Investigation of High Resolution Mass Spectrometry to Study the Formation and Evolution of Secondary Organic Aerosol

by

Kelly Louise Pereira

Doctor of Philosophy

University of York

Chemistry

September 2014

"Millions saw the apple fall, Newton was the only one who asked why?"

- Bernard M. Baruch

To the two most influential academics in my life.

Jacqui Hamilton and Kath Weatherhead

Your support, guidance and belief in me made this possible.

Abstract

Secondary organic aerosol (SOA) is well known to have adverse effects on climate, air quality and human health. However, the dynamic mechanisms occurring during SOA formation and ageing are poorly understood. In this study, a number of new instrumental methods based on liquid chromatography coupled to mass spectrometry were developed and validated to study the complex mechanisms controlling SOA formation and ageing. The method was tested on methyl chavicol, an oxygenated biogenic volatile organic compound that was recently identified as the main floral emission from an oil palm plantation in Malaysian Borneo. The photo-oxidation of methyl chavicol was investigated at the European Photoreactor. The SOA yield was determined to range between 19 - 31% depending on initial precursor (VOC:NO$_x$) mixing ratios. In total, 79 SOA compounds were observed and the structures of 10 compounds have been identified. The use of a time resolved aerosol collection method followed by offline mass spectrometry allowed the temporal evolution of individual compounds in the particulate phase to be observed. The majority of the observed initial SOA composition consisted of substituted nitrophenols. The photo-oxidation of two other aromatic systems (toluene and 4-methyl catechol) were also investigated. The photo-oxidation of toluene also resulted in the formation of substituted nitrophenols during initial aerosol growth. However, based on the volatility of these species and the amount of absorptive mass present, these compounds would not be expected to be in the aerosol phase. One possible explanation for this observation, is the formation of gas-phase clusters; suggesting that the presence of the nitro-group on the aromatic ring may be responsible for new particle formation. However, the structure of the nitrophenols were found to be critically important; highlighting the importance of studying SOA formation and evolution at a molecular level.

Table of Contents

List of Tables

List of Figures

Acknowledgements

Ten years ago I set myself one goal; achieve a PhD. Today, this goal is almost a reality. The last four years have been what can only be described, as life changing. I have met so many extremely talented people, travelled the world in pursuit of science and learnt things I never thought I was capable of learning. For this incredible opportunity, I would like to thank my supervisor, Jacqui Hamilton. Jacqui, you believed in me when I had lost all faith in myself. It was this resounding belief, which made me believe in myself. I cannot thank you enough for your support and guidance throughout this PhD. I would also like to express my greatest appreciation to my IPM, Jane Thomas-Oates for her guidance and support with my research over the years. One of things I wanted most during this PhD was to make you both proud, I hope I achieved this. I would also like to thank Ed Bergstrom, who was never too busy help or answer any technical questions I had regarding mass spectrometry.

Thank you to the atmospheric group, both past and present members, for your encouragement, support and friendship. In particular I would like to thank, Rachel, Marvin, Rosie, Jamie, Shalini and Sina.

This would not have been possible without my partner, Richard Procter. In the most darkest and loneliest of times you were the one making sure I was OK; whether this included a 3 am chat about the thesis, a motivational speech, or reassurance that everything was going to be fine. You understood how much achieving this PhD meant to me and supported me in every way possible. Words cannot express how grateful I am. I love you so much.

I would also like to thank my family, who have always supported me and have always been so proud. Dad, your story of how you persevered to get your qualifications in spite of the hardship you faced, kept me going in the most difficult of times, and will no doubt continue to inspire me. Mum, Georgia, Kim, thank you for the motivational speeches, you never doubted me once. I love you all very much.

Last but not least, I would like to thank my A-level chemistry teacher, Kath Weatherhead. Kath, without you I would of never of got this far. Your passion for chemistry is ultimately what led me down this path. I don't think I'll ever forget your dramatised impression of how a carbon atom has four bonds; memories I look back fondly on. Words cannot describe how grateful I am for your help and support at a time when I needed it the most.

Declaration

I hereby declare that the work presented in this thesis is my own (except where stated) and has not been submitted to any institution for any award. The majority of the work presented in Chapter 3 has been published in the peer-reviewed journal; Atmospheric Chemistry and Physics. The details of which are shown below:

Pereira, K. L., Hamilton, J. F., Rickard, A. R., Bloss, W. J., Alam, M. S., Camredon, M., Muñoz, A., Vázquez, M., Borrás, E., and Ródenas, M.: Secondary organic aerosol formation and composition from the photo-oxidation of methyl chavicol (estragole), Atmos. Chem. Phys., 14, 5349-5368, 10.5194/acp-14-5349-2014, 2014.

Chapter 4 is currently in the last stages of preparation for submission to the peer-reviewed journal; Environment Science and Technology. It is anticipated that this manuscript will be submitted prior to the viva.

Pereira, K. L., Hamilton, J. F., Rickard, A.R., Bloss, W., Alam, M. S., Camredon, Ward, M. W., Wyche, K. P., Muñoz, A., Vera, T., Vázquez, M., Borrás, E., Ródenas, M.: Observations of the Dynamic Mechanisms Controlling SOA Partitioning and Evolution: Investigating One Compound at a Time, in preparation, (2014).

Chapter 1 - Introduction to Secondary Organic Aerosol: Formation and Measurement

Techniques

1.1   Introduction

By definition, an aerosol is a solid or liquid particle suspended in a gas. In atmospheric science this definition refers to the suspension of a particle in air, and by extension, the atmosphere. Particulate air pollution is now well known to have adverse effects on climate and human health (Solomon et al., 2007). Aerosols can absorb and scatter solar radiation, influence cloud formation, affect air quality, and have detrimental effects on the human respiratory and cardiovascular system (Seaton et al., 1995; Peters et al., 1997; Keil and Haywood, 2003; Kappos et al., 2004; Brunekreef and Forsberg, 2005; Pope, 2006; Solomon et al., 2007). Numerous epidemiological studies have correlated human exposure to aerosol concentrations above 10 μg m^{-3} with increased morbidity and mortality rates (*cf.* (Pope, 2006)). The World Health Organisation (WHO) air quality guidelines (AQG) have recommended that the average annual aerosol concentration for fine particulate matter (< 2.5 μm in diameter) should be below 10 μg m^{-3} (WHO, 2006). However, currently 80% of the world's population live in regions where the aerosol concentration is around 20 ± 6.7 μg m^{-3}, exceeding that of the AQG (van Donkelaar et al., 2010). Furthermore, in some regions of the world where there is rapid economic and industrial developments such as China's mega cities, daily average aerosol concentrations are around 75 μg m^{-3}, increasing to ~ 160 μg m^{-3} or higher, during haze events; posing a significant risk to human health (Wang et al., 2013; Li et al., 2014).

A significant proportion $(20 - 90\%)$ of ambient aerosols are organic in nature, depending on source and ageing (Kanakidou et al., 2005). Organic aerosols can be directly emitted into the atmosphere (primary), or formed in the atmosphere through gas-particle conversion processes (secondary). Whilst the emission sources of primary organic aerosols are fairly well known (*e.g.* biomass burning, combustion), there is much uncertainty regarding the sources, composition and formation mechanisms of secondary organic aerosols (SOA). SOA constitutes a significant proportion of ambient particulate matter (Turpin and Huntzicker, 1995; Lim and Turpin, 2002; Zhang et al., 2005; Sullivan et al., 2006; Lanz et al., 2007). SOA is formed from the atmospheric oxidation of volatile organic compounds (VOCs) emitted in to the atmosphere from biogenic (*e.g.* vegetation) or anthropogenic sources (*e.g.* combustion). VOC oxidation can result in the formation of lower volatility species which can partition into the aerosol phase, forming SOA. The difficulty with studying SOA formation arises where the oxidation of a single VOC forms a wide variety of multi-functional oxidation products of differing volatilities (*e.g.* (Kroll and Seinfeld, 2008; Hallquist et al., 2009)). These compounds may undergo numerous oxidation steps, forming

a multitude of oxidation products; only some of which may contribute to SOA formation. Furthermore, once a compound partitions into the particulate phase it can undergo further oxidation steps (Claeys et al., 2004; Hearn et al., 2007; Perri et al., 2009; George and Abbatt, 2010) and reactive transformations (non-oxidative processes, *i.e.* oligomerisation) (Barsanti and Pankow, 2004; Gao et al., 2004a; Gao et al., 2004b; Iinuma et al., 2004; Kalberer et al., 2004; Tolocka et al., 2004), continually changing their chemical speciation and volatility (Kroll and Seinfeld, 2008). The sheer number of VOCs present in the ambient atmosphere (Goldstein and Galbally, 2007) and their continually evolving chemical composition, makes the identification of the species involved in SOA formation, growth and ageing, a highly complex and difficult task.

Current model simulations fail to predict observed SOA loadings in the ambient atmosphere (Heald et al., 2005; Volkamer et al., 2006; Hodzic et al., 2010; Ahmadov et al., 2012; Barsanti et al., 2013; Zhang et al., 2013; Zare et al., 2014). Whilst significant improvements have been made in recent years, models often under predict SOA loadings up to a factor of ~ 10 (Jimenez et al., 2009; Spracklen et al., 2011; Yu, 2011; Jathar et al., 2014; Langmann et al., 2014). Studies have shown that increasing the amount of anthropogenic SOA by 100 Tg yr^{-1} in modelled simulations, results in more accurate predictions of SOA loadings near source, but over predicts SOA loadings in remote regions (Heald et al., 2011; Spracklen et al., 2011). The inability to accurately simulate SOA loadings in the ambient atmosphere suggests there are additional sources of SOA formation which have not be identified and included in atmospheric models (*e.g.* (Kroll and Seinfeld, 2008; Hallquist et al., 2009)). To evaluate the effect of atmospheric aerosols on climate and human health, the sources, composition and mechanisms of SOA formation must be fully understood.

In the following sections, the processes behind SOA formation and the measurement techniques used to characterise SOA composition will be discussed. Initially, a brief background is given into the layers of atmosphere and its oxidising capacity. This is then followed by a discussion of the mechanisms occurring during VOC oxidation and the processes resulting in SOA formation. Finally, the techniques used to characterise SOA composition are discussed.

1.2   Layers of the Atmosphere

The atmosphere is comprised of many different layers, differentiated by changes in temperature and pressure with altitude (Figure 1.1). These layers can be broadly separated into the lower atmosphere, consisting of the troposphere and stratosphere, and the upper

atmosphere, consisting of the mesosphere, thermosphere and exosphere (the latter which is not shown in Figure 1.1). The troposphere is located in the lowest part of the atmosphere, extending from the earth's surface to approximately 10 - 15 km in height (Seinfeld and Pandis, 2012). The troposphere can be divided into two layers; the boundary layer (lower troposphere) and the free atmosphere (upper troposphere). Temperature inversions within the troposphere (*i.e.* nocturnal boundary layer/ entrainment zone) and the tropopause, generally prevent the majority of ground-level emissions from exceeding much beyond the boundary layer (~ 100 to 3000 m in altitude) (Stull, 1988; Finlayson-Pitts and Pitts, 2000; Harrison, 2001). As a result, the majority of ground-level emissions are concentrated close to the earth's surface, with the troposphere accounting for ~ 80% of the atmosphere's mass (Finlayson-Pitts and Pitts, 2000; Seinfeld and Pandis, 2012). It is in this region of the atmosphere where the following work will focus.
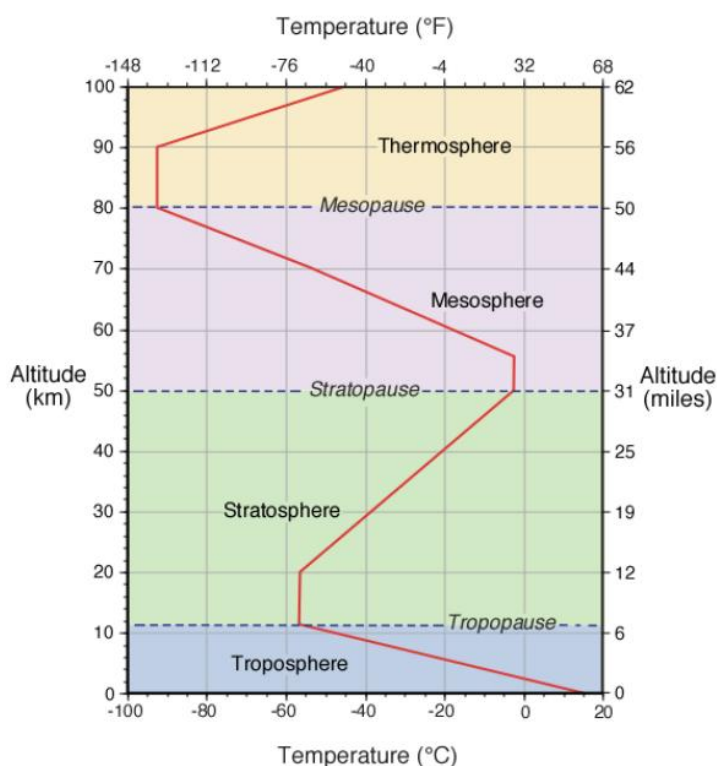
Figure 1.1 - Layers of the atmosphere, displaying changes in temperature with altitude. Taken from Pidwirny (2006).

1.3   Tropospheric Oxidants

VOCs emitted into the troposphere undergo oxidation primarily with hydroxyl radicals ($^{\bullet}$OH), ozone (O_3) and nitrate radicals ($^{\bullet}NO_3$) (Atkinson, 1997b, 2000; Calvert et al., 2000). In addition to these oxidants, atmospheric pollutants such as the oxides of nitrogen play an

important role in the photochemistry of the troposphere (Crutzen, 1979). Nitric oxide (NO) and nitrogen dioxide (NO_2) are known collectively as the oxides of nitrogen (NO_x). NO_x is primarily emitted into the atmosphere as nitric oxide (Atkinson, 2000). Nitric oxide can be directly emitted into the troposphere from anthropogenic (*e.g.* combustion) and natural sources (*e.g.* soils, natural fires), or formed in the troposphere from lightning strikes (Crutzen, 1979; Atkinson, 2000; Guenther et al., 2000; Schumann and Huntrieser, 2007; Bargsten et al., 2010). The effect of the oxides of nitrogen on the main atmospheric oxidants is discussed below.

1.3.1 Ozone: Sources and Formation

The main source of ozone in the troposphere is from the photolysis of nitrogen dioxide and subsequent reaction of the photoproduct, ground state oxygen ($O(^3P)$), with molecular oxygen (O_2) in the presence of air (M = air (O_2, N_2)) (Eq. 1.1 and 1.2) .

Eq. 1.1 $$NO_2 + h\nu \rightarrow NO + O(^3P) \qquad (\lambda < 410 \text{ nm})$$

Eq. 1.2 $$O(^3P) + O_2 + M \rightarrow O_3 + M$$
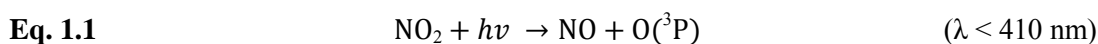
In addition to these reactions, ozone can also react with nitric oxide, forming nitrogen dioxide and molecular oxygen (Eq. 1.3). Considering only these reactions, a steady-state photo-chemical equilibrium can occur, resulting in no net loss, or formation of ozone (Figure 1.2).

Eq. 1.3 $$NO + O_3 \rightarrow NO_2 + O_2$$

The oxidation of VOCs with $^\bullet OH$, O_3 or $^\bullet NO_3$ can result in the formation of intermediate peroxy radicals (*i.e.* $HOO^\bullet$ and/or $ROO^\bullet$). These peroxy radicals can react with nitric oxide, forming nitrogen dioxide (Eq. 1.4 and Eq. 1.5); resulting in net ozone formation through reaction pathways Eq. 1.1 and Eq. 1.2 (Figure 1.3).

Eq. 1.4 $$ROO^\bullet + NO \rightarrow RO^\bullet + NO_2 \qquad (RO^\bullet = \text{alkoxy radical})$$

Eq. 1.5 $$HOO^\bullet + NO \rightarrow {}^\bullet OH + NO_2$$
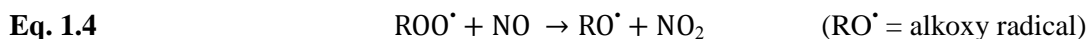
Relatively low levels of ozone in the troposphere is important due to the adverse effects ozone can have on human health and the environment (*e.g.* (Knowlton et al., 2004; Bell et al., 2007; Wang et al., 2007)), but also as the photolysis of ozone in the presence of water vapour is the main source of hydroxyl radicals in the troposphere (Atkinson, 1997a, 2000).

Net loss

O_3

NO NO_2

hv

O_2

O_3
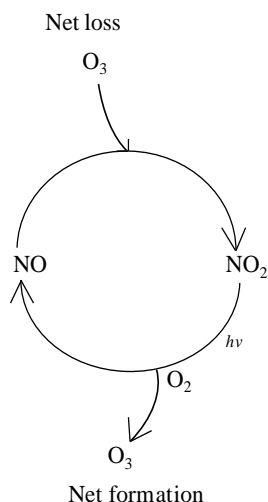
Net formation

Figure 1.2 - Steady state photochemical equilibrium between ozone (O_3) and the oxides of nitrogen. Adapted from Atkinson (2000).

VOC $\xrightarrow{\text{oxidation}}$ $\longrightarrow$ HOO$^{\cdot}$ $^{\cdot}$OH
                         ROO$^{\cdot}$ RO$^{\cdot}$

NO NO_2

hv

O_2

O_3
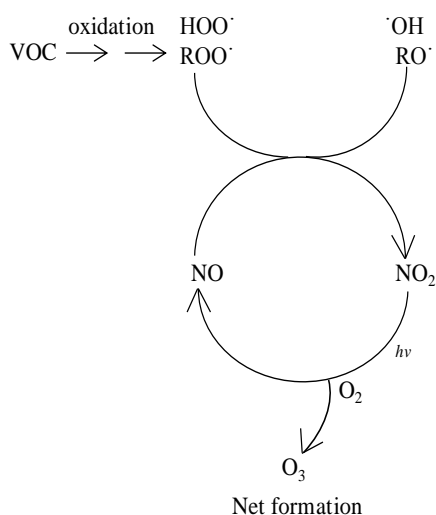
Net formation

Figure 1.3 - Net formation of ozone from the oxidation of VOCs in the presence of the oxides of nitrogen. Adapted from Atkinson (2000).

1.3.2   Hydroxyl Radical: Sources and Formation

The main source of hydroxyl radicals in the troposphere is from the photolysis of ozone in the presence of water vapour (Atkinson, 2000). The photolysis of ozone occurs at wavelengths $\geq$ 290 nm resulting in the formation of an excited oxygen atom, O(^{1}D), and molecular oxygen (Eq. 1.6) (Atkinson, 1997a; DeMore et al., 1997; Atkinson, 2000). The reaction of the excited oxygen atom with water vapour, results in the formation of hydroxyl radicals, as shown in Eq. 1.7.

Eq. 1.6 $\qquad\qquad$ $O_3 + h\nu \rightarrow O(^1D) + O_2$ $\qquad\qquad$ ($\lambda <$ 320 nm)

Eq. 1.7 $\qquad\qquad$ $O(^1D) + H_2O \rightarrow 2\,^{\bullet}OH$ $\qquad\qquad$ ~ 10%
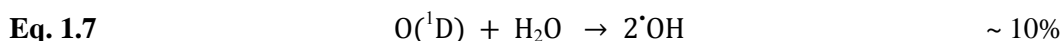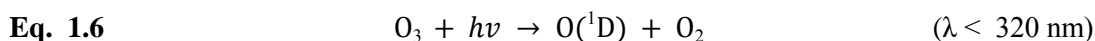
Additional (minor) sources of hydroxyl radicals in the troposphere include; (i) the photolysis of nitrous acid (HONO), formed from the heterogeneous reaction of nitrogen dioxide and water vapour on surfaces (Eq. 1.8 - 1.9) (Sakamaki et al., 1983; Akimoto et al., 1987; Sakamaki and Akimoto, 1988; Lammel and Cape, 1996; Alicke et al., 2003); (ii) reaction of alkenes with ozone (Atkinson, 1997b; Paulson et al., 1997; Donahue et al., 1998), and; (iii) the photolysis of formaldehyde and other carbonyl containing compounds in the presence of nitric oxide (Eq. 1.10 - 1.12) (Atkinson, 2000; Monks, 2005; Sander et al., 2006).

Eq. 1.8 $\qquad\qquad$ $HONO + h\nu \rightarrow \,^{\bullet}OH + NO$ $\qquad\qquad$ ($\lambda <$ 400 nm)

Eq. 1.9 $\qquad\qquad$ $2NO_2 + H_2O \rightarrow HONO + HNO_3$

Eq. 1.10 $\qquad\qquad$ $HCHO + h\nu \rightarrow H^{\bullet} + HCO^{\bullet}$ $\qquad\qquad$ ($\lambda <$ 334 nm)

Eq. 1.11 $\qquad\qquad$ $H^{\bullet} + O_2 + M \rightarrow HOO^{\bullet} + M$

Eq. 1.12 $\qquad\qquad$ $HOO^{\bullet} + NO \rightarrow \,^{\bullet}OH + NO_2$
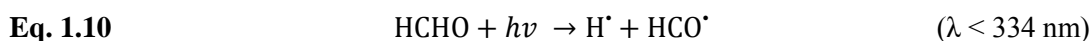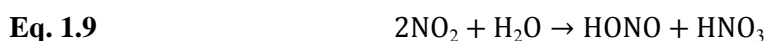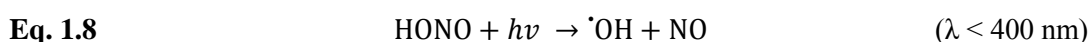
1.3.3   Nitrate Radical: Sources and Formation

The nitrate radical is formed from the reaction of nitrogen dioxide with ozone, as shown in Eq. 1.13 (Atkinson, 1997a; DeMore et al., 1997; Atkinson, 2000). During night time hours, the nitrate radical, along with ozone, are the dominant tropospheric oxidants (Winer et al., 1984; Paulson and Orlando, 1996; Geyer et al., 2003). During daylight hours, the nitrate radical undergoes rapid photolysis with a lifetime of ~ 5 seconds (Atkinson, 1997b, 2000). Photolysis degradation results in the formation of NO_2 and $O(^3P)$ as the major pathway (Eq. 1.14), and NO and O_2 as the minor pathway (Eq. 1.15) (Atkinson, 2000).

Eq. 1.13 $\qquad\qquad$ $NO_2 + O_3 \rightarrow \,^{\bullet}NO_3 + O_2$

Eq. 1.14 $\qquad\qquad$ $^{\bullet}NO_3 + h\nu \rightarrow NO_2 + O(^3P)$ $\qquad\qquad$ (~ 90%)

Eq. 1.15 $\qquad\qquad$ $^{\bullet}NO_3 + h\nu \rightarrow NO + O_2$ $\qquad\qquad$ (~ 10%)
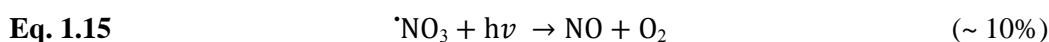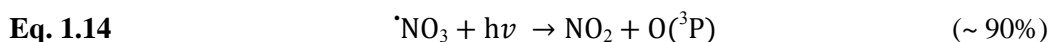
The nitrate radical is an important tropospheric oxidant. Typically, it was thought that hydroxyl radicals formed during daylight hours, would gradually decrease in concentration

to negligible amounts during the night (*e.g.* (Khan et al., 2011)). However, the reaction of the nitrate radical with unsaturated VOCs can result in the formation of night time peroxy radicals; resulting in the formation of night-time ˙OH through Eq. 1.12 (Platt et al., 1990; Geyer et al., 2003; Rivett et al., 2003; Khan et al., 2011).

1.4   VOC Oxidation

The mechanisms of VOC oxidation largely depend on the structure and functionality of the species, and the availability of the reactants. Generally, VOCs of the same class (*i.e.* alkenes, alkanes, aromatics *etc*) or functionality undergo similar initial oxidation pathways (Atkinson, 2000; Atkinson and Arey, 2003). VOCs which form an alkyl radical (R˙) upon oxidation, can proceed through the reaction pathways shown in Figure 1.4. The alkyl radical reacts rapidly and solely with O_2, forming an intermediate peroxy radical (ROO˙). These peroxy radicals can then undergo a number of reactions depending on the availability of the reactants and the "environment" in which oxidation occurs.
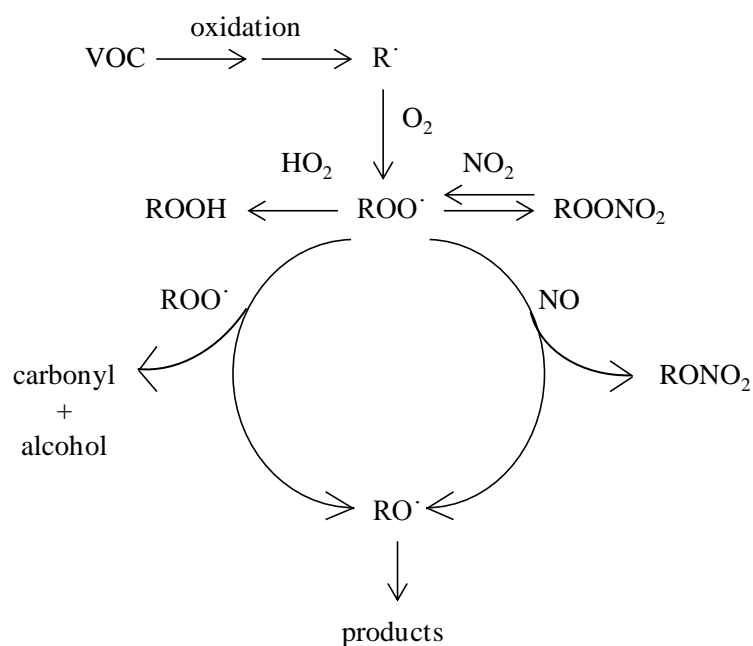
Figure 1.4 - Simplified VOC oxidation scheme for VOCs which produce an alkyl radical upon oxidation. Re-drawn from Atkinson (2000).

1.4.1   Alkanes

Alkanes react primarily with ˙OH and ˙NO_3, with the oxidation by ˙OH observed to dominate (Atkinson, 1997b, 2000; Atkinson and Arey, 2003). In both cases, oxidation

proceeds through hydrogen-atom (H-atom) abstraction from the carbon-hydrogen bonds (C-H bonds) as shown, for example, in Figure 1.5. H-atom abstraction results in the formation of an alkyl radical (R$^\bullet$), which can proceed through the reaction scheme show in Figure 1.4.
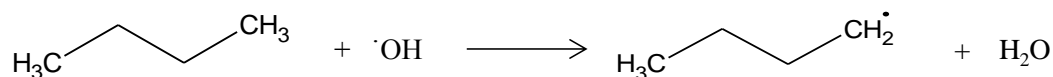
Figure 1.5 - An example of H-atom abstraction during the oxidation of an alkane (butane) with $^\bullet$OH.

The reaction of alkanes with ozone is considered to be of negligible importance due to its extremely slow rate of reaction ($< 10^{-22}$ cm^3 molecule^{-1} s^{-1} (Seinfeld, 1992; Atkinson, 1997b)) and is therefore, generally not considered as a reaction pathway (Atkinson, 1997b; Atkinson and Arey, 2003; Calvert et al., 2008).

1.4.2   Alkenes

Alkenes can react with $^\bullet$OH, O$_3$ and $^\bullet$NO$_3$. In contrast to the oxidation of alkanes, the oxidation of alkenes by $^\bullet$OH and $^\bullet$NO$_3$ proceeds mainly through the addition of the radical to the carbon-carbon double bond, with an example shown in Figure 1.6. In this reaction, the carbon-carbon double bond opens upon addition of the hydroxyl radical, forming an alkyl radical on the adjacent carbon atom.
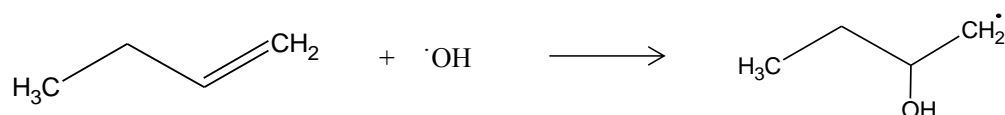
Figure 1.6 - Formation of the alkyl radical from the oxidation of an alkene with $^\bullet$OH

H-atom abstraction from the C-H bonds, as observed with the oxidation of alkanes, is considered to be a minor pathway; accounting for $< 5\%$ of the total reaction (Atkinson, 1989; Atkinson, 1997b).

As previously discussed, the reaction of an alkene with ozone does not result in the formation of an alkyl radical. Instead, an energy rich ozonide is formed which rapidly decomposes, forming a carbonyl and a biradical (Criegee intermediate), as shown in Figure 1.7. The Criegee intermediate can decompose or collisionally-stabilise forming a variety of products such as, carbonyls, esters, hydroperoxides and carboxylic acids (Atkinson, 1997b, 2000).
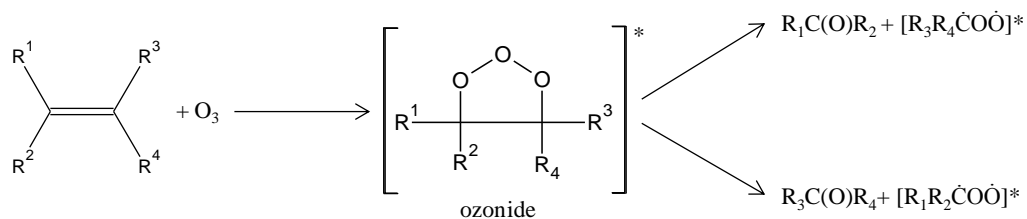
Figure 1.7 - Reaction of an alkene with ozone, displaying the formation and decomposition of the ozonide. * donates energy rich species. Re-drawn from Atkinson (2000).

1.4.3   Aromatics

Aromatics undergo oxidation with $^{\bullet}$OH and $^{\bullet}$NO$_3$, with the reaction with $^{\bullet}$OH dominating in the atmosphere (Atkinson, 2000; Atkinson and Arey, 2003). For both substituted and non-substituted aromatics, the major pathway of oxidation occurs through the addition of $^{\bullet}$OH to aromatic ring (Calvert et al., 2002; Atkinson and Arey, 2003). H-atom abstraction from the C-H bonds of the aromatic ring is a minor pathway, accounting for < 10% of the overall $^{\bullet}$OH reaction (Atkinson, 1989; Atkinson, 2000; Calvert et al., 2002; Atkinson and Arey, 2003). Substituted aromatics containing saturated or unsaturated hydrocarbon chain substituents, can undergo oxidation analogous to the mechanisms described above (Atkinson and Arey, 2003).

1.5   Gas-Particle Partitioning

The fundamental concept governing SOA formation is that it is mainly composed of semi-volatile compounds which partition between the gas and particulate phase (Pankow, 1994a, b). The partitioning of a species into the aerosol phase can be described by the absorptive partitioning co-efficient, K_p (Pankow, 1994b, a), or its inverse, the saturation concentration, C^* (Donahue et al., 2006). Both theorems dictate that the partitioning of a species into the aerosol phase depends upon its volatility (*i.e.* vapour pressure), its gas phase concentration and the amount of absorptive mass present (*i.e.* pre-existing aerosol particles into which semi-volatile species can be absorbed) (Pankow, 1994b, a; Odum et al., 1996; Donahue et al., 2006; Kroll and Seinfeld, 2008).

The absorptive partitioning co-efficient (K_p, m^3 µg^{-1}) is described in Eq. 1.18, where; P equals the mass concentration of the semi-volatile species, i, in the particulate phase (µg m^{-3}), G is the mass concentration of the semi-volatile species in the gas phase per volume of air (µg m^{-3}), M is the mass concentration of the total absorbing particulate phase (µg m^{-3}), R is the ideal gas constant (8.206×10^{-5} m^3 mol^{-1} K^{-1}), T is the temperature (K), f_{om} is the mass

fraction of the total suspended particulate concentration that is in the absorbing phase, MW_{om} is the average molecular weight of the absorbing phase (g mol^{-1}) (estimated value ~ 100 - 300 g mol^{-1} (Pankow, 1994b)), $p_{Li}°$ is the vapour pressure of the absorbing semi-volatile species as a liquid (Torr), and ζ is the activity co-efficient of the semi-volatile species in the particulate phase (assumed to be 1 (Pankow, 1994b; Donahue et al., 2006)).

Eq. 1.18
$$K_{pi} = \frac{P_i}{G_iM} = \frac{760RTf_{om}}{MW_{om}10^6\zeta_ip_{Li}°}$$

The saturation concentration (C^*, µg m^{-3}) equation is shown in Eq. 1.19; where C_i^{VAP} equals the concentration of the semi-volatile species in the gas phase (µg m^{-3}), C_i^{aer} is the concentration of the semi-volatile species in the particulate phase, and C_{OA} is the total organic aerosol concentration (µg m^{-3}). From Eq. 1.19 it can be observed that the saturation concentration does not include f_{om} or MW_{om}. Instead, this equation removes the estimated average molecular weight of the particulate absorbing mass, to provide a compound specific saturation concentration; where M_i equals the molecular weight of the absorbing semi-volatile species (Donahue et al., 2006).

Eq. 1.19
$$C_i^* = \frac{C_i^{VAP}C_{OA}}{C_i^{aer}} = \frac{M_i10^6\zeta_ip_{L,i}°}{760RT}$$

From both equations, it can be observed that providing some absorptive mass is present, a semi-volatile species can partition some of its mass into the aerosol phase. The fraction *F* of the semi-volatile species in the aerosol phase based on the amount of absorbing mass present, can be calculated as shown in Eq. 1.20. Multiplying the fraction of the semi-volatile species in the aerosol phase by its gas phase concentration, gives the concentration of the semi-volatile species in the particulate phase (Eq. 1.21) (Kroll and Seinfeld, 2008).

Eq. 1.20
$$F = \frac{1}{1 + C^*/M}$$

Eq. 1.21
$$C_i^{aer} = F \times C_i^{VAP}$$

The effect of the amount of absorbing mass on the fraction of species in the particulate phase is shown Figure 1.8. Here, it can be observed that if C^* is equal to the amount of absorptive mass present, the species will partition half of its gas phase mass into the aerosol phase (dashed line in Figure 1.8). Conversely, if $C^* < M$ the majority of its mass will reside in the particulate phase, and if $C^* > M$ the fraction of the species in the particulate phase

approaches zero. This is the result of a gas-particle equilibrium between the mass of the species in the gas phase and the amount of absorbing mass present (Pankow, 1994b, a).
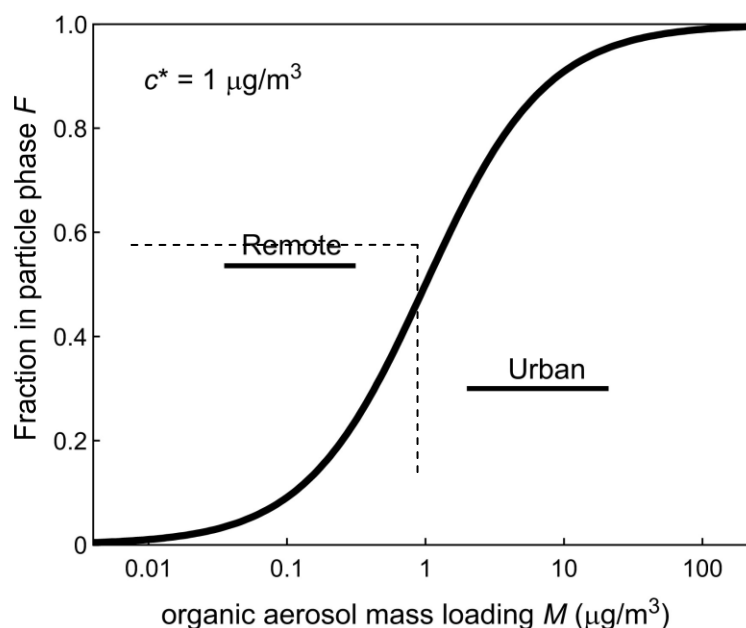
Figure 1.8 - The effect of the amount of absorbing mass present on the fraction of a species in the aerosol phase, displaying the approximate range of organic mass loadings expected in remote and urban environments. Figure obtained from Kroll and Seinfeld (2008).

The partitioning of a species into the aerosol phase is therefore largely dependent upon its vapour pressure (Kroll and Seinfeld, 2008; Donahue et al., 2009). One way to describe the partitioning of numerous, multifunctional species of differing volatilities, is to group them based on their saturation concentration ; a framework referred to as the volatility basis set (VBS) (Donahue et al., 2006; Donahue et al., 2009; Donahue et al., 2011a; Donahue et al., 2012). This framework characterises the partitioning of compounds with differing saturation concentrations at atmospheric loadings (1 to 100 µg m^{-3}), using the following definitions;

VOC = $C^* > 10^6$ µg m^{-3}. These compounds are of the highest volatility, the majority of which have been directly emitted into the troposphere and have not undergone oxidation. These compounds reside almost exclusively in the gas phase at atmospheric loadings.

IVOC = Intermediate volatility, C^* 10^3 to 10^6 µg m^{-3}. These compounds have lower saturation concentrations than the group discussed above, but also reside almost entirely in the gas phase.

SVOC - Semi-volatile, C^* 1 to 10^3 µg m^{-3}. These compounds have significant fractions of their mass in both the gas and particulate phase.

LVOC - Low volatility, C^* 10^{-2} to 1 µg m^{-3}. These compounds reside mostly in the particulate phase except in warm or remote (*i.e.* low atmospheric loadings) regions of the world (Donahue et al., 2009).

NVOC - Non volatile, C^* < 10^{-2} µg m^{-3}. These compounds are almost exclusively in the particulate phase. (Definition not included in recent studies (Donahue et al., 2013)).

ELVOC - Extremely low volatility, C^* < 10^{-3} µg m^{-3}. Similar to the group discussed above. Recently added definition (Donahue et al., 2013). These compounds are almost exclusively in the particulate phase and are suspected to be involved in new particle formation (see Section 1.6) (Donahue et al., 2013).

The effect of volatility on the partitioning of a species into the aerosol phase when a constant amount of absorptive mass is present, is shown in Figure 1.9. Here, it can be observed that the lower the saturation concentration (and thus higher K_p) of a compound, the more of its gas-phase mass is partitioned into the particulate phase.
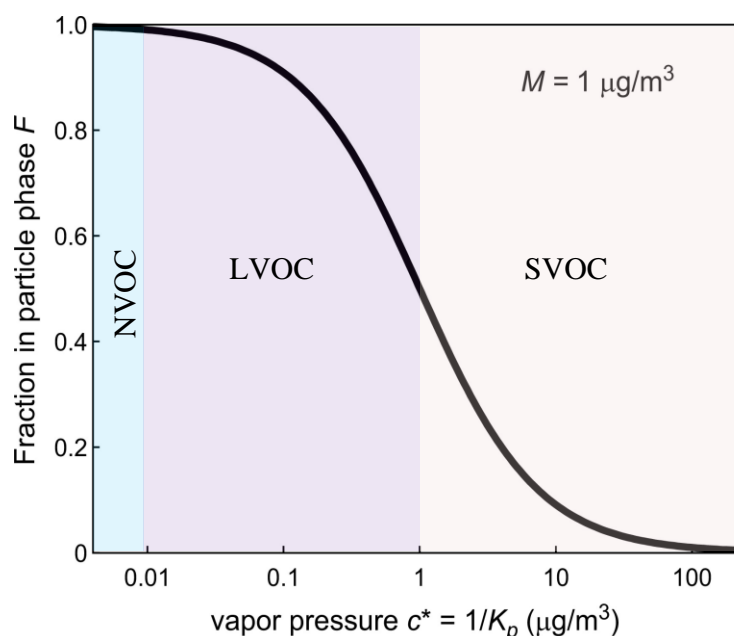
Figure 1.9 - Effect of vapour pressure on the fraction of a compounds mass that is partitioned into the aerosol phase. Displaying the VBS groupings. Adapted from Kroll and Seinfeld (2008).

1.6   New Particle Formation

In addition to the growth of SOA through gas-particle partitioning, new particle formation can also occur. The mechanisms of new particle formation in the atmosphere are currently not well understood (*e.g.* (Sogacheva et al., 2008; Zhang et al., 2011b; Riipinen et al., 2012; Bzdek et al., 2013)). It is generally accepted, that new particle formation occurs through the formation of stabilised gas-phase clusters (homogenous nucleation) of ~ 1 nm in diameter (Kulmala et al., 2004; Spracklen et al., 2006; Sipilä et al., 2010; Riipinen et al., 2012). These freshly nucleated clusters can then undergo growth to larger sizes through the condensation of low-volatility vapours, forming SOA (Kulmala et al., 2004; Zhang et al., 2004; Zhang et al., 2009; Riipinen et al., 2012).

New particle formation in the atmosphere does not continuously occur, but rather appears to be associated with particular meteorological conditions (*e.g.* (Sogacheva et al., 2008) and the abundance of sulfuric acid vapours (*cf.* (Kulmala et al., 2004)). Frequent "nucleation events" (*i.e.* observation of new particles and subsequent growth to ~ 50 nm in diameter) have been observed in many different environments throughout the world, such as; the remote Boral forest, suburban Helsinki, urban Atlanta, industrialised agricultural regions in Germany, and many more (Kulmala et al., 2004). There is now strong evidence that sulfuric acid vapours are involved in nucleation (Weber et al., 1995; Kulmala, 2003; Sihto et al., 2006; Sipilä et al., 2010; Donahue et al., 2013; Kulmala et al., 2013). However, recent studies have shown that sulfuric acid vapours alone cannot account for the high number of particles formed and the growth rates observed (Sipilä et al., 2010; Kirkby et al., 2011; Almeida et al., 2013). This suggests that other species which have not been identified, may be participating in nucleation along with sulfuric acid vapours (Sipilä et al., 2010). Recently, ELVOCs have been suggested to form stabilised gas-phase clusters with sulfuric acid vapours and drive nanoparticle growth, as shown in Figure 1.10 (Zhang et al., 2004; Donahue et al., 2011b; Pierce et al., 2011; Riipinen et al., 2011; Donahue et al., 2013; Kulmala et al., 2013; Ehn et al., 2014). However currently, the detailed chemical composition of these ELVOCs remains unknown (Donahue et al., 2013).
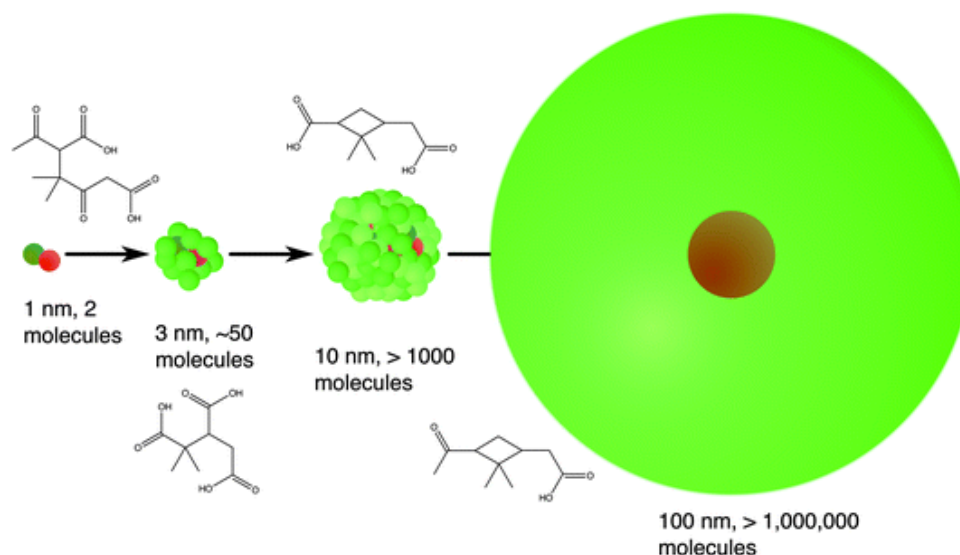
Figure 1.10 - Bimolecular homogenous nucleation of an ELVOC (3-methyl-1,2,3-butanetricarboxylic acid, MBTCA, dark green) and sulfuric acid (red), followed by the subsequent growth to larger particle diameters through the condensation of higher volatility species, such as cis-pinonic acid (light green). Taken from Donahue et al. (2013).

1.7 Chemical Characterisation of SOA

There is currently no 'perfect' instrument capable of providing detailed chemical composition of individual particles in the atmosphere as they form and evolve (Figure 1.11) (McMurry, 2000; Hallquist et al., 2009; Calvo et al., 2013). As a result, a wide variety of analytical techniques are used, often collaboratively, to determine SOA composition (Hallquist et al., 2009). Many of the significant advances in our understanding of the composition and formation of SOA can be attributed to mass spectrometry (Nizkorodov et al., 2011; Pratt and Prather, 2012a, b). There is now an extensive range of mass spectrometers used to study SOA, employing a wide variety of sample introduction techniques, ionisation methods and mass analysers (Nizkorodov et al., 2011; Laskin et al., 2012; Pratt and Prather, 2012a, b). These mass spectrometric techniques can be broadly separated into online and offline methods. Online methods can provide rapid sampling of particles, allowing near-real time measurements of particle size and composition (Canagaratna et al., 2007; Laskin et al., 2012; Pratt and Prather, 2012a).

Online mass spectrometric techniques, such as aerosol mass spectrometer (AMS, commercialised by Aerodyne Inc) has revolutionised the chemical characterisation of organic aerosol (OA). AMS can provide quantitative measurements of non-refractory species, including; sulfate, nitrate, ammonium, chloride and total organic matter, at high-

temporal resolution (Jimenez et al., 2003; Canagaratna et al., 2007; Zhang et al., 2011a). The AMS works by focussing sampled aerosol particles into a narrow beam, using an aerodynamic lens, and subjecting them to thermal vaporisation followed by electron ionisation. The high vaporisation temperature (600˚C) and electron energy used (70 eV) results in extensive fragmentation of the ions, preventing molecular identification (Canagaratna et al., 2007). However, the characteristic mass spectral fragment ions detected can provide information on the composition of bulk OA. This has led to significant advances in our understanding of the chemical speciation of ambient aerosol. For example, Zhang et al. (2007) found that non-refractory PM_1 ambient aerosol measured in various locations using the AMS, consisted of mainly organic material (18 - 70%) (Figure 1.12).
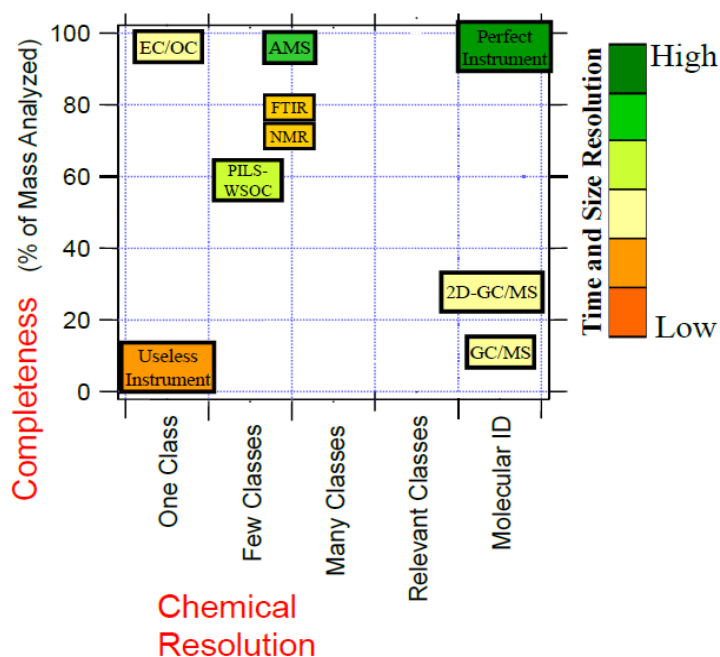
Figure 1.11 - Visual representation of some of the analytical techniques used to characterise OA composition, displaying the completeness of the aerosol mass which can be analysed, the size and time resolution and the chemical resolution which can be achieved. EC/OC = thermal optical elemental carbon/organic carbon analyser. PILS-WSOC = particle into liquid sampler combined with analysis for water soluble organic compounds. FTIR = Fourier transform infra-red spectroscopy. NMR = nuclear magnetic resonance. GC/MS = gas chromatography mass spectrometry. 2D-GC/MS = two-dimensional GC/MS. Taken from Hallquist et al. (2009).

Furthermore, the use of AMS followed by statistical multivariate techniques, such as positive matrix factorisation (PMF) can allow components of the sampled aerosol to be grouped in to "factors", providing information about chemical properties and the sources of

the sampled OA (Zhang et al., 2011a). Numerous groupings are used within the literature to describe the sources and chemical composition of OA. A few of these groups include; hydrocarbon-like organic aerosol (HOA), low-volatility oxygenated organic aerosol (LV-OOA) and semi-volatile oxygenated organic aerosol (SV-OOA) (Lanz et al., 2007; Jimenez et al., 2009; Zhang et al., 2011a). HOA represents OA from primary sources, having low O:C ratios < 0.1 and generally displaying characteristic fragmentation patterns of long-chain hydrocarbons similar to lubricants used in automotive engines (Zhang et al., 2005; Jimenez et al., 2009; Ng et al., 2010). LV-OOA is representative of aged relatively non-volatile OA with high O:C ratios, displaying strong correlations with non-volatile secondary species such as sulfate aerosol; whereas SV-OOA is correlated with more volatile species (*e.g.* ammonium nitrate aerosol) containing lower O:C ratios and is more indicative of freshly formed aerosol (Jimenez et al., 2009).
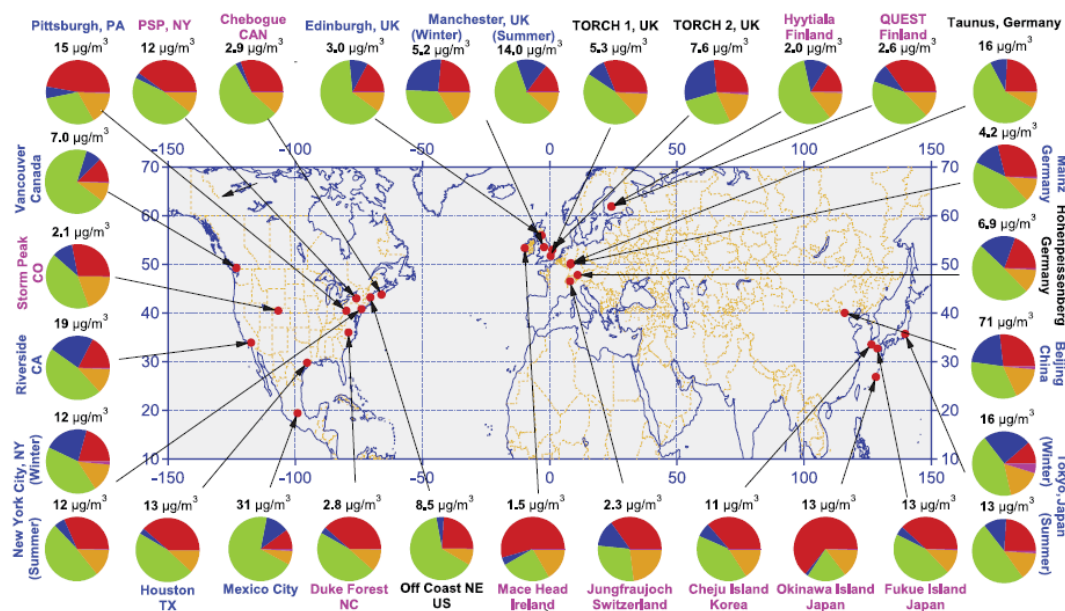
Figure 1.12 - Chemical composition and mass concentration of non-refractory PM$_1$ aerosol in urban area (blue), remote/rural areas (pink) and downwind of major cities (blank) using the AMS. Pie chats display the aerosol speciation; organics (green), sulfate (red), nitrate (blue), ammonium (orange) and chloride (purple). Taken from Zhang et al. (2007).

Using the AMS, the evolution of OA can be observed with the movement from HOA to SV-OOA through to LV-OOA as the OA becomes aged and increasingly more oxidised (Jimenez et al., 2009). This can be observed in Figure 1.13, where a high resolution time-of-flight AMS (HR-TOF-AMS) was used onboard an aircraft to measure the OA chemical speciation over Mexico city through to the outer rural areas over ~ 6 hours. From Figure 1.13, it can be observed that as the OA ages it becomes increasingly more oxidised and of

lower volatility, resulting in a decrease in the SV-OOA and an increase in LV-OOA as the OA evolves. However, whilst these techniques have been invaluable to our understanding of the processes occurring during SOA formation and ageing, they cannot currently provide the greater molecular and structural specificity that offline mass spectrometric techniques can offer (Zhang et al., 2007; Hallquist et al., 2009; Laskin et al., 2012). In order to investigate the mechanisms occurring during SOA formation and ageing, detailed chemical and structural speciation is required (Nizkorodov et al., 2011; Laskin et al., 2012).
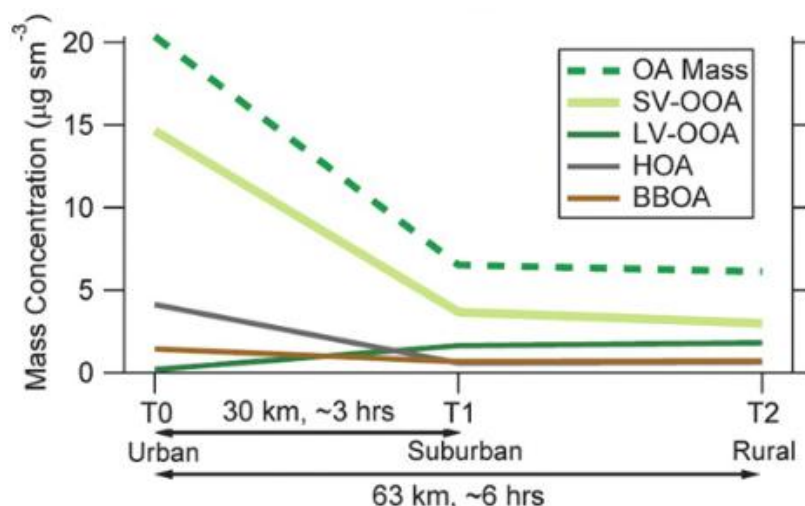
Figure 1.13 - Evolution of OA measured in Mexico city (0 hours) to the suburban (3 hours later) to the outer rural areas (6 hours later) using high resolution time-of-flight mass spectrometer (HR-TOF-AMS) onboard a National Science/National Center for Atmospheric Research (NSF/NCAR) C-130 aircraft. Factor analysis of HR-TOF-AMS, showing SV-OOA, LV-OOA, HOA, biomass burning oxygenated aerosol (BBOA). Taken from Jimenez et al. (2009).

Many different offline techniques (in contrast to near-real time analysis) can be used to study the molecular composition of OA. A few of these include; comprehensive two-dimensional gas chromatography mass spectrometry (GC×GC-MS), high performance liquid chromatography mass spectrometry (HPLC-MS), high performance liquid chromatography ultraviolet spectroscopy (HPLC-UV) and ultra-high resolution mass spectrometry techniques, such as the Fourier transform ion-cyclotron resonance mass spectrometer (FTICR-MS).

GC×GC-MS is capable of providing detailed chemical speciation of organic compounds in both the gas and particulate phase (Ledford et al., 1996). Comprehensive gas chromatography (GC×GC) utilises two columns in series which usually consist of differing

stationary phases, allowing the separation of compounds by two physical properties such as volatility and polarity (Arsene et al., 2011). The advantage of this technique in comparison to traditional gas chromatography mass spectrometry (GC-MS) is the additional chemical information obtained from the use of the secondary column. The secondary column provides another level of separation (usually orthogonal), resulting in structured chromatograms where compounds of a similar chemical speciation (*e.g.* aliphatics, aromatics *etc*) elute in groups (Figure 1.14); significantly aiding in compound identification.
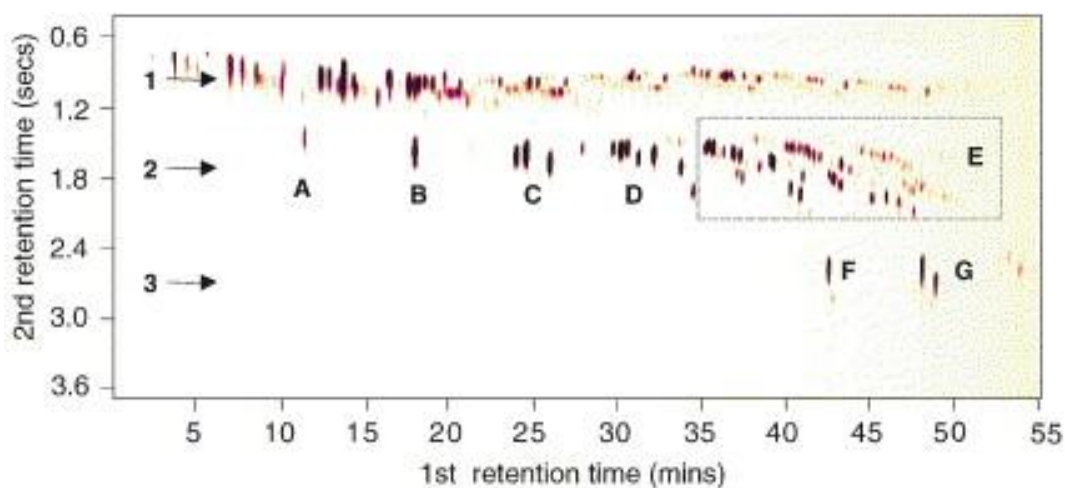
Figure 1.14 - Example of the chromatographic banding observed with the use of comprehensive two-dimensional gas chromatography for a leaded gasoline sample. 1 = Aliphatic band. 2 = Monoaromatic band. 3 = Polyaromatic band. A = Benzene. B = Toluene. C = Xylenes. D = C_3-substitued monoaromatics. E = higher aromatics. F = Napthalene. G = Methyl napthalenes. Taken from Hamilton and Lewis (2003).

GC×GC is capable of resolving thousands of compounds in ambient OA samples (Hamilton et al., 2004), and when coupled with mass spectrometry, can provide the detailed chemical speciation of compounds present in OA samples (Hamilton et al., 2004; Kallio et al., 2006; Robinson et al., 2011; Lee et al., 2012) and laboratory generated SOA (Hamilton et al., 2005; Webb et al., 2006; Hamilton et al., 2011). Whilst this technique can be extremely useful in providing the detailed chemical composition of OA, it is not suitable for the analysis of thermally labile or non-volatile compounds, due to the temperatures used to elute compounds from the column and some sample introduction techniques (*i.e.* thermal desorption) (Hamilton, 2010; Laskin et al., 2012).

Non-volatile compounds can be analysed using HPLC-MS. HPLC-MS is considered to be one of the most robust techniques for the chemical characterisation of OA, allowing a wide variety of polar to non-polar compounds to be isolated and detected, generally allowing a

broader range of species to be detected than with the use of GC×GC-MS (Laskin et al., 2012; Nozière et al., 2015). HPLC-MS can also be coupled with an ultra violet-visible detector (HPLC-UV-MS), allowing light absorbing compounds within OA samples to be to be targeted, whilst providing additional information on the functional groups and bonds of light absorbing species. This technique has been particularly useful in the analysis of organic nitrogen containing compounds (Kitanovski et al., 2012b).

FTICR-MS (reviewed by Marshall, 1985; Baykut and Eyler, 1986; Marshal and Grosshans, 1991; Marshall et al., 1998) can allow the elemental composition of thousands of compounds in complex mixtures to be identified (Marshall and Rodgers, 2008). This technique along with prior chromatographic separation (*i.e.* comprehensive two-dimensional gas chromatography, high performance liquid chromatography) and tandem mass spectrometry (discussed in Chapter 2), can provide both the chemical composition and structure of individual species, allowing molecular identification (Tolocka et al., 2004; Gómez-González et al., 2008; Laskin et al., 2009; Müller et al., 2009; Laskin et al., 2010; Laskin et al., 2012; Nguyen et al., 2012; Pereira et al., 2014). The use of these techniques with atmospheric simulation chamber experiments, used for generating SOA in controlled environments, can allow the mechanisms of SOA formation and evolution to be studied at a molecular level.

1.8   Thesis Outline

The aim of this thesis is to further investigate SOA formation and evolution using mass spectrometry. This will involve the use of a time resolved aerosol collection technique and the development of a number of new methods based on liquid chromatography coupled to mass spectrometry. A brief summary of the work present in each of the chapters is shown below.

Chapter 2 - This work shows the development and optimisation of a variety of HPLC-ESI-ITMS methods used for the compositional analysis of the SOA formed from the oxidation of 3-methyl furan, methyl chavicol and diesel exhaust emissions.

Chapter 3 - In this study, the SOA formed from the photo-oxidation of methyl chavicol is investigated. Methyl chavicol is an oxygenated biogenic volatile organic compound that was recently identified as the main floral emission from an oil palm plantation in Malaysian Borneo. The emissions of methyl chavicol observed may impact regional atmospheric chemistry, but little is known of its ability to form SOA.

Chapter 4 - In this study, the SOA composition formed during the photo-oxidation of methyl chavicol (biogenic oxygenated VOC), toluene (aromatic anthropogenic VOC) and 4-methyl catechol (aromatic anthropogenic oxygenated VOC) is investigated. The use of a time resolved aerosol collection method followed by offline mass spectrometric analysis allowed the dynamic processes occurring during SOA formation and ageing to be observed.

Chapter 5 - This work investigates the reliability and reproducibility of the chemical metrics used for describing the chemical properties of OA samples using ultra high resolution mass spectrometry.

Chapter 6 - Finally, a summary is given and future work is discussed.

Chapter 2 - Development of HPLC-ITMS for Complex Samples

2.1 Introduction

High performance liquid chromatography (HPLC) is a powerful tool for the separation of non-volatile compounds in complex mixtures. The coupling of prior chromatographic separation with mass spectrometry (MS) can allow individual species within complex mixtures to be isolated and identified; often allowing considerably more compounds to be observed compared with the use of mass spectrometry alone. LC-MS has been extensively used in the literature for the chemical characterisation of organic aerosol (OA). LC-MS can be used to detect and quantify pre-selected tracer compounds in ambient aerosol, such as; organic acids in OA samples collected in a Finnish coniferous forest (Anttila et al., 2005), nitrocatechols in biomass burning aerosol (Kitanovski et al., 2012b), nitrogen containing compounds in OA samples collected in Duke Forest in California, USA (Samy and Hays, 2013) and in the boreal forest in Finland (Laitinen et al., 2014). Alternatively, LC-MS can be used to the determine the molecular composition a wide variety of species present in ambient aerosol (Stone et al., 2009), or laboratory generated SOA, such as; β-caryophyllene (Kanawati et al., 2008; Alfarra et al., 2012), α- and β-pinene (Iinuma et al., 2007; Venkatachari and Hopke, 2008), methyl chavicol (Pereira et al., 2014) and benzene and 1,3,5-trimethyl benzene (Sato et al., 2012).

The most common type of HPLC column used for the analysis of OA, is reverse phase liquid chromatography (RP-LC). RP-LC consists of a polar mobile phase and a less polar stationary phase (typically C_{18} alkyl chains bonded to a silica surface (dimethyl octadecylsiliane)). RP-LC was developed in 1950, when the "normal" chromatography method consisted of using a polar stationary phase and a less polar mobile phase; the reverse to RP-LC and hence the name (Howard and Martin, 1950; Dorsey and Dill, 1989). RP-LC is an extremely versatile technique, allowing a wide range of polar and non-polar compounds to be separated. Using RP-LC, compounds are eluted in order of increasing hydrophobicity through increasing aqueous organic solvent content. Compound retention is achieved through the distribution of an analyte between the mobile phase (*i.e.* water and organic layer) and the stationary phase. However, the exact retention mechanisms are still under debate (Rafferty et al., 2011; Schure et al., 2013). Currently, it is not clear which mechanism (*i.e.* full partitioning of an analyte into the stationary phase, or absorption of an analyte into the stationary/mobile phase interface) is the most important for compound retention (Rafferty et al., 2011). Numerous studies have attempted to address this question, however the incomplete understanding of the interactions occurring between the stationary phase and the mobile phase, has made this particularly difficult (Carr et al., 1993; Carr et al., 1996; Vailaya and Horváth, 1998; Gritti and Guiochon, 2005; Rafferty et al., 2011).

The selection of a suitable chromatographic column is of critical importance for the separation and detection of analytes. One must consider the solubility of the analytes in the HPLC mobile phase composition, the chemical speciation of the analytes and their interaction with the chosen column stationary phase, and the compatibility of the HPLC mobile phase composition with the detection method. Atmospheric pressure mass spectrometry ionisation sources, such as electrospray ionisation (ESI), can allow HPLC to be successfully coupled with mass spectrometry. ESI converts analytes in the HPLC mobile phase eluant into gaseous ions, allowing the detection of these species using mass spectrometry (Bruins, 1998; Ho et al., 2003). ESI is well suited for analysis of small polar compounds and is considered to be a soft ionisation technique, generally resulting in little to no fragmentation of species during ionisation, with the exception of adduct formation which often results in extensive fragmentation. The minimal fragmentation of species during ionisation allows techniques such as tandem mass spectrometry (often abbreviated to MS/MS or MS^2, or MS^n where n > 2) to be performed; providing the structural information of species through fragmentation; often allowing compound identification (McLuckey and Wells, 2001; Nizkorodov et al., 2011).

Tandem (Latin meaning = *at length*) mass spectrometry can be performed using a wide variety of mass spectrometers. The quadrupole ion-trap mass spectrometer (ITMS) is one of these devices. The quadrupole ITMS can be referred to as a "tandem in-time" device, allowing the selection and fragmentation of precursor and subsequent product ions in real-time (McLuckey and Wells, 2001). The ability of this instrument to store ions within the ion trap during analysis, allows users to perform multiple MS^n experiments (March, 1997); significantly aiding in compound identification.

In the following work, the development and optimisation of a variety of HPLC-ESI-ITMS methods are shown. These methods were used for the chemical characterisation of 3-methyl furan, methyl chavicol and diesel SOA.

2.2   Experimental

2.2.1   Instrumentation

All of the method development shown in this Chapter was performed using an Agilent 1100 series high performance liquid chromatographer (HPLC, Berkshire, UK) coupled to a Bruker Daltonics HTC Plus ion trap mass spectrometer (IT-MS, Bruker Daltonics, Bremen, Germany). Ionisation was achieved using ESI. Oxygen free nitrogen (BOC, UK) was used

for the ESI dry gas flow. The mass spectrometer was operated in alternating polarity mode with a scan range of *m/z* 50 - 600.

2.2.2   Standards

In total, 39 standards were used for the development of the HPLC-ITMS methods shown in the chapter. Fourteen compounds were purchased from Sigma Aldrich (UK): (2Z)-but-2-enedioic acid (purity 99%), furan-2,5-dione (98%), Hexanedioic acid (99%), (3-acetyl-2,2-dimethylcyclobutyl)acetic   acid   (98%),   (acetyloxy)acetic   acid,   2,6,6-trimethylbicyclo[3.1.1]heptane-2,3-diol (99%), 5-oxohexanoic acid (97%), 4-oxopentanoic acid (97%) (4-methoxyphenyl)acetic acid (99%), 4-methoxybenzaldehyde (98%), Furan-2,5-dione (99%), 4-methoxybenzoic acid (99%), (2Z)-but-2-enedioic acid (99%), triethyl methanetricarboxylate (98%) and 2,5-dihydroxybenzoic acid (99.5%). Nine compounds were purchased from Fisher Scientific (UK): (2Z)-2-methylbut-2-enedioic acid (98%), 3-methylfuran-2,5-dione (98%), 3-methylfuran-2(5H)-one (90%),   furan-2(5H)-one (98%), furan-2-carbaldehyde (98%), 5-hydroxyfuran-2(5H)-one (99%), 2-hydroxypropane-1,2,3-tricarboxylic acid (99.5%), 2-hydroxyhexanoic acid (95%), and (1*E*)-prop-1-ene-1,2,3-tricarboxylic acid (98%). Two compounds were provided by the University College Cork: 3-methylbenzoic acid (purity unknown) and 2,6-dimethyl-4-nitrophenol (purity unknown).

2.2.3   Chromatography

Two HPLC stationary phases were investigated; hydrophilic interaction liquid chromatography (HILIC) and reverse phase liquid chromatography (RP-LC). For HILIC, a LUNA HILIC 150 mm × 4.6 mm, 5 µm particle size (Phenomenex, UK) column was used. Acetonitrile and water (LC-MS grade, Fisher Scientific, UK) were used for the mobile phase composition. The buffer consisted of either ammonium acetate or ammonium formate (HPLC grade, purity 99%, Sigma Aldrich, UK). The HPLC flow rate was set to 2 mL/min, with an injection volume of 60 µL. All samples were prepared in acetonitrile (LC-MS grade, Fisher Scientific, UK).

Two columns were used for RP-LC, these were; a Pinnacle C_{18} 150 mm × 4.6 mm, 5 µm particle size column (Thames Resteck, UK) and a Pinnacle C_{18} 200 mm × 4.6 mm, 5 µm particle size column. The mobile phase consisted of water (LC-MS grade, Fisher Scientific, UK) with 0.1% formic acid (Sigma Aldrich, UK) and methanol (LC-MS grade, Fisher Scientific, UK). The HPLC flow rate was set to 0.6 mL/min, with an injection volume of 60 µL (except where stated). All samples were prepared in 50:50 methanol:water (LC-MS

grade, Fisher Scientific, UK). A 5 minute pre-run consisting of the starting mobile phase conditions was performed before each sample injection.

2.2.4   Simulation Chamber Experiment

The photo-oxidation of 3-methyl furan was investigated at the EUPHORE chamber in Valencia, Spain. A description of the chamber setup and instrumentation can be found in Chapter 3, Section 3.2.1. Only a portion of the data was received for this experiment (see Section 2.3.1.5 for further information). From the data received, the initial mixing ratio of 3-methyl furan and NO in the chamber was determined as 682 ppbv and 46 ppbv respectively, corresponding to a VOC:NO$_x$ ratio of ~ 15:1. The average percentage relative humidity (%RH) was 37.8% and chamber temperature was 298.9 K throughout the experiment.

2.2.4.1 Sample Collection and Preparation

The SOA sample was collected onto a 47 mm quartz-fibre filter (Whatman, UK) at the end of the experiment, after the chamber covers had closed. The total aerosol volume sampled was 3 m^3. The filter was pre-fired at 500°C for 12 hours to remove any volatiles before sample collection. After sample collection, the filter was wrapped in foil and stored at -20°C until analysis. Prior to analysis, the filter was split into two portions. Approximately one eighth of the filter was kept for other analysis and the remainder transferred into a sample vial, suspended in 4 mL of water (optima LC-MS grade, Fisher, UK), covered in foil and left for two hours at room temperature. After this period, the sample was sonicated for 30 minutes and filtered through a Whatman PVDF 0.2 μm, 25 mm syringe filter (Whatman, UK). The sample extract was evaporated to dryness using a V10 vacuum solvent evaporator (Biotage, USA) and the residue redissolved in 1 mL of 50:50 methanol:water (optima LC-MS grade, Fisher, UK).

2.2.5   Diesel SOA

Two petroleum oil samples (automotive engine oil, group II base stock, ExxonMobil, UK) were used as a proxy for diesel SOA to develop a HPLC-ITMS method. One of these oil samples was oxidised by Neil Harris (PhD student, University of York). The oil sample was oxidised by heating the oil to 170 ˚C whilst continuously stirring and passing a flow of oxygen (BOC, UK) through the sample at 40 mL min^{-1}.

The solvents used for the removal of the water soluble and hydrocarbon fraction during liquid-liquid separation (see Section 2.3.3.1 for further information) were as follows:

methanol (optima LC-MS grade, Fisher Scientific, UK), water (optima LC-MS grade, Fisher Scientific, UK), hexane (reagent grade, Sigma Aldrich, UK). Evaporation of the water soluble fraction was achieved using a V10 solvent evaporator (Biotage, USA).

2.3 Results and Discussion

2.3.1 Development of a HPLC Method for SOA Analysis

In order to obtain both optimum separation and mass spectrometric response in a reasonable run time, two chromatographic separation methods were investigated; reverse phase liquid chromatography (RP-LC) and hydrophilic interaction liquid chromatography (HILIC). Eleven compounds were selected to develop a suitable HPLC-ITMS method, in the first instance concentrating on the species likely to be formed from the oxidation 3-methyl furan. These compounds consisted of a range of previously identified oxidation products and structurally similar alternatives (Bierbach et al., 1995; Gómez Alvarez et al., 2009; Tapia et al., 2011; Strollo and Ziemann, 2013). The eleven compounds and their structures are shown in Table 2.1.

Table 2.1 - Selected standards used for the development of a HPLC method for the chemical characterisation of 3-methyl furan SOA.
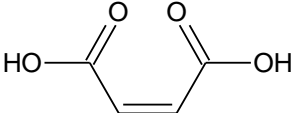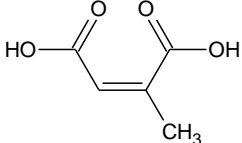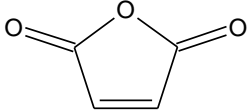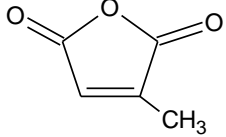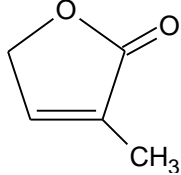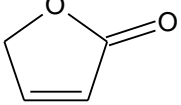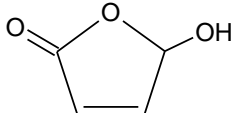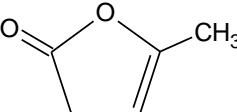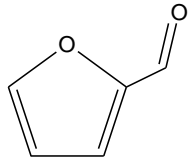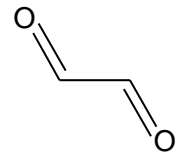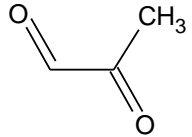
Compound no.	IUPAC name	Synonyms	MW [g mol^{-1}]	Compound structure
1	(2Z)-but-2-enedioic acid	Maleic acid	116	
2	(2Z)-2-methylbut-2-enedioic acid	Citraconic acid	130	
3	Furan-2,5-dione	Maleic anhydride	98	
4	3-methylfuran-2,5-dione	Citraconic anhydride	112	
5	3-methylfuran-2(5H)-one		98	
6	Furan-2(5H)-one	γ-cronto lactone	84	

Table 2.1 - continued........

Compound no.	IUPAC name	Synonyms	MW [g mol^{-1}]	Compound structure
7	5-hydroxyfuran-2-(5H)-one		100	
8	5-methylfuran-2(3H)-one	α-angelica lactone	98	
9	Furan-2-carbaldehyde		96	
10	Ethanedial	Glyoxal	58	
11	2-oxopropanal	Methyl glyoxal	72	

2.3.1.1 HILIC-ESI-ITMS

Hydrophilic interaction liquid chromatography (HILIC) is a technique used to separate small polar compounds (*e.g.* (Hemström and Irgum, 2006; Buszewski and Noga, 2012). HILIC was originally developed in 1990 (Alpert, 1990), although it wasn't until 2009 that this type of chromatography was used to characterise ambient aerosol (Stone et al., 2009). Since 2009, however, this technique has remained relatively redundant within aerosol science, with very few studies reporting the use of HILIC for the characterisation of ambient aerosol (Kitanovski et al., 2011; Kitanovski et al., 2012a; Kitanovski et al., 2012b).

HILIC is considered to be a variant of normal phase liquid chromatography (NP-LC) and the opposite of reverse phase liquid chromatography (RP-LC) (*e.g.* (Guo and Gaiki, 2011; Jandera, 2011; Moldoveanu and David, 2013)). Both NP-LC and HILIC consist of a polar stationary phase. However, unlike NP-LC, HILIC (analogous to RP-LC) uses aqueous organic solvents for the mobile phase composition, allowing this technique to be successfully coupled with ESI-MS (Cubbon et al., 2007). In contrast to RP-LC, HILIC elutes analytes in order of increasing hydrophilicity through increasing polar aqueous content (Alpert, 1990; Cubbon et al., 2007). The HILIC separation mechanism is still under debate (Wang and He, 2011; Xu et al., 2014). However, it is generally accepted that separation is achieved through liquid-liquid partitioning of an analyte from the hydrophobic mobile phase into a "water enriched" layer, close to the surface of the polar stationary phase (Alpert, 1990; Naidong, 2003; Buszewski and Noga, 2012). Once in this layer, the analyte can have intermolecular attractions (*i.e.* dipole-dipole, hydrogen bonding) with the polar stationary phase, resulting in retention. Increasing the mobile phase water content, results in the expansion of the water enriched layer; decreasing the strength of the intermolecular attractions between the analyte and the stationary phase, resulting in elution.

The three main types of HILIC stationary phases used include; neutral (*e.g.* cross-linked diol, cyano-propyl and amide), charged (*e.g.* amino) and zwitterionic (*e.g.* sulfobetaine and phosphorylcholine) (for further information see Jandera (2011) and Wang and He (2011)). The neutral, cross-linked diol stationary phase is considered to be one of the best for HILIC (Olsen and Pack, 2013). The majority of HILIC stationary phases are bonded to a silica surface which have un-bonded residual silanols present (Buszewski and Noga, 2012). Un-bonded silanols can influence compound separation through the absorption of analytes, and in some cases, can result in irreversible absorption (Jandera, 2011). During the manufacturing process of the cross-linked diol stationary phase, a silylating reagent is used to block the un-bonded silanols (Jandera, 2011; Olsen and Pack, 2013). Furthermore, its

polymeric structure (Figure 2.1) effectively shields the un-bonded silanols from the analyte (Guo and Gaiki, 2011); minimising unwanted secondary interactions observed with other HILIC stationary phases (Guo and Gaiki, 2005; Hao et al., 2008; Jandera, 2011; Buszewski and Noga, 2012).
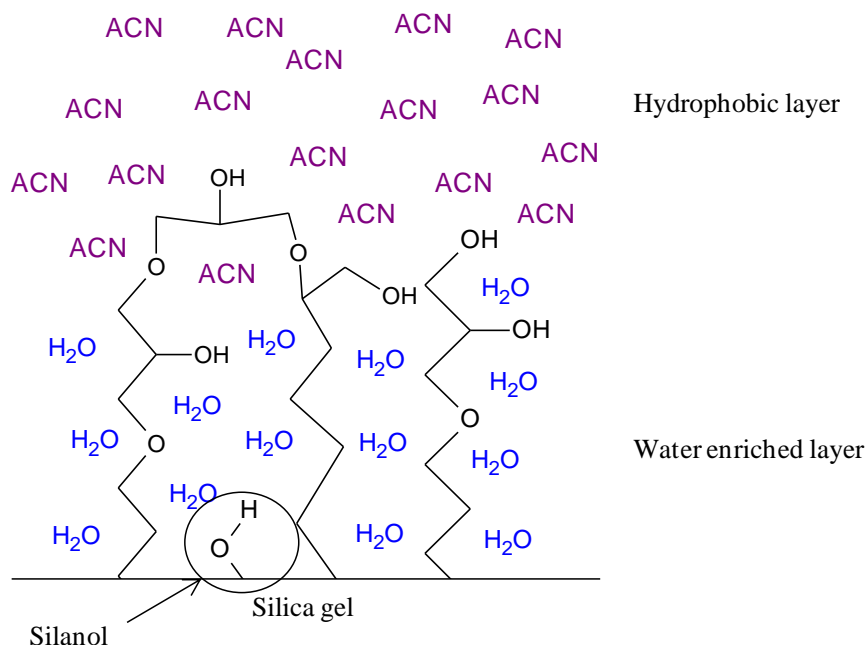
Figure 2.1 - Chemical structure of the HILIC cross-linked diol stationary phase with ether functionality. Displaying the hydrophobic (acetonitrile, ACN) and water enriched layer, and the shielding of a silanol by the polymeric cross-linked diol structure.

In this study, a LUNA HILIC cross-linked diol stationary phase was used to investigate its suitability for the separation of the small polar compounds shown in Table 2.1. Initially, a HILIC compatibility test was performed as recommended by the manufacture instructions. The HILIC compatibility test consists of a gradient elution program, where the retention time of a compound dictates whether HILIC is suitable for its separation. The gradient elution compatibility test is shown in Figure 2.2. Any compounds eluted between 0 to 2.5 minutes (elution region 1) have little to no interaction with the stationary phase, and are thus not well suited for separation using HILIC. Conversely, compounds eluted between 2.5 to 10 minutes (elution region 2) are ideally suited for the application of HILIC. Finally, any compounds eluted between 10 to 12.5 minutes (elution region 3) have strong interactions with the stationary phase, and through modification of the water content, may also be suitable for application of HILIC.
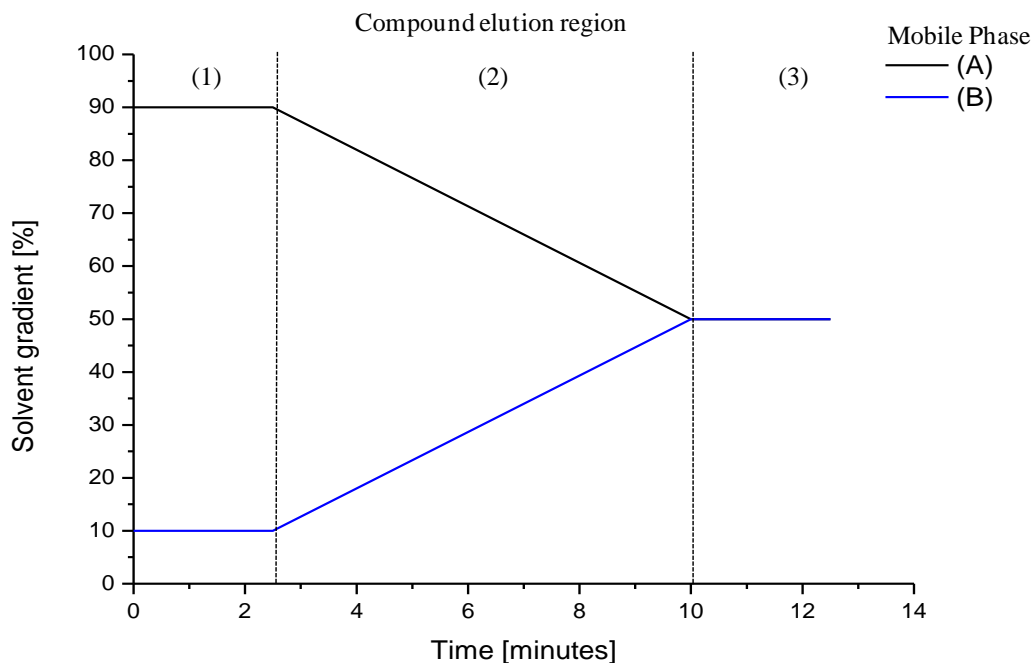
Figure 2.2 - Luna HILIC compound compatibility test, as recommend by manufacture instructions. Mobile phase; (A) = 90% acetonitrile, 10% of 50 mM ammonium formate or ammonium acetate; (B) = 80% water, 10% acetonitrile, 10%, 50 mM of ammonium formate or ammonium acetate. Compound elution region; (1) = little to no retention; (2) = ideal elution region; (3) = compounds strongly retained.

The HILIC compatibility test can be performed using either ammonium formate or ammonium acetate as the buffer. Initially 50 mM of ammonium formate was used. RP-LC was used prior to the investigation of HILIC. Of the seven external standards previously observed using RP-LC, only 4 were observed with the use of HILIC. These were; maleic acid (compound 1), citraconic acid (compound 2), citraconic anhydride (compound 4) and 5-methylfuran-2(3H)-one (compound 8). Only the deprotonated molecular species was observed for citraconic acid, and no adduct formation was observed for any of the identified species. All of these compounds eluted between 0 to 2.5 minutes, as shown in Figure 2.3. Compounds 4 and 8 were observed to elute at the same time as the extra-column volume, at 1.4 minutes into the gradient elution. The extra-column volume (also referred to as dead volume) is the time it takes for the sample to reach the detector from its injection point if there are no interactions; including the connecting lines and the column. Thus, the elution of compounds 4 and 8 in the extra-column volume suggests there is no interaction of these compounds with the stationary phase. The other two compounds, maleic acid and citraconic acid, displayed a slight interaction with the stationary phase, although both compounds co-eluted at 2 minutes into the gradient. The use of 50 mM of ammonium acetate provided slightly better separation of maleic and citraconic acid. However, as observed with the use

of ammonium formate, compounds 4 and 8 displayed no retention, eluting in the extra-column volume (Figure 2.4).
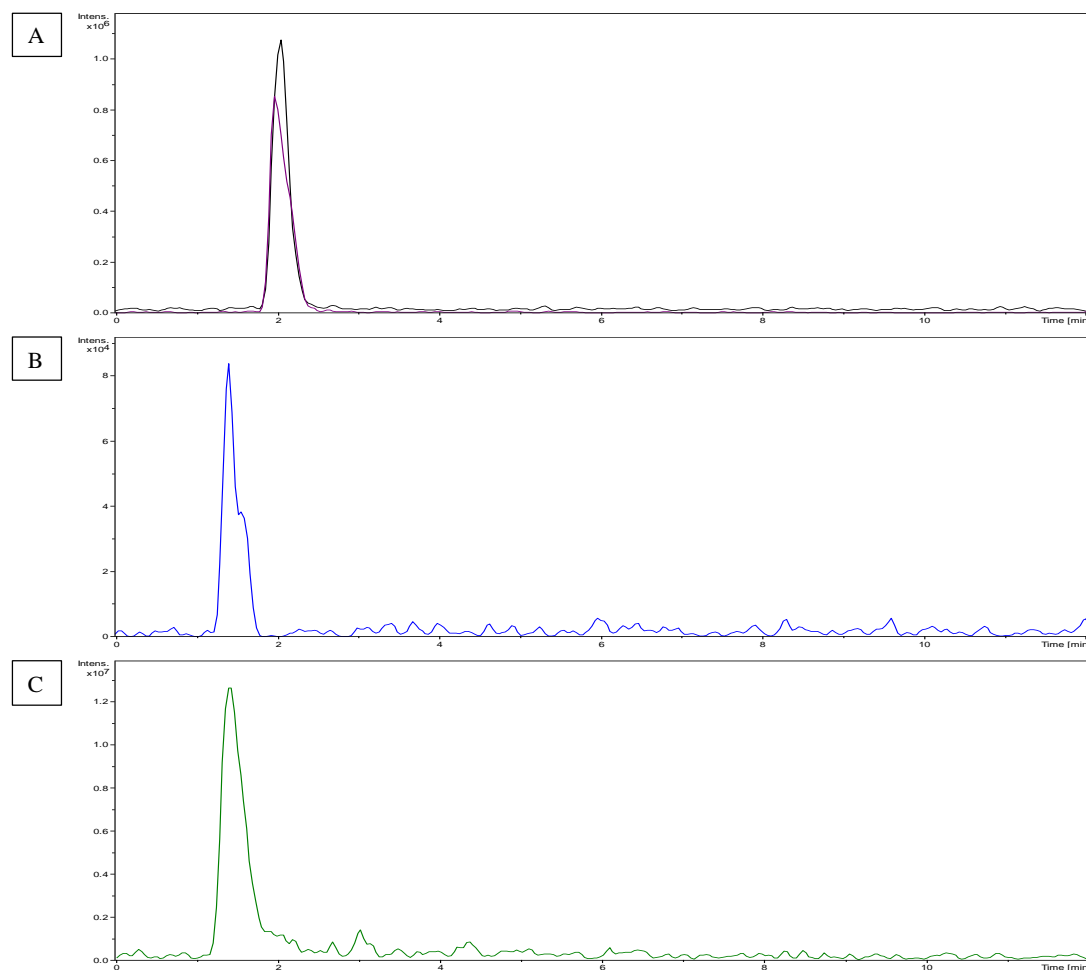
Figure 2.3 - Result of the LUNA HILIC compatibility test using 50 mM of ammonium formate; displaying the EICs of the observed external standards (Table 2.1) using HILIC-ESI-ITMS. A = Maleic acid (compound 1, black, *m/z* 115 (M-H)⁻) and citraconic acid (compound 2, purple, *m/z* 129 (M-H)⁻). B = Citraconic anhydride (compound 4, *m/z* 111 (M-H)⁻). C = 5-methylfuran-2(3H)-one (compound 8, *m/z* 99 (M+H)⁺).

The lack of chromatographic separation is most likely the reason why only four compounds were observed using HILIC. This is supported by the observation of a higher intensity peak eluted in extra-column volume when the external standards were run individually, in comparison to the prior blank samples (Figure 2.5). This suggests that due to the lack of chromatographic separation, the concentration of the external standards were too low to be identified (*i.e.* masked by higher intensity species which are also eluting in the extra-column volume).
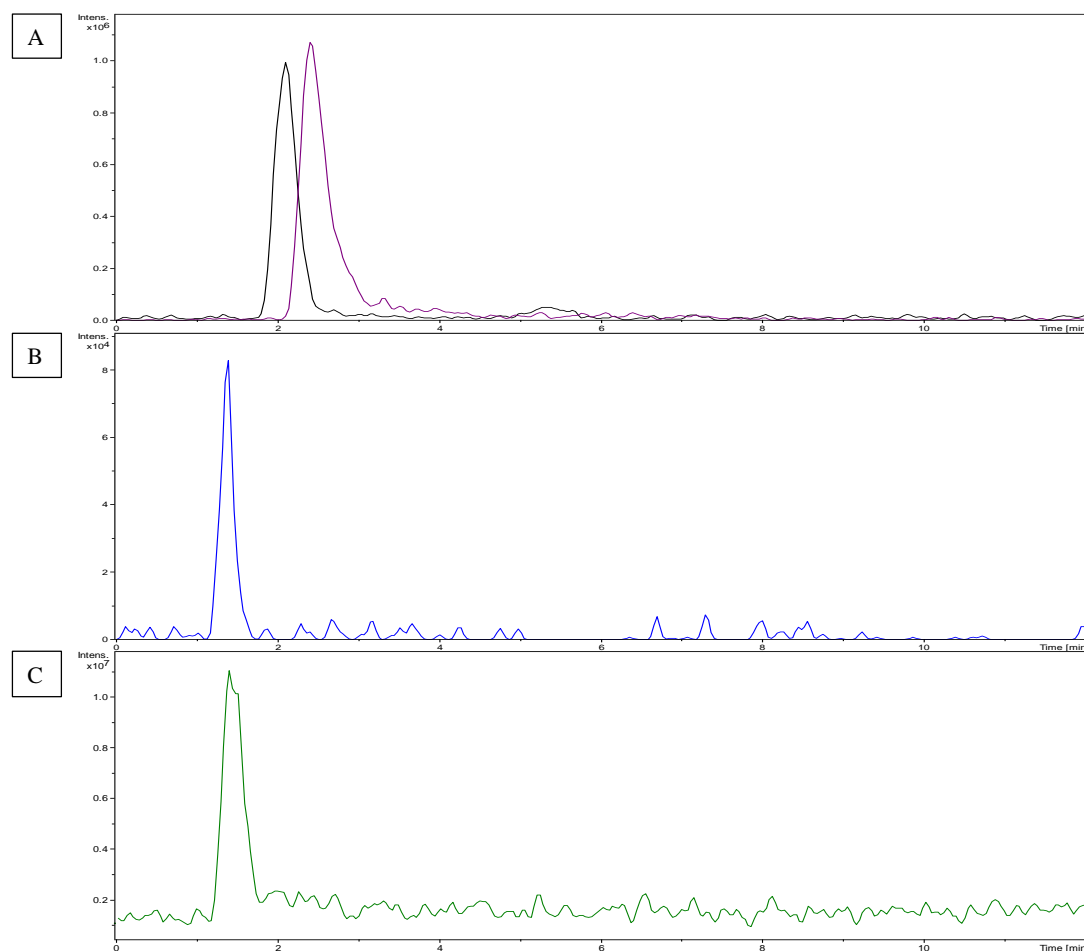
Figure 2.4 - Result of the LUNA HILIC compatibility test using 50 mM of ammonium acetate; displaying the EICs of the observed external standards (Table 2.1) using HILIC-ESI-ITMS. A = Maleic acid (compound 1, black, m/z 115 (M-H)$^-$) and citraconic acid (compound 2, purple, m/z 129 (M-H)$^-$). B = Citraconic anhydride (compound 4, blue, m/z 111 (M-H)$^-$). C = 5-methylfuran-2(3H)-one (compound 8, green, m/z 99 (M+H)$^+$).

The poor retention and resolution obtained with this column for the investigated standards has previously been observed in another study, with compounds of a similar chemical speciation, (see Nováková et al. (2009) for further information). In their study, the retention of ascorbic acid and dehydroascorbic acid was investigated using four HILIC columns of differing stationary phases; one of which was the LUNA HILIC. It was found that the LUNA HILIC displayed the lowest retention capability of all the stationary phases investigated (Nováková et al., 2009). However, it was noted that the retention of ascorbic acid and dehydroascorbic acid increased with very high concentrations of ammonium acetate, in excess of 100 mM (Nováková et al., 2009). In this study, numerous parameters such as the buffer concentration, pH, mobile phase composition and gradient elution were investigated. However, the best retention and resolution achieved was that shown in Figure

2.4. Consequently, HILIC was deemed unsuitable for the separation of the small polar compounds shown in Table 2.1, resulting in the return to RP-LC.
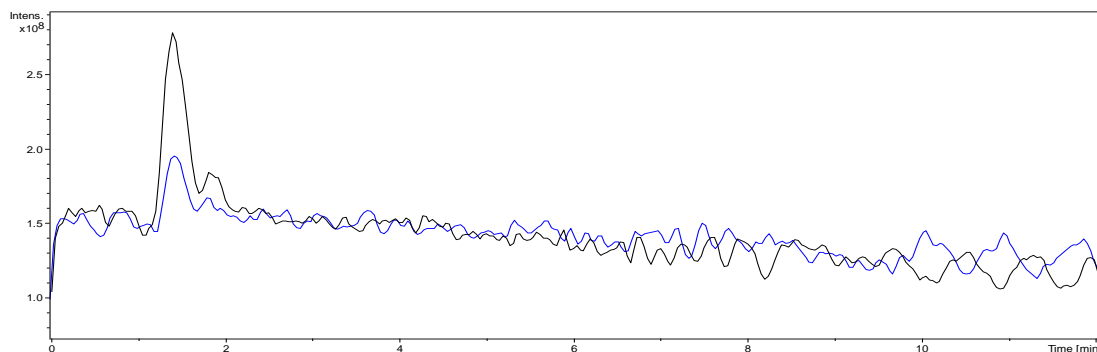
Figure 2.5 - An example of the higher intensity peak observed in the extra column volume when the external standards were run individually, in-comparison to the prior blank sample. Black = Total ion chromatogram (TIC) of 3-methyl-2(5H)furanone in acetonitrile at a concentration of 20 ppm (compound 5). Blue = TIC of acetonitrile (blank sample).

2.3.1.2 RP-LC-ESI-ITMS

On the return to RP-LC, a gradient elution method similar to the HILIC compatibility test was used. All of the small polar compounds shown in Table 2.1 were run on the gradient elution method shown in Figure 2.6.
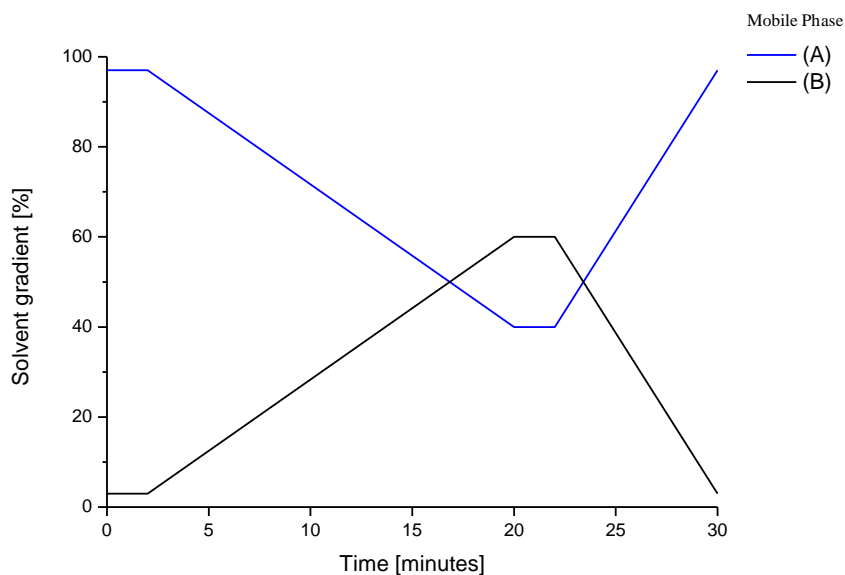
Figure 2.6 - Gradient elution method used for the separation of the small polar compounds shown in Table 2.1, using RP-LC-ESI-ITMS. Mobile phase; (A) = water with 0.1% formic acid. (B) = methanol.

In total, seven of the eleven external standards were observed using RP-LC. These were: maleic acid (compound 1), citraconic acid (compound 2), maleic anhydride (compound 3), citraconic anhydride (compound 4), 3-methylfuran-2(5H)-one (compound 5), 5-hydroxyfuran-2-(5H)-one (compound 7) and α-angelica lactone (compound 8). However, two compounds, citraconic anhydride and α-angelica lactone were deemed unsuitable for further analysis due to the observation of additional chromatographic peaks a few days after the standards had been prepared; suggesting these compounds are subject to further reaction and/or degradation. The retention times and the identified *m/z* values of the compounds observed are shown in Table 2.2. The EICs of the observed external standards (excluding compounds 4 and 8) is shown in Figure 2.7.
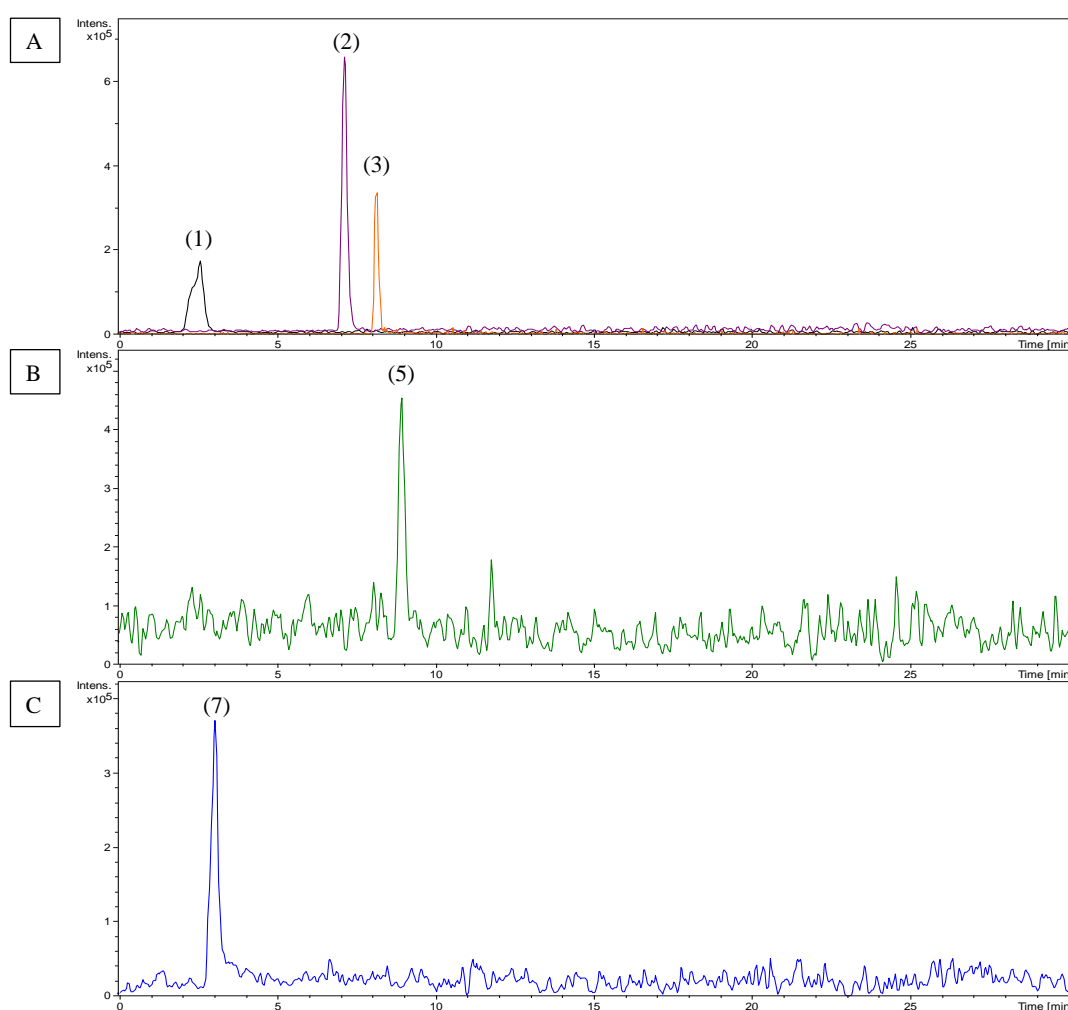
Figure 2.7 - EICs of the observed external standards (Table 2.1) at a concentration of 15 ppm using RP-LC-ITMS. The numbers in brackets refer to the compound numbers shown in Table 2.1. (1) = maleic acid, *m/z* 115 (M-H)$^-$. (2) = citraconic acid, *m/z* 129 (M-H)$^-$. (3) = maleic anhydride, *m/z* 97 (M-H)$^-$. (5) = 3-methylfuran-2-(5H)-one, *m/z* 99 (M+H)$^+$. (7) = 5-hydroxyfuran-2-(5H)-one, *m/z* 101 (M+H)$^+$.

Table 2.2 - The retention times (t_R) and the *m/z* ratios of the observed external standards (Table 2.1) using RP-LC-ESI-ITMS.

Compound no.	Compound name	t_R	[M-H]$^-$	[M+H]$^+$	[M+Na]$^+$
1	Maleic acid	2.6	115	-	-
2	Citraconic acid	7.1	129	-	153
3	Maleic anhydride	8.1	97	99	-
4	Citraconic anhydride[*]	-	111	113	-
5	3-methylfuran-2(5H)-one	8.9	-	99	121
6	γ-cronto lactone†	-		85	107
7	5-hydroxyfuran-2-(5H)-one	3.1	99	101	123
8	α-angelica lactone[*]	-	-	99	-
9	Furan-2-carbaldehyde	-	-	-	-
10	Glyoxal	-	-	-	-
11	Methyl glyoxal	-	-	-	-

[*] = Compound unstable; further reaction and/or degradation products observed (see text for further information). † = only observed at concentrations > 15 ppm.

No deprotonated or protonated molecular species (including adduct formation) were observed for three compounds, furan-2-carbaldehyde (compound 8), glyoxal (compound 9) and methyl glyoxal (compound 10). These species are relatively small and volatile and are thus not well suited for separation using RP-LC. Generally, these species are derivatized prior to chromatographic separation (Liggio and Mclaren, 2003; Kampf et al., 2011; Kocadağlı and Gökmen, 2014). The detection of these species using ESI-MS is possible, although this usually achieved after a suitable chromatographic method is used (*e.g.* ion chromatography) or derivatization is performed (Tan et al., 2010; Kirkland et al., 2013; Kocadağlı and Gökmen, 2014).

From Figure 2.7, it can be observed that all the compounds eluted on the slope of the gradient elution, displaying good interaction with the column stationary phase. Of the observed compounds, maleic acid (compound 1) displayed the least interaction with the column stationary phase, eluting 2.7 minutes into the gradient elution method. However, in contrast to the use of HILIC, no compounds eluted in the extra-column volume (t_R ~ 1.4 minutes) and no co-elution was observed, with all compounds displaying good separation. Furthermore, the use of RP-LC allowed an additional three external standards, which could not be observed with the use of HILIC, to be isolated and identified. As a result, this method

was deemed suitable for the separation of the small polar compounds shown in Table 2.1 and was used for the separation of the compounds likely to be found in 3-methyl furan SOA.

2.3.1.3 Optimisation of the ESI Source Parameters

Once a suitable HPLC method had been developed, the electrospray ionisation (ESI) source parameters were optimised. This was performed to ensure maximum sensitivity was achieved for the investigated compounds. The optimisation of the ESI source parameters included; the dry gas flow rate and the nebulizer pressure. These parameters were optimised through direct infusion of the HPLC mobile phase flow into the mass spectrometer, with a secondary flow connected through a tee from the direct infusion pump. This was performed to ensure the optimisation of the ESI source parameters included the large flow rate from the HPLC mobile phase (0.6 mL min^{-1}) and not just the small flow rate from the direct infusion pump (~ 240 μL h^{-1}). Two compounds, citraconic acid (compound 2) and triethyl methanetricarboxylate were used to optimise the ESI source parameters. The latter was used to represent highly oxidised high molecular weight compounds likely to be found in 3-methyl furan SOA. Both of these compounds were infused into the mass spectrometer through the direct infusion pump at an effective concentration of 5 ppm. The dry gas flow rate was investigated at 9, 10, 11 and 12 L min^{-1}. The dry gas flow rate was increased sequentially every two minutes into the analysis. The effect of the dry gas flow rate on the signal intensity of citraconic acid and triethyl methanetricarboxylate is shown in Figure 2.8.

From Figure 2.8, it can be observed that the dry gas flow rate had little effect on the signal intensity of citraconic acid, with the signal intensity remaining relatively stable throughout the analysis. However, for triethyl methanetricarboxylate a large increase in the signal intensity of this species was observed at a dry gas flow rate of 12 L min^{-1}. Subsequently, this was deemed the optimum flow rate.
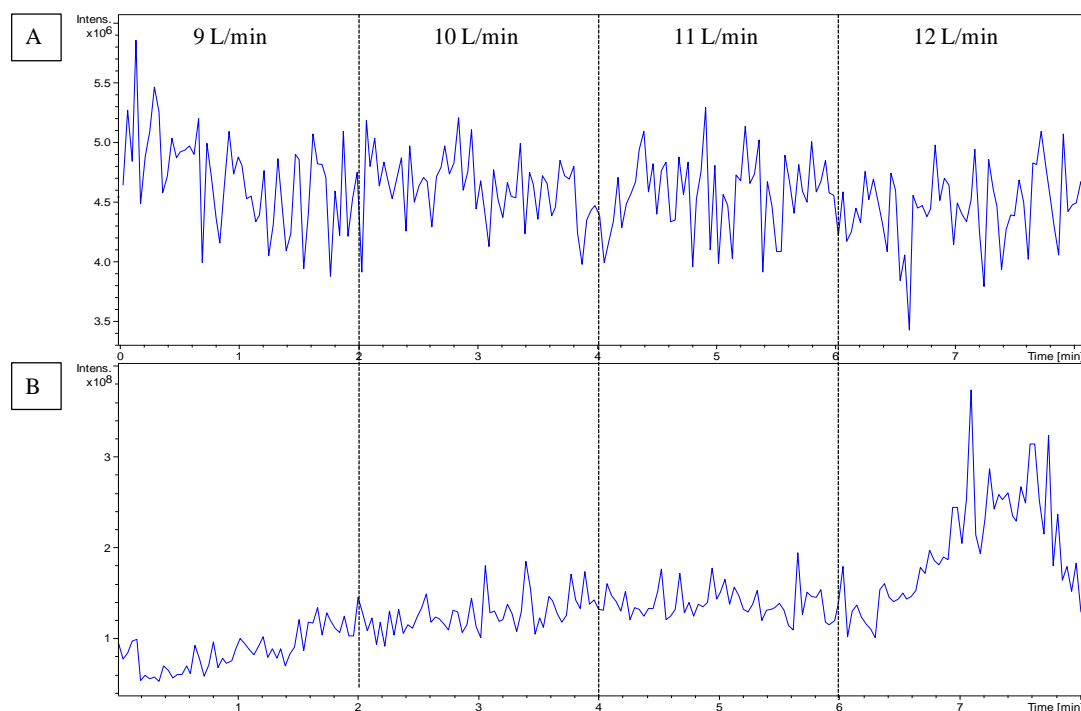
Figure 2.8 - Effect of the ESI dry gas flow rate on the signal intensity of citraconic acid and triethyl methanetricarboxylate. A = EIC of citraconic acid (compound 2), *m/z* 129 (M-H)⁻. B = EIC of triethyl methanetricarboxylate, *m/z* 233 (M+H)⁺.

The observed increase in the signal intensity of triethyl methanetricarboxylate at higher dry gas flow rates is presumably due to the larger amount of energy required to remove the ion from the surface of the droplet (desorption rate) during ionisation (Fenn, 1993; Banerjee and Mazumdar, 2012). Triethyl methanetricarboxylate contains considerably more polar functional groups than citraconic acid. Consequently, triethyl methanetricarboxylate will have stronger interactions with the solvent. The use of higher dry gas flow rates will increase solvent evaporation and thus result in an increase in the surface charge density within the droplet, thus presumably increasing the desorption rate (ion abundance) of the species (Fenn, 1993).

The nebuliser pressure was investigated at 50, 55, 60, 65 and 70 psi, using the same method as described above. The effect of the nebulizer pressure on the signal intensity of citraconic acid and triethyl methanetricarboxylate is shown in Figure 2.9. Here, little variation was observed in the signal intensity of both compounds with increasing dry gas pressure. As a result, the dry gas pressure of 70 psi used prior to optimisation was not changed. From these results, the optimum ESI parameters were determined as a dry gas flow rate of 12 L min⁻¹ with a nebulizer pressure of 70 psi.
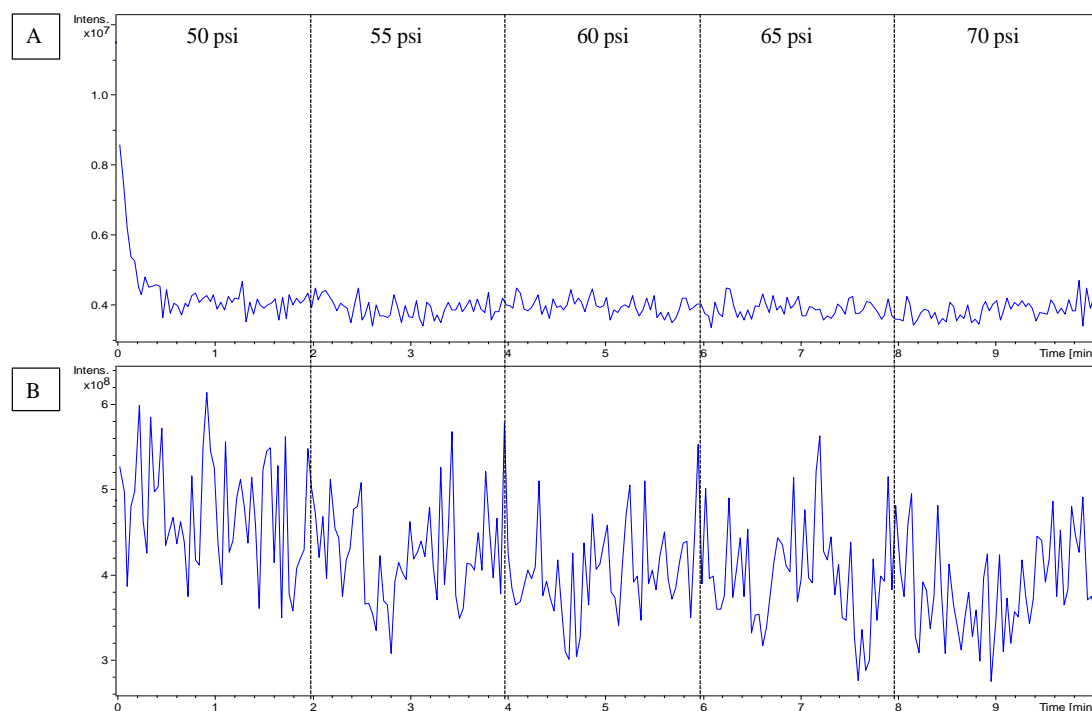
Figure 2.9 - Effect of the ESI dry gas pressure on the signal intensity of citraconic acid and triethyl methanetricarboxylate. A = EIC of citraconic acid (compound 2), *m/z* 129 (M-H)⁻. B = EIC of triethyl methanetricarboxylate, *m/z* 233 (M+H)⁺.

2.3.1.4 Calibrations

Calibrations were performed for maleic acid (compound 1), citraconic acid (compound 2), maleic anhydride (compound 3), 3-methylfuran-2-(5H)-one (compound 5) and 5-hydroxyfuran-2-(5H)-one (compound 7), using the developed RP-LC-ESI-ITMS method. The calibration of maleic anhydride (compound 3) was performed using the protonated molecular species, due to its higher signal intensity than the deprotonated molecular species. Calibrations ranged in concentration from 0.1 to 15 ppm and consisted of a minimum of 5 concentrations with 3 replicate measurements; with the exception of compound 5, where linearity was only observed over 4 concentrations. The calibration graphs of each of these compounds are shown in Figure 2.10.
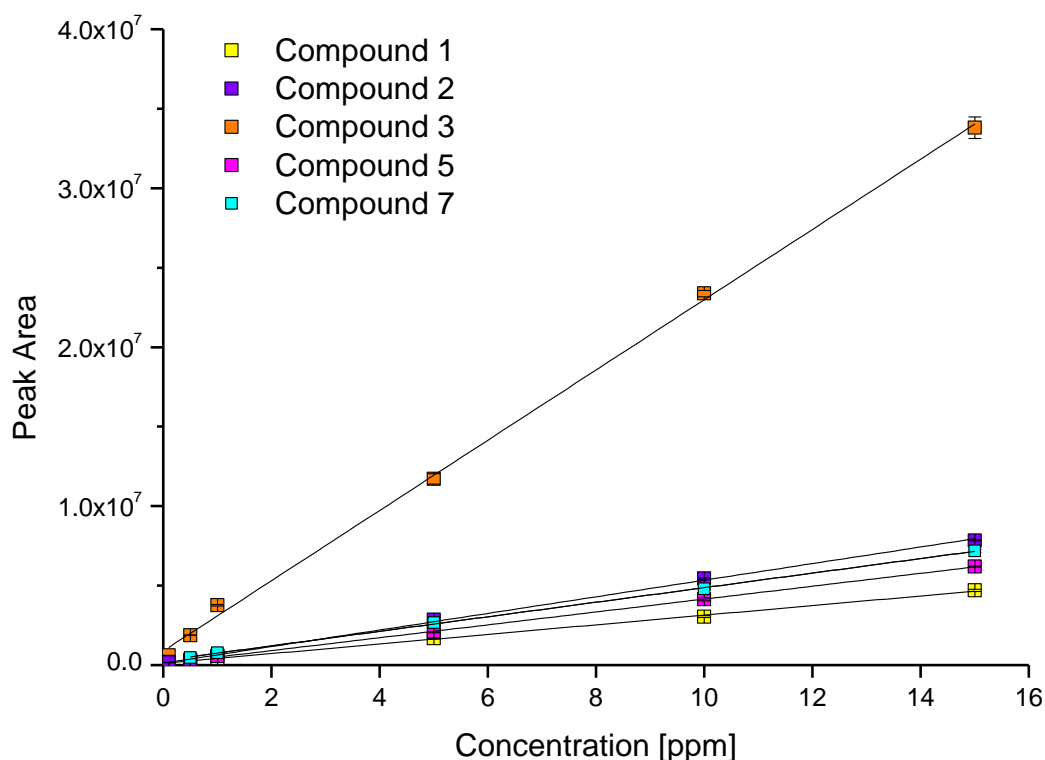
Figure 2.10 - Calibrations of compounds 1, 2, 3, 5 and 7 (Table 2.1) using the RP-LC-ESI-ITMS method. Compound 1 = maleic acid, m/z 115 (M-H)$^-$. Compound 2 = citraconic acid, m/z 129 (M-H)$^-$. Compound 3 = maleic anhydride, m/z 99 (M+H)$^+$. (5) = 3-methylfuran-2-(5H)-one, m/z 99 (M+H)$^+$. (7) = 5-hydroxyfuran-2-(5H)-one, m/z 101 (M+H)$^+$.

The minimum detectable chromatographic peak area (*ydl*), limit of detection (LOD) and limit of quantification (LOQ) were calculated for all the compounds using the equations given in Harris (2002). The *ydl* was calculated using the equation shown in Eq. 2.1; where *y*blank equals the average background signal of three blank samples at the retention time of the investigated compound, *t* equals the student's t-test at a 98% confidence interval for a sample size of three (*i.e.* three blank samples investigated), and s is the standard deviation of the chromatographic peak area of the second lowest concentration in the calibration graph.

Eq. 2.1 $$ydl = y\text{blank} + (t \; x \; s)$$

The LOD and LOQ were calculated using the equations shown in Eq. 2.2 and 2.3, respectively; where m equals the slope of the calibration graph. Here, a sample size of three was used for the student's t-test, for the three replicate measurements at each concentration. The generic approach of reporting the LOD as three times the signal to noise ratio (S/N = 3) was not used here, as this can induce up to 50% error in LOD value where the sample size is < 5 (Harris., 2002).

Eq. 2.2 $$\text{LOD} = t \; x \left(\frac{s}{m}\right)$$

Eq.2.3 $$\text{LOQ} = \left(\frac{\text{LOD}}{3}\right) x \; 10$$

The *ydl*, LOD and LOQ values obtained for the investigated compounds are shown in Table 2.3, along with the linearity of the calibration graphs (Pearson's correlation coefficient, R^2). From Table 2.2, it can be observed that all the compounds display very good linearity with R^2 values > 0.999. The precision of the replicate concentration measurements displayed very good reproducibility with the %RSD < 2.1 for all compounds. The LOD and LOQ values obtained for the investigated compounds were deemed to be in the excepted concentration range of the oxidation products likely to be found in 3-methyl furan SOA, with the LOD and LOQ values ranging between 0.01 to 0.07 ppm and 0.05 to 0.23 ppm, respectively.

Table 2.3 - The minimum detectable chromatographic peak area (*ydl*), limit of detection (LOD), limit of quantification (LOQ) and the linearity of the calibration graphs (R^2) for the small polar compounds shown in Table 2.1, using RP-LC-ESI-ITMS.

Compound no.*	Compound name	*ydl*	LOD [ppm]	LOQ [ppm]	Linearity of calibration (R^2)
1	Maleic acid	6.89×10^3	0.01	0.05	0.9996
2	Citraconic acid	1.91×10^4	0.03	0.10	0.9995
3	Maleic anhydride	6.20×10^4	0.03	0.10	0.9995
5	3-methylfuran-2-(5H)-one	4.78×10^4	0.06	0.21	0.9998
7	5-hydroxyfuran-2-(5H)-one	6.76×10^4	0.07	0.23	0.9998

* = Refer to Table 2.1.† = Range of the replicate measurements of the concentrations investigated.

2.3.1.5 Photo-oxidation of 3-methyl Furan

The photo-oxidation of 3-methyl furan was investigated at the European Photo-reactor chamber (EUPHORE) in Valencia, Spain. The experimental details can be found in Section 2.2.4. Furan and its alkyl derivatives, 2-methyl furan and 3-methyl furan, are primarily emitted in to the atmosphere from biomass burning and fossil fuel combustion (Graedel et al., 1986; Andreae and Merlet, 2001; Ciccioli et al., 2001; Gómez Alvarez et al., 2009; Strollo and Ziemann, 2013). In addition, ˙OH initiated VOC degradation can result in the formation of furan from the oxidation of 1,3-butadiene (Tuazon et al., 1999; Sprengnether et al., 2002), 2-methyl furan from the oxidation of cis-1,3-pentadiene (Ohta, 1984) and 3-methyl furan from the oxidation of isoprene (2-methyl-1,3-butadiene), which is the most abundant biogenic VOC emitted into the atmosphere (Atkinson et al., 1989; Ruppert and Becker, 2000; Lee et al., 2005; Robinson et al., 2011). The photo-oxidation of 3-methyl furan can result in the formation of unsaturated dicarbonyls in high yields (Gómez Alvarez et al., 2009; Tapia et al., 2011; Aschmann et al., 2013; Strollo and Ziemann, 2013). Unsaturated dicarbonyls can undergo acid catalysed oligomerisation reactions, forming high molecular weight species that can contribute to SOA formation and growth (Jang et al., 2002; Limbeck et al., 2003; Kalberer et al., 2004; Zhao et al., 2005).

A recent study found the photo-oxidation of 3-methyl furan resulted in significant SOA formation with a yield of 8.5 ± 2.5% (Gómez Alvarez et al., 2009). However, very few studies have investigated the SOA composition formed from the photo-oxidation of 3-methyl furan. Gómez Alvarez et al. (2009) tentatively identified two compounds in the aerosol phase, 3-hydroxypropenoic acid ($C_3H_3O_4$, MW 88 g mol^{-1}) and 4-keto-pentenoic acid ($C_5H_6O_3$, MW 114 g mol^{-1}) using gas chromatography mass spectrometry (GC-MS). In a separate study, Strollo and Ziemann (2013) identified a further eleven compounds in the aerosol phase formed from the photo-oxidation of 3-methyl furan, but were unable to provide detailed chemical or structural speciation.

In the following work, the SOA composition formed from the photo-oxidation of 3-methyl furan was investigated using the RP-LC-ESI-ITMS method developed in the previous sections. Initially, the RP-LC gradient elution method shown in Figure 2.6 was extended to incorporate the separation of high molecular weight species likely to be found in 3-methyl furan SOA (i.e. oligomers). The gradient elution method used for the analysis of the SOA sample is shown in Figure 2.11. From Figure 2.11, it can be observed that the slope of the gradient used for the separation of the compounds shown in Table 2.1 has not been changed, only the gradient has been extended over a longer run time and methanol content increased.
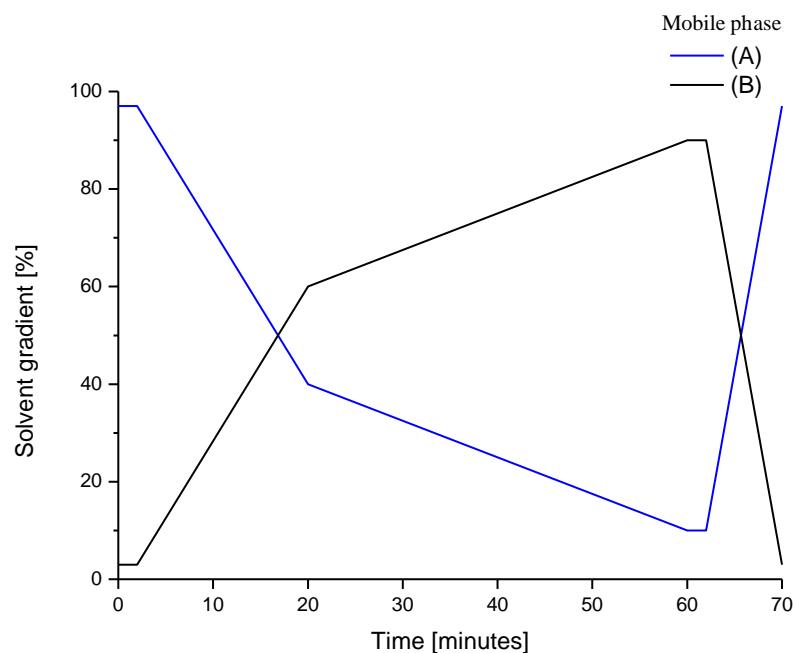
Figure 2.11 - Extended gradient elution for the analysis of 3-methyl furan SOA. Mobile phase; (A) = water with 0.1% formic acid. (B) = methanol. Data recording stopped at 60 minutes to exclude the column re-equilibration.

Unfortunately, a number of problems were encountered during this study. This project was originally designed as a collaborative project between University of York and the Mediterranean centre for environmental studies (CEAM), located in Valencia, Spain. However, due the loss of personnel, no gas phase data was obtained for the experiment performed at EUPHORE and the aerosol phase data received was incomplete. As a result, this project was abandoned shortly after the aerosol sample was received. However, a number of species were observed in the SOA filter sample, and of these compounds, four are discussed.

Four compounds were observed in the SOA filter sample at molecular weight of 114, 130 and two species at 192 g mol^{-1}. The EICs of these species are shown in Figure 2.12. Any chromatographic peaks that have not been numbered in Figure 2.12, were also observed in the prior blank sample and are thus not products of the photo-oxidation of 3-methyl furan. Of the four compounds observed in the SOA sample, one was identified. Compound 1 (MW 130 g mol^{-1}) shown in Figure 2.12A was identified as citraconic acid using the commercially available standard. The concentration of citraconic acid in the chamber was determined as 1.87 μg m^{-3}, representing 3.93% of SOA mass collected on the filter. Compound 2 (MW 114 g mol^{-1}, Figure 2.12B) co-eluted with citraconic acid. This compound was observed at *m/z* 113 (M-H)$^{-}$, *m/z* 115 (M+H)$^{+}$ and *m/z* 137 (M+Na)$^{+}$. Two peaks at *m/z* 97 and 70 were

observed in the mass spectrum at the same retention time as compound 2 and may be attributed to the loss of H_2O and C(O)OH from the protonated molecular species, respectively. Strollo and Ziemann (2013) identified three compounds at a molecular weight of 114 g mol^{-1} and suggested structures for these compounds based on the mechanism proposed by Aschmann et al. (2011, 2013) (Strollo and Ziemann, 2013). Of the three compounds shown in Strollo and Ziemann (2013), only one could result in the loss of H_2O and C(O)OH, suggesting the structure of this species is likely to be (2E)-3-methyl-4-oxobut-2-enoic acid, as shown in Figure 2.13. The high molecular weight of compounds 3 and 4 (MW 192 g mol^{-1} Figure 2.12C and D) suggest these species may be oligomers, although the structures of these compounds could not be identified.
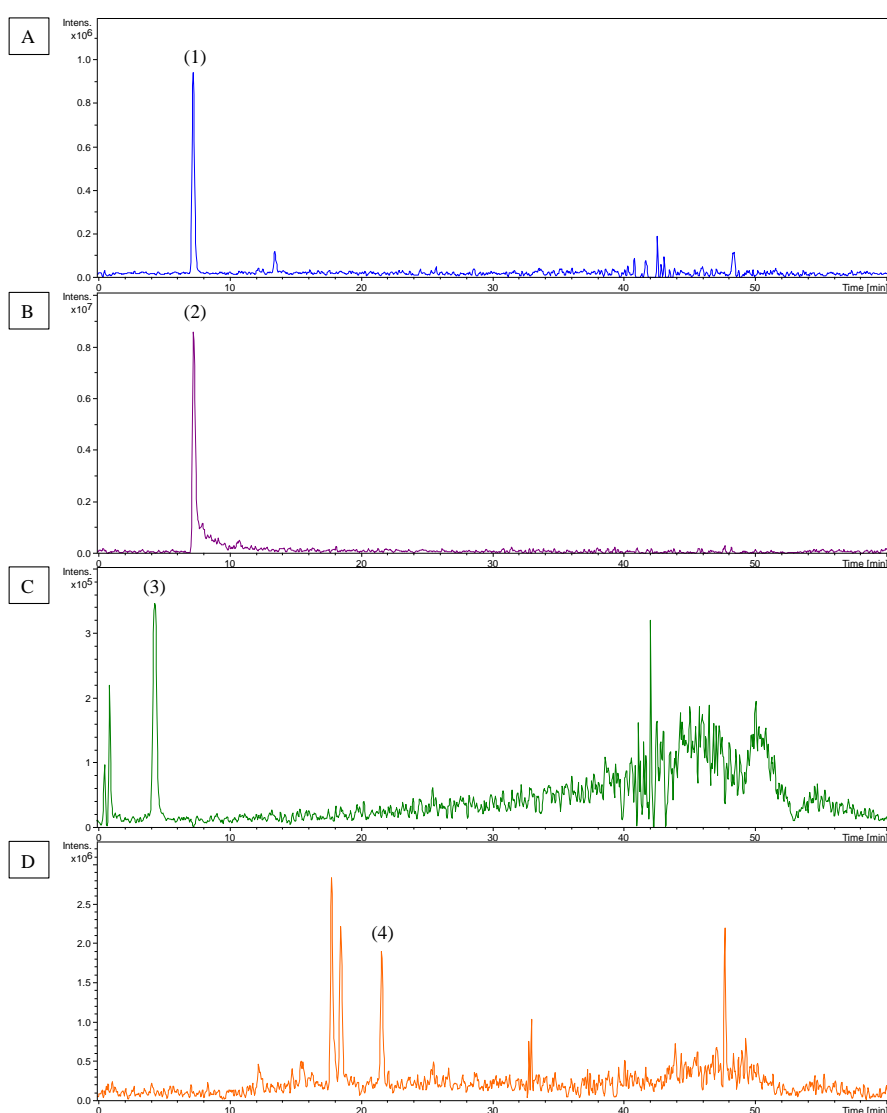
Figure 2.12 - EIC of the four compounds observed in the filter sample collected during the photo-oxidation of 3-methyl furan. Compound numbers; (1) = *m/z* 129 (M-H)$^-$. (2) = *m/z* 137 (M+Na)$^+$. (3) = *m/z* 191 (M-H)$^-$. (4) = *m/z* 193 (M+H)$^+$.
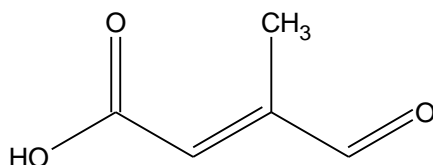
Figure 2.13 - Proposed structure for compound 2 ((2E)-3-methyl-4-oxobut-2-enoic acid) shown in Figure 2.12.

2.3.2   Long-term Monitoring of the ITMS Detector Stability

The ability to quantify components in SOA requires an instrument with sufficient detector stability between creating calibration graphs and analysing samples. In the following sections, a series of compounds have been tested for their use as external standards to monitor the ITMS detector stability and variation. The selected standards were subsequently used in Chapter 3 for the analysis of the SOA formed from the photo-oxidation of methyl chavicol.

2.3.2.1 External Standards: Selection and Characterisation

Initially, the ionisation efficiency, retention and peak shape of sixteen compounds was investigated, with the aim of selecting five compounds which could be used as external standards throughout the analysis of methyl chavicol SOA. These compounds consisted of a variety of differing functional groups and compound structures; three of which have previously been identified as methyl chavicol photo-oxidation products (Chapter 3, Section 3.1 and 3.3.5). The chosen compounds and their structures are shown in Table 2.4.

All the standards were run individually on the gradient elution method shown in Figure 2.14. For each of the compounds, the retention time and the *m/z* ratio of the protonated and/or deprotonated molecular species, including any adduct formation, if observed, was recorded and is shown in Table 2.5. Any compounds that eluted in the extra-column volume, displayed poor peak shape (*i.e.* peak broadening/tailing), was of low intensity, or only ionised in one ionisation mode, were deemed unsuitable and were excluded from further analysis (Table 2.5). This left seven remaining compounds: hexanedioic acid (compound 1), 2-hydroxyhexanoic acid (compound 2), cis-pinonic acid (compound 3), 4-methoxybenzoic acid (compound 4), 2,6-dimethyl-4-nitrophenol (compound 5), (4-methoxyphenyl)acetic acid (compound 11), 4-methoxybenzaldehyde (compound 13) and 3-methylbenzoic acid (compound 16).

Table 2.4 - The IUPAC names, molecular weight and compound structures of the selected compounds to be investigated as potential external standards throughout the analysis of methyl chavicol SOA.
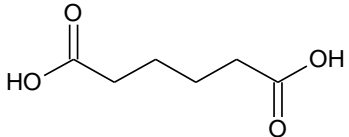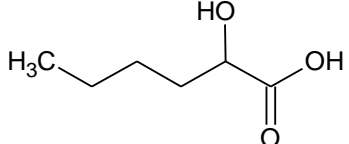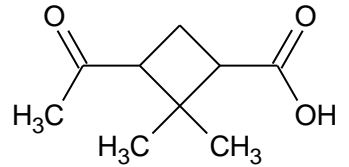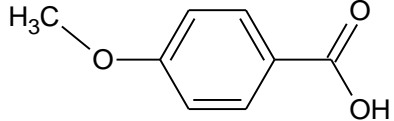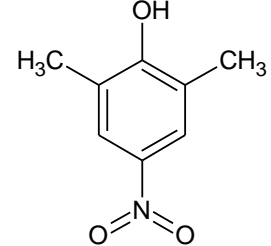
Compound no.	IUPAC name	Synonyms	MW [g mol^{-1}]	Compound structure
1	Hexanedioic acid	Adipic acid	146	
2	2-hydroxyhexanoic acid		132	
3	(3-acetyl-2,2-dimethylcyclobutyl)acetic acid	Cis-pinonic acid	184	
4	4-methoxybenzoic acid		152	
5	2,6-dimethyl-4-nitrophenol		167	

Table 2.4 - ....continued
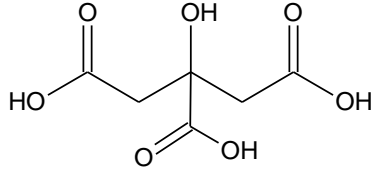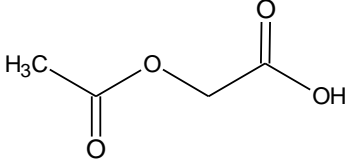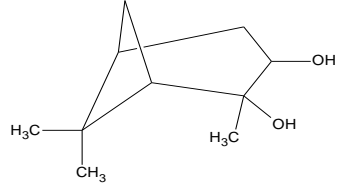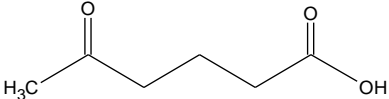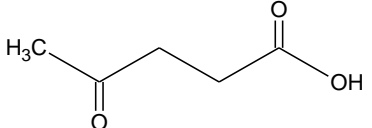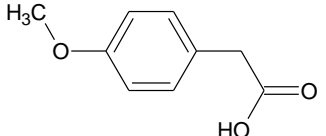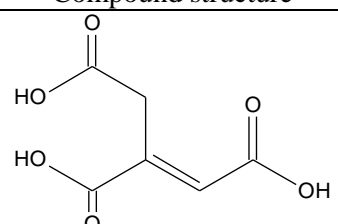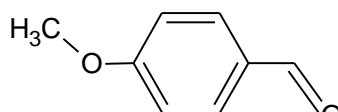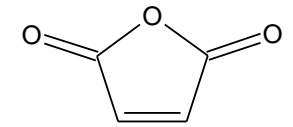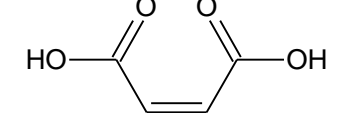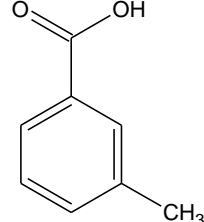
Compound no.	IUPAC name	Synonyms	MW [g mol^{-1}]	Compound structure
6	2-hydroxypropane-1,2,3-tricarboxylic acid	Citric acid	192	
7	(acetyloxy)acetic acid		118	
8	2,6,6-trimethylbicyclo[3.1.1]heptane-2,3-diol		170	
9	5-oxohexanoic acid		130	
10	4-oxopentanoic acid	Levulic acid	116	
11	(4-methoxyphenyl)acetic acid		166	

Table 2.4 - .....continued

Compound no.	IUPAC name	Synonyms	MW [g mol^{-1}]	Compound structure
12	(1*E*)-prop-1-ene-1,2,3-tricarboxylic acid		174	
13	4-methoxybenzaldehyde		136	
14	Furan-2,5-dione	Maleic anhydride	98	
15	(2Z)-but-2-enedioic acid	Maleic acid	116	
16	3-methylbenzoic acid		136	
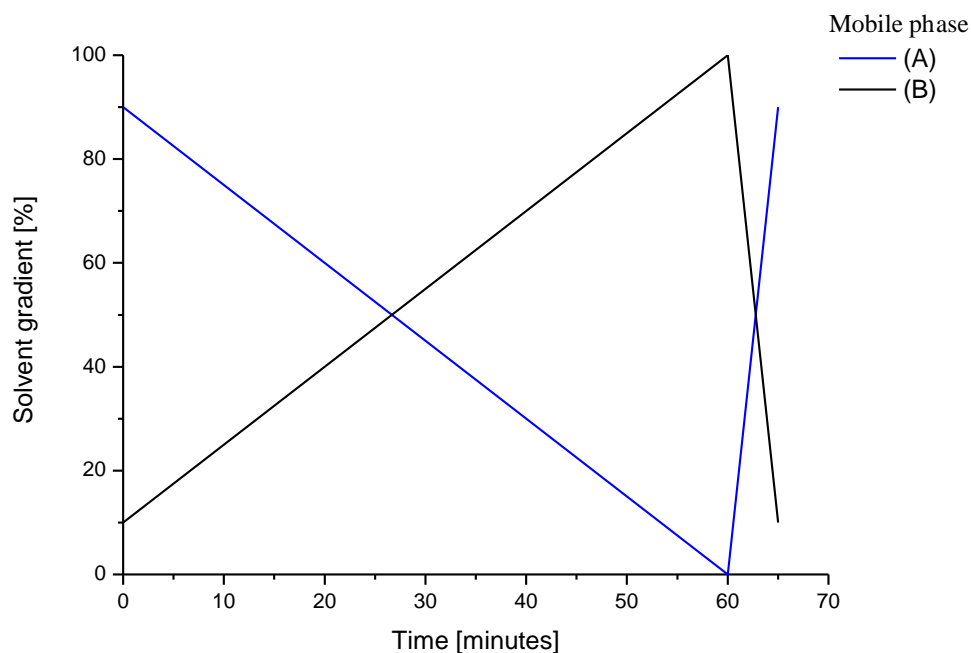
Figure 2.14 - RP-HPLC gradient elution method used for the characterisation of methyl chavicol SOA. (A) = H2O with 0.1% formic acid. (B) = methanol.

As a preliminary stability test, the remaining seven compounds were left at room temperature for two days and re-run using the same method. During this time period, the peak area of compound 11 decreased and a second chromatographic peak was observed, suggesting this compound was subject to further reaction and/or degradation (Figure 2.17). Consequently, compound 11 was excluded from further analysis. Finally, compound 16 was excluded due to the abundance of aromatic containing compounds in the remaining standards and its similar structure to 4-methoxybenzoic acid (compound 4), which is more likely to be an oxidation product of methyl chavicol.

A base peak chromatogram of the five selected external standards (compounds 1 to 5) in both positive and negative ionisation modes is shown in Figures 2.14 and 2.15, respectively. From Figures 2.15 and 2.16, it can be observed that all the selected external standards are well resolved and cover a wide range of the chromatogram. These five selected external standards were deemed suitable for monitoring of the ITMS detector variation.

Table 2.5 - The retention time and observed *m*/z ratios of the standard investigated (Table 2.4).

Compound no.	t_R	(M-H)⁻ (*m/z*)	(M+H)⁺ (*m/z*)	(M+Na)⁺ (*m/z*)
1	13.0	145	147	169
2	22.2	131	-	155
3	26.1	183	185	207
4	30.2	151	153	175
5	37.6	166	168	190
6	3.6 [a, b]	191	193	215
7	6.4 [b, c]	117	-	141
8	36.1	-	-	193
9	10.7	-	131 [b, c]	153 [b]
10	6.8 [b]	115	117	139
11	28.2	165 [d]	167	189
12	6.2	173 [b, c]	175 [c]	197
13	28.2	-	137	-
14	7.1 [b]	97	99	-
15	3.4 [a, b]	115	99	-
16	35.0	135	137	-

[a] = Eluted in the extra-column volume. [b] = Poor peak shape. [c] = Low intensity. [d] = Unstable/reactive (see text).
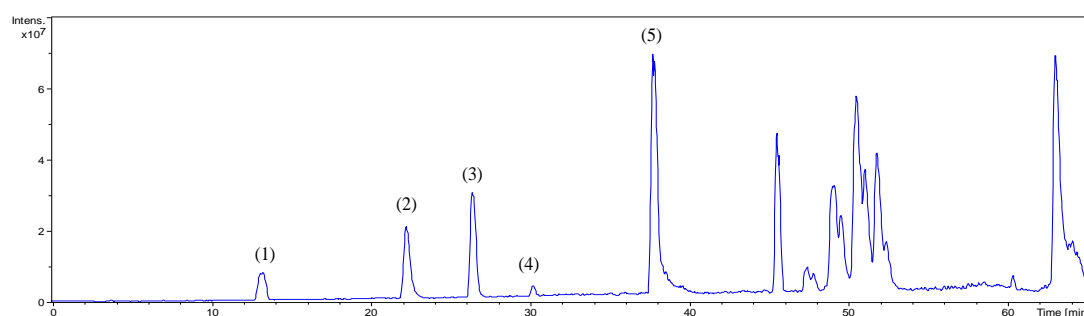
Figure 2.15 - Base peak chromatogram (BPC) of the five selected external standards at a concentration of 10 ppm, in negative ionisation mode. (1) = Hexanedioic acid, *m/z* 145 (M-H)⁻. (2) = 2-hydroxyhexanoic acid, *m/z* 131 (M-H)⁻. (3) = Cis-pinonic acid, *m/z* 183 (M-H)⁻. (4) = 4-methoxybenzoic acid, *m/z* 151 (M-H)⁻. (5) 2,6-dimethyl-4-nitrophenol, *m/z* 166 (M-H)⁻.
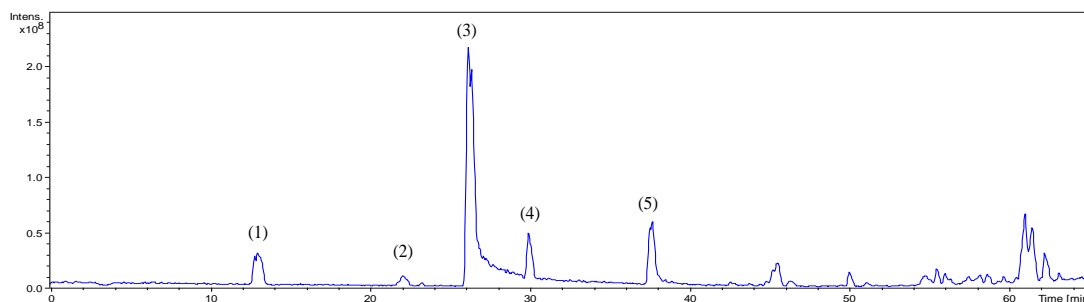
Figure 2.16 - BPC of the five selected external standards at a concentration of 10 ppm, in positive ionisation mode. (1) = Hexanedioic acid, *m/z* 169 (M+Na)[+]. (2) = 2-hydroxyhexanoic acid, *m/z* 155 (M+Na)[+]. (3) = Cis-pinonic acid, *m/z* 183 (M+H)[+]. (4) = 4-methoxybenzoic acid, *m/z* 153 (M+H)[+]. (5) 2,6-dimethyl-4-nitrophenol, *m/z* 168 (M+H)[+].
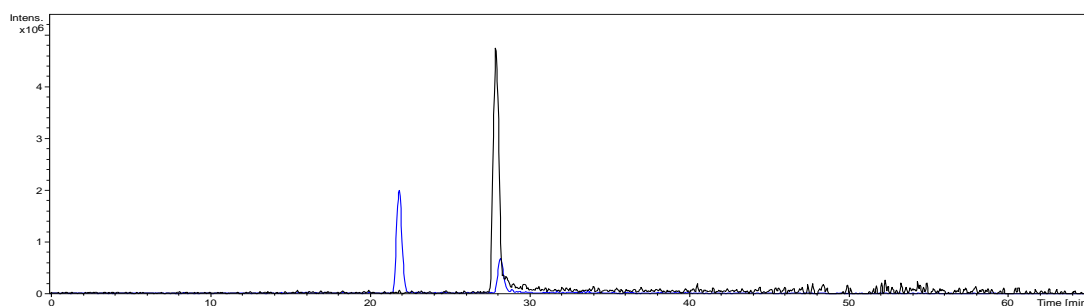
Figure 2.17 - EIC displaying the degradation or further reaction of (4-methoxyphenyl)acetic acid (compound 11, Table 2.4) after being left at room temperature for two days. Black = freshly made standard, *m/z* 165 (M-H)[-]. Blue = Analysis after two days at room temperature, *m/z* 165 (M-H)[-].

2.3.2.2 Long-term Monitoring of the ITMS Detector Variation

The five selected external standards (compounds 1 to 5, Table 2.4) were used to monitor the ITMS detector variation throughout the analysis of methyl chavicol SOA. These external standards were run numerous times before, after, and during the analysis of the SOA samples, over a period of approximately eight months. The measurement of the chromatographic peak areas of the external standards over time, allowed the stability and sensitivity of the instrument to be monitored; highlighting any issues with the instrument and the stability of the external standards.

The monitoring of the ITMS detector variation from July 2012 to May 2013 using the external standards in negative ionisation mode is shown in Figure 2.18. From Figure 2.18, it can be observed that all the external standards follow the same temporal profile, indicating there are no issues with the stability of the external standards. For example, if one of the

external standards were to degrade or react, a sudden decrease in the peak area of one of the compounds would be expected. This decrease would not follow the same temporal profiles of the other external standards; highlighting the degradation or reaction of the compound.

The ITMS detector variation from July 2012 to May 2013 using the external standards in positive ionisation mode is shown in Figure 2.19. Here, it can be observed that 2-hydroxyhexanoic acid (compound 2) does not follow the same temporal profile shape observed with the other external standards. As shown in Table 2.5, only the sodiated molecular species was observed for this compound in positive ionisation mode. The chromatographic peak areas of the protonated molecular species were integrated for all of the external standards, except compound 2; where the peak area of the sodiated molecular species was used. Adduct ions such as sodium and potassium can result in the formation of sodiated $(M+Na)^+$ and potassiated $(M+K)^+$ molecular species during ionisation. The main source of sodium and potassium ions is from glassware, including the HPLC mobile phase containers and laboratory glass wear (*e.g.* (Ma and Kim, 1997; Mortier et al., 2004; Yang et al., 2013)). The formation of these adducts, however, are not reproducible (Kruve et al., 2013), accounting for the variation in the temporal profile shape observed with compound 2 in positive ionisation mode.

Adduct formation was observed for all the external standards in positive ionisation mode. The relative amount of the $(M+H)^+$ versus $(M+Na)^+$ varied over time. However, it was generally observed that the $(M+Na)^+$ increased the older the standard became. Adduct formation also appeared to result in a decrease in the protonated molecular species signal intensity. In some cases (*i.e.* last point in September for compound 1, Figure 2.19), the protonated molecular species was not observed at all. Therefore, the external standards were less useful for monitoring the ITMS detector variation in positive ionisation mode. From these results, it is suggested that fresh standards should be prepared before measuring the ITMS detector variation in positive ionisation mode.
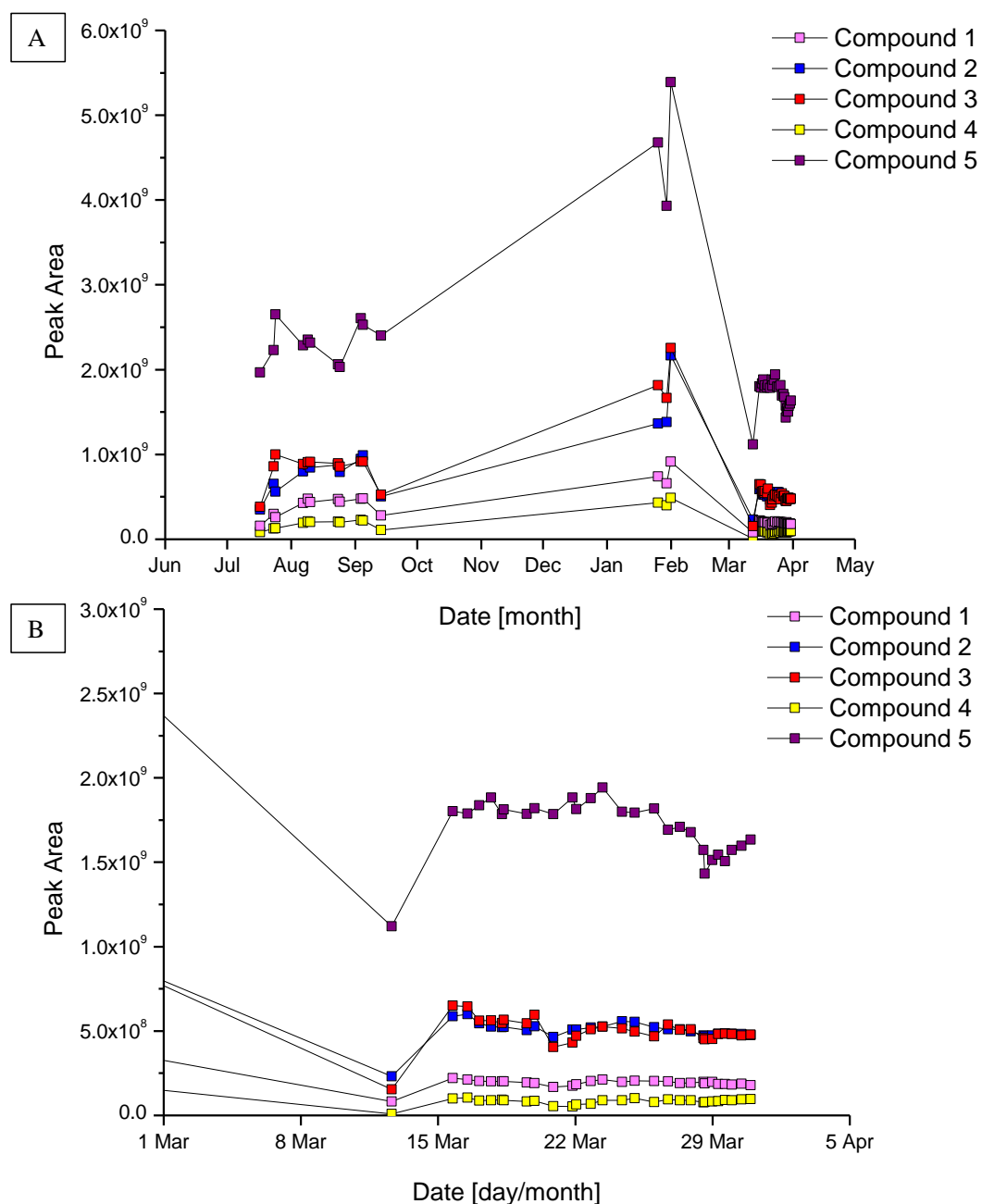
Figure 2.18 - Long term monitoring of the ITMS detector variation using selected external standards (compounds 1 to 5, Table 2.4) in negative ionisation mode throughout the ATMECH project (Chapter 3). A = Period of analysis, between July 2012 to May 2013. B = zoomed in view of March 2013 to April 2013. (1) = Hexanedioic acid, m/z 145 (M-H)$^-$. (2) = 2-hydroxyhexanoic acid, m/z 131 (M-H)$^-$. (3) = Cis-pinonic acid, m/z 183 (M-H)$^-$. (4) = 4-methoxybenzoic acid, m/z 151 (M-H)$^-$. (5) 2,6-dimethyl-4-nitrophenol, m/z 166 (M-H)$^-$.
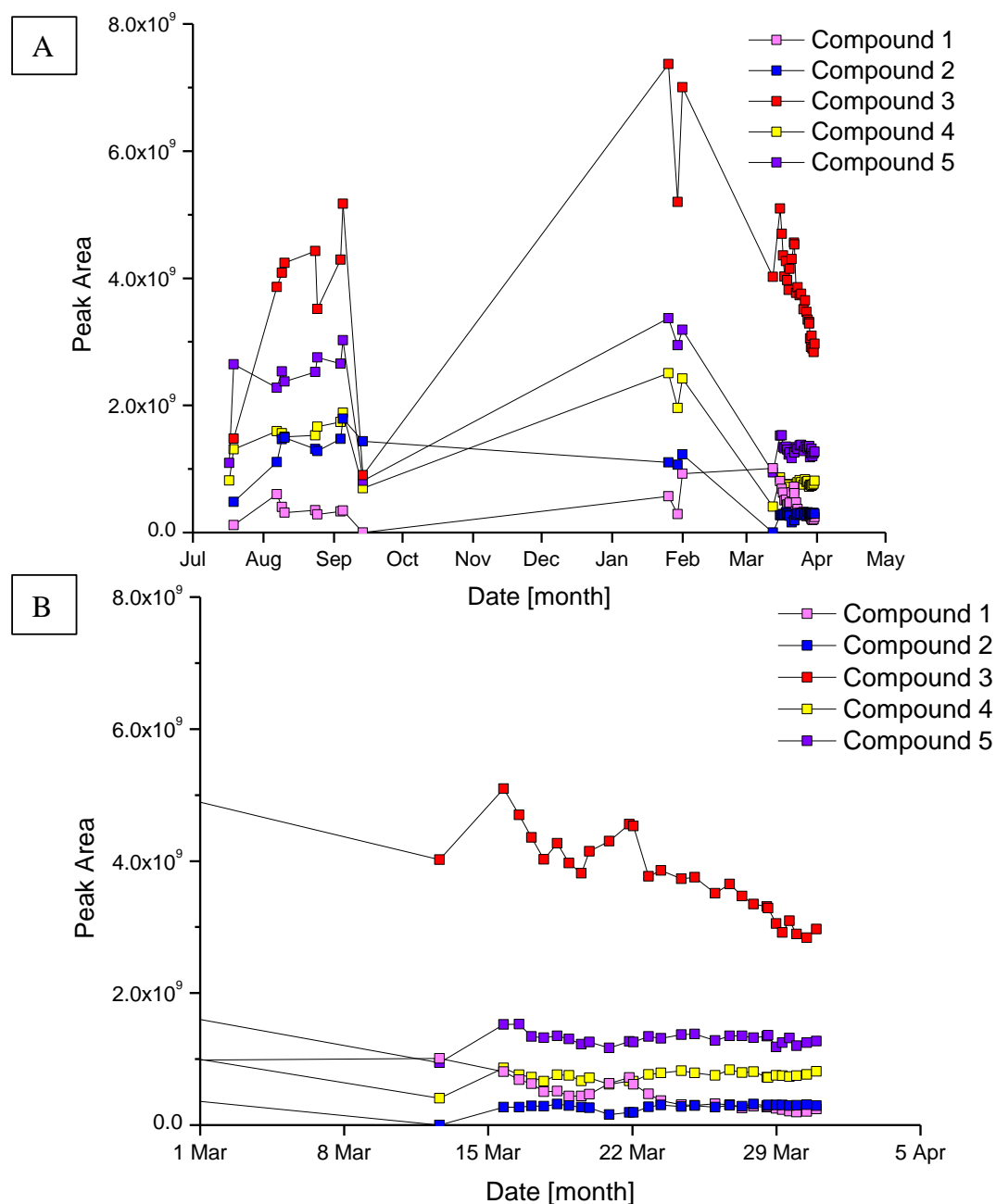
Figure 2.19 - Long term monitoring of the ITMS detector variation using selected external standards (compounds 1 to 5, Table 2.4) in positive ionisation mode throughout the ATMECH project (Chapter 3). A = Period of analysis, between July 2012 to May 2013. B = zoomed in view of March 2013 to April 2013. (1) = Hexanedioic acid, *m/z* 147 (M+H)[+]. (2) = 2-hydroxyhexanoic acid, *m/z* 155 (M+Na)[+]. (3) = Cis-pinonic acid, *m/z* 185 (M+H)[+]. (4) = 4-methoxybenzoic acid, *m/z* 153 (M+H)[+]. (5) 2,6-dimethyl-4-nitrophenol, *m/z* 168 (M+H)[+].

2.3.3   Increasing Sample Complexity

As a part of the recently funded Natural Environment Research Council (NERC) COMbustion PARTicles in the atmosphere (Com-Part) project, the University of York will be investigating the SOA composition formed from the oxidation of diesel exhaust emissions. Diesel is a petroleum product with a carbon range of ~ C_8 to C_{25} and has been suggested to be an important SOA precursor in urban areas, due to the relatively low volatility gaseous species emitted from diesel exhaust fumes (Robinson et al., 2007; Gentner et al., 2012; Jathar et al., 2013; Gordon et al., 2014). The compositional analysis of the gas phase species emitted from diesel exhaust fumes is usually determined using gas chromatography and often results in an unidentified complex mixture (UCM). The further oxidation of these species is likely to result in an extremely complex mixture with upwards of ~ 10^4 compounds in the aerosol phase.

Few studies have investigated the SOA composition formed from the oxidation of diesel exhaust emissions (Robinson et al., 2007; Chirico et al., 2010; Gordon et al., 2014) and no studies have provided the detailed chemical composition of these species. As a result, it is difficult to predict the main compounds likely to be found in diesel SOA and to develop a suitable HPLC-ITMS method for the isolation and identification of these species. To address this problem, a petroleum oil sample (automotive engine oil) was oxidised at high temperatures with O_2 ($O^{\bullet}$ radical oxidation) and used as a proxy of diesel SOA for the development of an HPLC-ITMS method. Two petroleum oil samples were used for method development; a non-oxidised oil sample (translucent) and an oxidised oil sample that was yellow in appearance.

2.3.3.1 Extraction Procedure

Only the water soluble fraction of the oil samples were analysed. The water soluble fraction was removed from the oil samples using liquid-liquid separation. Each oil sample was poured into a separating funnel consisting of 10 mL of hexane, 5 mL of methanol and 5 mL of water and shaken (Figure 2.20). Once the mixtures had separated, the water soluble fraction (*i.e.* methanol and water) and the hydrocarbon fraction (*i.e.* hexane) were collected into separate vials as shown in Figure 2.21. The middle section where both layers met was discarded to ensure none of the hydrocarbon layer was obtained in the water-soluble fraction. The water soluble fraction was evaporated to dryness, the weight of the remaining residue determined, and the sample re-suspended in 10 mL of 50:50 methanol:water.
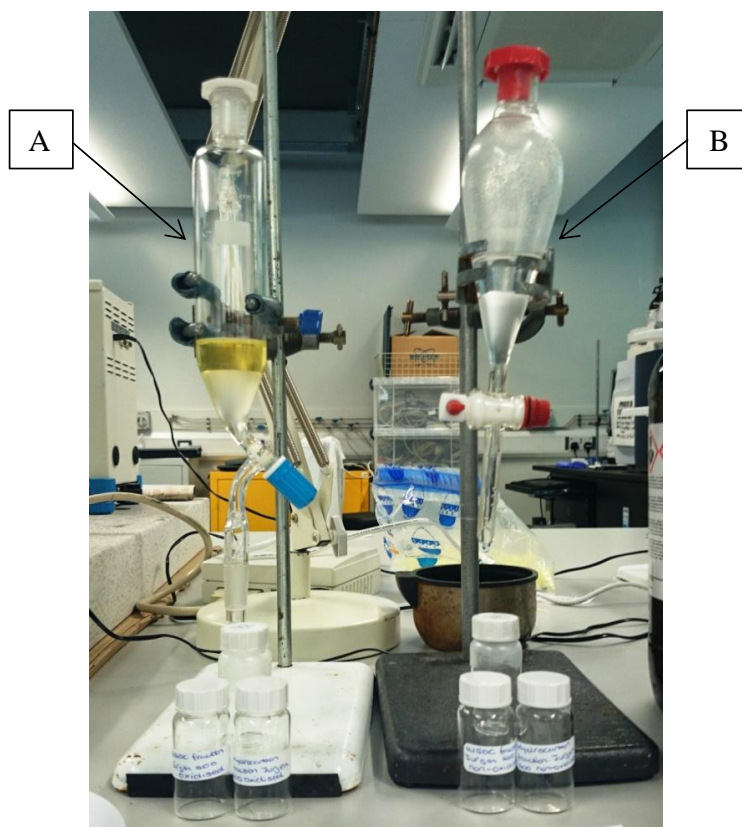
Figure 2.20 - Liquid-liquid separation of the hydrocarbon and water soluble fraction of the oxidised oil sample (A) and the non-oxidised oil sample (B).
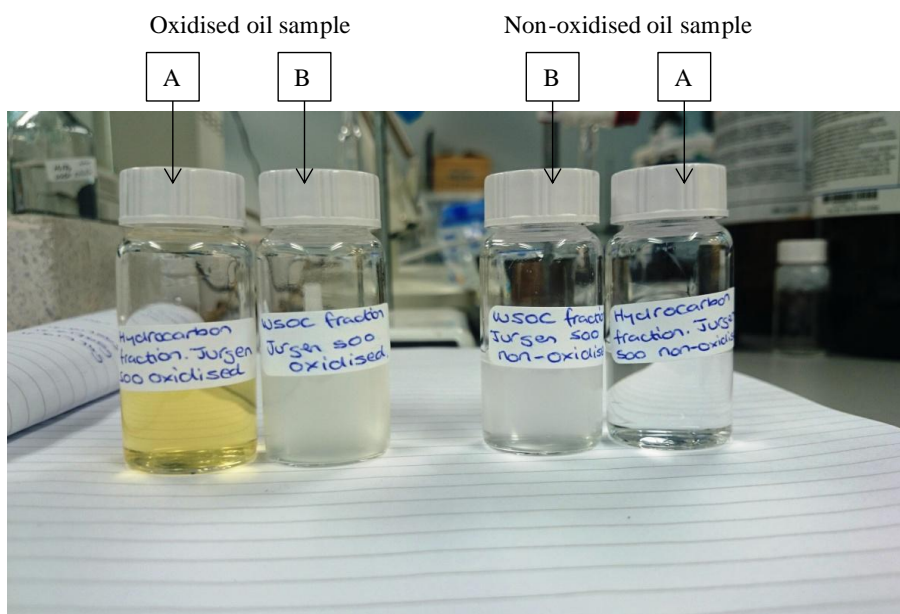
Figure 2.21 - The hydrocarbon (A) and water soluble (B) fractions of the oxidised and non-oxidised oil samples.

2.3.3.2 Results

Initially, the same gradient elution method shown in Figure 2.14, was used for the analysis of the water soluble fraction of the oil samples. The RP-LC column length was extended by an extra 5 cm to increase compound resolution. The total ion chromatograms (TICs) of the non-oxidised and oxidised oil samples in negative and positive ionisation modes, is shown in Figures 2.22 and 2.23, respectively. From Figures 2.22 and 2.23, it can be observed that there is a significant amount of unresolved compounds present in the oxidised oil sample (*i.e.* UCM). These compounds elute between ~ 25 to 55 minutes into the gradient elution, suggesting these species are of high molecular weight and are not very oxidised (*i.e.* displaying strong interactions with the column stationary phase).

The oxidised oil sample was used for the development of the HPLC-ITMS method. The UCM in the oxidised oil sample allowed the sample complexity expected to be present in diesel SOA, to be considered in the development of an HPLC-ITMS method. Figure 2.24A shows a base peak chromatogram (BPC) of the oxidised oil sample in negative ionisation mode. A BPC normalises the signal intensities of all the ions to the highest intensity species (base peak) in each series of mass spectra (*i.e.* 3 mass spectra per 0.04 minutes); whereas the TIC sums the signal intensities of the species in each series of mass spectra.

From Figure 2.24A, it appears that few compounds elute between the extra-column volume (t_R 4.8) to ~ 25 minutes in to the gradient. However, there are a number of low concentration species present in this elution region that cannot be observed. These compounds could be observed by reducing the internal diameter of the connecting lines from the RP-LC column to the mass spectrometer. The use of a smaller diameter tubing decreases the amount of volume within the connecting lines. This decreases the diffusion of separated analytes within these lines, essentially concentrating the species, increasing peak height and allowing more compounds to be observed. This can be observed in Figure 2.24B, where the internal diameter of the connecting lines was reduced from 0.02" to 0.01". Here, more species can be observed between the extra-column volume (t_R 4.8) to ~ 25 minutes in to the gradient.
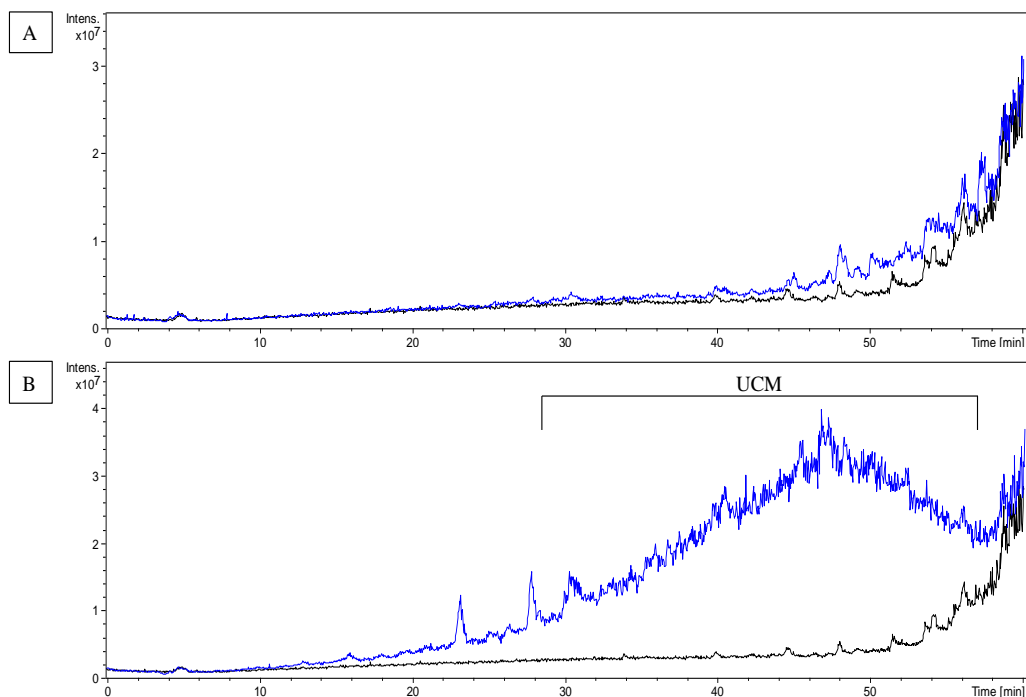
Figure 2.22 - TIC of the water soluble fraction of the non-oxidised oil sample and the oxidised oil sample at 100 ppm using the HPLC-ITMS in negative ionisation mode. Black = sample blank (methanol:water). Blue; A = non-oxidised oil sample. B = oxidised oil sample.
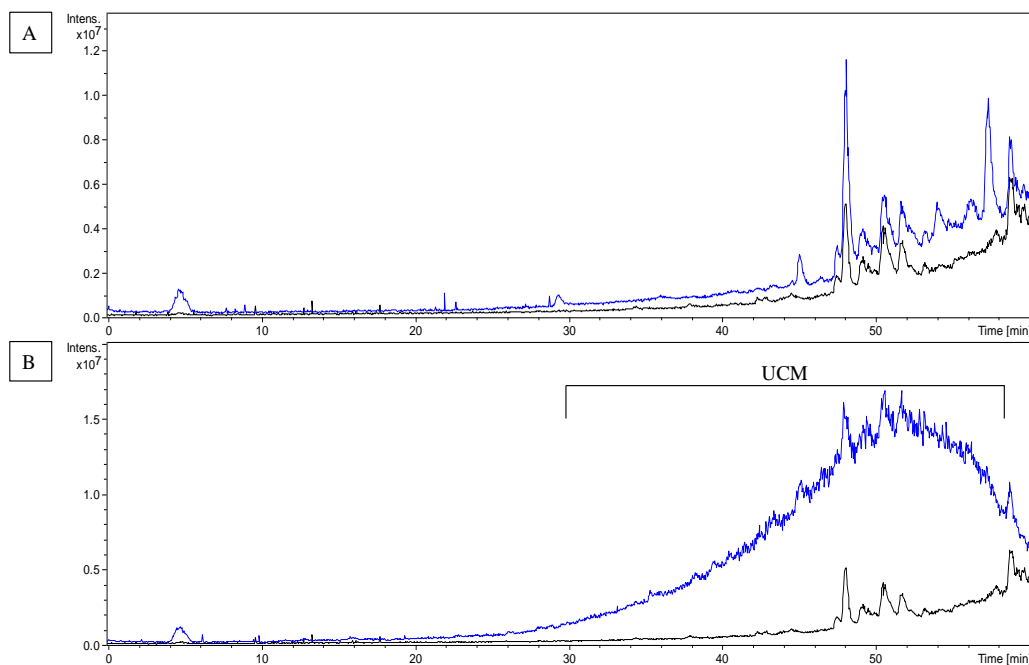
Figure 2.23 - TIC of the water soluble fraction of the non-oxidised oil sample and the oxidised oil sample at 100 ppm using the HPLC-ITMS in positive ionisation mode. Black = sample blank (methanol:water). Blue; A = non-oxidised oil sample. B = oxidised oil sample.

Many of the compounds observed in Figure 2.24B display poor resolution and appear to co-elute. To increase compound separation, the gradient elution method was extended to a longer run time. The gradient elution method used is shown in Figure 2.25. The use of the longer gradient elution method provided much better separation as shown in Figure 2.24C. In this chromatogram, considerably more compounds can be observed, suggesting the majority of these species co-eluted using the previous gradient elution method. However, from Figure 2.24C it can be observed that many compounds are still eluting towards the end of the gradient (70 -75 minutes), suggesting the methanol content needs to be increased to elute the remaining compounds which display very strong interactions with the column stationary phase. In order to keep the same separation but increase the methanol content, the gradient would need to be further extended over a longer run time. The extension of the gradient elution method will be decided once a diesel SOA sample has been run on this method (*i.e.* dependant on whether a higher methanol content is required). The development of a HPLC method for the analysis of complex samples, as shown here, is often a balance between achieving good compound separation, but in a reasonable run time.
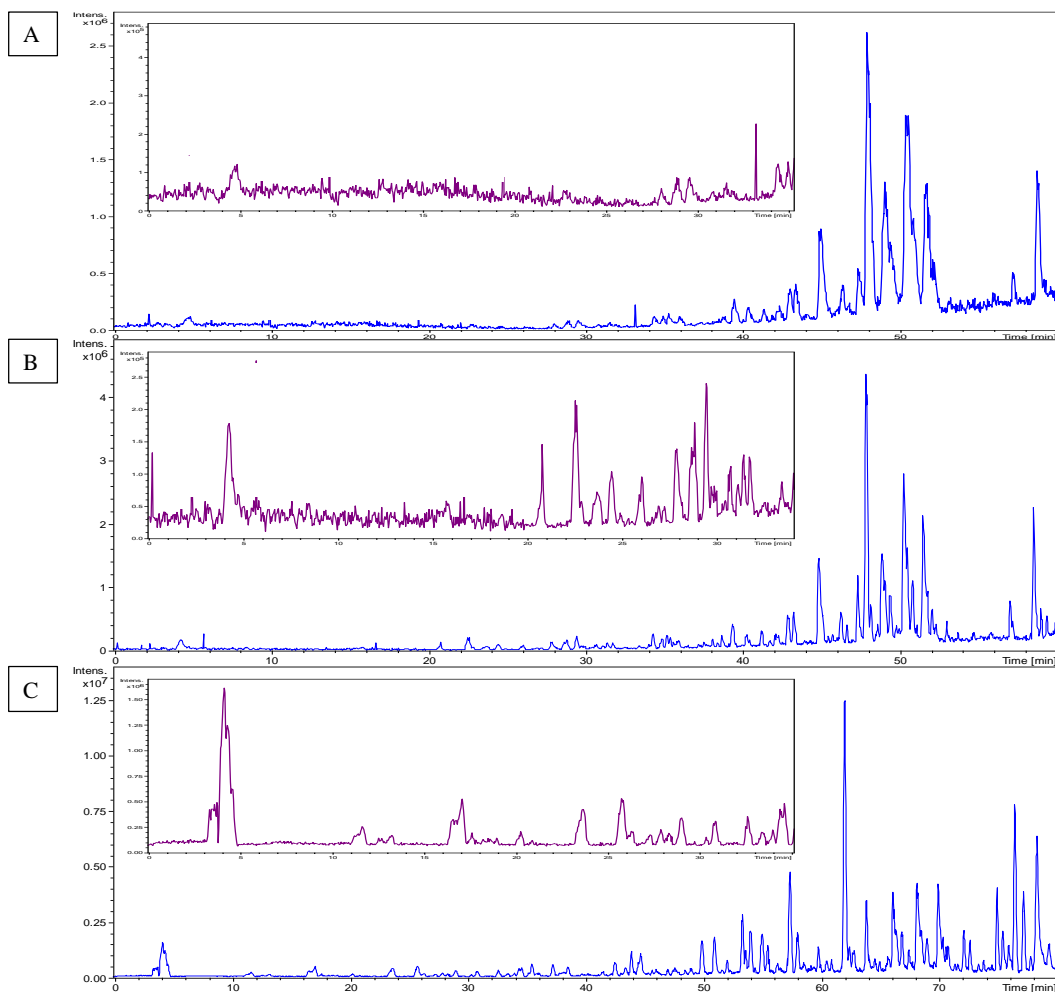
Figure 2.24 - BPC of the water soluble fraction of the oxidised oil sample at 100 ppm in negative ionisation mode using RP-LC-ESI-ITMS. A = oxidised oil sample using the gradient elution method shown in Figure 2.14 . B = peek tubing internal diameter reduced from 0.02" (shown in A) to 0.01" C = gradient elution method extended (Figure 2.25). Blue = full sample run time. Purple = zoomed in view.
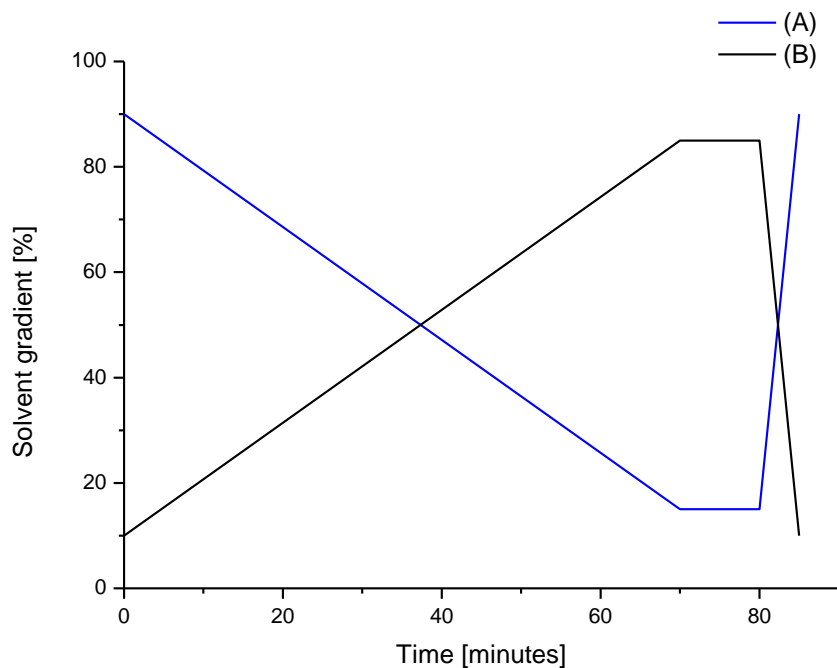
Figure 2.25 - Extended gradient elution method for the analysis of the water soluble fraction of the oxidised oil sample. Mobile phase; (A) = water with 0.1% formic acid. (B) = methanol.

Related families of species within the oxidised oil sample can be observed through the use of EICs. For example, compounds containing increasing numbers of CH_2 groups in their compound structures can be observed by sequentially adding *m/z* 14 to an observed chromatographic peak, as shown in Figure 2.26. From Figure 2.26, it can be observed that the compounds shift to higher retention times with increasing numbers of CH_2 groups, displaying stronger interactions with column stationary phase as the hydrocarbon backbone of the species increases.

Whilst related families of species can be observed in the oxidised oil sample, the lack of known compounds in the sample makes it difficult to determine if there are any issues with the RP-LC method. For example, during the development of this HPLC method, an internal diameter of 0.005" was chosen for the connecting lines. However, this internal diameter resulted in significant peak splitting which could not be observed in the oxidised oil sample. The peak splitting was only observed when a selection of compounds suspected to be present in diesel SOA were run on the developed method. Peak splitting is usually observed when the analytes within the mobile phase eluant do not reach column at the same time, and/or if there is a sample overload on the column which prevents the analytes from fully interacting the stationary phase. In both cases, one chromatographic peak, representing one compound, will display a distorted peak shape, which in the most severe of cases, will

appear to be two separate peaks. The observed peak splitting is shown in Figure 2.27A for a 1 ppm standard of 2,5-dihydroxybenzoic acid. Increasing the internal diameter of the peak tubing from 0.005" to 0.02" improved the peak splitting, but did not remove it entirely (Figure 2.27B). The peak splitting was removed by decreasing the sample injection volume as shown in Figure 2.28. From Figure 2.28, it can be observed that an injection of 45 μL displayed a slightly distorted peak shape. As a result, a sample injection volume of 30 μL was chosen for further analysis; the injection volume which displayed good peak shape and maximum peak height.
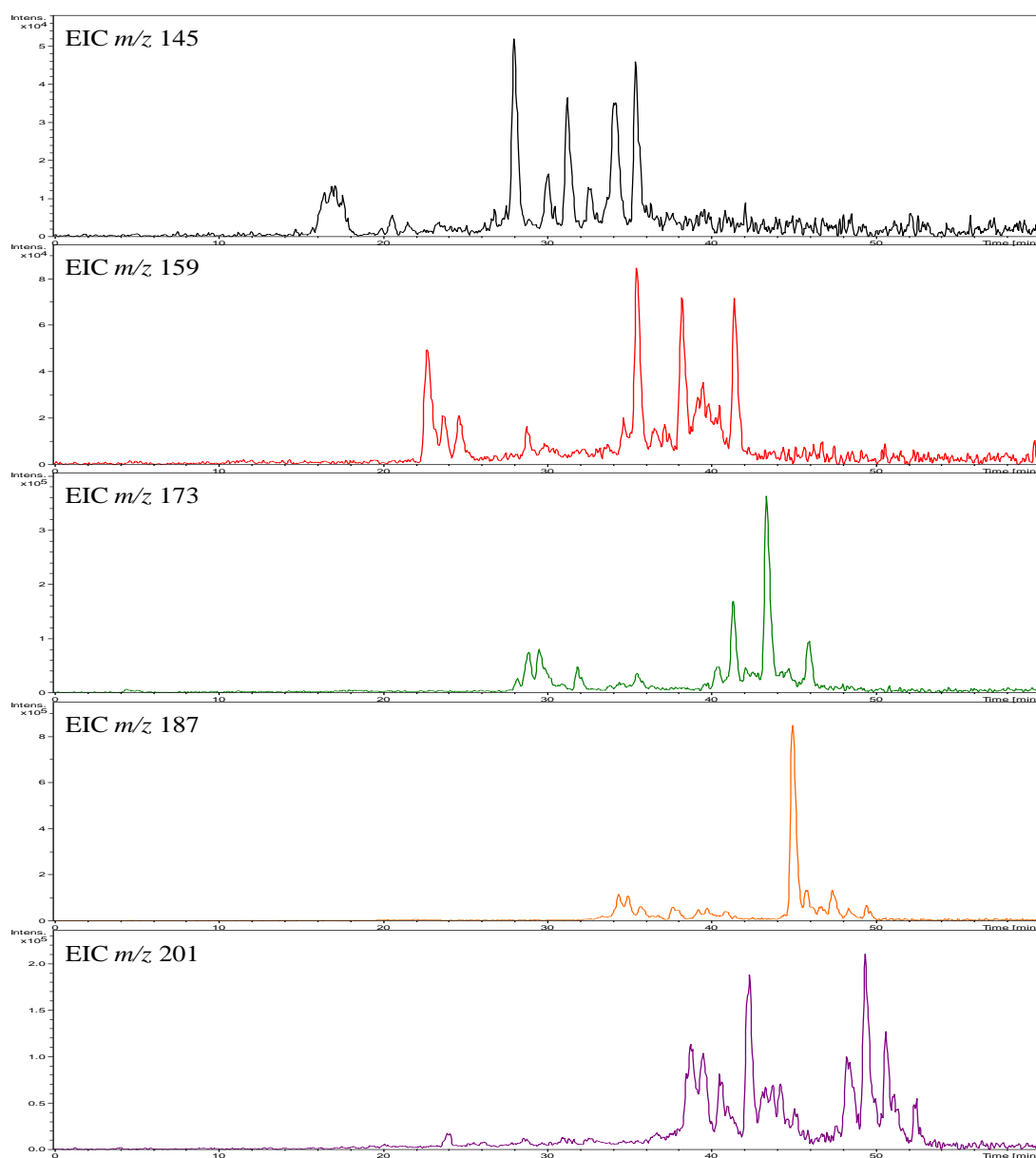
Figure 2.26 - EICs of related families of species, displaying increasing numbers of CH_2 groups in the compound structures demonstrated using the water soluble fraction of the oxidised oil sample.
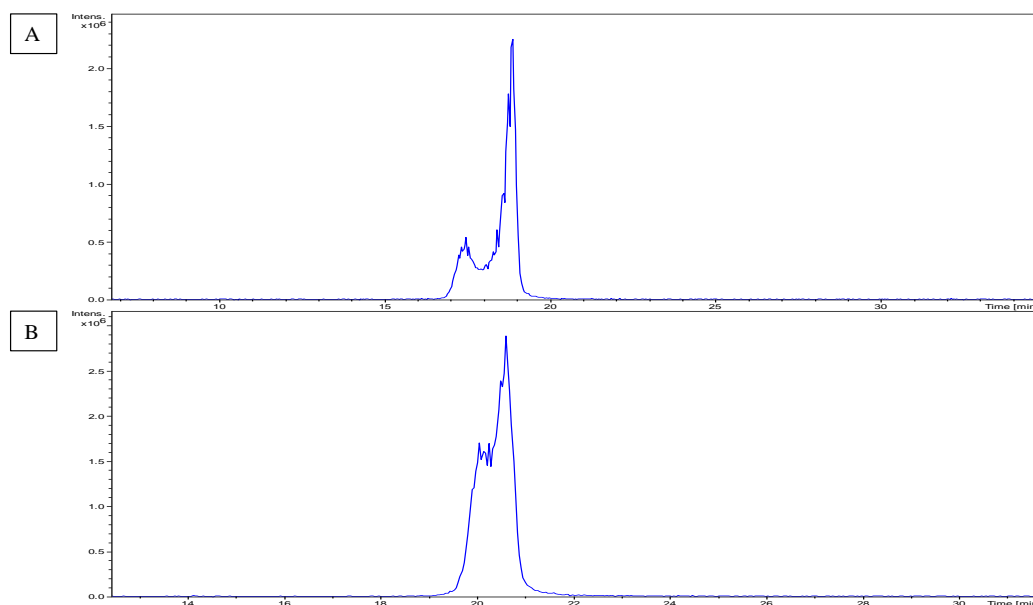
Figure 2.27 - An example of the peak splitting observed using a 1 ppm standard of 2,5-dihydroxybenzoic acid using the HPLC-ITMS A = internal diameter of 0.005" for the connecting lines. B = internal diameter of 0.02" for the connecting lines. Please note, a different gradient elution method was used in (A) (gradient similar to Figure 2.25, except the methanol content was increased to 100% at 70 minutes). The gradient elution method used in (B) is shown in Figure 2.25.

For the analysis of diesel SOA, the gradient elution method shown in Figure 2.25 will be used (potentially increasing the amount of methanol content if required), with an injection volume of 30 µL and an internal diameter of 0.02" for the connecting lines.
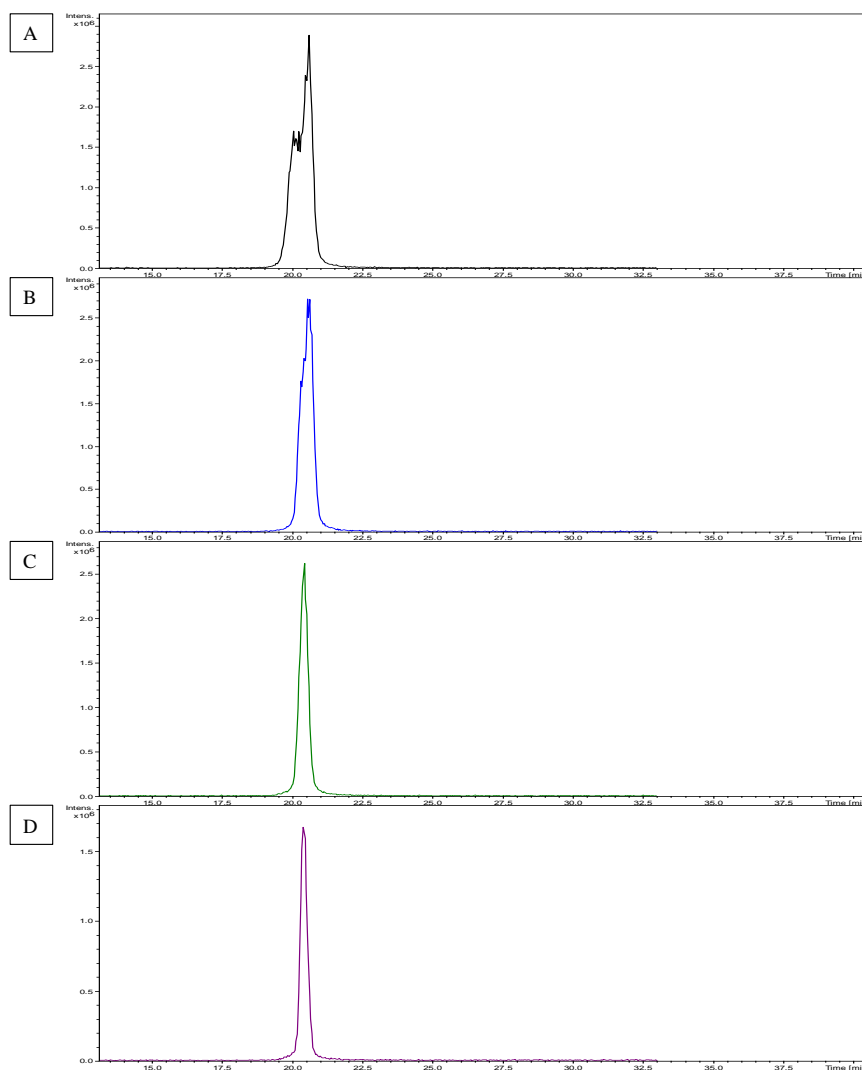
Figure 2.28 - EIC of 2,5-dihydroxybenzoic acid (*m/z* 154 (M-H)⁻) at a concentration of 1 ppm in negative ionisation mode, using RP-LC-ESI-ITMS. Sample injection volume; A = 60 µL. B = 45 µL. C = 30 µL. D = 15 µL.

2.4   Summary

Two HPLC stationary phases, HILIC and RP-LC, were investigated for the separation of eleven small polar compounds likely to be found in 3-methyl furan SOA. Of the eleven compounds, only four were observed using HILIC. Two compounds, citraconic anhydride and 5-methyfuran-2(3H)-one eluted in the extra-column volume, displaying no interaction with the stationary phase. The other two compounds, maleic and citraconic acid, displayed little interaction with the column stationary phase and were observed to co-elute. As a result, HILIC was found to be unsuitable for the separation of these compounds. Of the eleven compounds, seven were observed using RP-LC. All of these compounds displayed good interactions with the column stationary phase and were well resolved.

Calibrations were performed for five of the seven compounds which could be observed using RP-LC. Two compounds, citraconic anhydride and α-angelica lactone were excluded from further analysis due to the observation of additional chromatographic peaks, suggesting the further reaction and/or degradation of these species. The remaining five compounds; maleic acid, citraconic acid, maleic anhydride, 3-methylfuran-2(5H)-one and 5-hydroxyfuran-2-(5H)-one, all displayed a linear detector response ($R^2 > 0.999$) over a concentration range of 0.1 to 15 ppm. The LOD and LOQ values were deemed to be in the expected concentration range of the oxidation products likely to be found in 3-methyl furan SOA, with the LOD and LOQ values ranging between 0.01 to 0.07 ppm and 0.05 to 0.23 ppm, respectively.

The developed HPLC-ITMS method was used to investigate the SOA composition formed from the photo-oxidation of 3-methyl furan. Four chromatographic peaks were discussed, one was identified (using the commercially available standard) and a tentative structure was proposed for another. The identified compound, citraconic acid was found to represent a large proportion of the SOA mass collected on the filter (3.93%). However, due to lack of data received the project was abandoned.

Five external standards were chosen from sixteen compounds to monitor the ITMS detector variation during the analysis of methyl chavicol SOA (Chapter 3). This was a long-term study ranging over approximately eight months. The chromatographic peak areas of the external standards were monitored over time to allow any issues with the stability of the instrument to be highlighted immediately. All of the external standards were stable over the course of the analysis. The monitoring of the ITMS detector variation worked very well in negative ionisation mode. However, in positive ionisation this method was less useful due to formation of adducts which appeared to effect the signal intensity of the protonated molecular species.

Finally, a HPLC-ITMS method was developed for the analysis of diesel SOA. In this study a petroleum oil sample was oxidised to replicate the UCM expected to be present in diesel SOA and used to develop a suitable HPLC-ITMS method. Whilst this oil sample was extremely useful for method development, the lack of known compounds made it difficult to identify any problems with the method; highlighting the importance of also using known compounds for method development.

Chapter 3 - Secondary Organic Aerosol Formation and Composition from the Photo-oxidation of Methyl Chavicol (Estragole).*

*The majority of the work presented in this chapter has been published in the peer-reviewed journal; Atmospheric Chemistry and Physics. Please refer to Pereira et al. (2014).

3.1   Introduction

Approximately 90% of all global VOC emissions are from biogenic sources (Guenther et al., 1995). The most abundant biogenic emissions are attributed to isoprene (35-40%), monoterpenes (11-25%) and oxygenated VOCs (reactive other VOCs and other VOCs, 20-30%) (Guenther et al., 1995; Guenther et al., 2000). The largest source of biogenic VOC emissions are from vegetation; including trees which account for ~ 71% of emissions (Guenther et al., 1995), shrubs and crops, with a small emission source from grasslands and soils (Zimmerman, 1979; Guenther et al., 1995; Guenther et al., 2000; Wiedinmyer et al., 2004). Oxygenated VOCs (OVOCs) have received more attention recently due to the advances in instrumentation to detect and quantify these compounds in the ambient atmosphere. Despite this, significant uncertainties still remain in our knowledge of the sources, chemical composition and atmospheric oxidation mechanisms of OVOCs; in particular higher molecular weight species (> C_5) (Singh et al., 2000; Schade and Goldstein, 2001; Bouvier-Brown, 2008; Steiner et al., 2008; Taipale et al., 2012).

Methyl chavicol ($C_{10}H_{12}O$), also known as estragole and 1-allyl-4-methoxybenzene, is a C_{10} aromatic biogenic OVOC emitted from a variety of pine trees (including *ponderosa pine*), shrubs (*clausena dunniana, straggley baeckea*) and common herbs (*basil, fennel, tarragon*) (Mirov, 1961; Simon et al., 1990; Werker et al., 1994; De Vincenzi et al., 2000; Barazani et al., 2002; Southwell et al., 2003; Holzinger et al., 2005; Adams, 2007; Bouvier-Brown et al., 2009; Holzinger et al., 2010). A recent publication identified significant methyl chavicol emissions above the canopy of an oil palm plantation in Malaysian Borneo, with a mean midday flux of 0.81 mg m^{-2} h^{-1} and a mean mixing ratio of 3.0 ppbv (maximum mixing ratio observed ~ 7.0 ppbv) (Misztal et al., 2010). Methyl chavicol emissions from palm oil plantations were estimated to result in a global emission of ~ 0.5 Tg y^{-1} (Misztal et al., 2010).

There are currently 43 oil palm producing countries, with the majority of oil palm plantations concentrated in Indonesia and Malaysia (Figure 3.1) (FAOSTAT, 2012; MPOB, 2012). In 2011, there were approximately 7.7 million hectares (Mha) of oil palm plantations in Indonesia (USDA, 2013) and 5.0 Mha in Malaysia (MPOB, 2012). The increasing demand for palm oil for uses in food products and biofuels is resulting in the rapid expansion of oil palm agriculture (Fitzherbert et al., 2008). This rapid expansion in the oil palm agriculture is resulting in large areas of forestry being replaced with palm oil plantations (Fitzherbert et al., 2008). Consequently, methyl chavicol emissions are likely to have a considerable effect on regional chemistry in locations where oil palm plantations are

significant. Despite this, there have been few literature reports which have investigated the atmospheric fate of methyl chavicol, including gas-phase degradation, SOA formation, composition and yields.
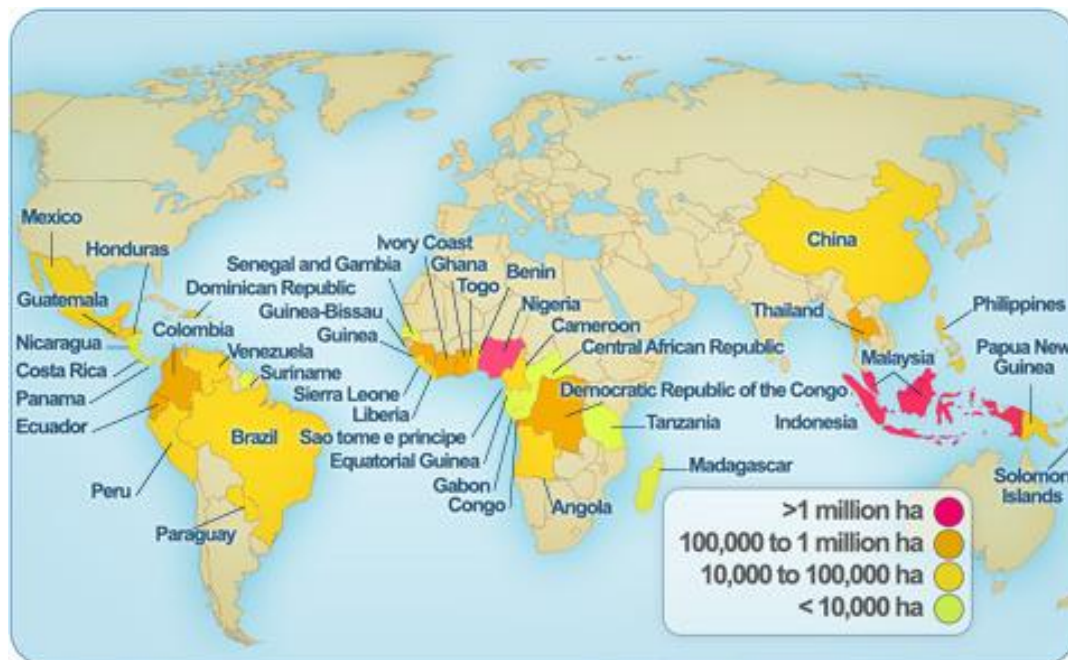
Figure 3.1 - The location and amount of oil palm plantations worldwide. Taken from MPOB, (2012).

The gas phase products formed from the oxidation of methyl chavicol with hydroxyl radicals ($^{\bullet}$OH) and ozone (O_3) has been investigated by Lee et al. (2006a, b) and more recently by Bloss et al. (2012) and Gai et al. (2013). The gas phase reactivity of methyl chavicol with $^{\bullet}$OH and O_3 has been reported by Bloss et al. (2012) and by Gai et al. (2013), who in addition investigated the gas phase reactivity of methyl chavicol with $^{\bullet}$NO$_3$. In the study performed by Lee et al. (2006b), the photo-oxidation of methyl chavicol resulted in a significant SOA yield (yield 40%) and the formation of two abundant structurally unidentified gas phase compounds at MW 136 g mol^{-1} ($C_8H_8O_2$, yield 42 $\pm$ 9%) and MW 150 g mol^{-1} ($C_9H_{10}O_2$, yield 23 $\pm$ 5%), detected using proton transfer reaction mass spectrometry (PTR-MS).

Bouvier-Brown et al. (2009) identified MW 136 g mol^{-1} as 4-methoxybenzaldehyde in the aerosol phase at Blodgett forest (California, US) and suggested the identification of pinonaldehyde (MW 150 g mol^{-1}) in previous studies (Holzinger et al., 2005), could be in part attributed to 4-methoxybenzene acetaldehyde (MW 150 g mol^{-1}) identified in Lee et al. (2006b). In addition, Cahill et al. (2006) tentatively identified 4-methoxybenzene

acetaldehyde in aerosol samples collected in the Sierra Nevada Mountains (California, US). More recently, Gai et al. (2013) identified a further two abundant gas phase products, MW 122 g mol^{-1} 4-methoxytoluene, and MW 166 g mol^{-1} 4-methoxybenzeneacteic acid, and identified MW 136 g mol^{-1} and MW 150 g mol^{-1} as 4-methoxybenzaldehyde and 4-methoxybenzene acetaldehyde, respectively, in support of the literature. However, the aerosol phase composition and mechanisms of formation from the oxidation of methyl chavicol has largely been unexplored.

The aim of this study is to characterise the SOA oxidation products formed from the photo-oxidation of methyl chavicol and determine their formation mechanisms. Experiments were performed at the European Photoreactor chamber in Valencia, Spain, as a part of the atmospheric chemistry of methyl chavicol (ATMECH) project. Aerosol samples were collected every 30 minutes using a particle into liquid sampler (PILS) and filters were collected at the end of each experiment. The automated sampling of the PILS provided added convenience over the use of filters for time resolved collection of SOA. SOA composition was investigated using an extensive range of instruments, including; high performance liquid chromatography ion trap mass spectrometry (HPLC-ITMS), high performance liquid chromatography quadrupole time-of-flight mass spectrometry (HPLC-QTOFMS) and Fourier transform ion cyclotron resonance mass spectrometry (FTICR-MS).

3.2   Experimental

3.2.1   Chamber Simulation Experiments

Experiments were performed at the European Photoreactor (EUPHORE) in Valencia, Spain. The EUPHORE facility comprises of two 200 m^3 hemispheric reaction chambers made of fluorinated ethylene propylene foil (FEP), with housings which may be closed to exclude sunlight (Figure 3.2). The simulation chambers are situated on the roof of the Mediterranean Centre for Environmental Studies (CEAM) building. Chamber temperature is near ambient and chamber pressure is maintained at approximately 100 Pa above ambient. Dry scrubbed air is used within the chamber and two large fans ensure homogenous mixing. Further technical information regarding the chamber design and installation can be found in the literature (Becker, 1996; Klotz et al., 1998; Volkamer et al., 2001; Bloss et al., 2005).

A series of experiments was performed during May 2012 as a part of the atmospheric chemistry of methyl chavicol project (ATMECH). The experiments performed, initial mixing ratios, chamber temperatures and relative humidities are presented in Table 3.1. The chamber was cleaned before each experiment by flushing with scrubbed dry air overnight.

Methyl chavicol was introduced into the chamber through a heated air stream. "Classical" photo-oxidation experiments were performed, where no additional $^\bullet$OH source was added into the chamber. The initial source of $^\bullet$OH in these experiments was from the photolysis of HONO, formed from the heterogeneous reaction of NO_2 and H_2O on the chamber walls (Carter et al., 1981, 1982; Sakamaki et al., 1983; Pitts et al., 1984; Svensson et al., 1987; Rohrer et al., 2005).

Figure 3.2 - EUPHORE simulation chamber. Black circle displays the PILS sampling inlet, discussed in Section 3.2.2.

An extensive range of monitors was used to measure chamber temperature (temperature sensor, model PT100), pressure (Barometer, model AIR-DB-VOC), humidity (Hygrometer Watz, model Walz-TS2), solar intensity (J_{NO2} Filter Radiometer), ozone (UV detector, Monitor Labs, model 9810) and NO_x (Teledyne API, model NO_X_API-T200UP; photolytic converter). PTR-MS (Ionikon Analytik) and Fourier transform infra red (FTIR Nicolet Magna, model 550), coupled to a white-type mirror system with an optical path length of 616 m, were used to monitor methyl chavicol decay and product formation. Laser induced fluorescence (LIF) was used to measure $^\bullet$OH and HO_2. The LIF is composed of a copper vapour laser that pumps a tunable dye laser at an output of 616 nm. The chamber dilution rate was calculated by measuring the decay of an inert tracer gas, sulphur hexafluoride

(SF$_6$), using FTIR; typical pseudo-first-order rate constants of 2×10^{-5} s^{-1} were obtained, corresponding to a dilution lifetime around 14 hours. The formation and evolution of SOA was measured using a scanning mobility particle sizer (TSI Incorporated, model 3080) consisting of a differential mobility analyzer (model 3081) and a condensation particle counter (model 3775).

Table 3.1 - The initial experimental mixing ratios, temperature and relative humidity range for the experiments discussed.

| Exp. type | Exp. ID | Exp. date | Exp. description | Initial mixing ratio[a] | | | | VOC:oxidant | Experimental range | |
				MC^{b} [ppbv]	NO [ppbv]	NO_2 [ppbv]	O_3 [ppbv]	ratio	Chamber temp [K]	RH [%]
Chamber Blank	$MC_{(0)}$	08.05.12	Chamber Blank	< LOD	< LOD	1	< LOD	-	294-311	0.9–4.7
Photo-oxidation	MC_{MNOx}	23.05.12	Medium NO_x	570	50	2	31	~ 11:1	299-308	0.8-5.8
	$MC_{[low]}$	11.05.12	High NO_x	212	38	8	9	~ 5:1	298-308	0.9–14.7
	$MC_{[high]}$	15.05.12	High NO_x	460	92	3	5	~ 5:1	297-306	2.1-10.7

[a] = On the opening of the chamber covers. [b] = FTIR measurement.

3.2.2 Aerosol Sampling and Sample Preparation

3.2.2.1 PILS

A Brechtel Manufacturing Incorporated (California, US) model 4002 particle into liquid sampler (PILS) was used for aerosol collection (Figure 3.3). The PILS was first manufactured in 2001 by Brechtel Manufacturing; based on the original PILS design shown in Weber et al. (2001). A schematic diagram of the PILS is shown in Figure 3.4. The PILS relies on the growth of sampled water soluble particles in a supersaturated environment of water vapour. Sampled air consisting of gaseous and particulate phase species enter the PILS at a flow rate of ~ 13 L min^{-1}. A chosen impactor size of PM$_1$ or PM$_{2.5}$ typically limits particles with diameters larger than 1 or 2.5 μm, respectively, from entering the instrument. Inorganic and organic gases are removed from the sampled air through the use of acidic, basic and activated carbon denuders. The denuders consist of either concentric cylindrical-shaped glass coated in a solution, or a stainless steel block covered in impregnated carbon strips, both which remove certain gaseous species on to the internal wall coating. Particles with diameters below the chosen impactor size enter into the PILS condensation chamber, where the sampled air flow mixes with a smaller turbulent heated air flow of steam (100 °C, ~ 1.51 L min^{-1}). The sampled air flow cools the smaller heated air flow of steam, resulting in adiabatic cooling and the formation of a supersaturated environment of water vapour. In this environment, particles grow into droplets with diameters ranging between 1 and 10 μm (Orsini et al., 2003). Particles with diameters above 1 μm are captured on the quartz impactor plate. Particles below this diameter are removed from the PILS through the exhaust flow. A continued flow of high purity water washes the quartz impactor plate (wash flow) and the set sample volume (sample flow) transfers the particle/water mixture into sealed vials, located in the carousel.

The PILS inlet was connected to the chamber outlet using approximately 1.5 meters of 1/3" stainless steel tubing. The location of the PILS inlet in the chamber is shown in Figure 3.2. Aerosol samples were collected using a PM$_1$ impactor. The activated carbon, acidic and basic denuders were prepared as per manufacturer instructions. The wash flow rate was set at 240 μL min^{-1} and consisted of optima LC-MS grade water (Fisher Scientific, UK). The sample flow rate transferred the aerosol water mixture into sealed vials at a flow rate of 200 μL min^{-1}, for 30 minutes per sample. Samples were collected before the addition of methyl chavicol or NO into the chamber and continued sampling until after the chamber was closed. After sample collection, punctured vial caps were replaced and securely sealed with

parafilm. All vials were wrapped in foil to minimise potential degradation from photolysis and were stored at -20°C °C until analysis. Collected PILS samples were evaporated to dryness using a V10 vacuum solvent evaporator (Biotage, USA) and redissolved in 300 μL of 50:50 methanol:water (optima LC-MS grade, Fisher, UK), with the exception of experiment $MC_{[high]}$, which was redissolved in 500 μL.
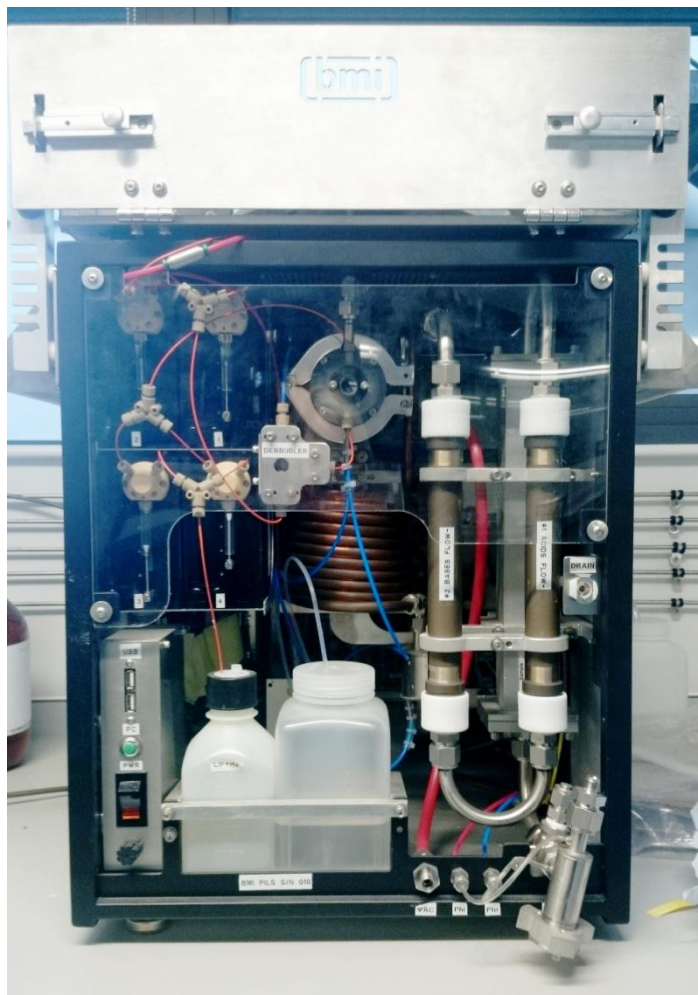
Figure 3.3 - Brechtel Manufacturing particle into liquid sampler (model 4002).

The PILS sample dilution amount is usually determined by spiking a known concentration of lithium fluoride into the sample flow. However, no internal standard was used due to the potential effects on the analytical method and SOA composition (*e.g.* adduct formation, ion suppression). PILS samples were evaporated to dryness to eliminate the unknown sample dilution amount. The re-suspension of samples into a smaller volume, concentrated the aerosol compounds, almost certainly allowing more SOA species to be observed. The re-suspension of the PILS samples into 50:50 methanol:water was performed to be more compatible with the high performance liquid chromatography (HPLC) mobile phase and to

increase the electrospray ionisation (ESI) efficiency (*cf.* (Kebarle and Verkerk, 2009)). The PILS collection efficiency has previously been determined, where no appreciable loss has been found for the particle diameter range investigated (30 nm to 1 μm) (Orsini et al., 2003).
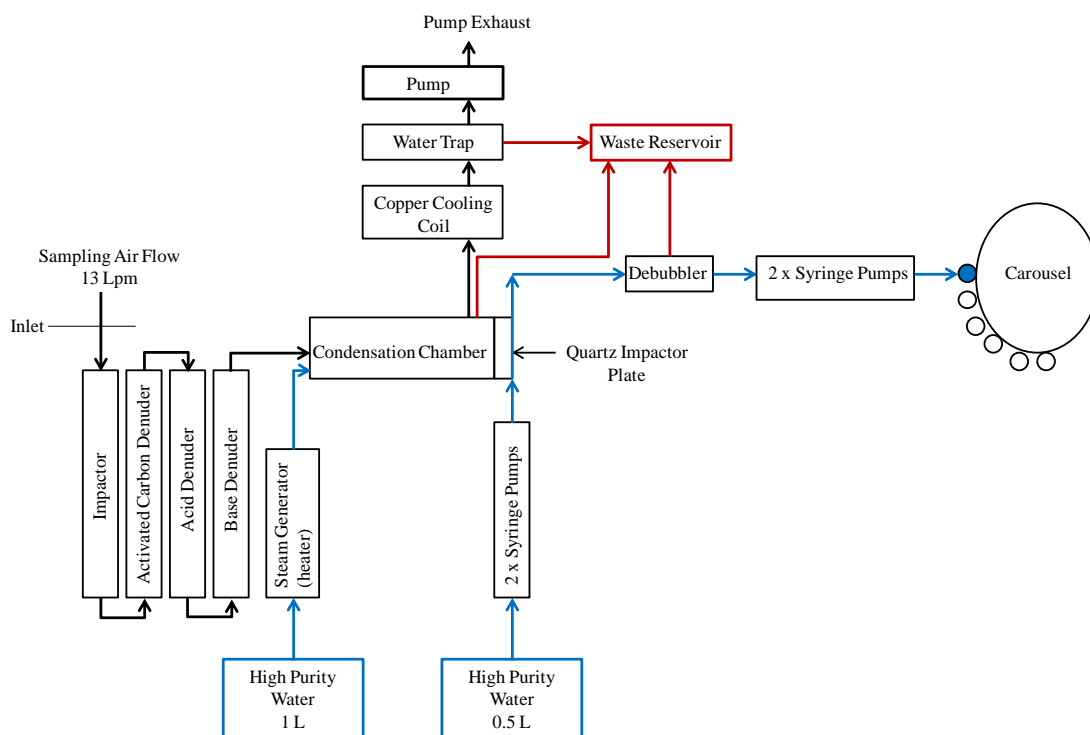
Figure 3.4 - Schematic of the PILS, adapted from the manufacturer's manual (also shown in Soroshian et al. (2006)) Coloured arrows; black = sampling air flow, blue = water flow, red = waste flow.

3.2.3 HPLC-ITMS

SOA composition was investigated using an Agilent 1100 series high performance liquid chromatograph (HPLC, Berkshire, UK) coupled to a HTC Plus ion trap mass spectrometer (IT-MS, Bruker Daltonics, Bremen, Germany). A reversed phase Pinnacle C_{18} 150 mm $\times$ 4.6 mm, 5 μm particle size column (Thames Resteck, UK) was used. The HPLC mobile phase composition consisted of (A) water (optima LC-MS grade, Fisher, UK) with 0.1% formic acid (Sigma Aldrich, UK) and (B) methanol (optima LC-MS grade, Fisher, UK). Gradient elution was used, starting at 90% (A) 10% (B), moving to 0% (A) 100% (B) over 60 minutes, returning to the initial starting conditions at 65 minutes. A 5 minute pre-run consisting of the starting mobile phase composition was performed before each sample injection. The flow rate was set at 0.6 mL min^{-1} with a sample injection volume of 60 μL. Electrospray ionisation (ESI) was used, with a dry gas flow rate of 12 L min^{-1}, a dry gas

temperature of 365ºC and nebuliser gas pressure of 70 psi (oxygen free nitrogen, OFN, BOC, UK). The MS was operated in alternating polarity mode, scanning from *m/z* 50 to 600. Tandem MS was achieved through the automated MS[2] function within the Esquire software (Bruker Daltonics, software version 5.2).

3.2.4 FTICR-MS

A solariX Fourier transform ion cyclotron resonance mass spectrometer with a 9.4-T superconducting magnet (Bruker Daltonics, Coventry, UK) was used and externally calibrated using L-Arginine (Sigma Aldrich, UK, purity 98%). Samples were introduced into the ESI source through direct infusion, using a Hamilton 50 µL syringe (Hamilton, Switzerland) at a flow rate of 120 µL hour[-1]. Spectra were acquired in both positive and negative ionisation modes over a scan range of *m/z* 50 – 800. The ESI parameters were set to a dry gas flow rate of 3.7 L min^{-1}, dry gas temperature of 220 °C, and a nebulizer gas pressure of 1.2 bar (nitrogen, BOC, UK). Broadband detection mode was used, with 64 spectra averages obtained for each spectrum. Ion accumulation in the ICR cell was set to 0.5 seconds with a source accumulation time of 0.002 seconds. The collision radio frequency (RF) and ion cooler time was set to favour lower masses at 1300 Vpp (volts peak-to-peak) and 0.010 seconds, respectively. An approximate resolution of 38,000 at *m/z* 400 was obtained for both ionisation modes.

The spectral analysis was performed using DataAnalysis 4.0 software (Bruker Daltonics, Breman, Germany). Monoisotopic elemental formulae were calculated using the following restrictions; unlimited C, H and O were allowed and up to 3 N atoms, O:C < 3, H:C > 0.5, DBE < 20, and in positive mode, Na and K adducts were also allowed. The accuracy of the molecular formulae (elemental composition) assignment is shown by the error; where the error equals the difference between the exact and measured mass for the assigned molecular formula. The mass error (also referred to as mass accuracy) is displayed in ppm and is calculated by dividing the mass error by the exact mass for the assigned molecular formula and multiplying by 10^6. The molecular formula score refers to the fit of the theoretical and measured isotopic distribution and abundance for the assigned molecular formula, and is displayed in percent. The molecular formula score is not calculated for a signal to noise (S/N) ratio below 5. The combination of a high score and low mass accuracy will result in few potential molecular formula assignments for a compound at a given *m/z*. A compound with an *m/z* below 300, with a high score (100%) and low mass accuracy (< 5 ppm) results in only one potential molecular formula (Kind and Fiehn, 2006).

3.2.5   HPLC-QTOFMS

A Dionex ultimate 3000 HPLC (Thermo Scientific Inc, UK) was coupled with an ultra high resolution quadrupole time-of-flight mass spectrometer (HPLC-QTOFMS) (maXis 3G, Bruker Daltonics, Coventry, UK). The HPLC utilised the same reverse phase Pinnacle C_{18} column and mobile phase composition as described in the HPLC-ITMS analysis. The gradient elution runtime was shortened, starting at 90% (A) 10% (B), moving to 0% (A) 100% (B) over 50 minutes and returning to the initial starting conditions at 55 minutes. A 5 minute pre-run was performed before each sample injection using the starting mobile phase composition. The flow rate was set to 0.6 mL min^{-1} and the column temperature controlled at 20°C. A user defined autosampler method was created, drawing 58 μL of sample into the sample loop, followed by 2 μL of a 10 ppm external standard mix and 20 μL of 50:50 methanol:water (optima LC-MS grade, Fisher, UK). The HPLC-QTOFMS was externally calibrated using ESI-L low concentration tuning mix (Agilent Technologies, UK). ESI was used and the parameters were set to a dry gas flow rate of 10 L min^{-1}, dry gas temperature of 350°C and a nebulizer pressure of 4 bar (nitrogen, BOC, UK). Tandem mass spectra were acquired for a mass range of *m/z* 50 to 800 using the auto MS^2 function within the Compass 1.3 micrOTOF-SR3 software, control version 3.0 (Bruker Daltonics, UK). The three most abundant precursor ions per spectrum were automatically selected by the software and subjected to collision induced dissociation (CID). The collision energy for CID fragmentation was set at 8.0 eV at a collision RF of 800.0 Vpp. The spectral analysis was performed using DataAnalysis 4.0 software (Bruker Daltonics, Breman, Germany). The molecular formula error and score was automatically calculated by the DataAnalysis software using the same methods as described in the FTICR-MS analysis.

3.2.6   Standards and Calibrations

A 10 ppm external standard (ES) mix was used to monitor the ITMS detector variation over the course of the sample analysis (Chapter 2, Section 2.3.2). The ES mix was also used for the optimisation of the HPLC-QTOFMS method, internal mass calibration and to determine the retention time shift of the SOA compounds due to the shortening of the gradient elution. The ES mix consisted of 5 compounds, 4-methoxybenzoic acid (Sigma Aldrich, UK, purity 99%), hexanedioic acid (Sigma Aldrich, UK, purity 99%), cis-pinonic acid (Sigma Aldrich, UK, purity 99%), 2-hydroxyhexanoic acid (Acros Organics, Belgium, purity 95%) and 2,6-dimethyl-3-nitrophenol (provided by University College Cork). These compounds were selected based on their range of retention times, stability, variety of functional groups and

ionisation efficiency in both positive and negative ionisation modes. Calibrations were performed using the HPLC-ITMS for any structurally identified SOA compounds where standards were commercially available. Calibrations ranged in concentration from 0.02 to 2 ppm and consisted of a minimum of 5 concentrations, with 3 replicate measurements.

3.3   Results and Discussion

3.3.1   Photo-oxidation of Methyl Chavicol

Four experiments carried out as part of the ATMECH campaign are discussed here: (i) $MC_{(0)}$; a chamber background experiment, where no VOCs or NO_x were added to the chamber and the chamber housing was opened to expose the chamber to light. None of the methyl chavicol SOA compounds identified were observed in this experiment. (ii) $MC_{[high]}$, a photo-oxidation experiment with high initial mixing ratios of methyl chavicol (460 ppbv) and NO (92 ppbv); (iii) $MC_{[low]}$, a photo-oxidation experiment with lower mixing ratios of methyl chavicol (212 ppbv) and NO (38 ppbv), with a similar initial VOC:NO_x ratio (~5:1) to $MC_{[high]}$ and; (iv) MC_{MNOx}, a photo-oxidation experiment with similar mixing ratios of methyl chavicol (570 ppbv) to $MC_{[high]}$, but with a lower VOC:NO_x ratio (~11:1) (*i.e.* NO 50 ppbv). The VOC/NO_x ratio used in $MC_{[high]}$ and $MC_{[low]}$ represents the lower MC/NO_x ratio of an agro-industrialized oil palm plantation site in northern Borneo (Hewitt et al., 2009; MacKenzie et al., 2011); where the boundary layer (500-800 m) NO_x concentration (75th percentile) was ~ 0.6 ppbv (Hewitt et al., 2009), with a methyl chavicol abundance of ~ 3 ppbv at midday (MacKenzie et al., 2011), corresponding to a MC/NO_x ratio of 5.

3.3.2   Overview of Experiments

The temporal evolution of NO_x, O_3, methyl chavicol and SOA growth are shown in Figure 3.5 and show similar profiles to previous aromatic photo-oxidation experiments, with initial aerosol formation occurring when the photochemical system enters into a relatively "low NO" state (*cf.* (Rickard et al., 2010)). The maximum SOA mass observed, corrected for wall loss and chamber dilution, was 420, 126 and 391 µg m^{-3} in $MC_{[high]}$, $MC_{[low]}$ and MC_{MNOx}, respectively. It is worth noting that the methyl chavicol concentration was fluctuating from the opening of the chamber covers to the first 30 minutes of $MC_{[high]}$, Figure 3.5B. As a result, the amount of methyl chavicol reacted during this time period could not be determined. However, no SOA formation occurred until ~ 40 minutes into the experiment and thus the results of $MC_{[high]}$ have not been affected.
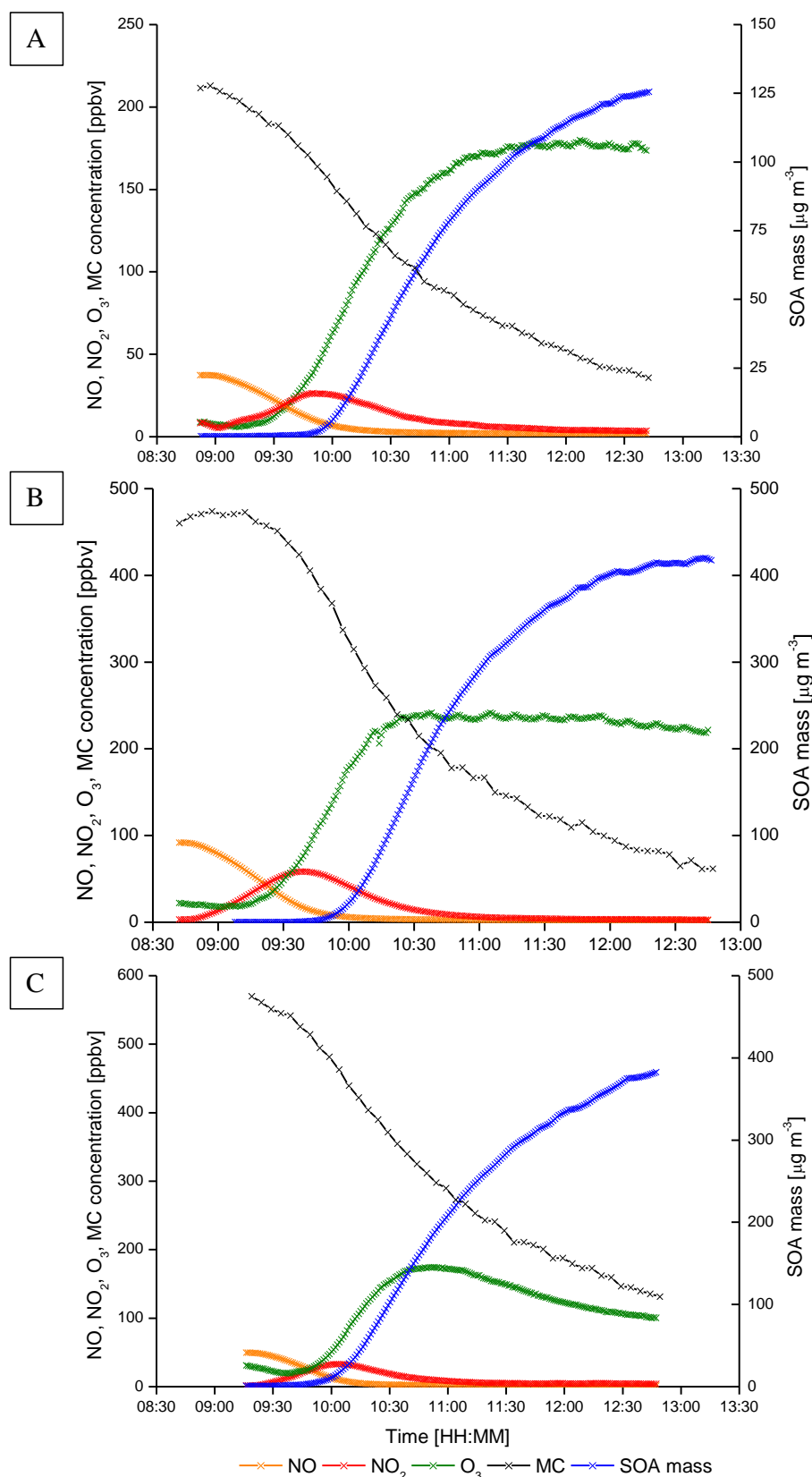
Figure 3.5 - Temporal evolution of NO, NO_2, O_3 methyl chavicol (MC) and SOA mass (corrected for wall loss and chamber dilution) in experiments during ATMECH. A = $MC_{[low]}$. B = $MC_{[high]}$. C = MC_{MNOx}.

3.3.3   Calculation of the SOA Yields

The SOA yield (Y) was calculated using the equation given in (Odum et al., 1996) (Eq.3.1), where the amount of aerosol mass formed [ΔM_0, µg m^{-3}] was divided by the amount of methyl chavicol reacted [ΔMC, µg m^{-3}], assuming spherical aerosol shape with a density of 1.4 g cm^{-3}. To accurately calculate the SOA yield, the amount of methyl chavicol reacted and SOA mass formed must be corrected for chamber dilution and wall loss. Small leaks within the chamber walls and the continued sampling of chamber air result in a decrease in chamber volume. To maintain chamber volume and thus pressure, scrubbed dry air is added into the chamber at a rate proportional to the rate at which the chamber air is sampled and lost, resulting in the dilution of the chamber contents.

Eq. 3.1
$$Y = \frac{\Delta M_0}{\Delta MC}$$

The rate of chamber dilution can be calculated by measuring the concentration decay of an inert tracer gas (SF_6) over time, using FTIR. The use of the integrated first order rate law (Eq. 3.2) provides the rate of dilution over the time period investigated; where C_0 is the initial concentration of SF_6, C is the concentration of SF_6 at each time step, t (s) is time period between C_0 and C, and k (s^{-1}) is the rate constant. For a first order rate of reaction, a plot of ln[C/C$_0$] *vs.* time results in a straight line, where the slope is equal to the rate of chamber dilution (Eq. 3.3).

Eq. 3. 2
$$-kt = ln\left(\frac{C}{C_0}\right)$$

Eq. 3.3
$$ln[C] = kt + ln[C_0]$$

Losses of semi-volatile and particulate phase species can also occur at the chamber walls. Particles are lost to the chamber walls through deposition. The rate of particle deposition depends on particle size, turbulence within the chamber, chamber geometry and particle charges (Crump and Seinfeld, 1981; McMurry and Grosjean, 1985). The rate of particle deposition is measured at the end of an experiment, when SOA formation has stopped. The chamber housing is closed to prevent further reaction from photolysis and the particle volume distribution measured over a certain time period, using the SMPS. The particle wall loss rate is calculated using the same method as discussed above (Eq. 3.2 and 3.3); except the rate is equal to the rate of particle wall loss and chamber dilution (total loss); as chamber dilution is still occurring. The subtraction of the known dilution rate from the total loss rate,

gives the rate of particle wall loss; which is assumed to be constant throughout an experiment (Pierce et al., 2008).

Losses of semi-volatile species to the chamber walls can occur through deposition, reaction at the chamber walls, and/or uptake onto particles already deposited on the walls of the chamber (Loza et al., 2010). This loss process is often not considered in SOA chamber studies (Loza et al., 2010; Shiraiwa et al., 2013), primarily because the chamber walls are chemically inert and thoroughly cleaned before and after experiments. As such, the reaction or deposition of semi-volatile species to the chamber walls is often considered to be a negligible loss process (Loza et al., 2010). Potential wall losses of methyl chavicol were not considered in these experiments, although recent studies have shown that wall losses can be significant for certain gas phase species (Loza et al., 2010; Hildebrandt et al., 2011; Loza et al., 2014; Zhang et al., 2014). It is therefore possible, that the SOA yields reported from these experiments may be underestimated.

The amount of methyl chavicol reacted ($MC_{reacted}$) and SOA mass formed (SOA_{formed}) corrected for chamber losses can be represented as shown in Eq. 3.4 and 3.5, respectively. The amount of methyl chavicol reacted was corrected for chamber dilution through the use of Eq. 3.6. The rate of dilution (k dilution, s^{-1}) determined from Eq. 3.3 was multiplied by the change in time between steps x (tx) and y (ty), to provide an overall dilution rate for the sampled time period. This rate of dilution was multiplied by the average amount of methyl chavicol measured during this time period, to provide the amount of methyl chavicol diluted. The addition of the amount diluted by the amount reacted between time steps x and y, gives the amount of methyl chavicol reacted corrected for chamber dilution during this time period. The cumulative sum of the amount of methyl chavicol reacted corrected for chamber dilution between the initial time step (1) to n (Eq. 3.7), gives the total amount of methyl chavicol reacted ($MC_{totalreacted}$) at time step n (tn).

Eq. 3.4 $$MC_{reacted} = MC_{measured} + MC_{dilution}$$

Eq. 3.5 $$SOA_{formed} = SOA_{measured} + SOA_{dilution} + SOA_{wall\,loss}$$

Eq. 3.6 $$MC_{reacted} = (MC_{tx} - MC_{ty}) + k_{dilution}\left(\frac{MC_{tx} + MC_{ty}}{2}\right)\Delta t_{(tx-ty)}$$

Eq. 3.7 $$MC_{totalreacted(tn)} = \sum_1^n (MC_{reacted})_i$$

A size dependent particle wall loss rate was calculated using Eq. 3.8; where $N(D_p,t)$ is the particle number concentration, $\beta(d_p)$ is the particle number loss coefficient and D_p is the

particle diameter (see (Bowman et al., 1997) and (Cocker et al., 2001) for further information).

Eq. 3.8
$$\frac{\mathrm{d}N(\mathrm{D_p}, t)}{\mathrm{d}t} = -\beta(\mathrm{D_p})N(\mathrm{D_p}, t)$$

Once the chamber dilution and wall loss corrections have been applied, the SOA yield can be calculated for each time step, using Eq. 3.1; where the maximum SOA yield for any one of the time steps, is reported as the overall yield for the experiment investigated.

3.3.4 SOA Yields

The SOA yields were determined as 19%, 31% and 23% for experiments $MC_{[low]}$, $MC_{[high]}$ and MC_{MNOx}, respectively. As expected, a larger SOA yield was obtained at higher initial mixing ratios ($MC_{[low]}$ 19%, $MC_{[high]}$ 31%). At higher initial mixing ratios, higher concentrations of the gas phase oxidation products are formed. This results in more species being able to reach their saturation concentration and partition into the aerosol phase, increasing SOA mass and subsequently, the SOA yield (Pankow, 1994b, a; Odum et al., 1996; Song et al., 2005). Furthermore, as the amount of aerosol mass increases, more species of higher volatility can absorb onto pre-existing aerosol particles (Pankow, 1994b, a; Odum et al., 1996); furthering increasing the amount of aerosol mass formed and thus accounting for the larger yield observed in $MC_{[high]}$.

3.3.5 Gas Phase Product Formation

Four compounds, 4-methoxytoluene (MW 122 g mol^{-1}), 4-methoxybenzaldehyde (MW 136 g mol^{-1}), 4-methoxybenzene acetaldehyde (MW 150 g mol^{-1}) and (4-methoxyphenyl)acetic acid (MW 166 g mol^{-1}) have previously been identified in the literature as the oxidation products formed from the photo-oxidation methyl chavicol (Lee et al., 2006b; Bouvier-Brown et al., 2009; Gai et al., 2013). The structures of these compounds are shown in Table 3.2,. along with 4-methoxybenzoic acid (MW 152 g mol^{-1}), which is suggested to be a further oxidation product of 4-methoxybenzaldehyde (MW 136 g mol^{-1}). All three experiments were investigated for the presence of these compounds using PTR-MS.

PTR-MS is an online technique used for the detection of VOCs in air (Hewitt et al., 2003; Blake et al., 2009). PTR-MS utilises a hollow-cathode ionisation source to ionise reagent gas molecules to protonated molecular species (Blake et al., 2009). These protonated molecular species (in the majority of cases) act as proton donors, undergoing proton transfer

reactions with sampled VOCs; resulting in the ionisation and detection of these species. The most common reagent gas used in PTR-MS is water vapour, forming hydronium ions $(H_3O)^+$ upon ionisation.
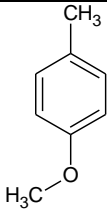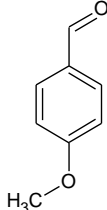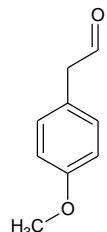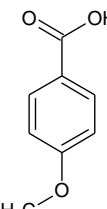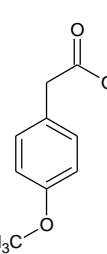
Generally, gas phase species containing alcohol or carboxylic acid functional groups undergo dissociation (fragmentation) on proton transfer from a hydronium ion (H_3O^+) (Spanel et al., 1997; Spanel and Smith, 1998; Blake et al., 2009). These compounds usually have high proton affinities which results in large excess energy being released upon proton transfer; causing fragmentation. This is often observed through the neutral loss of H_2O from an alcohol group or the hydroxyl group of a carboxylic acid (Spanel et al., 1997; Spanel and Smith, 1998). This fragmentation can result in only a proportion of the protonated molecular species being observed, or in some instances (*e.g.* 1-propanol (Schwarz et al., 2009)), result in the protonated molecular species not being observed at all (Spanel et al., 1997; Spanel and Smith, 1998). Two compounds, MW 152 and 166 g mol^{-1} were observed in MC$_{[high]}$ and MC$_{[low]}$ and may be attributed to the two carboxylic acid containing compounds, 4-methoxybenzoic acid and (4-methoxyphenyl)acetic acid, respectively. The identification of two species at the expected MW of 4-methoxybenzoic acid and (4-methoxyphenyl)acetic acid, suggests these compound do not undergo extensive fragmentation, although it is possible only a proportion of the compound concentration is observed.

Five compounds with a MW of 122, 136, 150, 152 and 166 g mol^{-1} were observed in MC$_{[high]}$ and MC$_{[low]}$ and may be attributed to 4-methoxytoluene, 4-methoxybenzaldehyde, 4-methoxybenzene acetaldehyde, 4-methoxybenzoic acid and (4-methoxyphenyl)acetic acid, respectively. In both experiments, all of these compounds were observed above the limit of detection (defined as 3 = S/N). The concentration of MW 136 g mol^{-1} (suspected product, 4-methoxybenzaldehyde) was determined using the calibrated response factor of α-pinene. The responses of all the other compounds are shown in normalised counts per second (ncps); where the counts per second (cps) of the trace gas is normalised per 10^6 H$_3$O$^+$ ion count rates (see (Ellis and Mayhew, 2013) for further information). The temporal evolutions of MW 136, 150 and 166 g mol^{-1} from the opening to the closing of the chamber covers in MC$_{[high]}$, MC$_{[low]}$ and MC$_{MNOx}$ are shown in Figure 3.6. Only a few measurements were obtained for MW 122 and 152 g mol^{-1} during the experiments. These compounds were observed above the LOD in only two out of approximately three measurements and as a result, the temporal profiles of these species are not shown in Figure 3.6.

As previously discussed, experiments MC$_{[high]}$ and MC$_{[low]}$ were performed at similar VOC/NO$_x$ ratios; except in MC$_{[low]}$, a lower initial mixing ratio was used. It would be

expected that the chemistry in both experiments (and thus the oxidation products formed) would be comparable due to the similarity of the VOC/NO$_x$ ratio, but in MC$_{[low]}$, lower concentrations of the oxidation products would be expected, due to the lower initial mixing ratio. This can be observed from the temporal profiles of MW 136, 150 and 166 g mol^{-1} where in both experiments the temporal evolution of these compounds are very similar, but in MC$_{[low]}$ the signal intensities/concentrations are lower (Figure 3.6A and B). The effect of the VOC/NO$_x$ ratio on product formation and evolution can be observed by comparing experiments MC$_{[high]}$ and MC$_{MNOx}$. Both experiments were performed at similar initial mixing ratios, except in MC$_{MNOx}$ a higher VOC/NO$_x$ ratio (lower NO$_x$ concentration) was used. In MC$_{MNOx}$, only one compound was observed above the limit of detection, MW 136 g mol^{-1} (4-methoxybenzaldehyde). As shown in Figure 3.6, the temporal evolution of this compound in MC$_{MNOx}$ is considerably different to that observed in MC$_{[high]}$; where in MC$_{MNOx}$ a delay in formation of $\sim$ 60 minutes is observed. Furthermore, a significant decrease in the maximum concentration of MW 136 g mol^{-1} (4-methoxybenzaldehyde) was observed in MC$_{MNOx}$, decreasing from $\sim$ 200 ppbv in MC$_{[high]}$ to $\sim$ 5 ppbv in MC$_{MNOx}$.

Table 3.2 - The compound structures of the methyl chavicol gas-phase oxidation products.

Compound name	MW [g mol^{-1}]	Compound structure
4-methoxytoluene	122	
4-methoxybenzaldehyde	136	
4-methoxybenzene acetaldehyde	150	
4-methoxybenzoic acid	152	
(4-methoxyphenyl)acetic acid	166	
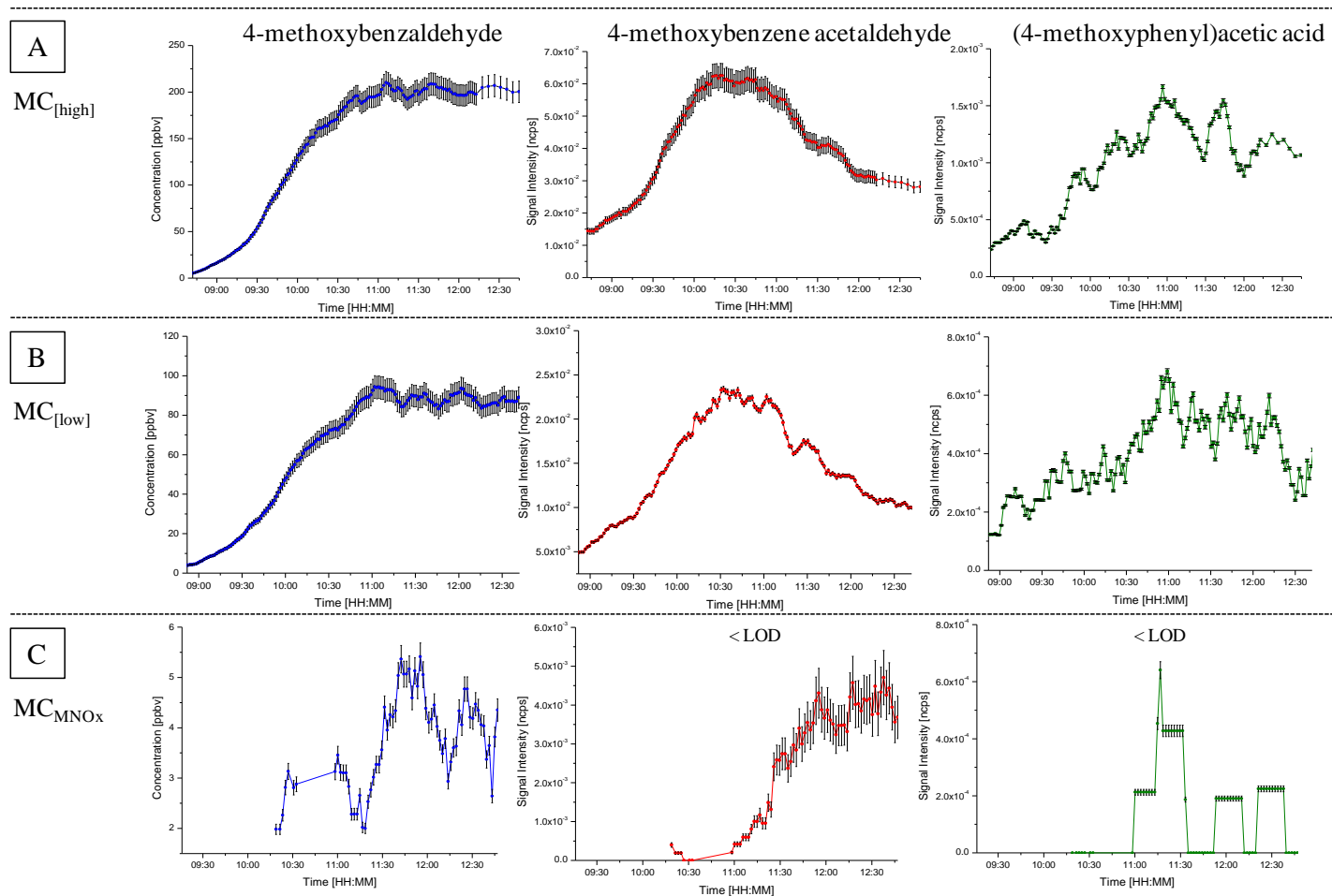
Figure 3.6 - PTR-MS gas phase evolution of (from left to right): 4-methoxybenzaldehyde (MW 136 g mol^{-1}), 4-methoxybenzene acetaldehyde (MW 150 g mol^{-1}) and (4-methoxyphenyl)acetic acid (MW 166 g mol^{-1}) in experiments $MC_{[high]}$ (A), $MC_{[low]}$ (B) and MC_{MNOx} (C), respectively.

3.3.6 SOA Composition

The PILS samples were analysed using a series of complementary analytical techniques. Initially, the HPLC-ITMS was used to screen the PILS samples for SOA species. Any compounds observed in the PILS samples before the introduction of methyl chavicol and NO into the chamber in $MC_{[high]}$, $MC_{[low]}$ and MC_{MNOx} were excluded from further analysis. Compounds which displayed changes in their chromatographic peak areas (and thus concentration) were investigated further. In $MC_{[high]}$, 79 SOA compounds were observed in the PILS samples using HPLC-ITMS. Of these compounds, 75 were also observed in the $MC_{[low]}$ experiment. Four compounds, MW 236, 248, 272 and 290 g mol^{-1} were not observed in the lower concentration experiment. In $MC_{[high]}$, the intensities of these compounds in the HPLC-ITMS analysis were observed just above the limit of detection (defined as 3 = S/N). The similarity of the oxidation products formed, but the lower initial mixing ratio in $MC_{[low]}$, suggests these compounds were not observed in the $MC_{[low]}$ experiment due to a decrease in the formation yields at lower initial mixing ratios.

In $MC_{[high]}$, fragmentation data was obtained for 76 of the 79 SOA compounds using HPLC-ITMS[2]. In many cases it was not possible to identify the compound structures of the SOA species due to the low mass resolution of the ITMS and lack of commercially available standards. This resulted in the use of the FTICR-MS to aid in the identification of the SOA molecular formulae and compound structures. The use of FTICR-MS significantly aided in compound identification, providing the molecular formulae for 67 of the 79 SOA compounds with average error of 0.64 ppm for negative ionisation mode and 5.23 ppm for positive ionisation mode. FTICR-MS[2] could not be performed due to the lack of prior chromatographic separation and the low concentration of the SOA compounds. Instead, HPLC-QTOFMS[2] was used to obtain high mass resolution compound fragmentation data for the SOA compounds. The HPLC-QTOFMS identified the molecular formulae of 74 of the 79 SOA compounds with an average error of 4.37 ppm for negative ionisation mode and 17.85 ppm for positive ionisation mode. The use of the HPLC-QTOFMS was complementary to the FTICR-MS, allowing the comparison of two high mass resolution data sets to determine the molecular formulae of the SOA compounds, as shown in Tables 3.3, 3.4 and 3.5. The use of prior chromatographic separation with the QTOFMS and its inherently better detection limits were advantageous and allowed the molecular formulae of the 12 low concentration SOA compounds not identified using FTICR-MS to be determined. Of the 79 SOA compounds, the FTICR-MS and the HPLC-QTOFMS were in agreement of the molecular formulae for 52 SOA compounds. Only one high resolution

mass spectrometric technique provided the molecular formulae for 17 SOA compounds and for 10 SOA compounds the molecular formulae provided by the HPLC-QTOFMS and FTICR-MS were not in agreement. A complete list of the observed SOA species including the molecular formulae identification and associated errors can be found in Tables 3.3 and 3.4. Of the 79 SOA compounds, the structures of 10 have been assigned and are shown in Table 3.5. The structures of (4-methoxyphenyl)acetic acid and 4-methoxybenzoic acid have been confirmed using the retention time and fragmentation patterns of commercially available standards. All other compound structures have been determined from the deprotonated or protonated molecular species fragmentations obtained from the HPLC-ITMS[2] and HPLC-QTOFMS[2].

A Van Krevelen plot of the 79 SOA compounds is shown in Figure 3.7. The average O:C and H:C ratio was determined as 0.44 and 1.37, respectively. In comparison to other aromatic photo-oxidation studies, the H:C ratio of methyl chavicol SOA fits considerably well. The H:C ratio of benzene and 1,3,5-TMB SOA was previously determined to range between 1.35 to 1.42 and 1.68 to 1.72, respectively (Sato et al., 2012). In their study, the higher H:C ratio observed for 1,3,5-TMB SOA in comparison to benzene SOA, was suggested to be the result of the starting precursor 1,3,5-TMB (H:C = 1.3) having a higher H:C ratio than benzene (H:C = 1) (Sato et al., 2012). Methyl chavicol has a H:C ratio of 1.2. Considering this, it would be expected that methyl chavicol SOA would have a H:C ratio (H:C = 1.37) higher than benzene SOA (H:C = 1.35 to 1.42) and lower than 1,3,5-TMB SOA (H:C = 1.68 to 1.72). It is important to note however, that the SOA H:C ratio is not just indicative of the H:C ratio of the starting precursor. The H:C ratio will increase with increasing numbers of ring-opening oxidation products formed (*i.e.* increasing saturation); thus the H:C ratio is also largely dependent on the mechanisms of oxidation (*e.g.* (Forstner et al., 1997; Sato et al., 2012). From Figure 3.7 it can be observed that the majority of the oxidation products formed appear to retain the aromatic ring, with H:C ratios less than ~ 1.5. There are however, a number of oxidation products observed with H:C ratios greater than ~ 1.5, suggesting these are ring-opened species. Of the 79 compounds, 45 had a DBE greater than 4 (average DBE for all compounds = 5), further suggesting that the aromatic ring is retained upon oxidation for the majority of observed compounds. In contrast to the H:C ratio, the O:C ratio of benzene SOA (O:C = 0.62 - 0.71) was found to be higher than 1,3,5-TMB SOA (O:C = 0.25 - 0.47) (Sato et al., 2012). This is the result of 1,3,5-TMB containing three methyl substituents on the aromatic ring which are unlikely to undergo extensive oxidation (Sato et al., 2012). Methyl chavicol has two aromatic substituents, a methoxy group, and a hydrocarbon chain (HC) which contains alkene functionality

(discussed in more detail in Section 3.3.8). The methoxy group and the alkyl proportion of the HC chain, similar to the methyl substituents in 1,3,5-TMB, are unlikely to undergo extensive oxidation. However, the alkene functionality on the HC will undergo oxidation. Thus, it would be expected that the O:C ratio of methyl chavicol SOA would be higher than 1,3,5-TMB SOA, but not as oxidised as benzene SOA. An average O:C ratio of 0.44 for methyl chavicol SOA, suggests that the majority of compounds formed have not undergone extensive oxidation.

Table 3.3 - The molecular formulae (MF) and associated errors of the identified SOA compounds in experiment $MC_{[high]}$ using FTICR-MS and HPLC-QTOFMS in negative ionisation mode.

t_R	MW [g mol^{-1}]	FTICR-MS MF	Error [ppm]	Score [%]	HPLC-QTOFMS MF	Error [ppm]	Score [%]
14.3	138				$C_7H_6O_3$	-9.7	100
30.1	152	$C_8H_8O_3$[a]	0.3	100	$C_8H_8O_3$	-1.4	100
28.1	166	$C_9H_{10}O_3$	0.8	100	$C_9H_{10}O_3$	1.2	100
33	168	$C_8H_8O_4$	0.7	100	$C_8H_8O_4$	0.2	100
12.5	180	$C_9H_8O_4$	0.9	100	$C_9H_8O_4$	2.6	100
16.1	182	$C_9H_{10}O_4$	0.8	100	$C_9H_{10}O_4$	-0.3	100
17.6	191	$C_{10}H_9NO_3$	0.7	100	$C_{10}H_9NO_3$	-3.2	100
33.7	194	$C_{11}H_{14}O_3$	0	100	$C_{11}H_{14}O_3$	-0.9	0[b]
22.6	196	$C_{10}H_{12}O_4$	1	100	$C_{10}H_{12}O_4$	13.5	100
25.2	196	$C_{10}H_{12}O_4$	1	100	$C_{10}H_{12}O_4$	2.5	100
28.6	196	$C_{10}H_{12}O_4$	1	100	$C_{10}H_{12}O_4$	9.4	100
20.2	198	$C_{10}H_{14}O_4$[a]	0.9	100	$C_{10}H_{14}O_4$	2.4	100
20.7	199	$C_8H_9NO_5$	0.2	100	$C_8H_9NO_5$	-0.2	100
39.6	209	$C_{10}H_{11}NO_4$[a]	0	100	$C_{10}H_{11}NO_4$	4.3	100
27.8	210	$C_{11}H_{14}O_4$	0.9	100	$C_{11}H_{14}O_4$	1.4	100
31.7	210	$C_{11}H_{14}O_4$	0.9	100	$C_{11}H_{14}O_4$	2.8	11.88
21.3	213	$C_9H_{11}NO_5$	0.7	100	$C_9H_{11}NO_5$	0.5	100
21	214	$C_{11}H_{18}O_4$	0.4	100	$C_{11}H_{18}O_4$	2	100
18.6	236	$C_8H_{12}O_8$[a]	0.5	100	$C_8H_{12}O_8$	28.5	0[b]
31.8	238	$C_{12}H_{14}O_5$	0.9	100	$C_{12}H_{14}O_5$	9.9	100
22.2	243	$C_{10}H_{13}NO_6$	0.6	100	$C_{10}H_{13}NO_6$	-0.7	100
35.9	252	$C_{13}H_{16}O_5$	1.6	100	$C_{13}H_{16}O_5$	8.1	30.3
11.8	277	$C_9H_{11}NO_9$	0.5	100	$C_9H_{11}NO_9$	-5.2	100
12.8	277	$C_9H_{11}NO_9$	0.2	100	$C_9H_{11}NO_9$	0.9	100
28.8	292	$C_{15}H_{16}O_6$	1.2	100			
23.3	296	$C_{18}H_{16}O_4$	-0.2	100	$C_{18}H_{16}O_4$	3.5	100
36.1	317	$C_{16}H_{15}NO_6$	-0.3	100	$C_{16}H_{15}NO_6$	1.8	100
36.2	428	$C_{18}H_{20}O_{12}$	-0.1	100	$C_{18}H_{20}O_{12}$	-0.8	100

[a] Compound observed in positive and negative ionisation mode. [b] The measured isotopic distribution and abundance does not match for the selected molecular formula.

Table 3.4 - The molecular formulae (MF) and associated errors of the identified SOA compounds in experiment MC[high] using FTICR-MS and HPLC-QTOFMS in positive ionisation mode.

t_R	MW [g mol^{-1}]	FTICR-MS MF	Error [ppm]	Score [%]	HPLC-QTOFMS MF	Error [ppm]	Score [%]
34.3	98				$C_6H_{10}O$*	18	100
36.4	98				$C_6H_{10}O$*	14	100
44	98	$C_4H_2O_3$*	23.6	100	$C_6H_{10}O$*	12.7	100
33.7	120				$C_4H_8O_4$	31.3	100
28.2	146	$C_7H_{14}O_3$	-1.9	100	$C_8H_{12}O$*	30.1	100
18.5	151				$C_4H_9NO_5$	-21.2	100
30.2	152	$C_8H_8O_3$[a]	1.2	100	$C_8H_8O_3$	2.5	100
10.9	162	$C_{10}H_{12}O_2$	3.9	100	$C_{10}H_{12}O_2$	54.3	100
13.9	162	$C_{10}H_{12}O_2$	3.9	100	$C_6H_{12}O_5$	4.9	100
22.6	162	$C_{10}H_{10}O_2$	3.9	100	$C_{10}H_{10}O_2$	30.8	100
27.3	164				$C_{10}H_{12}O_2$	16.6	100
12.1	168	$C_9H_{12}O_3$*	4.7	100	$C_9H_{12}O_3$*	12.1	100
27.9	170	$C_8H_{10}O_4$*	4.4	100	$C_{11}H_{12}O_3$	-2.6	100
20.5	174				$C_8H_{14}O_4$*	-5.5	100
14.5	177				$C_5H_7NO_6$	-26.2	100
26.8	178				$C_{10}H_{14}O_2$	5	100
22.5	180	$C_{10}H_{12}O_3$*	4.2	100	$C_{10}H_{12}O_3$*	2	100
27.6	180				$C_{10}H_{12}O_3$	-7.8	100
36	180	$C_{10}H_{12}O_3$*	4.2	100	$C_7H_{16}O_5$*	2.9	100
23.3	182	$C_{10}H_{14}O_3$*	4.1	100	$C_{10}H_{14}O_3$*	-2.3	3.57
33.5	182	$C_{10}H_{14}O_3$*	4.4	100	$C_{10}H_{14}O_3$*	-43.3	1.18
10.2	184				$C_8H_8O_5$	48	0.02
15.7	188	$C_8H_{12}O_5$*	4.6	100	$C_8H_{12}O_5$*	-3.8	100
17.8	190	$C_{10}H_9NO_3$	1.4	100	$C_{10}H_9NO_3$	-0.9	100
19	190	$C_8H_{14}O_5$*	5.1	100	$C_8H_{14}O_5$*	-0.8	100
41.2	192	$C_9H_{20}O_4$*	3.9	100	$C_9H_{20}O_4$*	37.7	0[b]
19.8	196	$C_{10}H_{12}O_4$*	5	100	$C_{10}H_{12}O_4$*	9.4	100
10.8	198	$C_{13}H_{10}O_2$*	4.2	100	$C_{13}H_{10}O_2$*	-27.8	0.3
14.1	198	$C_{13}H_{10}O_2$*	3.9	100	$C_{13}H_{10}O_2$*	-22.9	3.11
16.3	198	$C_{10}H_{14}O_4$*	4.2	100	$C_{10}H_{14}O_4$*	24	100
20.2	198	$C_{10}H_{14}O_4$*[a]	4.2	90.07	$C_{10}H_{14}O_4$*	1.3	100
23.4	199				$C_{10}H_{17}NO_3$	-27.4	100
14.8	204	$C_{12}H_{12}O_3$*	16	100			
39.7	209	$C_{10}H_{11}NO_4$[a]	0.9	100	$C_{10}H_{11}NO_4$	6.9	100
19.1	212	$C_{11}H_{16}O_4$*	4.2	100			
33	212	$C_{11}H_{16}O_4$*	5.1	100	$C_{10}H_{18}O_6$	23.4	0.5
21.4	214	$C_{11}H_{18}O_4$*	5	100			
37.2	219	$C_{10}H_{20}O_5$*	3.7	100	$C_{10}H_{20}O_5$*	-33.9	0.9
37.9	219	$C_{10}H_{20}O_5$*	3.7	100	$C_{10}H_{20}O_5$*	-28	3.42

Table 3.4 - Continued...

t_R	MW [g mol^{-1}]	FTICR-MS MF	Error [ppm]	Score [%]	HPLC-QTOFMS MF	Error [ppm]	Score [%]
20.9	226	$C_{12}H_{18}O_4$*	5.4	100	$C_{12}H_{18}O_4$*	14.2	100
30.4	232	$C_{10}H_{16}O_6$	5.3	100	$C_{10}H_{16}O_6$	-10.7	100
36.2	234	$C_{11}H_{16}O_4$*	5.5	100	$C_{10}H_{18}O_6$	-11.7	100
45.6	234	$C_{11}H_{22}O_5$*	7	100	$C_{11}H_{22}O_5$*	-35.5	0.13
18.8	237	$C_8H_{12}O_8$[a]	-2.9	100	$C_8H_{12}O_8$	5.5	100
33.8	238	$C_{13}H_{18}O_4$*	5.4	100	$C_{13}H_{18}O_4$*	33.1	0 [b]
41.5	240	$C_9H_{14}O_6$*	5	100	$C_9H_{20}O_7$	-1.9	100
17.1	244	$C_{11}H_{16}O_6$*	5.6	100			
47.4	248	$C_{12}H_{24}O_5$*	4.7	100	$C_{12}H_{24}O_5$*	43.2	0 [b]
37.7	250	$C_{11}H_{22}O_6$*	6.2	100	$C_{11}H_{22}O_6$*	-17.4	4.07
43.2	256	$C_{14}H_{24}O_4$*	-3.3	100	$C_{14}H_{24}O_4$*	6.6	100
35.6	268	$C_{15}H_{24}O_4$*	4	100	$C_{15}H_{24}O_4$*	-19.6	3.2
44.1	276	$C_{17}H_{24}O_3$*	6.2	100	$C_{14}H_{28}O_5$*	27	0.02
8.9	286	$C_{19}H_{10}O_3$	5.2	100	$C_{19}H_{10}O_3$	-4.9	100
44.5	289	$C_{15}H_{15}NO_5$	-12.9	0.96	$C_{18}H_{27}NO_2$	-28.6	100
44	302	$C_{16}H_{30}O_5$*	6.2	100	$C_{16}H_{30}O_5$*	8	92.45

* Identified as [M+Na]$^+$, the Na adduct has been removed from molecular formula and molecular weight corrected. [a] Compound observed in positive and negative ionisation mode. [b] The measured isotopic distribution and abundance does not match for the selected molecular formula.

Table 3.5 - The 10 structurally identified SOA compounds including; retention time (t_R), molecular formula (MF) identification and associated errors using HPLC-ITMS, FTICR-MS and HPLC-QTOFMS
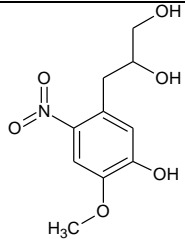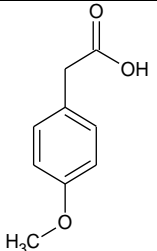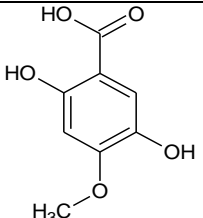
Compound	IUPAC name	Compound structure	MC[high]					
			MW [g mol^{-1}]	t_R	FTICR-MS MF	FTICR-MS MF error [ppm]	HPLC-QTOFMS MF	HPLC-QTOFMS MF error [ppm]
1	3-(5-hydroxy-4-methoxy-2-nitrophenyl)propane-1,2-diol		243	22.2	$C_{10}H_{13}NO_6$	0.6	$C_{10}H_{13}NO_6$	-0.7
2	(4-methoxyphenyl)acetic acid		166	28.1	$C_9H_{10}O_3$	0.8	$C_9H_{10}O_3$	1.2
3	2,5-dihydroxy-4-methoxybenzoic acid		184	10.2	a		$C_8H_8O_5$	48

Table 3.5 - Continued.......
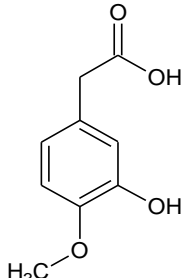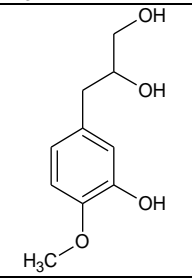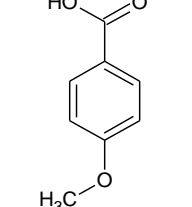
Compound	IUPAC name	Compound structure	MC[high]					
			MW [g mol^{-1}]	t_R	FTICR-MS MF	FTICR-MS MF error [ppm]	HPLC-QTOFMS MF	HPLC-QTOFMS MF error [ppm]
4	(3-hydroxy-4-methoxyphenyl)acetic acid		182	16.1	$C_9H_{10}O_4$	0.8	$C_9H_{10}O_4$	-0.3
5	3-(3-hydroxy-4-methoxyphenyl)propane-1,2-diol		198	20.2	$C_{10}H_{14}O_4$	0.9	$C_{10}H_{14}O_4$	2.4
6	4-methoxybenzoic acid		152	30.1	$C_8H_8O_3$	0.3	$C_8H_8O_3$	-1.4

Table 3.5 - Continued......
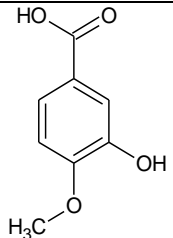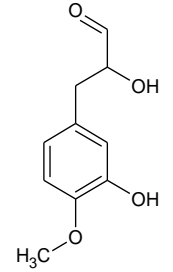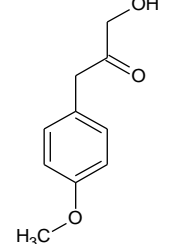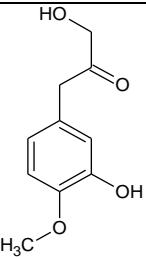
Compound	IUPAC name	Compound structure	MC[high]					
			MW [g mol⁻¹]	t_R	FTICR-MS MF	FTICR-MS MF error [ppm]	HPLC-QTOFMS MF	HPLC-QTOFMS MF error [ppm]
7	3-hydroxy-4-methoxybenzoic acid		168	33.0	$C_8H_8O_4$	0.7	$C_8H_8O_4$	0.2
8	2-hydroxy-3-(3-hydroxy-4-methoxyphenyl)propanal		196	25.2	$C_{10}H_{12}O_4$	1	$C_{10}H_{12}O_4$	2.5
9	1-hydroxy-3-(4-methoxyphenyl)propan-2-one		180	27.6	a		$C_{10}H_{12}O_3$	-7.8

Table 3.5 - Continued....

| Compound | IUPAC name | Compound structure | MC[high] | | | | | |
			MW [g mol^{-1}]	t_R	FTICR-MS MF	FTICR-MS MF error [ppm]	HPLC-QTOFMS MF	HPLC-QTOFMS MF error [ppm]
10	1-hydroxy-3-(3-hydroxy-4-methoxyphenyl)propan-2-one		196	19.8	$C_{10}H_{12}O_4$*	5	$C_{10}H_{12}O_4$*	9.4

[a] = Deprotonated or protonated molecular species not observed in FTICR-MS spectra due to low concentration. * Identified as [M+Na]$^+$, the Na adduct has been removed from molecular formula and molecular weight corrected.
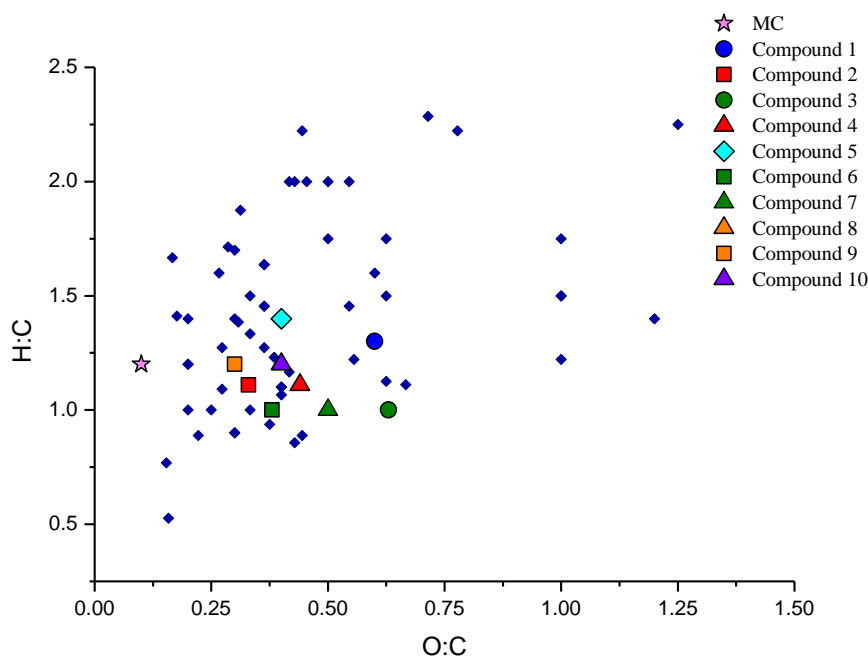
Figure 3.7 - Van Krevelen plot of the 79 SOA compounds observed in $MC_{[high]}$. Blue diamonds represent structurally unidentified compounds. Legend shows the structurally identified compounds 1 to 10, refer to Table 3.5 for compound identification. For the structurally identified compounds; related generations of compounds are shown in the same colour. The movement of the structurally identified compounds along the horizontal axis to higher O:C ratios, displays increasing oxidation through the addition of ˙OH. The diagonal movement towards lower H:C ratios, displays an decrease in the HC chain by CH_2. Compounds 8 and 10 are structural isomers; compound 8 is hidden by compound 10.

3.3.7   Calibrations

Calibrations were performed for 4-methoxybenzoic acid and (4-methoxyphenyl)acetic acid using the commercially available standards (Figure 3.8). Detector variation during sample analysis was determined for both compounds by measuring the chromatographic peak area of 4-methoxybenzoic acid in the 10 ppm ES mix (Chapter 2, Section 2.3.2.2). A 6% relative standard deviation is shown as the concentration error (i.e. plus/minus sign) and includes a detector variation of ~ 5% (based on 4 replicate measurements) plus a negligible amount for the PILS collection efficiency (see Section 3.2.2). The highest concentration of 4-methoxybenzoic acid and (4-methoxyphenyl)acetic acid observed in any one the PILS samples is reported. The percentage SOA mass was calculated by using the maximum amount of SOA formed. No corrections have been applied for wall loss or chamber dilution.

The concentrations of 4-methoxybenzoic acid and (4-methoxyphenyl)acetic acid in $MC_{[high]}$ were determined as 1.26 ± 0.08 and 0.41 ± 0.02 µg m^{-3}; representing a percentage SOA mass

of 0.44 ± 0.03 and 0.14 ± 0.01%, respectively. In MC$_{[low]}$, the concentration of 4-methoxybenzoic acid was determined as 0.23 ± 0.01 µg m^{-3}, corresponding to a percentage SOA mass of 0.26 ± 0.02%. The HPLC-ITMS intensity of (4-methoxyphenyl)acetic acid in the MC$_{[low]}$ experiment was observed below the limit of quantification (defined as 5 = S/N) and thus the concentration and percentage SOA mass for this compound could not be determined.
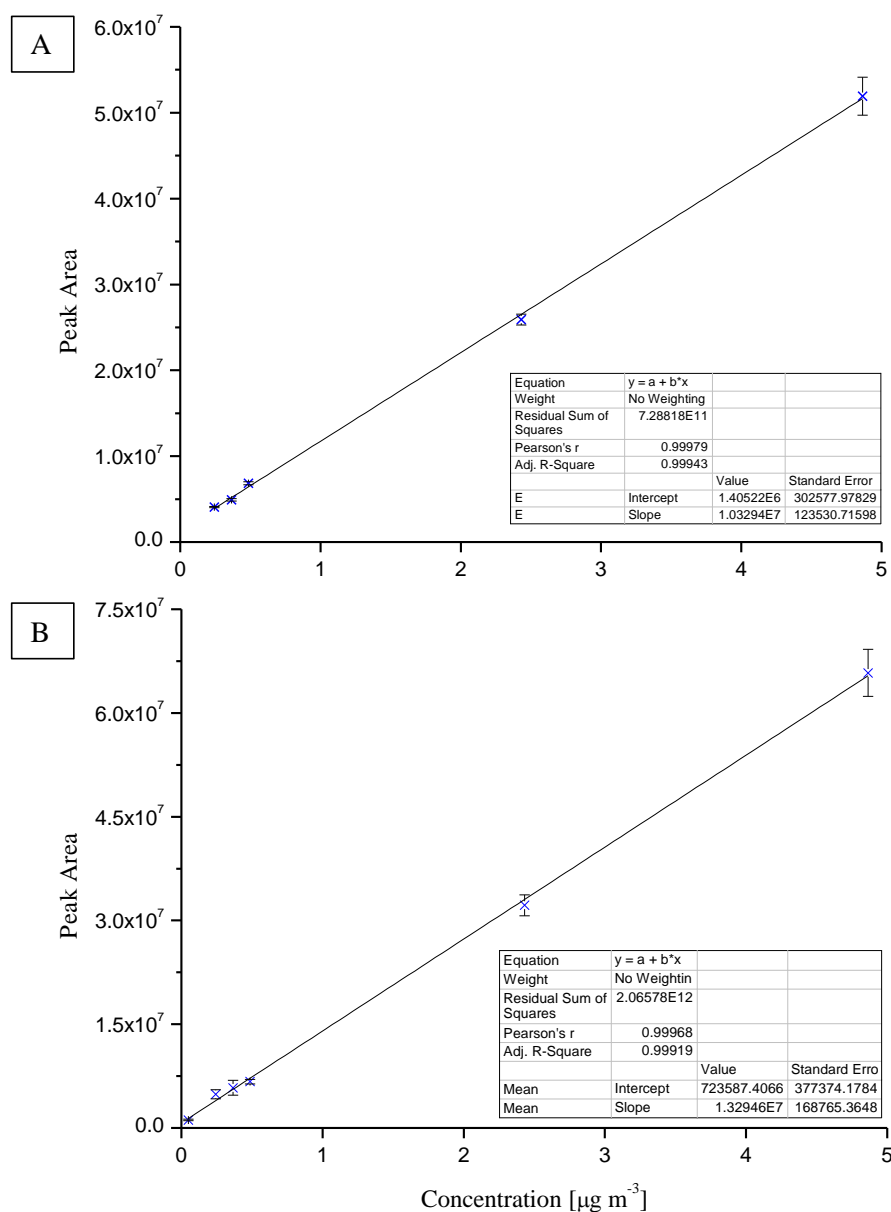
Figure 3.8 - HPLC-ITMS calibrations of (4-methoxyphenyl)acetic acid and 4-methoxybenzoic acid using the commercially available standards. A = (4-methoxyphenyl)acetic acid. B = 4-methoxybenzoic acid.

3.3.8   Compound Structure Assignment

The product ions of two deprotonated molecular species are discussed here as examples to illustrate the methodology used to assign SOA compound structures. Compound 1 with a MW of 243 g mol^{-1} was assigned the molecular formula $C_{10}H_{13}NO_6$ with 5 double bond equivalents (DBE). Compound 1 contains the same number of carbon atoms and one more degree of saturation than the original VOC precursor, methyl chavicol ($C_{10}H_{12}O$). In addition, compound 1 was identified in the first PILS sample containing SOA (shortest reaction time, between 41 to 71 minutes into the $MC_{[high]}$ experiment). The similarity of the carbon number, degree of saturation, and the identification of this compound during the initial particle growth, would suggest the structure of compound 1 was similar to that of the precursor, a substituted methoxyphenyl. The product ions of *m/z* 242 [M-H]$^-$ (compound 1) are summarized in Table 3.6. Compound 1 was identified as 3-(5-hydroxy-4-methoxy-2-nitrophenyl)propane-1,2-diol using the observed fragments discussed below and shown in Figure 3.9.

The highest intensity fragment ion at *m/z* 224 is due to the loss of water (H_2O) occurring through hydrogen abstraction, Figure 3.9A. The base peak loss of H_2O would suggest the presence of an aliphatic alcohol, most likely terminal. The loss of H_2O results in an intermolecular rearrangement of the fragment ion, resulting in the formation of a double bond, indicated by the increase in the DBE by 1. The fragment ion at *m/z* 182 has formed as a result of a subsequent loss of C_2H_2O from *m/z* 224, which is supported by the decrease in the DBE by 1 for the remaining fragment ion. The fragment ion at *m/z* 182 results from a total loss of $C_2H_4O_2$, suggesting the presence of a second hydroxyl group on the leaving group, most likely on the adjacent carbon to the first alcohol group, Figure 3.9B. The fragment ion at *m/z* 167 has formed as a result of an odd electron cleavage (OE), resulting in the formation of $[C_7H_5NO_4]^{\bullet-}$ and the loss of $[C_3H_7O_2]^{\bullet}$, Figure 3.9C. OE cleavages are unusual in CID and are often associated with resonance stabilised ring structures and nitrogen containing functional groups (Hayen et al., 2002; Fu et al., 2006; Holčapek et al., 2007; Holčapek et al., 2010).

Table 3.6 - Deprotonated molecular species fragmentation for compound 1, obtained from the use of the HPLC-ITMS[2] and the HPLC-QTOFMS[2]

MF	[M-H]⁻	DBE	Fragment ion [m/z]	Fragment ion MF	DBE	Loss [Da]	Electron fragmentation	Fragment ion MF error [ppm]	MF Score [%]	Fragmentation shown
$C_{10}H_{13}NO_6$	242	5	**224**	**$C_{10}H_{10}NO_5$**	**6**	**18**	**EE**	**-2.1**	**100**	**Figure 3.9A**
			182	$C_8H_8NO_4$	5	(18+42) = 60	EE	-1	100	Figure 3.9B
			167	$C_7H_5NO_4$	5*	(18+57) = 75	OE	8.8	100	Figure 3.9C
			137	$C_7H_5O_3$	4**	105	OE	-19.2	100	Figure 3.9C

The highest intensity fragment ion is shown in bold. DBE = double bond equivalent. Electron fragmentation, EE = even electron, OE = odd electron. MF = molecular formula. *DBE was manually calculated, as automated DBE calculation is incorrect for radical fragment ions (DBE = 5.5 - 0.5 (for one 'hydrogen atom deficiency') = 5, see Pellegrin (1983) for the calculation of DBE and DBE correction for radical ions). **DBE manually calculated, (DBE = 5 - 1 (for two 'hydrogen atom deficiencies') = 4).
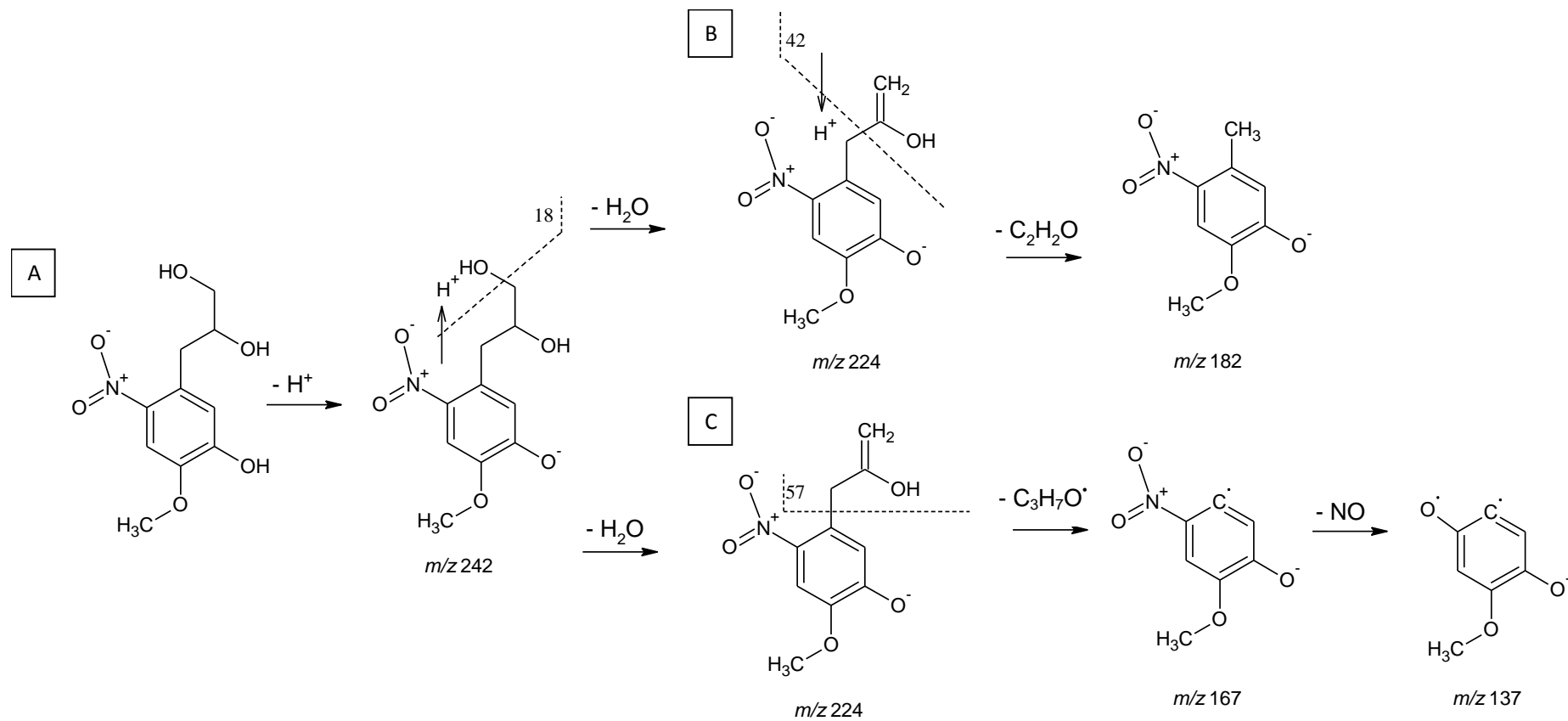
Figure 3.9 - Proposed deprotonated molecular species fragmentation for compound 1 in negative ionisation mode. Dashed lines indicate the location of fragmentation.

Assuming the remaining deprotonated radical fragment ion at m/z 167 $[C_7H_5NO_4]^{\cdot-}$ is a substituted methoxyphenyl, the subtraction of the methoxy $[OCH_3]$ and aromatic $[C_6H_2]^-$ group from the molecular formula would leave N_1O_3 unaccounted for. This suggests either a nitrate group $(R-ONO_2)$, or a hydroxyl $(R-OH)$ and a nitro $(R-NO_2)$ group are attached to the ring. The presence of a nitrate group on the ring is likely to result in the loss of NO_2 or ONO_2 from the fragmentation of the carbon-oxygen or oxygen-nitrogen bond during CID (Zhao and Yinon, 2002; Holčapek et al., 2010). Furthermore, the lability of the nitrate group often results in spontaneous fragmentation in the softest ESI conditions, resulting in the fragment ions ONO_2 and NO_2 at m/z 63 and m/z 47, respectively (Yinon et al., 1997; Holčapek et al., 2010). However, no fragment ion at m/z 63 for ONO_2 was observed. A peak at m/z 137 (intensity 1.33%) was observed and was attributed to $[C_7H_5O_3]^{\cdot-}$, the loss of NO from the fragment ion at m/z 167 $[C_7H_5NO_4]^{\cdot-}$, Figure 3.9C. The loss of NO is a typical for nitro functional groups in negative ionisation mode using CID (Yinon et al., 1997; Fu et al., 2006; Schmidt et al., 2006; Holčapek et al., 2010). The rearrangement of bonds from R-NO2 to R-ONO results in the loss of NO (Schmidt et al., 2006). Nitro functional groups usually result in the loss of NO and NO_2. However, the loss of only NO has been observed for some compounds containing a nitro functional group and has previously been suggested to be the result of an electron donating substituent in the para position to the nitro group, enhancing the loss of NO by resonance stabilisation (Bursey and McLafferty, 1966; Bursey, 1969).

The location of phenyl substitutions has proved to be difficult to determine using CID due to the lack of ring fragmentation as a result of resonance stabilisation. In addition, the N-containing compounds that were observed to undergo ring fragmentation exhibited complex re-arrangements making the identification of these compound structures a difficult task. The most likely locations of phenyl substitutions can be identified however, by considering the formation mechanisms of these compounds in the gas phase (Calvert et al., 2002; Ziemann and Atkinson, 2012). Methyl chavicol has two phenyl substituents, a methoxy group and an hydrocarbon (HC) chain, both of which are ortho, para directing (March, 1992). The stronger activating group of the two phenyl substituents, the methoxy group, will determine the most energetically favoured and resonance stabilised position of an addition to the ring (March, 1992). The para position to the methoxy group is occupied by the HC chain and therefore the initial oxidation of a hydroxyl radical to the ring of methyl chavicol would be most energetically favoured at the ortho position to the methoxy group (Ziemann and Atkinson, 2012). The location of the nitro group on the ring is more difficult to assign. Assuming the hydroxyl radical is already attached to the ring, the most strongly activating

group would now be the hydroxyl group, which is also ortho, para directing (March, 1992). The ortho position to the hydroxyl group is more sterically hindered by the adjacent HC chain and hydroxyl group, compared to the para position, which is only sterically hindered by the HC chain. It is therefore suggested that the nitro group is located in the para position to the hydroxyl group. The suggested location of the nitro and hydroxyl group on the ring is also supported by the mechanism suggested in Bursey and McLafferty (1966) and Bursey (1969), where the loss of only NO is observed for a nitro functional group during CID when an activating group is located in the para position to the nitro group.

Compound 5, with a MW of 198 g mol^{-1} was assigned the molecular formula $C_{10}H_{14}O_4$ with 4 DBE. The product ions of m/z 197 [M-H]$^-$ (compound 5) are summarized in Table 3.7. Compound 5 was identified as 3-(3-hydroxy-4-methoxyphenyl)propane-1,2-diol from the product ions discussed here and shown in Figure 3.10. Both compounds 1 and 5 exhibit similar HC chain fragmentation, with the loss of 18 Da (H_2O) and 42 Da ($C_2H_2O_2$), Figure 3.10A and B. The product ion [$C_7H_7O_2$]$^{\cdot-}$ at m/z 123 resulted from an even electron (EE) loss of $C_3H_6O_2$, unlike the OE loss of [$C_3H_7O_2$]$^{\cdot}$ observed for compound 1, Figure 3.10C. Compound 5 does not have a nitro group present on the ring and as a result the resonance stabilization of the aromatic ring is lower than in compound 1. The decrease in resonance stabilisation results in an EE cleavage and the abstraction of a hydrogen from the leaving group to the aromatic ring. Hydrogen abstraction from the loss group results in an intermolecular re-arrangement and the loss of $C_3H_6O_2$. Therefore, the same HC chain has been suggested for both compounds 1 and 5. Assuming a methoxyphenyl sub-structure, the deprotonated product ion would leave [C_6H_3O]$^-$ from product ion [$C_7H_7O_2$]$^-$ at m/z 123, suggesting a hydroxyl group is attached to the aromatic ring.

Table 3.7 - Deprotonated molecular species fragmentation for compound 5, obtained from the use of the HPLC-ITMS^2 and the HPLC-QTOFMS^2

MF	[M-H]$^-$	DBE	Fragment ion [*m/z*]	Fragment ion MF	DBE	Loss [Da]	Electron fragmentation	Fragment ion MF error [ppm]	MF Score [%]	Fragmentation shown
$C_{10}H_{14}O_4$	197	4	**179**	**$C_{10}H_{11}O_3$**	**5**	**18**	**EE**	**-19.3**	**100**	**Figure 3.10A**
			137	$C_8H_9O_2$	4	(18+42) = 60	EE	-0.5	100	Figure 3.10B
			123	$C_7H_7O_2$	4	74	EE	-3.4	100	Figure 3.10C

The highest intensity fragment ion is shown in bold. DBE = double bond equivalent. Electron fragmentation, EE = even electron. MF = molecular formula.
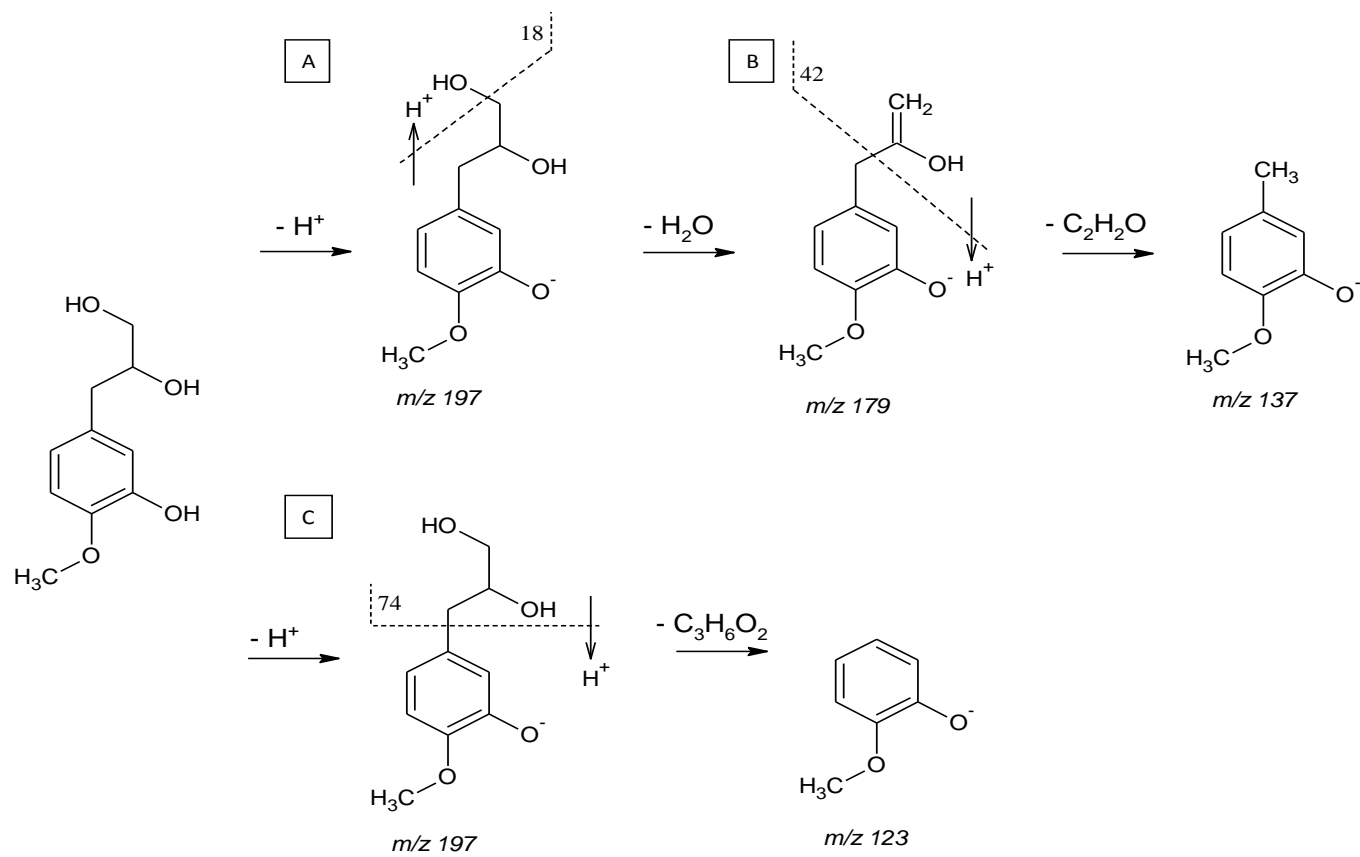
Figure 3.10 - Proposed deprotonated molecular species fragmentation for compound 5 in negative ionisation mode. Dashed lines indicate the location of fragmentation.

3.3.9 Mechanism of Formation

A proposed mechanism for the formation of compounds 1, 5, 8, 9 and 10 is shown in Figures 3.11 and 3.12. The formation of these compounds can be rationalised as the products of methyl chavicol oxidation by considering typical gas phase oxidation mechanisms (Calvert et al., 2002; Ziemann and Atkinson, 2012). The reaction rate constants of methyl chavicol with $^\bullet$OH and O_3 have previously been determined as $5.20 \pm 0.78 \times 10^{-11}$ and $1.03 \pm 0.23 \times 10^{-17}$ cm^3 molecule^{-1} s^{-1}, respectively (Gai et al., 2013).

The proportion of methyl chavicol reacting with $^\bullet$OH and O_3 can be calculated using Eq. 3.8 and Eq. 3.9, respectively; where $k_{MC + OH}$ is the rate constant of the reaction of methyl chavicol with $^\bullet$OH (cm^3 molecule^{-1} s^{-1}), $k_{MC + O3}$ is the rate constant of the reaction of methyl chavicol with O_3 (cm^3 molecule^{-1} s^{-1}), [OH] and [O_3] is the measured concentration of $^\bullet$OH (ppbv) and O_3 (ppbv), respectively. The proportion of methyl chavicol reacting with $^\bullet$OH and O_3 during MC$_{[low]}$ and MC$_{[high]}$ is shown in Figure 3.13; where throughout both experiments the reaction of methyl chavicol with $^\bullet$OH is observed to dominate over the reaction with O_3. The increasing proportion of methyl chavicol reacting with O_3 throughout both experiments is due to increasing O_3 concentration as the chemistry in both the experiments progresses (*i.e.* conversion of NO to NO$_2$, followed by the photolysis of NO$_2$ to form O_3).

Eq. 3.8
$$\% \, OH = \left(\frac{k_{MC+OH}[OH]}{(k_{MC+OH}[OH] + k_{MC+O3}[O_3])} \right) \times 100$$

Eq. 3.9
$$\% \, O_3 = \left(\frac{k_{MC+O3}[O_3]}{(k_{MC+O3}[O_3] + k_{MC+OH}[OH])} \right) \times 100$$

The initial oxidation of methyl chavicol will proceed mainly through the $^\bullet$OH radical addition mechanism (Atkinson, 1997b; Calvert et al., 2002; Ziemann and Atkinson, 2012) and can attack the ring and/or the HC chain. $^\bullet$OH radical addition can occur on either carbon of the double bond of the HC chain, resulting in the formation of primary and secondary β-hydroxyalkyl radicals, with the secondary β-hydroxyalkyl radical pathway being the most favoured (approximately 85% using Peeters et al. (2007) $^\bullet$OH addition structure activity relationship) (Cvetanovic, 1976; Atkinson, 1997b, 2000). The resulting β-hydroxyalkyl radicals react predominantly with O_2 to form β-hydroxyperoxy radicals. The high concentration of NO at the beginning of MC$_{[high]}$ and MC$_{[low]}$ will result in the conversion of NO to NO$_2$ (leading to O_3 formation) and the formation of β-hydroxyalkoxy radicals as the

major pathway. β-hydroxyalkoxy radicals can react with O_2, decompose or isomerise. Decomposition and isomerisation are expected to be the dominant pathways, with the exception of the $HOCH_2CH_2O^\bullet$ radical (from ethene + $^\bullet OH$), for which decomposition and reaction with O_2 can be competitive (Atkinson, 1997b, a; Fuchs et al., 2011).

For both types of β-hydroxyalkoxy radicals formed, decomposition followed by rapid reaction with O_2 leads to the formation of formaldehyde, HO_2 and (4-methoxyphenyl)acetaldehyde (Atkinson, 1997b; Orlando et al., 2003). Isomerisation through a 1, 5 H-atom shift from the aromatic ring to the HC chain is suggested to be of minor importance due to the resonance stability of the ring. The reaction with O_2 (minor pathway) would result in the loss of HO_2 and the formation of the observed first generation compound, 1-hydroxy-3-(4-methoxyphenyl)propan-2-one (compound 9), Figure 3.11(A). Further oxidation of this compound through the addition of a hydroxyl radical to the ring results in the formation of 1-hydroxy-3-(3-hydroxy-4-methoxyphenyl)propan-2-one (compound 10), Figure 3.11(B). As discussed in the previous Section, the initial hydroxyl addition to the ring will occur at the ortho position to the methoxy group, the position which is most energetically favoured and resonance stabilised. Compound 8, 2-hydroxy-3-(3-hydroxy-4-methoxyphenyl)propanal, is also suggested to be a second generation compound which has formed through the oxidation of the primary β-hydroxyalkoxy radicals with O_2 (the less favoured pathway) and has been further oxidised by the addition of a hydroxyl radical to the ring, Figure 3.12(A).
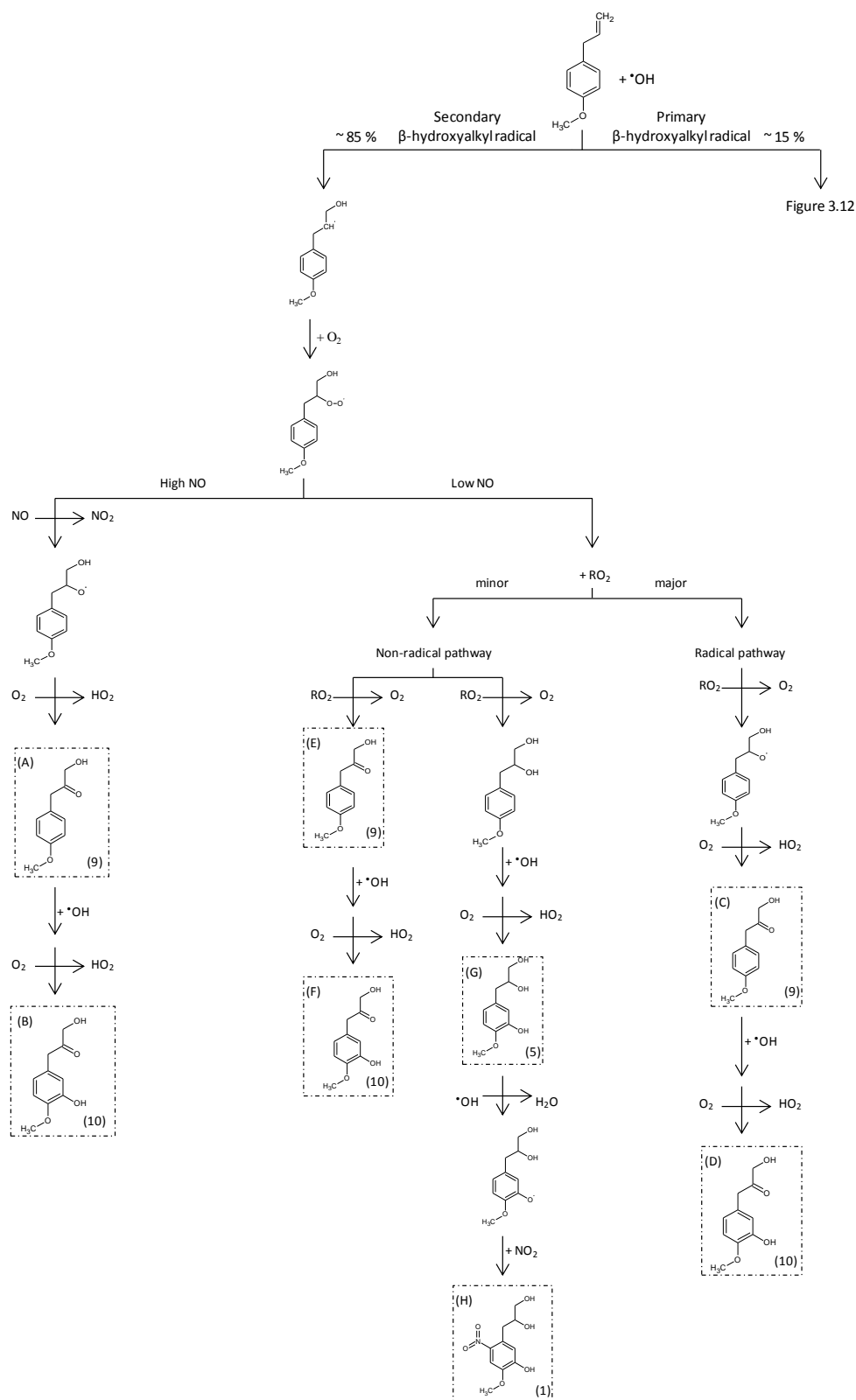
Figure 3.11 - Mechanism of formation for the identified SOA compounds through the secondary β- hydroxyalkyl radical pathway, compounds 1, 5, 9 and 10, shown in brackets, refer to Table 3.5 for compound identification. See text for the explanation of the mechanism, letters refer to the text explanation. Boxes highlight identified SOA compounds.
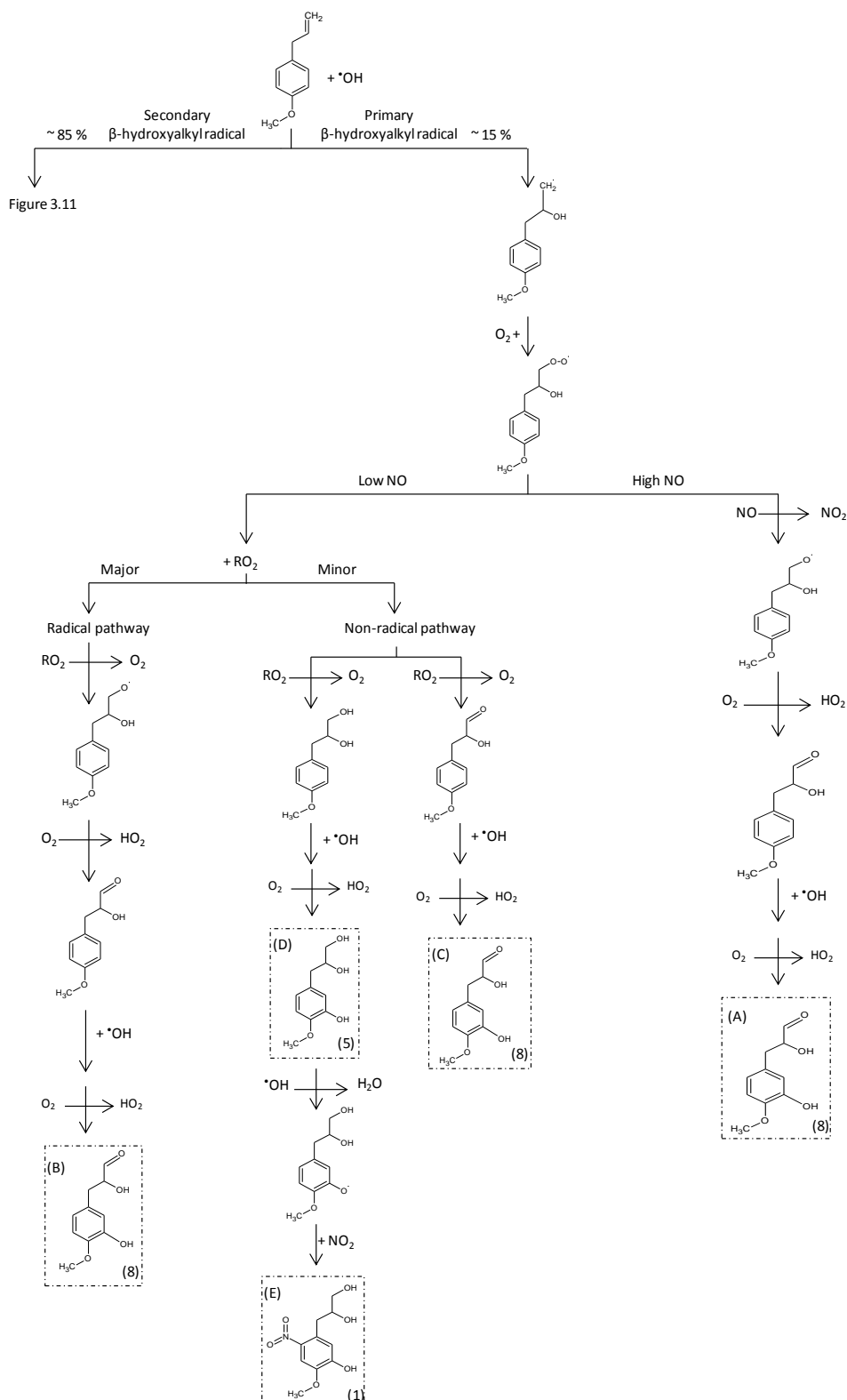
Figure 3.12 - Mechanism of formation for the identified SOA compounds through the primary β-hydroxyalkyl radical pathway, compounds 1, 5 and 8, shown in brackets, refer to Table 3.5 for compound identification. See text for the explanation of the mechanism, letters refer to the text explanation. Boxes highlight identified SOA compounds.
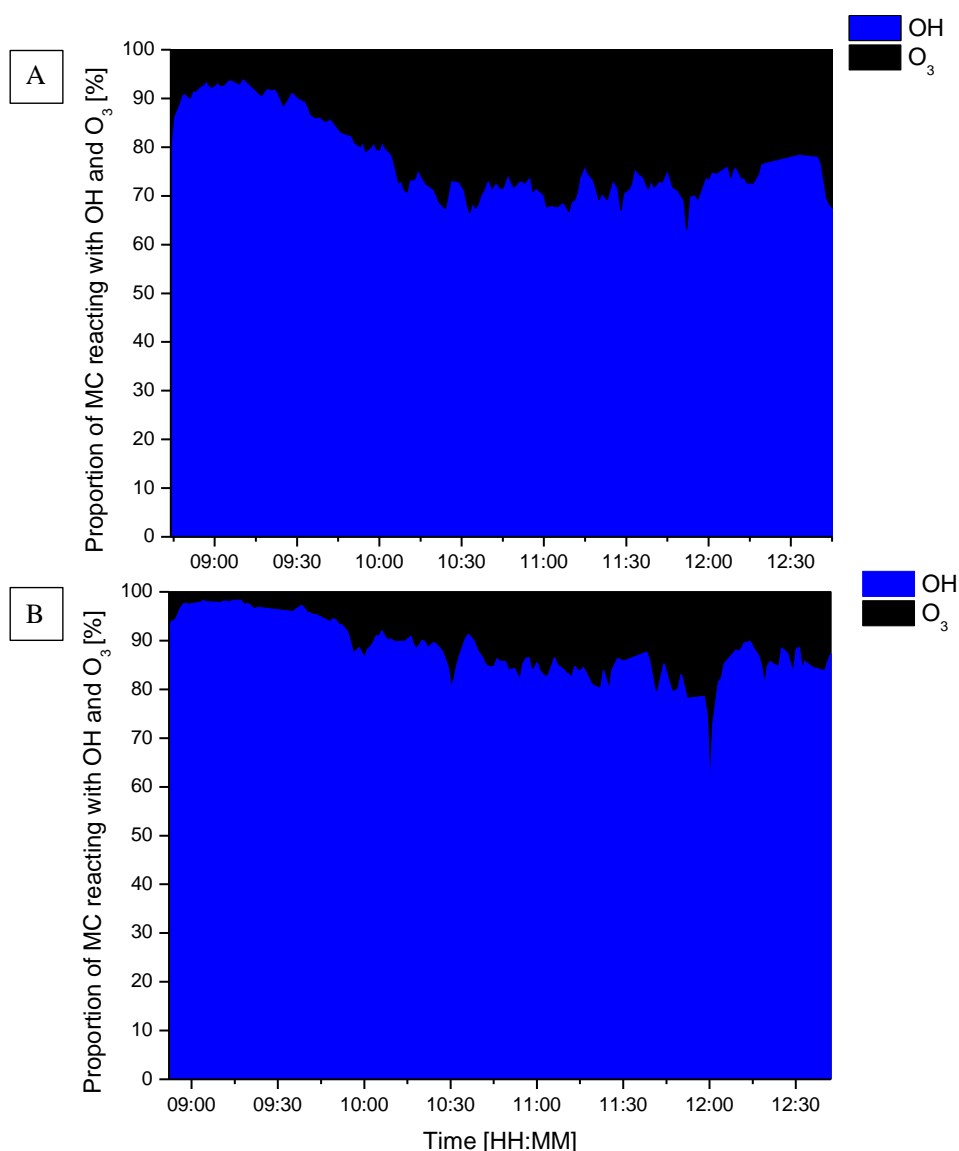
Figure 3.13 - Proportion of methyl chavicol (MC) reacting with ·OH and O_3 at each measured time point during $MC_{[high]}$ (A) and $MC_{[low]}$ (B).

As a relatively "low NO_x state" is entered in $MC_{[high]}$ and $MC_{[low]}$ the RO_2 + HO_2 (dominate pathway) or RO_2 reaction will begin to dominate over the competing reaction with NO (Stockwell et al., 1990; Atkinson, 1997b). The cross/self reaction of β-hydroxyperoxy radicals will proceed mainly through two pathways; the radical pathway and non-radical pathway (hydrogen abstraction), with the radical pathway accounting for approximately 30 - 80% of the RO_2 + RO_2 reaction (Madronich and Calvert, 1990; Atkinson, 1997b). The radical pathway (major pathway) will result in the formation of β-hydroxyalkoxy radicals with the loss of O_2. The β-hydroxyalkoxy radicals can then undergo oxidation through the same mechanisms as discussed above, resulting in a secondary pathway for the formation of compounds 8, 9 and 10, Figure 3.12 (B), Figure 3.11(C) and (D), respectively. A third minor

pathway to the formation of compounds 8, 9 and 10 can also occur through the $RO_2 + RO_2$ non radical pathway; where one peroxy radical abstracts a hydrogen atom from another peroxy radical, resulting in the formation of an alcohol and carbonyl, respectively, with the loss of O_2 (Howard and Ingold, 1968; Madronich and Calvert, 1990). The hydrogen atom is abstracted from the carbon bonded to the peroxy radical, thus the abstraction of a hydrogen atom from a secondary β-hydroxyperoxy radical will result in the formation of 1-hydroxy-3-(4-methoxyphenyl)propan-2-one (compound 9), Figure 3.11(E). The further oxidation of this compound though the reaction with $^•OH$ will result in the formation of 1-hydroxy-3-(3-hydroxy-4-methoxyphenyl)propan-2-one (compound 10), Figure 3.11(F). Moreover, the abstraction of a hydrogen from a primary β-hydroxyperoxy radical followed by the further oxidation of an $^•OH$ radical to the ring, will result in the formation of 2-hydroxy-3-(3-hydroxy-4-methoxyphenyl)propanal (compound 8), Figure 3.12(C).

The formation of the diol on the HC chain of compound 1 [3-(5-hydroxy-4-methoxy-2-nitrophenyl)propane-1,2-diol], and compound 5 [3-(3-hydroxy-4-methoxyphenyl)propane-1,2-diol], could have occurred through two mechanisms; unimolecular isomerisation of the β-hydroxyalkoxy radical through a 1,5 H-atom shift, or the self/cross RO_2 reactions of the β-hydroxyperoxy radicals through the non-radical pathway. The isomerisation pathway would seem unlikely due to the formation of a alkyl radical on the carbon where the H-atom was abstracted, which could decompose, isomerise, or react with $O_{2,}$ with the latter resulting in the formation of a more oxidised product than observed. Decomposition would result in the formation of a compound with fewer carbon atoms than required, and isomerisation would still result in an alkyl radical. The self/cross reactions of β-hydroxyperoxy radicals would appear to be the more likely pathway, particularly under low NO_x conditions. After the formation of a diol on the HC chain, the further oxidation *via* hydroxyl radical addition to the ring would result in the formation of the third generation SOA compound, 3-(3-hydroxy-4-methoxyphenyl)propane-1,2-diol (compound 5), Figure 3.11(G) and Figure 3.12(D). Further addition of NO_2 to the ring of compound 5 through the hydrogen atom abstraction pathway leads to the formation of a fourth generation SOA compound 3-(5-hydroxy-4-methoxy-2-nitrophenyl)propane-1,2-diol (Compound 1), Figure 3.11(H) and Figure 3.12(E). A hydroxyl radical can abstract a hydrogen atom from the oxygen-hydrogen bond of the hydroxyl group on the substituted phenol, resulting in the formation of a phenoxy radical and the loss of H_2O (Atkinson, 1994; Forstner et al., 1997; Atkinson, 2000). The phenoxy radical can then react with NO_2 to form a substituted nitrophenol (Atkinson, 1994; Forstner et al., 1997; Atkinson, 2000).

Compounds 2, 3, 4, 6 and 7, contain acid functional groups and less carbon atoms than the original VOC precursor, methyl chavicol. These compounds appear to be later generation SOA species and could have formed through a number of potential mechanisms, such as reactions with ozone (O'Neal and Blumstein, 1973; Neeb et al., 1996; Calvert et al., 2000; Orzechowska and Paulson, 2005), and/or with hydroxyl radicals (Forstner et al., 1997; Gai et al., 2013), although the detailed reaction mechanisms for the formation of organic acids from hydroxyl radicals has not been properly established (Carlton et al., 2009). Compounds 4 and 7 appear to be the further oxidation products of compounds 2 and 6, through the addition of a hydroxyl radical to ring. In addition, compound 3 appears to be the further oxidation product of compound 7, through a second addition of a hydroxyl radical to the ring. Here it is suggested, that the second addition of the hydroxyl radical to the ring of compound 7 will be in the para position to the hydroxyl group, the most resonance stabilised and least sterically hindered position.

3.3.10 The Effect of NO$_x$ on SOA Formation

Interestingly, a larger SOA yield was obtained in MC$_{[high]}$ than in MC$_{MNOx}$, where a higher NO$_x$ level was used. For the vast majority of VOC precursors (particularly those containing 10 carbon atoms or fewer), SOA yields are observed to significantly decrease with increasing NO$_x$ (Kroll and Seinfeld, 2008). The SOA yields of isoprene (Kroll et al., 2006), monoterpenes (α-pinene and β-pinene (Hatakeyama et al., 1991; Pandis et al., 1991; Zhang et al., 1992; Presto et al., 2005; Ng et al., 2007b)) and simple aromatics (toluene (Hurley et al., 2001; Johnson et al., 2004), m-xylene (Song et al., 2005) and benzene (Ng et al., 2007a)) have all been found to decrease with increasing NO$_x$. Generally, the reverse is observed for larger VOCs containing 10 or more carbon atoms. The SOA yields of two sesquiterpenes (aromadendrene and longifolene) (Ng et al., 2007b), pinonaldehyde and n-tridecanal (Chacon-Madrid and Donahue, 2011; Chacon-Madrid et al., 2013) and cyclododecane (Cappa et al., 2013) have all been found to increase with increasing NO$_x$. However, this trend of larger VOC precursors displaying higher SOA yields with increasing NO$_x$ should be used with caution. Recent studies have found a number of VOCs containing 10 or more carbon atoms do not follow this trend, with the SOA yields of dodecane, 2-methylundecane, hexylcyclohexane (Cappa et al., 2013), naphthalene and its alkyl derivatives (1-methylnapthalene, 2-methylnapthalene and 1,2-dimethylnapthalene) (Chan et al., 2009) found to decrease with increasing NO$_x$. Moreover, the photo-oxidation of benzene and ozonolyisis of limonene has been found to show little or no NO$_x$ dependence (Martín-Reviejo and Wirtz, 2005; Zhang et al., 2006), suggesting the importance of other factors on

SOA formation, such as the VOC compound structure (branched, straight chain, cyclic, aromatic), reactivity, product volatility and stability (dissociation / photolysis degradation) (Kanakidou et al., 2005; Chacon-Madrid and Donahue, 2011; Cappa et al., 2013).

The effect of the NO_x ratio on SOA formation can be significant. In some cases, SOA formation can be completely suppressed in high NO_x or NO environments (Presto et al., 2005; Surratt et al., 2010; Eddingsaas et al., 2012). This so called "NO_x effect" is the result of competitive RO_2 chemistry. In high NO_x environments, VOCs which form hydroxyperoxy radicals (RO_2) upon oxidation, will preferentially react with NO, resulting in the conversion of NO to NO_2 (leading to O_3 formation) and formation of a hydroxyalkoxy radicals ($RO^•$).. The hydroxyalkoxy radicals can then undergo dissociation (decomposition), isomerisation or reaction with O_2 or NO_2, with the latter (providing sufficient NO_2 concentration is available), resulting in the formation of organic nitrates (R1a). It is worth noting however, if the NO_2 concentration is high, hydroxyperoxy radicals (RO_2) can react with NO_2, forming peroxy nitrates, as shown in R1b. These species are short lived, undergoing thermal dissociation back to the reactants with lifetimes of approximately 0.1-1 s at 298 K (Zabel, 1995; Atkinson, 1997b, 2000). Although whilst these species are short lived, they are also of low volatility, and have subsequently been suggested to be important in the initial stages of SOA formation (Kroll and Seinfeld, 2008).

R1a $\qquad\qquad\qquad\qquad RO^• + NO_2 \rightarrow RONO_2$

R1b $\qquad\qquad\qquad\qquad RO_2 + NO_2 \rightarrow ROONO_2$

At low NO concentrations, hydroxyperoxy radicals can react with HO_2 or as previously discussed, undergo cross/self reactions with other hydroxyperoxy radicals resulting in the formation of hydroxyalkoxy radicals (R2a), or alcohol and carbonyl containing species (R2b). Alternatively, hydroxyperoxy radicals can react with HO_2 resulting in the formation of hydroperoxides (R2c); a low volatility species which has also been suggested to be involved in the initial stages of SOA formation in the oxidation of a variety of VOCs (*e.g.* α- and β-pinene, isoprene (Bonn et al., 2004; Kroll et al., 2006)).

R2a $\qquad\qquad\qquad\qquad RO_2 + RO_2 \rightarrow 2RO^• + O_2$

R2b $\qquad\qquad\qquad\qquad RO_2 + RO_2 \rightarrow ROH + R{=}O + O_2$

R2c $\qquad\qquad\qquad\qquad RO_2 + HO_2 \rightarrow ROOH + O_2$

The level of NO_x used can therefore have a considerable effect on the chemical speciation and the yield distribution of the oxidation products formed. As a result, this can affect the timing of SOA formation, the amount of aerosol mass formed and the SOA yields. The NO_x effect can however, be insightful into the mechanisms which produce sufficiently low volatility species to result in SOA formation. For example, the photo-oxidation of α-pinene in the presence of high NO (VOC/NO_x ~ 0.45), results in the complete suppression of SOA formation *via* homogenous nucleation (Presto et al., 2005). Therefore, the α-pinene oxidation products formed in high NO environments are not of low enough volatility and are not formed in sufficient quantities to be able to overcome their saturation concentrations. Consequently, no SOA is formed until a relatively low NO environment has been entered (*i.e.* after sufficient time has passed for the saturation concentration to be achieved, or when species of lower volatility are able to form through reaction pathways which are favoured in high NO_2 environments (*e.g.* organic nitrates (R1a) and/or peroxynitrates (R1b)) and/or low NO environments, (*e.g.* peroxides (R2c)).

In all three methyl chavicol photo-oxidation experiments, SOA formation did not begin until a relatively low NO environment was entered (< ~ 32 ppbv) (Section 3.3.2, Figure 3.5). This delay in SOA formation until a relatively low NO environment is entered is often observed in classical photo-oxidation experiments with VOCs which display increasing SOA yields with decreasing NO_x; in contrast to that of methyl chavicol (*cf.* (Kroll and Seinfeld, 2008)). The time dependent growth curves of the photo-oxidation experiments discussed are shown in Figure 3.14; where the amount of aerosol mass formed (ΔM_0, μg m^{-3}) was plotted against the amount of methyl chavicol reacted (ΔMC, μg m^{-3}) at each measured time period, over the duration of the experiment. The delay in SOA formation until a relatively low NO environment is entered, can be observed in Figure 3.14; where the growth curve does not display a gradual increase in aerosol mass at the beginning of the experiment, remaining at $\Delta M_0 = ~ 0$ for a certain period of time. As previously discussed (Section 3.2.2), the first 30 minutes of the $MC_{[high]}$ experiment was removed in Figures 3.14 due to the fluctuating VOC precursor concentration. As a result, a number of the data points in $MC_{[high]}$ where $\Delta M_0 = ~ 0$ cannot be observed.
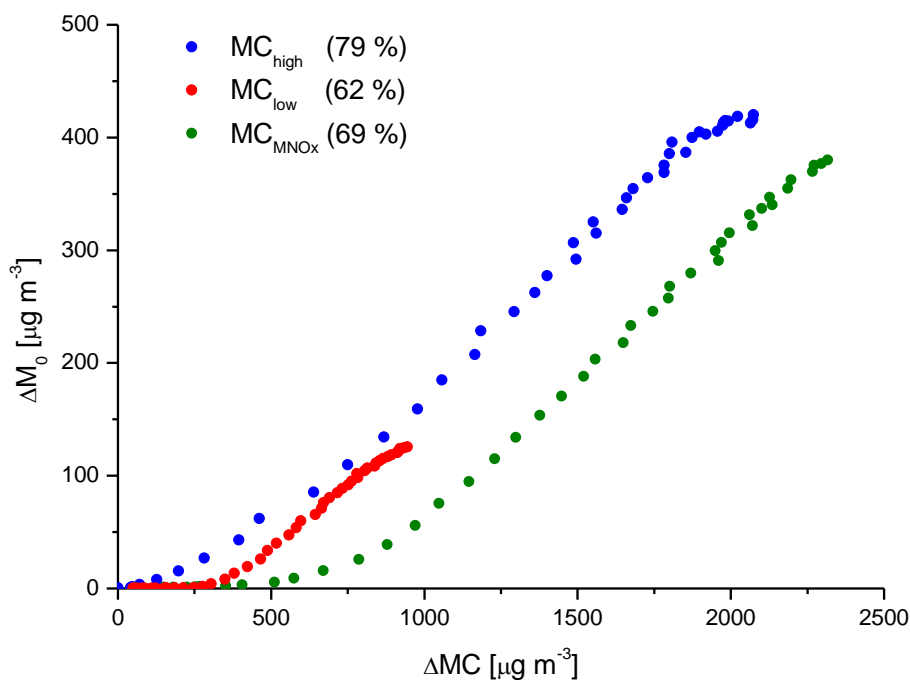
Figure 3.14 - Time dependent growth curve of experiments $MC_{[low]}$, $MC_{[high]}$ and MC_{MNOx}. The total amount of methyl chavicol reacted in each experiment is shown in brackets.

It is worth noting that a time dependent methyl chavicol photo-oxidation growth curve has previously been shown in literature; where no significant delay in SOA formation was observed (Ng et al., 2006). However, there are a number of key differences between this study and the study performed by Ng et al. (2006). In contrast to the classical photo-oxidation experiments performed here, Ng et al. (2006) added an additional source of ˙OH radicals (HONO) into the chamber before initiating photo-oxidation. The addition of HONO results in a burst of ˙OH radicals when photo-oxidation is initiated. The higher ˙OH concentration at the beginning of the experiment results in a faster rate of oxidation, and thus a faster rate of SOA formation (Ng et al., 2007a). Furthermore, Ng et al. (2006) used ammonium sulfate seed, compared to the nucleation only experiments performed here. The use of ammonium sulfate seed has been shown to increase the amount of aerosol mass formed from the oxidation of aromatic precursors, in the initial stages of SOA formation (Kroll et al., 2007; Lu et al., 2009; Huang et al., 2013). Moreover, the VOC/NO_x investigated in Ng et al. (2006) was lower ($VOC/NO_x \sim 0.8$) than the VOC/NO_x investigated in this study ($VOC/NO_x \sim 5$). As shown in Figure 3.14, the use of a higher NO_x level (*i.e.* lower VOC/NO_x ratio) resulted in a larger amount of aerosol mass formed for a smaller amount of methyl chavicol reacted; where in the initial stages of SOA formation the $MC_{[high]}$ growth curve increases from $\Delta M_0 = \sim 0$ faster than in MC_{MNOx}.

Interestingly, initial SOA formation in $MC_{[high]}$ and MC_{MNOx} was observed at approximately the same time (~ 40 minutes) after the opening of the chamber covers (Figure 3.15). In both experiments, SOA formation did not begin until the NO concentration had decreased to ~ 60% of the initial (maximum) concentration. However, in $MC_{[high]}$ more aerosol mass was formed for a smaller amount of methyl chavicol reacted (Figure 3.14). At the time of initial SOA formation in $MC_{[high]}$ and MC_{MNOx}, the experimental conditions (chamber temperature and relative humidity), $^{\bullet}OH$ and O_3 concentrations were all relatively similar; see Table 3.8 and Figures 3.17 and 3.18. The only considerable difference between these experiments which could account for a larger amount of aerosol mass formed for a smaller amount of methyl chavicol reacted in $MC_{[high]}$, is the NO_x concentration. However, no SOA formation was observed until a relatively low NO environment was entered, suggesting that the higher NO_2 concentration in $MC_{[high]}$ is enhancing SOA formation.

Recently, a number of studies have found the SOA yields of certain VOCs in low NO environments, increase with increasing NO_2 concentrations. The SOA yields of α-pinene were found to be significantly greater in high NO_2 environments (~ 25%), than in high NO (~ 8%) (Eddingsaas et al., 2012). Moreover, α-pinene SOA formation was found to occur immediately in low NO, high NO_2 environments; but not in high NO environments, where a delay in SOA formation was observed (Eddingsaas et al., 2012). The photo-oxidation of methacrolein (isoprene oxidation product) has also been found to have a larger SOA yield in high NO_2 environments, than in high NO (Surratt et al., 2010). This study found the SOA yield of methacrolein increased when ~ 350 ppbv of additional NO_2 was added into the chamber (instead of NO) (5.1%), than when ~ 290 ppb of additional NO was added (2.9%). Moreover, in the presence of ~ 500 ppb of NO the SOA yield of methacrolein was found to be the lowest of all experiments investigated (< 2%,); suggesting the importance of the NO_2 concentration on SOA formation.
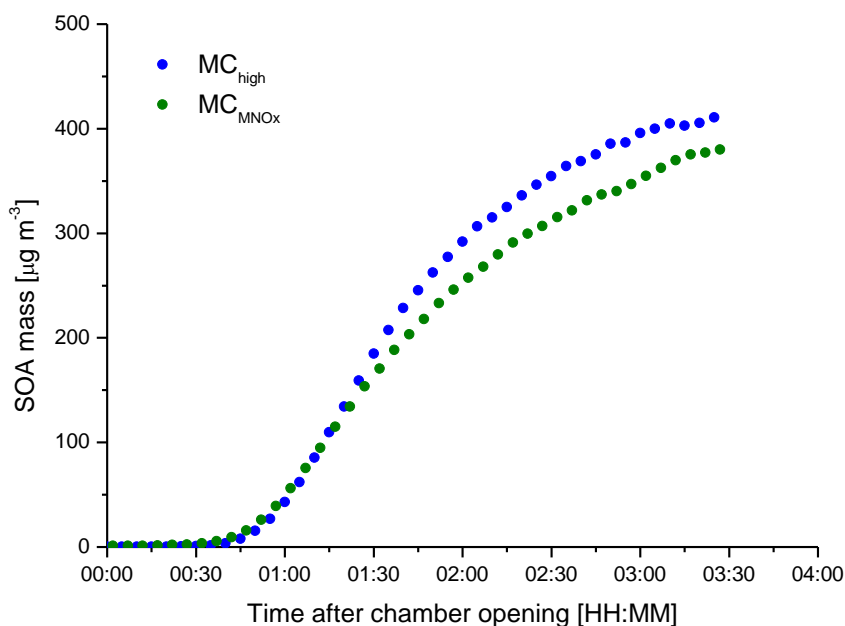
Figure 3.15 - Amount of aerosol mass formed (corrected for wall loss and chamber dilution) in $MC_{[high]}$ and MC_{MNOx} after the opening of the chamber covers.

Table 3.8 - Experimental conditions and oxidant concentrations at time of initial SOA formation in $MC_{[high]}$ and MC_{MNOx}

Exp.	Measured oxidant concentration					Experimental conditions	
	$^{\bullet}$OH	O_3	NO	NO_2		RH	Chamber temp
	[molecules cm^{-3}]	[ppbv]	[ppbv]	[ppbv]		[%]	[K]
$MC_{[high]}$	2.27×10^6	43	32	52		3	302
MC_{MNOx}	2.55×10^6	40	17	30		1	304

One explanation for the larger SOA yields observed at higher NO_2 concentrations has been suggested to be the result of increased acidity of the oxidation products formed (*i.e.* formation of peroxy nitrates and/or increased nitric acid concentrations from the heterogeneous reactions of NO_2 and H_2O, or $^{\bullet}$OH and NO_2 on the chamber walls) (Jang et al., 2002; Hu et al., 2007). Acid-catalysed reactions have been found to significantly increase SOA formation (Jang et al., 2002). However, for these reactions to occur, the aerosol, or components of the aerosol, must be aqueous to allow proton transfer and/or dissolution of acidic gases onto particles. In both $MC_{[high]}$ and MC_{MNOx} the percentage relative humidity at the time of initial SOA formation was below 3% (Table 3.8). At these low percentage relative humidities, acid-catalysed reactions are very unlikely to affect SOA formation. A more likely explanation is that the oxidation products formed from the reaction

with NO_2 are of low volatility and are likely to be influencing SOA formation in the initial stages of aerosol growth.
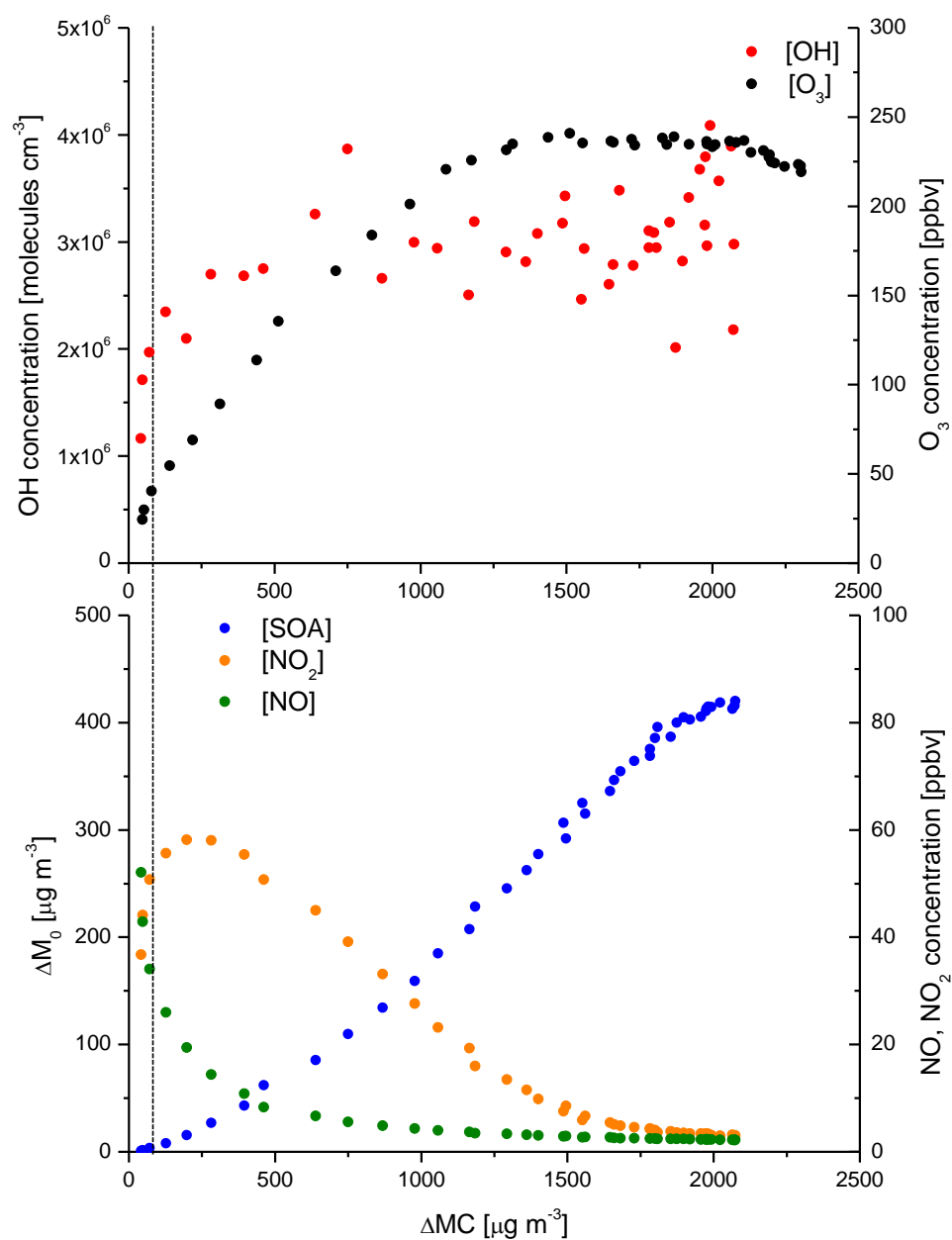
Figure 3.16 - The temporal evolution of ˙OH, O_3, NO and NO_2 concentration and SOA mass, plotted against the amount of methyl chavicol reacted in $MC_{[high]}$. Dashed black line indicates the time of initial SOA growth. The first 30 minutes of the $MC_{[high]}$ experiment has been removed due to the fluctuating methyl chavicol concentration; see Section 3.2.2.
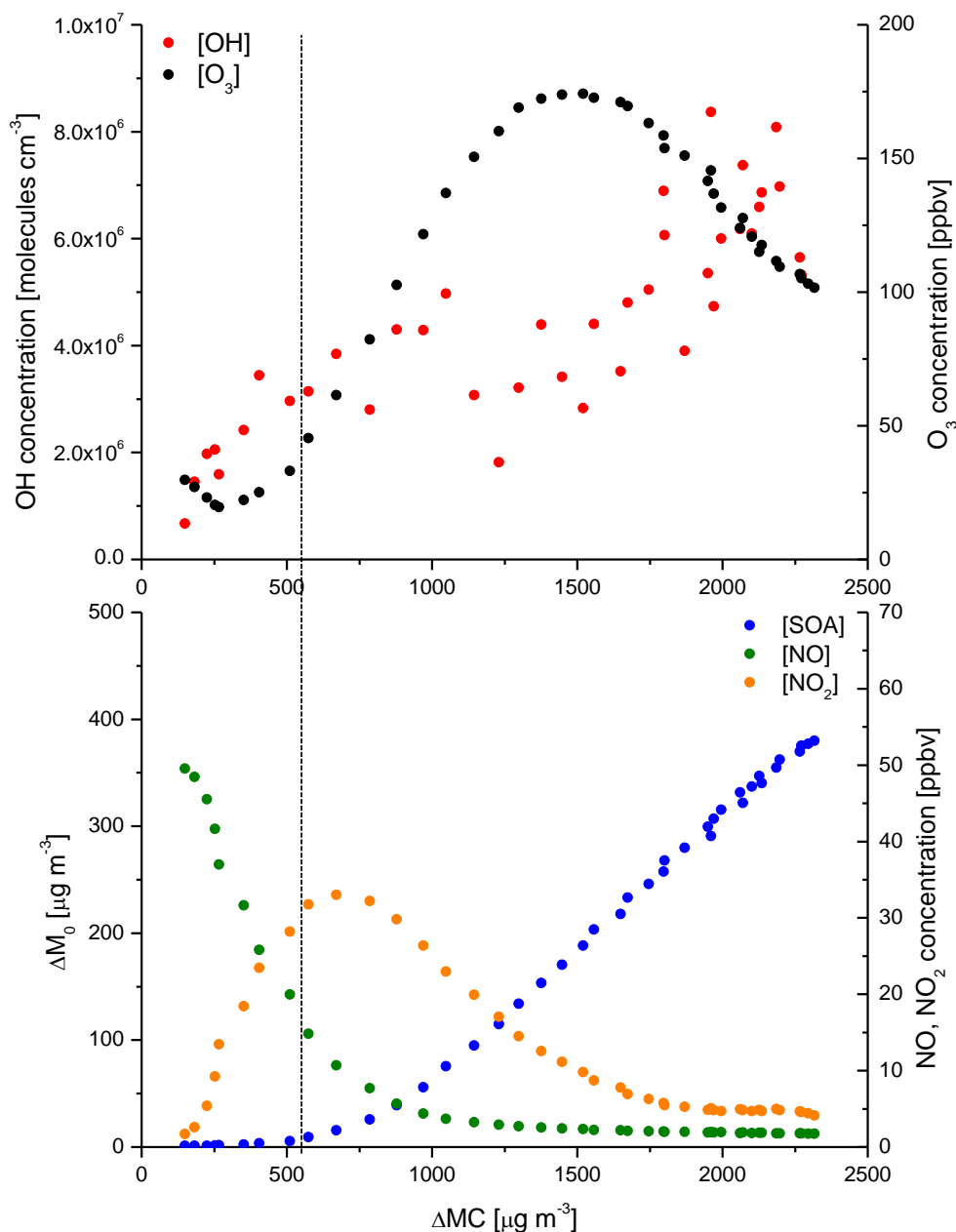
Figure 3.17 - The temporal evolution of ˙OH, O_3, NO and NO_2 concentration and SOA mass, plotted against the amount of methyl chavicol reacted in MC_{MNOx}. Dashed black line indicates the time of initial SOA growth.

3.3.11 Atmospheric Relevance

The SOA yield obtained in this study for the photo-oxidation of methyl chavicol, in $MC_{[low]}$ (18%), $MC_{[high]}$ (29%) and MC_{MNOx} (23%) are comparatively lower than the 40% SOA yield reported previously (Lee et al., 2006b), although there are a number of key differences between the two studies. Lee et al. (2006b) used ammonium sulfate seed (compared to the

nucleation only experiments presented here), which as discussed previously, has been shown to increase the SOA yields of aromatic precursors (Kroll et al., 2007; Lu et al., 2009; Huang et al., 2013). In addition, the percentage relative humidity (%RH) was approximately 5 times greater in the study performed by Lee et al. (2006b). Recent publications have shown that the SOA mass formed from a substituted aromatic compound (*p*-xylene), increases with increasing% RH, approximately by a factor of 2 over a %RH range of 5 to 75% (Healy et al., 2009; Zhou et al., 2011). Nevertheless, it is clear the photo-oxidation of methyl chavicol results in significant SOA formation. Recent literature has shown oxygenated biogenic VOCs containing 10 carbon atoms (including eucalyptol, verbenone, linalool) resulted in an SOA yield between 16 to 20%, with the use of neutral (Lee et al., 2006b; Varutbangkul et al., 2006; Iinuma et al., 2008) or acidic (Iinuma et al., 2008) seed. It is difficult to directly compare SOA yields from the oxidation of a similar VOC precursors in the literature due to the limitations of using chamber derived data (Camredon et al., 2007). However, reported SOA yields of methyl chavicol were the highest of all oxygenated VOCs investigated (SOA yield 26-40%) (Lee et al., 2006b; Varutbangkul et al., 2006). Although these experiments are at concentrations higher than the real atmosphere, they suggest that methyl chavicol can act as an important SOA precursor in regions where methyl chavicol emissions are significant, such as downwind from pine forests and oil palm plantations. Furthermore, the results of this study indicate that as the concentration of NO_x increases (*i.e.* increasing amount of oil palm processing plants with the expansion of oil palm agriculture) the SOA mass formed from methyl chavicol is also likely to increase.

Aerosol loadings where methyl chavicol emissions are significant, such as northern Borneo, have been found to range from 5 $\mu g\ m^{-3}$ (800 meters above the oil palm plantation) to 100 $\mu g\ m^{-3}$ (in a chimney plume of an near-source oil palm processing plant) (MacKenzie et al., 2011). The aerosol loadings formed in these experiments are considerably higher ($MC_{[low]}$ 126, $MC_{[high]}$ 430 and MC_{MNOx} 391 $\mu g\ m^{-3}$) than the aerosol loadings observed in ambient conditions. It is therefore likely that more compounds are observed in the aerosol phase in this study than would be at atmospherically relevant conditions; due to more higher volatility species partitioning into the aerosol phase at higher mass loadings (Pankow, 1994b, a; Odum et al., 1996). However, the structurally identified compounds were characterized as semi- to low-volatility oxygenated organic aerosol; where at atmospherically relevant conditions a sizable fraction of these compounds would be expected to exist in the aerosol phase (Donahue et al., 2012).

The SOA compounds identified in this study will be representative of methyl chavicol oxidation products formed in polluted environments (high NO_x) and downwind of pollution sources (low NO_x, high O_3). At the start of the chamber experiments, the high NO concentrations will be representative of methyl chavicol emissions directly next to a high NO source, such as a processing plant (MacKenzie et al., 2011). Here, the peroxy radicals $(ROO^{\bullet})$ will preferentially react with NO forming alkoxy radicals $(RO^{\bullet})$ and NO_2 (leading to O_3 formation). As a relatively low NO environment in the chamber is entered (*i.e.* the majority of NO has been converted to NO_2), the RO_2 radicals will increasingly react with RO_2 or (primarily) HO_2; instead of NO. The oxidation products formed whilst the NO concentration is relatively low but the NO_2 concentration is near maximum, will be representative of the methyl chavicol oxidation products formed in polluted environments, (*i.e.* agro-industrialized oil palm plantation site (MacKenzie et al., 2011)). As the chamber experiment progresses, the NO_2 concentration decreases, approaching zero (as the NO_x is not replenished in the chamber) and the O_3 concentration increases from the photolysis of NO_2. This chamber scenario then corresponds to an environment representative of the products formed downwind of an agro-industrialized oil palm plantation; where there is less pollution (low NO_x), but O_3 is present.

Four compounds with a MW of 122, 136, 150 and 166 g mol^{-1} were observed in the gas phase using PTR-MS and may be attributed to 4-methoxytoluene, 4-methoxybenzaldehyde, 4-methoxybenzene acetaldehyde and (4-methoxyphenyl)acetic acid, respectively, in agreement with Lee et al. (2006b), Spada et al. (2008) and Gai et al. (2013). These compounds are formed as a result of decomposition leading to higher volatility species and are therefore not included in Figures 3.11 and 3.12. The gas phase oxidation mechanisms of these compounds can be observed in Gai et al (2013). In contrast to Cahill et al. (2006) and Bouvier-Brown et al. (2009) 4-methoxybenzaldehyde (MW 136 g mol^{-1}) and 4-methoxybenzene acetaldehyde (MW 150 g mol^{-1}) were not identified in the aerosol phase in this study. Compound vapour pressures were calculated using the UManSysProp website (http://ratty.cas.manchester.ac.uk/informatics/) at 298.15 K, using the Nannoolal vapour pressure and boiling point extrapolation method (Nannoolal et al., 2004; Nannoolal et al., 2008) and the saturation concentration (C^{*}, µg m^{-3}) determined (Donahue et al., 2006). The calculated volatility of these compounds suggests they are intermediate VOCs (4-methoxybenzaldehyde, $C^{*} = 4.96 \times 10^{5}$ µg m^{-3} and 4-methoxybenzene acetaldehyde, $C^{*} = 3.02 \times 10^{5}$ µg m^{-3}). The use of gas phase scrubbers for organics in the PILS sampler used in this study may indicate that previous ambient observations are due to positive artefacts from gas phase absorption to filters.

The saturation concentration (C^*, µg m^{-3}) (Donahue et al., 2006) and O:C ratio were determined for all the identified compounds and plotted in a O:C /$\log_{10} C^*$, µg m^{-3} volatility basis set space (Jimenez et al., 2009; Donahue et al., 2013), as shown in Figure 3.18. All of the identified SOA compounds retained the aromatic ring, with O:C ratios between 0.30 to 0.63 and H:C ratios between 1.11 and 1.40. The oxidation of methyl chavicol and its early generation products resulted in the formation of low vapour pressure and a high O:C ratio species, due to the lack of ring fragmentation. This resulted in the movement of the SOA compounds to lower volatilities and higher O:C ratios, thus functionalisation rather than fragmentation was mainly observed. The majority of the structurally identified SOA species underwent oxidation on the aromatic ring, through the addition of ˙OH and/or NO_2. The formation of compound 1 (3-(5-hydroxy-4-methoxy-2-nitrophenyl)propane-1,2-diol) through the addition of a NO_2 group on the aromatic ring resulted in the movement of this species to the low volatility oxygenated organic aerosol region (LVOOA), and just outside the extremely low volatility oxygenated organic aerosol (ELVOOA) nucleator region proposed by Donahue et al (2013). Ring addition appears to be an important pathway, resulting in the formation of low volatility species with high O:C ratios, which may also be important for other aromatic compounds. Only structures for 8 of the 79 compounds detected could be tentatively identified; however, 2 structures were confirmed with authentic standards. Further work is required to characterise the SOA formed from methyl chavicol oxidation with different oxidants (O_3, ˙NO_3), RH and seed aerosol.
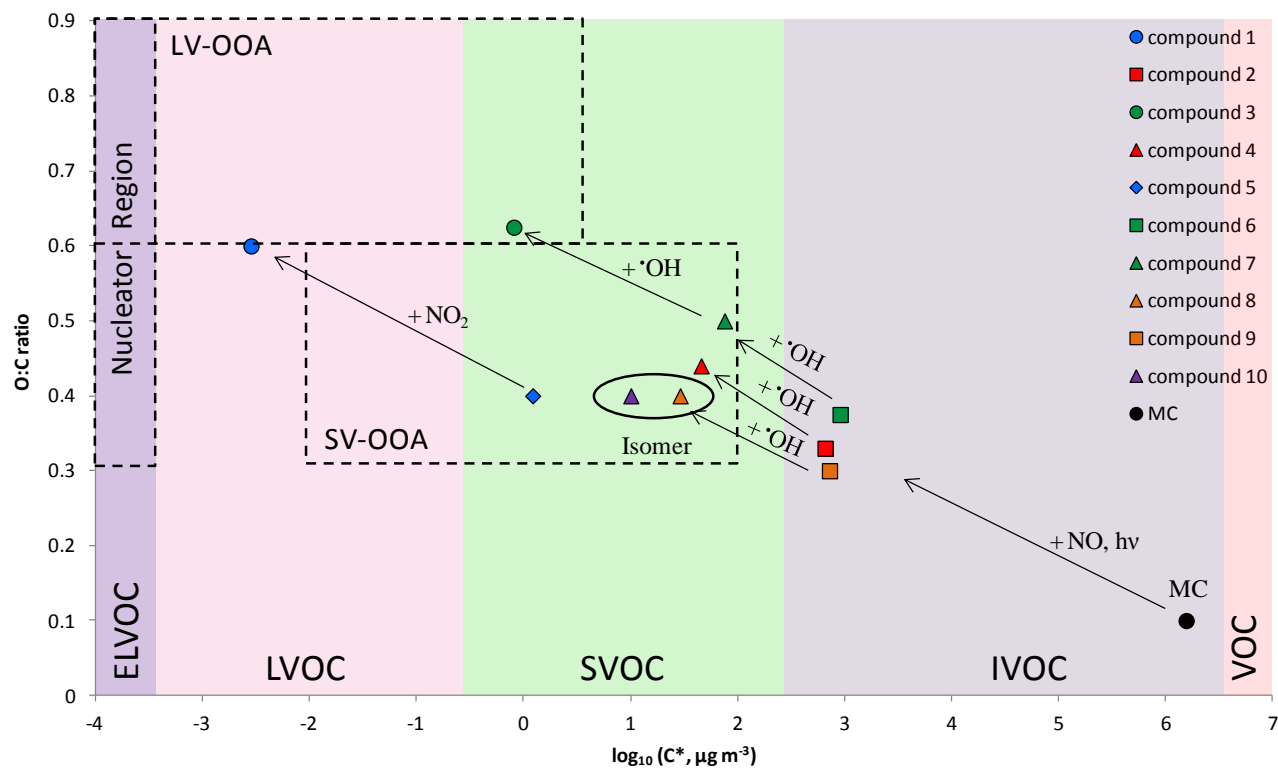
Figure 3.18 - Oxygen to carbon ratio (O:C) and saturation concentration $\log_{10} C^*$ (Donahue et al., 2006) space to show the movement of the identified SOA compounds to lower volatilities upon oxidation in $MC_{[high]}$. Related generations of compounds are shown in the same colour. The change of shape but use of the same colour indicates a change in the SOA compound structure through the reaction with ${}^\bullet$OH radicals or NO_2. See legend for SOA compound identification and refer to Table 3.5. O:C/$\log_{10} C^*$ space with associated volatilities have been redrawn from Donahue et al. (2013) and Jimenez et al. (2009).

Chapter 4 - Observations of the Dynamic Mechanisms Controlling SOA Partitioning and Evolution: Investigating One Compound at a Time

4.1   Introduction

The difficulty with studying SOA formation arises where the oxidation of a single VOC forms a wide variety of multi-functional oxidation products of differing volatilities (Kroll and Seinfeld, 2008; Hallquist et al., 2009). These compounds may undergo numerous oxidation steps, forming a multitude of oxidation products; only some of which may contribute to SOA formation and subsequent growth. Furthermore, once a compound partitions into the condensed phase it can undergo further oxidation steps (Claeys et al., 2004; Hearn et al., 2007; Perri et al., 2009; George and Abbatt, 2010) and reactive transformations (non-oxidative processes, *i.e.* oligomerisation) (Barsanti and Pankow, 2004; Gao et al., 2004a; Gao et al., 2004b; Iinuma et al., 2004; Kalberer et al., 2004; Tolocka et al., 2004), continually changing their chemical speciation and volatility (Kroll and Seinfeld, 2008). The sheer number of VOCs present in the ambient atmosphere (Goldstein and Galbally, 2007) and their continually evolving gas and aerosol phase chemical composition, makes the identification of the species involved in SOA formation, growth and ageing, a highly complex and difficult task.

Atmospheric simulation chambers can afford mechanistic insight into SOA formation processes under simplified conditions. The oxidation of a single VOC may be investigated in a controlled environment using a variety of oxidants, with and without the use of irradiation; providing significant insight into the mechanisms of SOA formation. Bulk particle measurement techniques, such as aerosol mass spectrometry (AMS) and high resolution time-of-flight aerosol mass spectrometry (HR-TOF-AMS) (DeCarlo et al., 2006), provide near-real time chemical speciation (*e.g.* sulfate, nitrate, ammonium and oxidised organic carbon) of non-refractory aerosol; allowing changes in particle oxidation to be observed. However, whilst these techniques have been invaluable to our understanding of the chemical and physical transformations occurring during particle evolution, they do not provide the detailed chemical composition and structural speciation that offline mass spectrometric techniques can offer (Zhang et al., 2007; Hallquist et al., 2009; Laskin et al., 2012). Consequently, our knowledge of the physical and chemical changes occurring during aerosol formation, growth and ageing, is limited.

Aromatic hydrocarbons are considered to be one of the most important SOA precursors, contributing significantly to SOA formation in urban areas (Zi-feng et al., 2009; Liu et al., 2012). Aromatics are known to be highly reactive, and with their large emission rates are deemed to be a high photochemical ozone creation potentials (Derwent et al., 2007). However, despite their important impact on urban air quality, aromatic photo-oxidation

mechanisms are still poorly understood (Bloss et al., 2005). For aromatic compounds such as alkyl-benzenes typically emitted from gasoline, new particle formation in smog chamber simulations occurs when a relatively "low NO environment" is entered, suggesting that low NO chemistry is vital for producing sufficiently low volatility oxidation products to initiate nucleation (Johnson et al., 2004; Kroll and Seinfeld, 2008). This has previously been attributed to the formation of peroxides formed through the $RO_2 + HO_2$ reaction pathway, although little compositional evidence has been found in aromatic systems to support this. The ability to study the molecular composition of SOA at high time resolution could provide this information, and significantly aid in our understanding of SOA formation and ageing.

SOA formation during the photo-oxidation of the mono-aromatic compounds, toluene (aromatic anthropogenic VOC), 4-methyl catechol (aromatic anthropogenic oxygenated VOC (OVOC)) and methyl chavicol (biogenic aromatic OVOC) were investigated at the European Photoreactor chamber in Valencia, Spain. Time resolved sub-micron aerosol samples were collected every 30 minutes using a particle into liquid sampler (PILS) and analysed offline using; high performance liquid chromatography ion-trap mass spectrometry (HPLC-ITMS), high performance liquid chromatography quadrupole time-of-flight mass spectrometry (HPLC-QTOFMS) and Fourier transform ion cyclotron mass spectrometry (FTICR-MS). The particle phase temporal profiles of a wide variety of individual multifunctional photochemical products are provided, with detailed chemical and structural speciation for these compounds. The use of a time resolved aerosol collection method followed by offline state-of-the-art mass spectrometric analysis, has allowed the temporal evolution of individual compounds in the particulate phase to be observed.

4.2   Experimental

4.2.1   Chamber Experiments, Aerosol Collection and Analysis

Experiments were performed at the European Photoreactor chamber in Valencia, Spain. A series of experiments were performed during July 2009 as a part of the toluene oxidation experiments in a chamber (TOXIC) project, and during May 2012 as a part of the atmospheric chemistry of methyl chavicol (ATMECH) project. The chamber setup and instrumentation used has previously been described in detail and can be found in Chapter 3, Section 3.2.1. All of the chamber instrumentation used during the TOXIC project was the same as discussed for the ATMECH project. The only exception was that PTR-MS was not used to monitor precursor degradation and product formation. Instead, a Fourier transform infra red spectrometer (FTIR, Nicolet Magna, model 550) coupled to a white-type mirror

system (optical path length 616 m) was used. The VOC precursors investigated, initial mixing ratios, chamber humidity and temperature for the experiments discussed, are shown in Table 4.1. Aerosol samples were collected, prepared and analysed using the same methodology as discussed previously (Chapter 3, Section 3.2.2 to 3.2.5). The aerosol samples collected from the TOXIC project were re-dissolved in 500 µL of 50:50 methanol:water (optima, LC-MS grade, Fisher Scientific, UK) and analysed using only HPLC-ITMS.

4.2.2   Temporal Profiles

Temporal profiles were created by measuring the chromatographic peak areas of the observed SOA compounds in each 30 minute PILS sample using the HPLC-ITMS (see Section 4.3 for further information). Replicate injections of the same SOA sample could not be performed due to the lack of sample volume. Instead, the precision of the measured peak areas (shown through the use of error bars on the temporal profiles) was determined by measuring the chromatographic peak area of an external standard, with the closest chemical and structural speciation to the SOA compound.

For the ATMECH project, the precision of the detector for all the nitro-aromatics was determined using a 10 ppm standard of 2,6-dimethyl-3-nitrophenol (provided by University College Cork, Sigma Aldrich, UK, purity 95%) and was found to be 1.8% based on 3 replicate measurements. The ITMS precision for (4-methoxyphenyl)acetic acid and 4-methoxybenzoic acid was determined using a 10 ppm standard of 4-methoxybenzoic acid (Sigma Aldrich, UK, purity 99%). For this compound, the precision of the detector was found to be 4.4% based on 3 repeats. These values were rounded up to 5% to account for a small loss of particles during collection (Chapter 3, Section 3.2.2.1). For the TOXIC project, the precision of the detector for all the nitro-aromatics was determined using a 1 ppm standard of 4-nitrocatechol (Sigma Aldrich, UK, purity 97%) and was found to be 5.8% based on 4 replicate measurements. The ITMS detector variation was slightly higher during this period and so a 7 %RSD was applied.

No wall loss or chamber dilution corrections have been applied to any of the temporal profiles, aerosol mass and particle number concentrations shown in the following work. This was performed as the concentration of many of the SOA compounds could not be determined due to the lack of commercially available standards. Furthermore, it was not known if the aerosol composition was consistent across the sampled size range and thus, a size dependent wall loss correction could not be applied.

Table 4.1 - Initial mixing ratios of the oxidants and VOC precursors investigated, including chamber humidity and temperature for the experiments performed during the TOXIC and ATMECH project.

Project	Date	Exp.	Exp. Description	Initial mixing ratio[a]			Oxidant initial mixing ratio[a]			VOC:NO$_x$	Experimental range[b]	
				Toluene [ppbv]	Methyl chavicol [ppbv]	4-Methyl Catechol [ppbv]	NO [ppbv]	NO$_2$ [ppbv]	O$_3$ [ppbv]		RH [%]	Temperature [K]
TOXIC	20.07.09	Tol$_{low}$	Low NO$_x$	535	-	-	41	0	0	~13:1	0.2 – 2.9	297 - 308
	21.07.09	Tol$_{high}$	High NO$_x$	560	-	-	105	0	0	~5:1	1.1 – 2.1	297 - 309
	28.07.09	4-MCat		-	-	591	120	2	0	~5:1	0.2 – 8.8	298 - 305
ATMECH	15.05.12	MC$_{[high]}$		-	460	-	92	3	5	~5:1	2.1 -10.7	297 - 306

[a] = On the opening of the chamber covers. [b] = From the opening to the closing of the chamber covers.

4.3   Results and Discussion

Initially, the PILS samples were screened for SOA species using HPLC-ITMS. Any compounds present before the introduction of the VOC precursor and NO into the chamber were excluded from further analysis. Only compounds that displayed changes in their chromatographic peak areas were investigated further. Peak areas of the observed SOA compounds were measured in each 30 minute PILS sample, allowing the temporal evolution of individual species in the particulate phase to be observed.

4.3.1   Aerosol Partitioning and Evolution

4.3.1.1 Photo-oxidation of Methyl Chavicol

Initially, the SOA composition formed from the photo-oxidation of methyl chavicol, experiment $MC_{[high]}$ was investigated. In this experiment, 79 SOA compounds were observed in the PILS SOA samples using HPLC-ITMS (Chapter 3, Section 3.3.6). Temporal profiles were created for 70 of the 79 SOA species. The other 9 compounds were excluded due to the majority of chromatographic peaks observed being below the limit of detection (defined as S/N = 3). The temporal evolutions of the individual SOA compounds varied considerably, with different rates of aerosol partitioning, formation and loss observed. Nevertheless, three main temporal profile shapes could be distinguished. The majority of SOA compounds displayed a relatively slow increase in particle phase concentration, following initial aerosol growth, after which the concentration either plateaued or began to decrease towards the end of the experiment (~ 4 hours). Of the 79 SOA compounds, 51 species displayed this type of temporal profile (hereafter referred to as TP 1) and an example is shown in Figure 4.1A.

The majority of these compounds were first observed in the aerosol phase between 71 to 101 minutes into the experiment, when the SOA mass in the chamber was rapidly increasing (59 to 187 μg m^{-3}, Figure 4.1D). All of these compounds displayed a gradual increase in their particulate phase concentration, with the majority reaching maximum concentration at ~ 175 minutes into the experiment, when SOA formation in the chamber had plateaued. The structures of 5 of these species have previously been determined (Chapter 3, Section 3.3.6) and were identified as; 3-hydroxy-4-methoxyphenyl)acetic acid, 3-(3-hydroxy-4-methoxyphenyl)propane-1,2-diol, 4-methoxybenzoic acid, 3-hydroxy-4-methoxybenzoic acid and 2-hydroxy-3-(3-hydroxy-4-methoxyphenyl)propanal. The compound structures, the

proposed mechanistic generation and the time period these compounds were first observed in the aerosol phase are shown in Table 4.2.
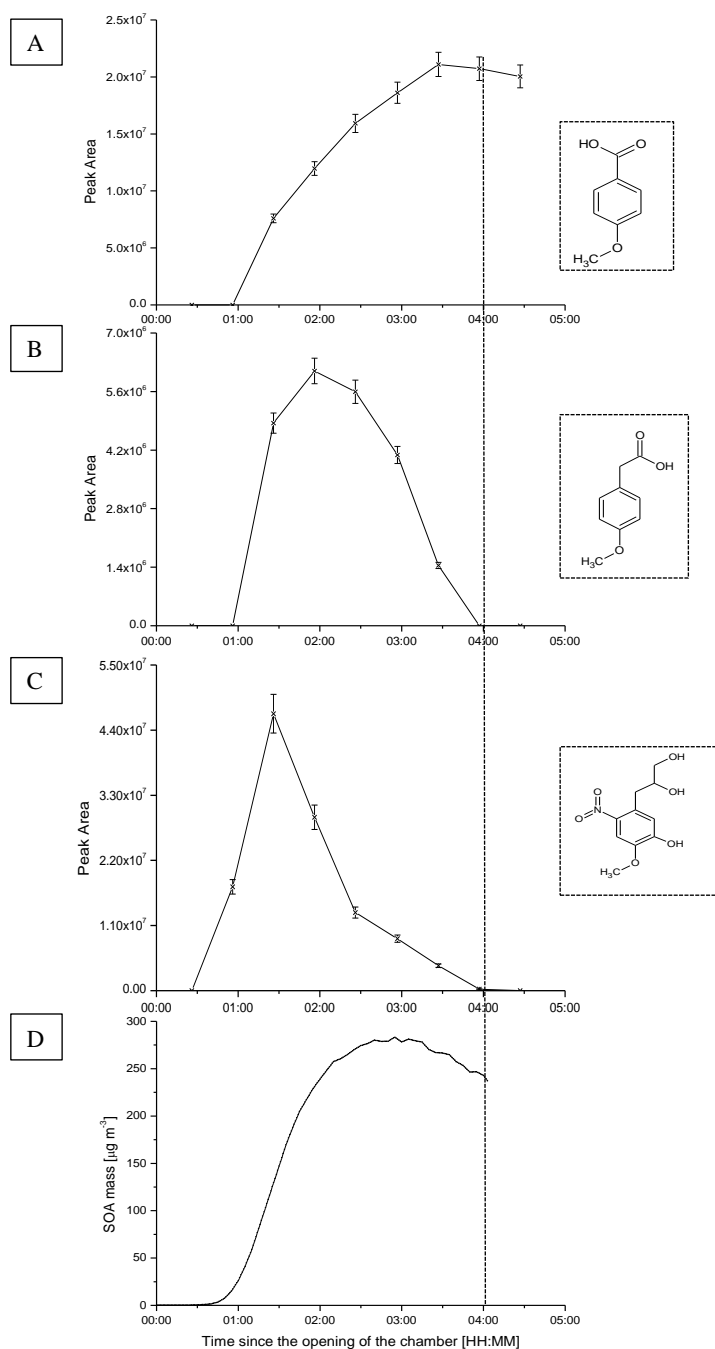
Figure 4.1 - Types of the characteristic particle phase temporal profiles observed in MC[high]. A = TP 1, 4-methoxybenzoic acid. B = TP 2, (4-methoxyphenyl)acetic acid. C = TP 3, 3-(5-hydroxy-4-methoxy-2-nitrophenyl)propane-1,2-diol. D = SOA mass . Temporal profiles are plotted using the average PILS sampling time. Error bars display a 5 %RSD (Section 4.2.2) Dashed line = closing of the chamber covers.

Table 4.2 - The compound structures, timing of aerosol partitioning and maximum concentration observed for the SOA compounds displaying TP 1.
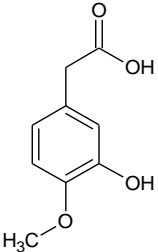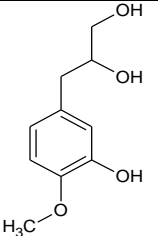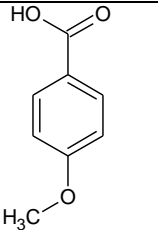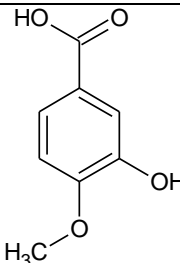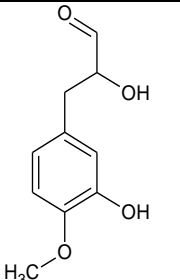
Compound no.	IUPAC name	MW [g mol⁻¹]	MF	Structure	First observed in the aerosol phase [minutes]	Maximum aerosol concentration [minutes]	Proposed mechanistic generation
1	(3-hydroxy-4-methoxyphenyl)acetic acid	182	$C_9H_{10}O_4$		71 - 101	162 - 192	[a]
2	3-(3-hydroxy-4-methoxyphenyl)propane-1,2-diol	198	$C_{10}H_{14}O_4$		71 - 101	162 - 192	3rd
3	4-methoxybenzoic acid	152	$C_8H_8O_3$		71 - 101	192 - 222	[a]

Table 4.2 - Continued.....

Compound no.	IUPAC name	MW [g mol^{-1}]	MF	Structure	First observed in the aerosol phase [minutes]	Maximum aerosol concentration [minutes]	Proposed mechanistic generation
4	3-hydroxy-4-methoxybenzoic acid	168	$C_8H_8O_4$		101 - 131	192 - 222	a
5	2-hydroxy-3-(3-hydroxy-4-methoxyphenyl)propanal	196	$C_{10}H_{12}O_4$		71 - 101	222 - 252	3rd

^{a} = Suspected > 4th generation species, most likely formed through the reaction with ozone (Chapter 3, Section 3.3).

The vapour pressures of these compounds were calculated using the UManSysProp online facility for calculating properties of individual organic molecules and ensemble mixtures (http://umansysprop.seaes.manchester.ac.uk/), employing the Nannoolal vapour pressure (Nannoolal et al., 2008) and boiling point (Nannoolal et al., 2004) extrapolation method. The calculated saturation concentration (C^*, μg m^{-3}) of the structurally identified compounds ranged from 9.17×10^2 to 1.23×10^0 μg m^{-3}, characterising these species as intermediate- to semi-volatile organic compounds (Donahue et al., 2006). The gradual increase in the particulate phase concentration observed with this type of temporal profile is likely the result of a faster formation rate than loss and increasing gas-particle absorption (uptake) as the aerosol mass progressively increases (Pankow, 1994b, a). The peak area of 4-methoxybenzoic acid (typical TP1 profile shape) was divided by the SOA mass at each measured time period, throughout the experiment. A linear relationship was observed between the increasing peak area of 4-methoxybenzoic acid and increasing SOA mass (Figures 4.2A and B). A Pearson's correlation coefficient (R^2) of 0.8736 was obtained when the aerosol mass was > 130 μg m^{-3}, and an R^2 of 0.9895 when the SOA mass was > 231 μg m^{-3}. This suggests that gas-particle partitioning is likely to be the main mechanism driving the partitioning of this species into the aerosol phase, particularly after ~ 2 hours into the experiment when the SOA mass is > 231 μg m^{-3}. This type of temporal profile shape has previously been observed with the uptake of glyoxal onto ammonium sulfate seed particles (Galloway et al., 2011) and the oxidation products, caryophyllonic and nocaryophyllonic acid, formed from the ozonolysis of β-caryophyllene (Van Eijck et al., 2013).

The second type of temporal profile shape observed (TP 2) displayed a rapid increase and then decrease in aerosol concentration, as shown in Figure 4.1B. These species were short lived, remaining in the aerosol phase for a maximum of 2.5 hours, and could not be detected in the aerosol samples at the end of the experiment. Only 3 compounds displayed this type of temporal profile and the structure of one was identified as (4-methoxyphenyl)acetic acid (Chapter 3, Section 3.3.6, Table 3.5, compound 2). The two unidentified species consisted of one highly oxygenated compound, $C_8H_{12}O_8$, and one species, $C_{11}H_{14}O_4$, which contained one more carbon atom than the original VOC precursor. All of these compounds reached peak concentration up to 30 minutes after partitioning into the aerosol phase (*i.e.* in the following PILS sample) and displayed a rapid loss process after maximum concentration was observed. The rapid decrease in the aerosol phase concentration observed for these compounds could be due a variety of loss processes, such as; (i) photolysis or further reaction of the compound in the gas phase; (ii) insufficient precursor/oxidant concentration, and/or; (iii) in-particle phase/heterogeneous reactions.

For the identified species, (4-methoxyphenyl)acetic acid, photolysis degradation is considered to be negligible (Jenkin et al., 1997). However, the identification of an oxidation product, with an additional $^{\bullet}$OH group on the aromatic ring (3-hydroxy-4-methoxyphenyl)acetic acid (Chapter 3, Section 3.3.6, Table 3.5, compound 4) indicates further gas phase and/or heterogeneous reactions are occurring. Routes (i) and (ii) will result in a decrease in the compounds gas phase concentration, which could result in net re-evaporation into the gas phase. Recently, Vanden et al. (2010) found ambient SOA and laboratory generated α-pinene SOA did not follow the reversible gas-particle partitioning equilibrium assumed for liquid state particles (Vaden et al., 2011). The removal of gas phase organics did not result in the complete re-evaporation the SOA species into the gas phase, indicating the SOA studied was not liquid-like, and that re-evaporation was slow and kinetically limited (Vaden et al., 2011). For an experimental time of ~ 4 hours, approximately 45% of the SOA remained in the aerosol phase, whether the SOA was liquid or solid state, aged or not (Vaden et al., 2011). Considering this, gas phase loss processes are unlikely to solely account for the removal of a species from the aerosol phase. It is therefore likely that these species are also being lost as a result of heterogeneous or in-particle phase reactions, changing their chemical composition and resulting in the compound not being observed at the end of the experiment.

The third type of temporal profile shape (TP 3) was similar to TP 2 discussed above, except these compounds appeared in the aerosol phase earlier in the experiment (between 41 to 71 minutes) and a slower decrease in the aerosol concentration was observed (*i.e.* longer lifetime) (Figure 4.1C). Interestingly, all 8 species that displayed this type of temporal profile contained nitrogen. Seven of these organic nitrogen (ON) species were first observed in the aerosol phase when initial SOA growth was observed in the chamber (41 - 71 minutes into the experiment) and reached peak concentration within the next 30 minutes. The complex re-arrangements observed for these compounds during collision induced dissociation (CID) in the mass spectrometer made the structural identification particularly difficult. The compound structure of one of these compounds was identified as 3-(5-hydroxy-4-methoxy-2-nitrophenyl)propane-1,2-diol (Chapter 3, Section 3.3.6) and the structures of two have been tentatively assigned as substituted nitrophenols; 5-methoxy-4-nitro-2-(prop-2-en-1-yl)phenol and 1-hydroxy-3-(2-hydroxy-4-methoxy-5-nitrophenyl)propan-2-one (see Section 4.3.5 for the discussion of the structural assignment). The compound structures, time period these compounds were first observed in the aerosol phase and the proposed mechanistic generation are shown in Table 4.3. The calculated saturation concentrations and O:C ratios of the structurally identified compounds ranged

from 4.37×10^2 to 2.86×10^{-2} µg m^{-3} and 0.4 to 0.6 respectively, classifying these species as semi- to low volatility oxygenated organic compounds (SVOOC – LVOOC) (Donahue et al., 2006).
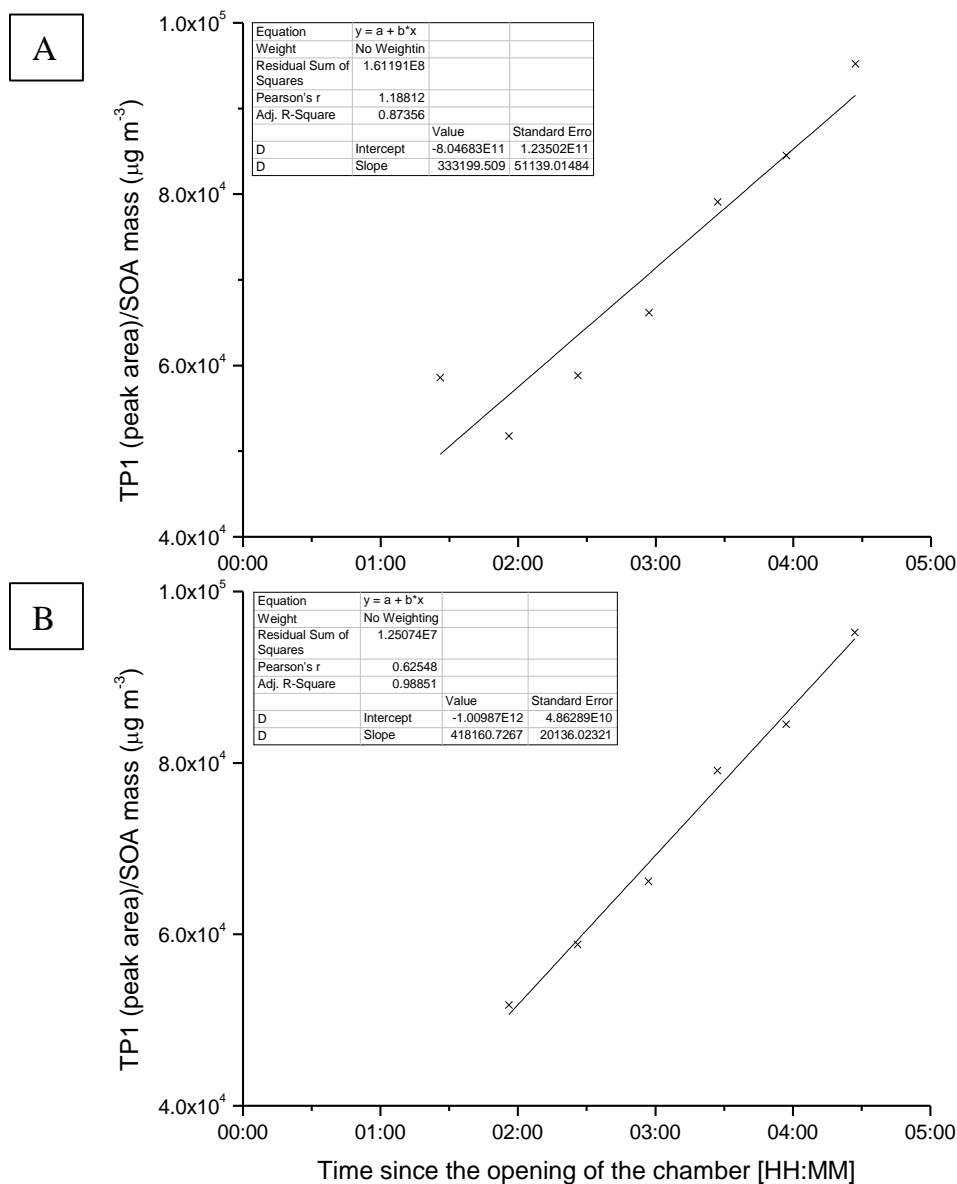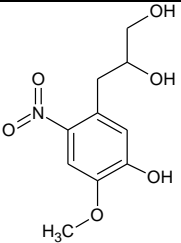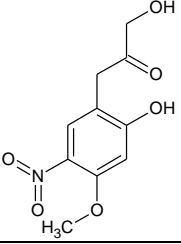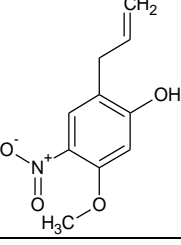
Figure 4.2 - Relationship of the peak area of 4-methoxybenzoic acid (typical TP1 profile shape) divided by increasing SOA mass, throughout MC$_{[high]}$. A = SOA mass > 130 µg m^{-3}. B = SOA mass > 231 µg m^{-3}.

Table 4.3 - The compound structures, timing of aerosol partitioning and maximum concentration observed for the SOA compounds displaying TP 3.

Compound no.	IUPAC name	MW [g mol^{-1}]	MF	Structure	First observed in the aerosol phase [minutes]	Maximum aerosol concentration [minutes]	Proposed mechanistic generation
1	3-(5-hydroxy-4-methoxy-2-nitrophenyl)propane-1,2-diol	243	$C_{10}H_{13}NO_6$		41 - 71	71 - 101	3rd
2	1-hydroxy-3-(2-hydroxy-4-methoxy-5-nitrophenyl)propan-2-one	241	$C_{10}H_{11}NO_6$		41 - 71	71 - 101	3rd
3	5-methoxy-4-nitro-2-(prop-2-en-1-yl)phenol	209	$C_{10}H_{11}NO_4$		41 - 71	71 - 101	2nd

The decrease in the particulate phase concentration observed for these species may be the result of a number of competing processes, such as; the low formation rates of the gas phase nitro-aromatics as the NO_2 concentration is depleted in the chamber (as NO_x is not replenished), photolysis/further reaction of the gas phase species leading to re-volatilisation from the aerosol phase and/or in-particle phase/heterogeneous chemistry. However, the observation of only one additional nitrogen containing compound later in the experiment suggests that either; (i) these compounds are entirely removed from the aerosol phase through re-volatilisation and do not partition back into the aerosol phase, or; (ii) upon further reaction lose nitrogen. The complete removal of these species from the particulate phase through re-volatilisation would appear unlikely due to the low volatility of these compounds and the potential kinetic limitations of re-evaporation (Vaden et al., 2011). A more likely explanation for the lack of further nitrogen containing oxidation products, is that upon further reaction nitrogen is being lost. A number of recent studies have found that nitrophenols can lose HONO in the gas or particulate phase (Bröske et al., 2003; Bejan et al., 2006; Kleffmann, 2007), possibly explaining why only one further nitrogen containing oxidation product was observed.

4.3.1.2 The Effect of Volatility on Aerosol Partitioning

The role of volatility in the partitioning of a species into the aerosol phase can clearly be observed in the time profiles of individual compounds. The addition of an NO_2 group to the aromatic ring leads to a large decrease in the vapour pressure (VP) of $\sim$ 3 orders of magnitude. This can be observed at a molecular level here, where the substituted nitrophenol 3-(5-hydroxy-4-methoxy-2-nitrophenyl)propane-1,2-diol (compound 1, Table 4.3, calculated VP = -12.54 $\log_{10}$ (P_{L}, atm)) can be observed in the aerosol phase before its phenol precursor 3-(3-hydroxy-4-methoxyphenyl)propane-1,2-diol (compound 2, Table 4.2, calculated VP = -9.82 $\log_{10}$ (P_{L}, atm)), as shown in Figure 4.3. However, It should be noted that the calculation of the vapour pressure using the UManSysProp website, which uses the structure activity relationship to calculate the vapour pressure, is only based on a few experimental measurements of compounds containing a nitro group.

The addition of an $^{\bullet}$OH group to the aromatic ring is shown to have a smaller impact on volatility. This can be observed by comparing pairs of precursors and products; where the addition of a $^{\bullet}$OH radical to the aromatic ring of the two precursors, 4-methoxybenzoic acid and (4-methoxyphenyl)acetic acid resulted in the formation of 3-hydroxy-4-methoxybenzoic acid and (3-hydroxy-4-methoxyphenyl)acetic acid, respectively. The calculated reduction in vapour pressure upon the oxidation of the precursors is only $\sim$1 order of magnitude (VP = -

1.12 and -1.20 $\log_{10}$ ($P_{\tilde{L}}$, atm) respectively). In both cases, the product did not partition into the aerosol phase before its precursor, as shown in Figure 4.4. Whilst it is well known that a lower volatility species will partition into the aerosol phase before a higher volatility species (assuming no loss processes affect partitioning and the aerosol mass concentration and interactions are the same in both cases) (Donahue et al., 2006; Kroll and Seinfeld, 2008), the volatility effect of individual functional groups upon species oxidation, and the timescale of their aerosol partitioning, has not been shown previously.
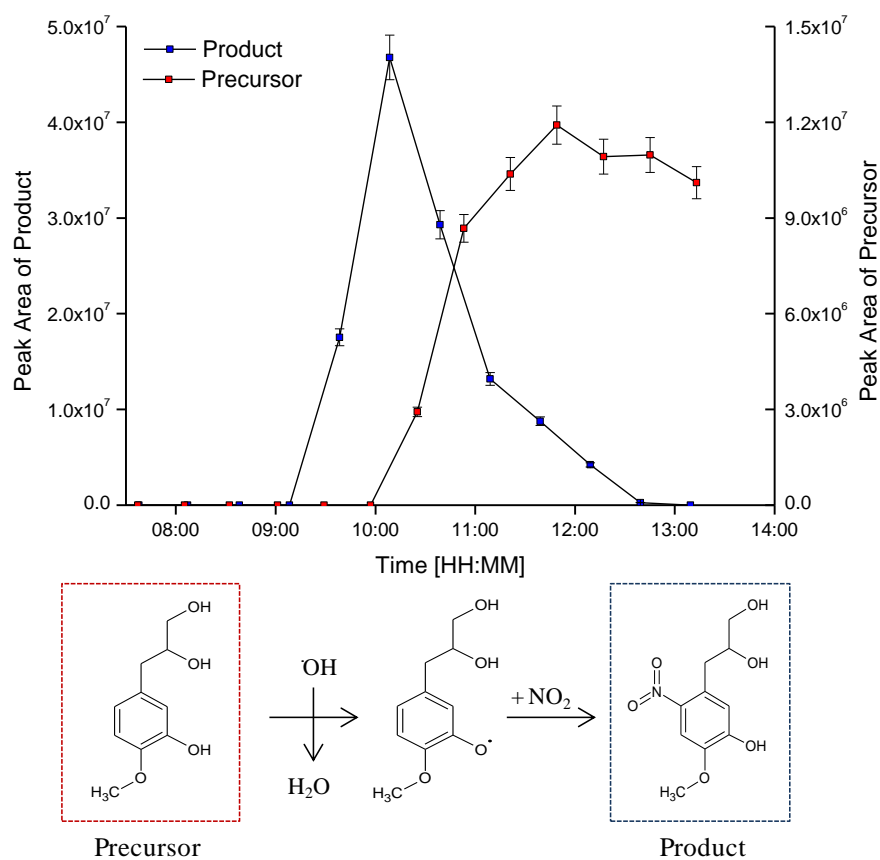
Figure 4.3 - Temporal profiles of the precursor 3-(3-hydroxy-4-methoxyphenyl)propane-1,2-diol and its oxidation product 3-(5-hydroxy-4-methoxy-2-nitrophenyl)propane-1,2-diol in the particulate phase, showing the timings of aerosol partitioning during experiment MC$_{[high]}$.
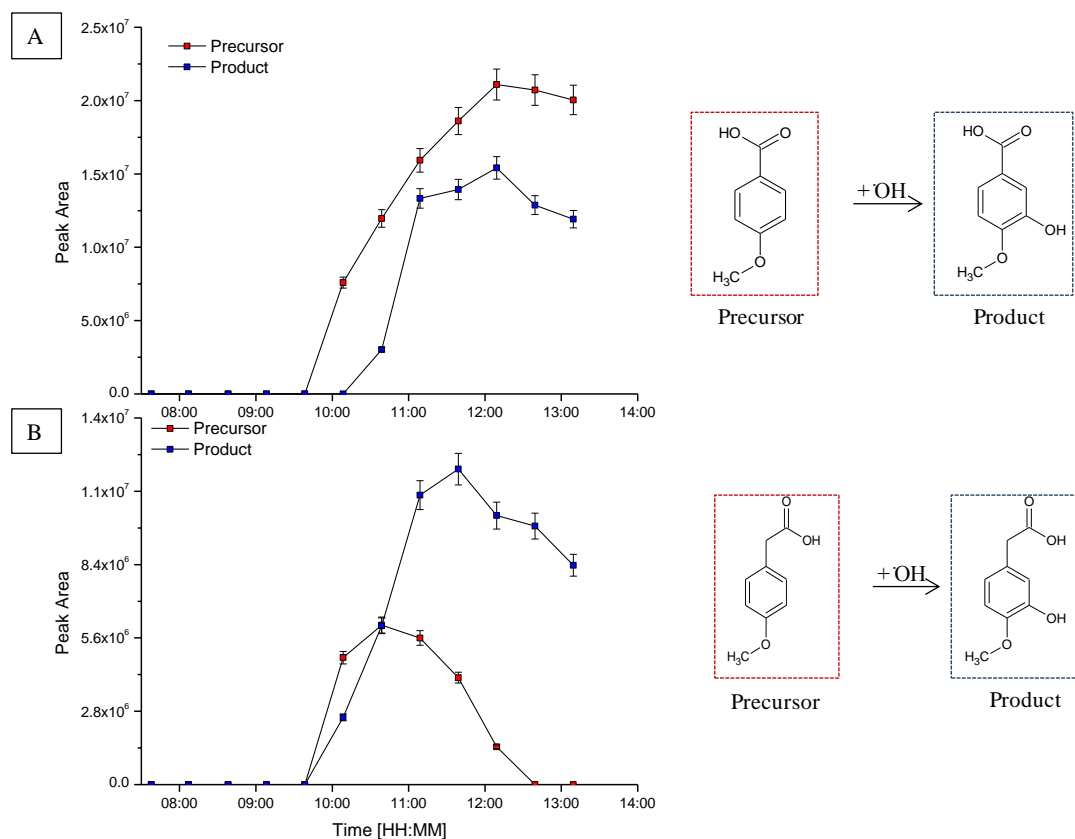
Figure 4.4 - Temporal profiles of two precursors and their oxidation products in the particulate phase showing the timings of aerosol partitioning during experiment $MC_{[high]}$. (A) precursor = 4-methoxybenzoic acid, oxidation product = 3-hydroxy-4-methoxybenzoic acid. (B) precursor = (4-methoxyphenyl)acetic acid, oxidation product = (3-hydroxy-4-methoxyphenyl)acetic acid.

4.3.1.3 Importance of ON Species in SOA Formation and Growth

During the first PILS sample of the experiment (0 to 11 minutes) no detectable SOA formation occurred, with particle number, diameter and mass similar to that of the chamber background. In the second PILS sampling time period (11 to 41 minutes into the experiment), new particle formation was observed in the chamber, although little growth in the aerosol mass (0.22 to 1.85 μg m^{-3}) or diameter was observed in this period, as shown in Figure 4.5. No SOA compounds were identified in the PILS sample taken during this period. During the third PILS sampling period (41 to 71 minutes into the experiment), maximum particle number was observed at 67 minutes and the aerosol diameter and mass (1.85 to 63.5 μg m^{-3}) rapidly increased. In this PILS sample, 14 SOA compounds were observed.

Figure 4.5 - Particle diameter *vs*. time with a coloured contour plot displaying increasing particle number (A) and particle mass (B) during $MC_{[high]}$. Dashed lines display the sampling period of the first three PILS samples from the opening of the chamber covers. Chamber covers opened at 08:42, 19 minutes into the first PILS sample.

These 14 SOA compounds consisted of eight ON species ($C_9H_{11}NO_9$, $C_{10}H_9NO_3$, $C_{10}H_{13}NO_6$, $C_{10}H_{11}NO_6$, $C_9H_{11}NO_9$, $C_{10}H_{11}NO_4$, $C_5H_7NO_6$ and $C_{10}H_{17}NO_3$), one oligomer ($C_{18}H_{20}O_{12}$), three oxidised compounds ($C_{10}H_{14}O_3$, $C_{11}H_{18}O_5$ and $C_{10}H_{12}O_5$), and one compound at MW 121 g mol^{-1}; whose molecular formula could not be identified due to a large error in the mass accuracy. Of the ON compounds, the structures of three were identified as substituted nitrophenols; 3-(5-hydroxy-4-methoxy-2-nitrophenyl)propane-1,2-diol (Compound 1, Table 4.1, MW 243 g mol^{-1}, $C_{10}H_{13}NO_6$), 1-hydroxy-3-(2-hydroxy-4-methoxy-5-nitrophenyl)propan-2-one (see Section 4.3.1.4 for compound identification, MW

241 g mol^{-1} C$_{10}$H$_{11}$NO$_6$) and 5-methoxy-4-nitro-2-(prop-2-en-1-yl)phenol (see Section 4.3.1.4 for compound identification, MW 209 g mol^{-1} C$_{10}$H$_{11}$NO$_4$).

The formation mechanism of 3-(5-hydroxy-4-methoxy-2-nitrophenyl)propane-1,2-diol from the photo-oxidation of methyl chavicol has previously been determined (Chapter 3, Section 3.3.9). The formation of the diol on the hydrocarbon chain of 3-(5-hydroxy-4-methoxy-2-nitrophenyl)propane-1,2-diol occurs through RO$_2$ + RO$_2$ self/cross reactions, favoured in relatively "low NO environments". Thus, this compound requires both a relatively low NO environment for the formation of the diol on the hydrocarbon chain and sufficient NO$_2$ concentration for the addition of a nitro group to the aromatic ring. The NO$_2$ concentration was divided by the NO concentration at each measured time period during MC$_{[high]}$. This provided a temporal profile of the NO$_2$/NO ratio (ppbv/ppbv). The temporal profile of 3-(5-hydroxy-4-methoxy-2-nitrophenyl)propane-1,2-diol was found to display a direct correlation with the temporal profile of the NO$_2$/NO ratio (ppbv/ppbv) as shown in Figure 4.6. All of the ON compounds except C$_{10}$H$_{17}$NO$_3$ (MW 199 g mol^{-1}) and C$_5$H$_7$NO$_6$ (MW 177 g mol^{-1}) were also observed to follow the same correlation with the NO$_2$/NO ratio (ppbv/ppbv). Furthermore, all of the nitrogen containing compounds except C$_{10}$H$_{17}$NO$_3$ and C$_5$H$_7$NO$_6$, displayed a TP 3 evolution and characteristic mass spectral fragmentation patterns suggesting these compounds contained resonance stabilised ring structures (see Section 4.3.1.4). Based on the molecular formulae, C$_5$H$_7$NO$_6$ and C$_{10}$H$_{17}$NO$_3$ cannot contain a benzene ring structure, with C$_5$H$_7$NO$_6$ containing too few carbons atoms and DBEs (DBE = 3) and C$_{10}$H$_{17}$NO$_3$ containing too many hydrogen atoms. Thus, these compounds cannot be substituted nitrophenols, potentially explaining why a TP3 evolution and correlation with the NO$_2$/NO ratio (ppbv/ppbv) was not observed for these species. As a result, these compounds are not included in the remaining discussion.

The structurally identified nitrogen containing species were characterised as semi- to low volatility oxygenated organic compounds, with 3-(5-hydroxy-4-methoxy-2-nitrophenyl)propane-1,2-diol just fractionally outside the extremely low volatility (ELVOC) region proposed in Donahue (2013). Of the structurally unidentified compounds, one was determined to have a molecular formula of C$_9$H$_{11}$NO$_9$. This compound has an O:C ratio of 1 and is thus also likely to be an extremely low volatility oxygenated organic compound. The low volatility of these compounds and observation of these species during initial SOA growth, as shown in Figure 4.7, suggests that these compounds are among the least volatile species and are thus likely to be involved in the initial SOA growth.
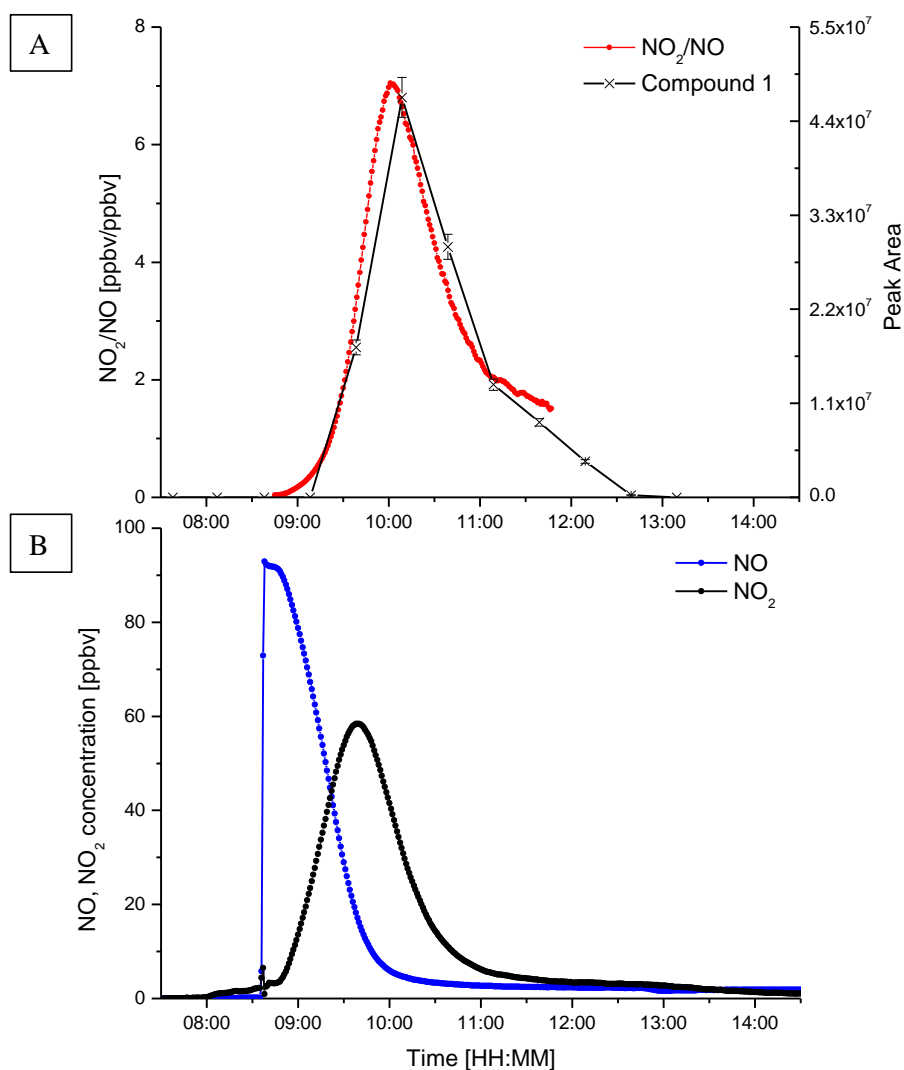
Figure 4.6 - Correlation of the NO_2/NO concentration ratio (ppbv/ppbv) with the particle phase temporal profile of 3-(5-hydroxy-4-methoxy-2-nitrophenyl)propane-1,2-diol (compound 1, Table 4.3) in experiment $MC_{[high]}$. (A) Black = temporal profile of 3-(5-hydroxy-4-methoxy-2-nitrophenyl)propane-1,2-diol. Red = temporal profile of the NO_2/NO ratio (ppbv/ppbv). (B) Blue = NO concentration. Black = NO_2 concentration.
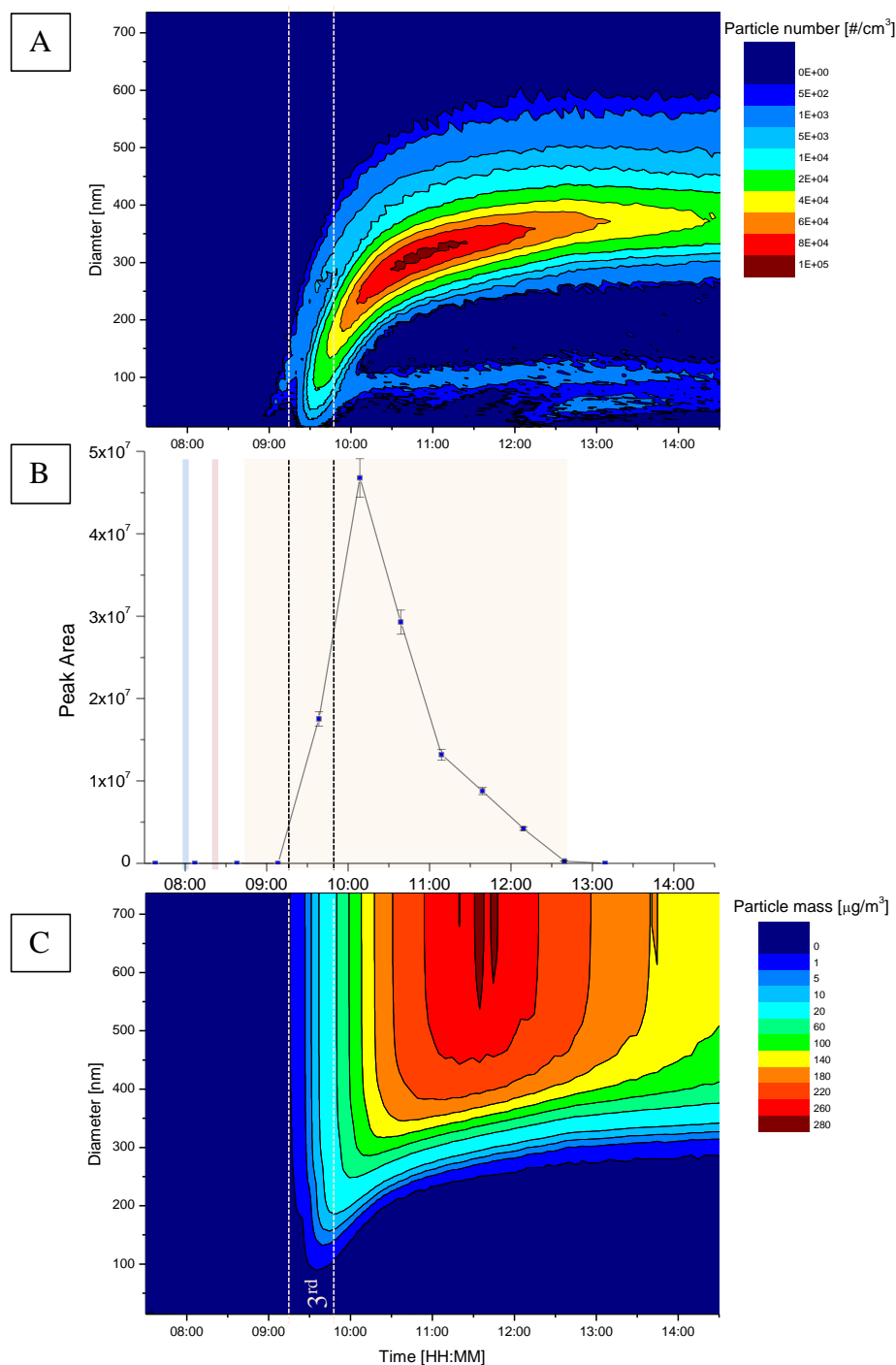
Figure 4.7 - Particle diameter *vs*. time with a coloured contour plot displaying increasing particle number (A) and particle mass (C), compared with the aerosol phase temporal profile of 3-(5-hydroxy-4-methoxy-2-nitrophenyl)propane-1,2-diol (B) (compound 1, a Compound observed in positive and negative ionisation mode. [b] The measured isotopic distribution and abundance does not match for the selected molecular formula.

Table 3.4) during $MC_{[high]}$. Shaded areas; Blue = NO addition. Red = methyl chavicol addition. Orange = opening to the closing of the chamber covers. Dashed lines display the first PILS sampling period where SOA was first observed (3rd sample from the opening of the chamber covers).

4.3.1.4 ON Compound Structure Assignment

The fragmentation data of the structurally unidentified nitrogen containing compounds, $C_{10}H_{11}NO_4$ (MW 209 g mol^{-1}) and $C_{10}H_{11}NO_6$ (MW 241 g mol^{-1}) observed in $MC_{[high]}$, are shown in Tables 4.4 and 4.5, respectively. The molecular formulae of both these compounds were determined from the FTICR-MS and HPLC-QTOF-MS. The molecular formula of MW 209 g mol^{-1} was determined as $C_{10}H_{11}NO_4$, with a molecular formulae error of 0.9 ppm with a score of 100% for the FTICR-MS analysis, and an error of 6.9 ppm with a score of 100% for the HPLC-QTOFMS analysis. The molecular formulae of MW 241 g mol^{-1} was determined as $C_{10}H_{11}NO_6$ with an error of 0.7 ppm with a score of 100% for the FTICR-MS analysis, and error of -3.8 ppm with a score of 100% for the HPLC-QTOF-MS analysis. Tentative structures have been proposed for these compounds based on the observed fragment ions and losses. The identification of both of these compounds in the first PILS SOA sample (between 41 to 71 minutes into $MC_{[high]}$) and the similarity of the carbon number and degree of saturation (DBE) to the original VOC precursor, methyl chavicol, suggests the structures of these compounds are likely to be similar to that of the VOC precursor; a substituted methoxyphenyl.

The fragmentation patterns of $C_{10}H_{11}NO_4$ (MW 209 g mol^{-1}) is discussed here and shown in Figure 4.8. This compound was assigned as 5-methoxy-4-nitro-2-(prop-2-en-1-yl)phenol (Table 4.3, compound 3) containing 6 DBE. The highest intensity fragment ion at *m/z* 193 is the result of an odd electron (OE) cleavage of $^{\bullet}CH_3$ from the methoxy group ($R-OCH_3$). OE cleavages are unusual in CID and are often associated with resonance stabilised ring structures (Holčapek et al., 2010; Pereira et al., 2014). The loss of $^{\bullet}CH_3$ suggests that a methoxy group is attached to an aromatic ring and the ring is resonance stabilised (Figure 4.8A). The fragment ion at *m/z* 178 suggests a loss of C_2H_6 from the deprotonated molecular species. This appears to be an unlikely neutral loss, suggesting that the double bond on the hydrocarbon chain (HC) has opened and gained two hydrogen atoms. Considering the formation mechanisms, isomerisation through a 1,5 H-atom shift is suggested to be of minor importance due to the resonance stability of the ring (Pereira et al., 2014). It is possible that the double bond could become saturated from the addition of an $^{\bullet}OH$ radical and subsequent further reactions. However, there is no indication that the HC chain contains any elements

other than carbon and hydrogen. Furthermore, the molecular formula of remaining fragment ion, $C_8H_4NO_4$, has very few hydrogen atoms and a high number of DBEs (DBE = 7), making it difficult to propose an aromatic structure which adheres to this. A more likely alternative is the loss of NO (Figure 4.8B), which would also support the presence of a resonance stabilised ring structure. The loss of NO is often observed with resonance stabilised ring structures where an electron donating functional group (*e.g.* an alcohol group) is located in the para position to the nitro group (Bursey and McLafferty, 1966; Bursey, 1969; Schmidt et al., 2006; Pereira et al., 2014).

Fragment ion *m/z* 163 is the result of a loss of CH_3NO from the deprotonated molecular species (Figure 4.8C), or a consecutive loss of NO from fragment ion *m/z* 193 (Figure 4.8D). Both losses suggest a nitro group is attached to the aromatic ring with an electron donating substituent in the para position to the nitro group. The loss CH_3NO also supports the loss of NO (fragment ion *m/z* 178). The loss of CH_3NO suggests the nitro group is located next to the methoxy group, undergoing an intermolecular re-arrangement and resulting in the loss of CH_3 from the methoxy group and NO from the nitro group (Figure 4.8C). Fragment ion *m/z* 145 is the result of a consecutive loss of H_2O and CH_3NO (CH_5NO_2) from the deprotonated molecular species (Figure 4.8D), or the loss of H_2O from fragment ion *m/z* 163 (Figure 4.8C). Hydrogen atom abstraction directly from a resonance stabilised aromatic ring is unlikely. However, if the NO_2 group has already been lost, the decrease in resonance stabilisation is more likely to allow H-atom abstraction to occur directly from the ring. Alternatively, H-atom abstraction may occur from the HC chain, resulting in the loss of H_2O.

The fragmentation patterns of $C_{10}H_{11}NO_6$ (MW 241 g mol^{-1}) is shown in Figure 4.9. The deprotonated molecular species (M-H)$^-$ at *m/z* 240 was observed below the MS^2 threshold in the HPLC-QTOFMS^2 analysis. Consequently, the fragmentation data could not be obtained for this compound using this technique. Instead, the HPLC-ITMS^2 was used. This compound was assigned as 1-hydroxy-3-(2-hydroxy-4-methoxy-5-nitrophenyl)propan-2-one (Table 4.3, compound 2) containing 6 DBE. The highest intensity fragment ion at *m/z* 222 is from the loss of H_2O, suggesting the presence of an alcohol group on the HC, most likely in the terminal position (Figure 4.9A) (Pereira et al., 2014). The second fragment ion at *m/z* 210, suggests the loss of NO, which is further supported by the loss of CH_3NO resulting in a fragment ion at *m/z* 195 (Figures 4.9B and C). This suggests that an NO_2 group is located on the aromatic ring next to the methoxy group and an electron donating substituent is in the para position to the NO_2 group; as observed with the fragmentation of 5-methoxy-4-nitro-2-(prop-2-en-1-yl)phenol discussed above.

The fragment ion at *m/z* 193 can be attributed to the loss of HNO_2, which is most likely the result of the NO_2 group abstracting a hydrogen atom from the methoxy group (Figure 4.9D). Finally, the fragment ion at *m/z* 166 can be attributed to the loss of $C_3H_6O_2$ from the deprotonated molecular species, which is mostly likely to be the loss of the HC chain. The loss of $C_3H_6O_2$ contains too few hydrogen atoms to be fully saturated. Furthermore, the loss of H_2O (fragment ion *m/z* 222), suggests that the double bond on the hydrocarbon chain has opened. Therefore, it is likely that a ketone is attached on the adjacent carbon atom to the alcohol group (Figure 4.9E); with the leaving group ($C_3H_6O_2$) abstracting a hydrogen atom from the aromatic ring, most likely after the loss of NO_2.

Table 4.4 - Deprotonated molecular species fragmentation for $C_{10}H_{11}NO_4$ (MW 209 g mol^{-1}), obtained from the use of the HPLC-ITMS[2] and the HPLC-QTOFMS[2]

[M-H]$^-$	m/z	DBE	Fragment ion [m/z]	Fragment ion MF	DBE	EF	Loss [Da]	Suspected loss	Fragment ion MF error [ppm]	Fragment ion score [%]	Fragmentation shown
$C_{10}H_{10}NO_4$	208	6	**193**	**$C_9H_7NO_4$**	**6***	**OE**	**15**	**$^\bullet CH_3$**	**7.0**	**100**	**Figure 4.8A**
			178	$C_8H_4NO_4$	7	EE	30	C_2H_6†	5.7	100	Figure 4.8B
			163	$C_9H_7O_3$	6	EE	45	CH_3NO or NO from m/z 193	-0.1	100	Figure 4.8C
			145	$C_9H_5O_2$	7	EE	63	CH_5NO_2 (H_2O + CH_3NO) or H_2O from m/z 163	2.7	100	Figure 4.8C and D

The highest intensity fragment ion is shown in bold. Electron fragmentation (EF), EE = even electron, OE = odd electron. MF = molecular formula. *DBE was manually calculated, as automated DBE calculation is incorrect for radical fragment ions (DBE = 6.5 - 0.5 (for one 'hydrogen atom deficiency') = 6, see (Pellegrin, 1983) for the calculation of DBE and DBE correction for radical ions). † = Loss of C_2H_6 seems unlikely, suspected loss of NO (see text for further explanation).
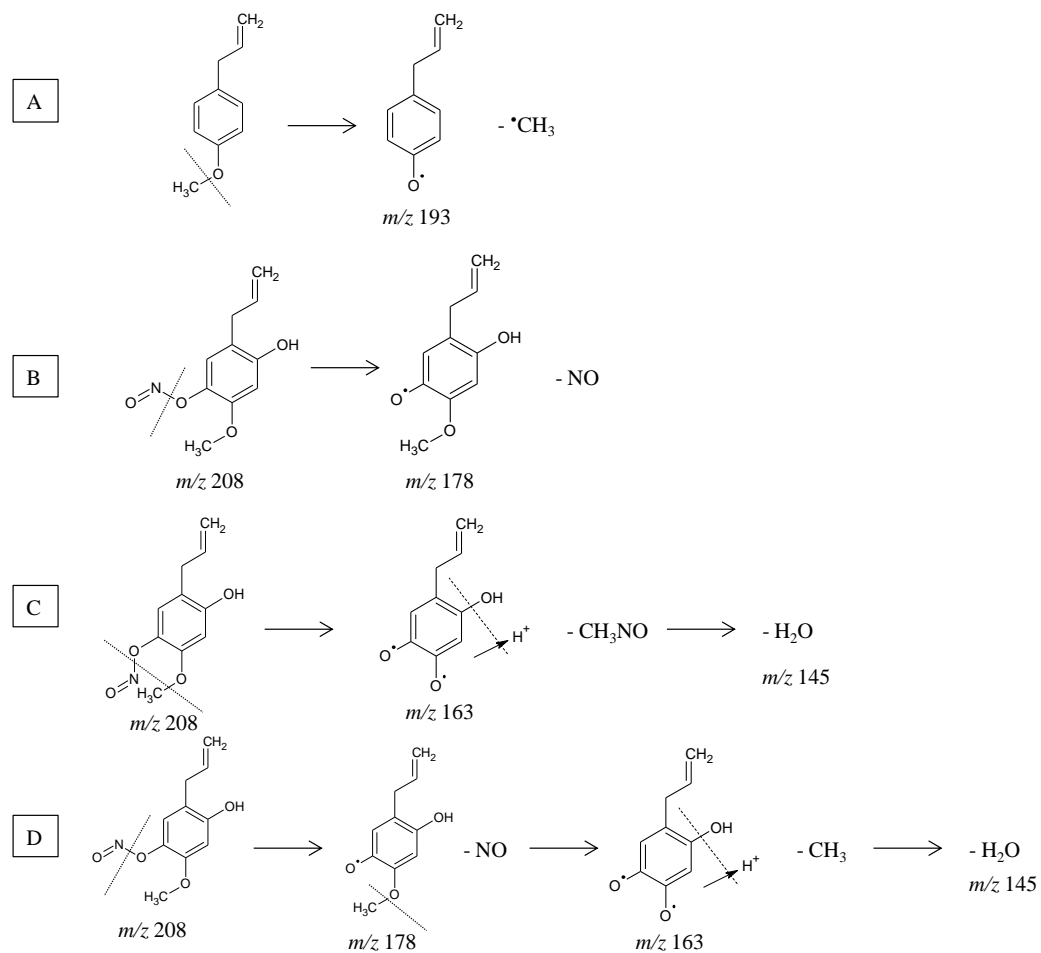
Figure 4.8 - Proposed deprotonated molecular species fragmentation for $C_{10}H_{11}NO_4$ (MW 209 g mol^{-1}) in negative ionisation mode. Dashed lines indicate the location of fragmentation.

Table 4.5 - Deprotonated molecular species fragmentation for $C_{10}H_{11}NO_6$ (MW 241 g mol^{-1}), obtained from the use of the HPLC-ITMS^2

(M-H)$^-$	Fragment ion [m/z]	Loss [Da]	Suspected Loss	Fragmentation shown
240	**222**	**18**	**H_2O**	**Figure 4.9A**
	210	30	NO	Figure 4.9B
	195	45	CH_3NO	Figure 4.9C
	193	47	HNO_2	Figure 4.9D
	166	74	$C_3H_6O_2$	Figure 4.9E

The highest intensity fragment ion is shown in bold.
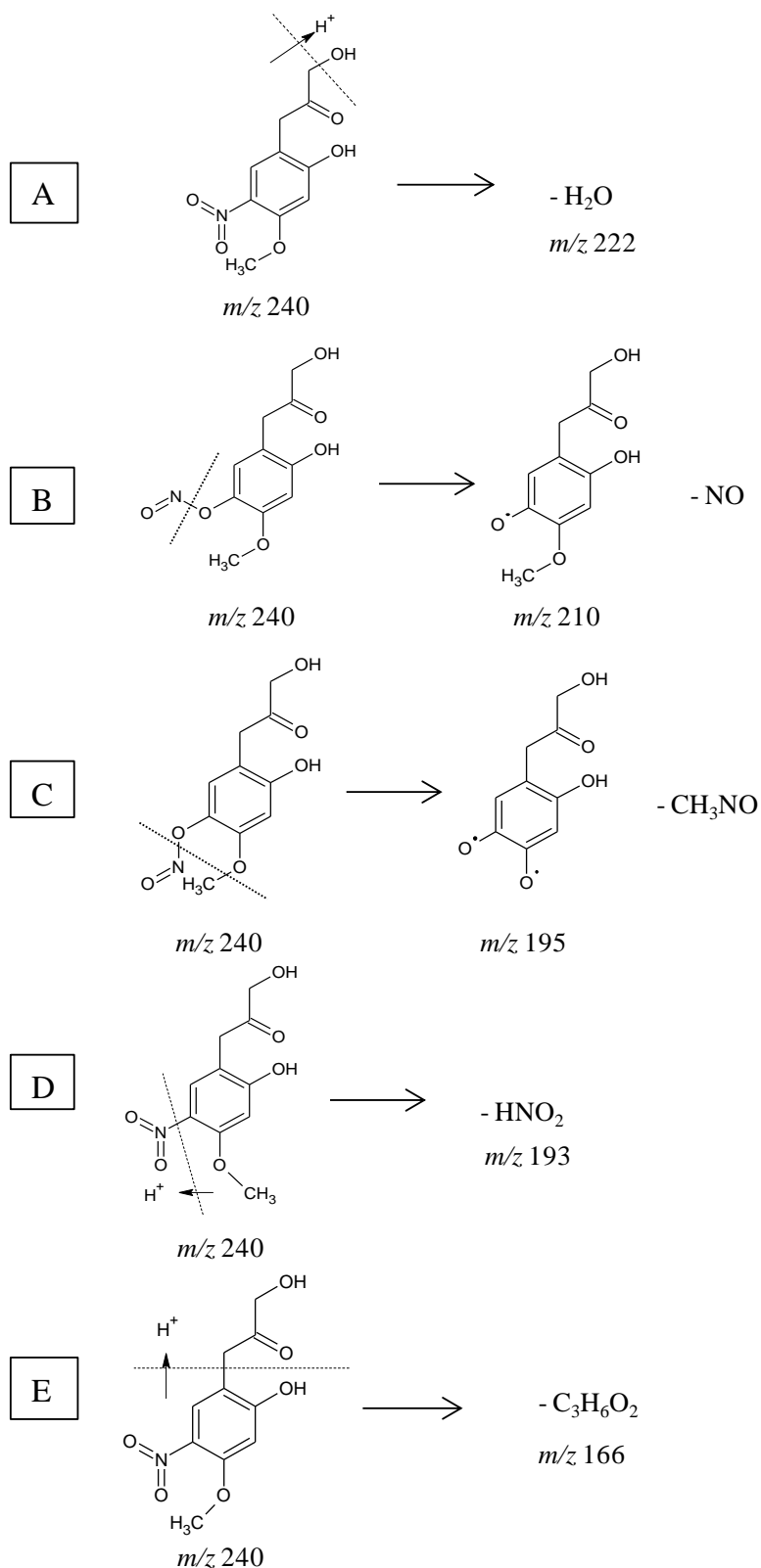
Figure 4.9 - Proposed deprotonated molecular species fragmentation for $C_{10}H_{11}NO_6$ (MW 241 g mol^{-1}) in negative ionisation mode. Dashed lines indicate the location of fragmentation.

4.3.2 Photo-oxidation of Toluene and 4-methylcatechol

Owing to the clear importance of nitrophenols in methyl chavicol SOA formation, three other aromatic systems, toluene, 4-methylcatechol and benzaldehyde were also investigated. However, very little aerosol mass was formed during the photo-oxidation of benzaldehyde (< 2.83 µg m^{-3}) and no SOA compounds were observed in the SOA samples. As a result, photo-oxidation of benzaldehyde is not discussed further.

Two toluene photo-oxidation experiments were investigated; (i) Tol$_{low}$, a VOC/NO$_x$ ratio ~ 13, where 535 ppbv of toluene and 41 ppbv of NO was added into the chamber, and; (ii) Tol$_{high}$, a higher VOC/NO$_x$ ratio ~ 5, where 560 ppbv of toluene and 105 ppbv of NO was added into the chamber (Table 4.1). In both experiments, two nitrogen containing compounds were observed in the PILS SOA samples and are assigned as; methyl-nitrophenol (C$_7$H$_7$NO$_3$, MW 153 g mol^{-1}) a second generation product and methyl nitro-catechol (C$_7$H$_7$NO$_4$, MW 169 g mol^{-1}) a third generation product. Both of these compounds are two major toluene photo-oxidation products (Forstner et al., 1997; Jang and Kamens, 2001; Hamilton et al., 2005; Sato et al., 2007). The deprotonated molecular species of methyl-nitrophenol in the HPLC-ITMS^2 analysis was below the MS^2 threshold, subsequently no fragmentation data was obtained for this compound. However, no other deprotonated molecular species were observed at this *m/z* in the PILS SOA samples. As this compound is known to be a major toluene photo-oxidation product and no other ions were observed at this *m/z*, it very likely that this peak is the result of methyl-nitrophenol. The exact locations of the aromatic substitutions of methyl nitro-catechol are unclear and are discussed in Section 4.3.2.1, but based on known mechanisms and the structural elucidation of the fragmentation patterns, the most likely structure is 3-methyl-4-nitrocatechol.

The temporal profiles of methyl-nitrophenol and methyl nitro-catechol were observed to follow the same TP 3 shape observed previously for the methyl chavicol nitrophenols. Again, both of these compounds also displayed a direct correlation with the temporal profile of the NO$_2$/NO (ppbv/ppbv) ratio (Figure 4.10), although the more volatile species, methyl-nitrophenol, was slightly delayed in experiment Tol$_{high}$, partitioning into the aerosol phase up to 30 minutes later than the methyl nitro-catechol (Figure 4.11). The saturation concentration of methyl-nitrophenol and methyl nitro-catechol was determined as 1.12×10^5 and 1.41×10^3 µg m^{-3}, respectively, characterising these species as intermediate-VOCs. The gas concentrations of methyl-nitrophenol and methyl nitro-catechol in both toluene experiments are not known. However, in order for methyl-nitrophenol and methyl nitro-catechol to partition into the aerosol phase without any absorptive mass present, a gas phase

concentration of 17.95 ppmv and 0.20 ppmv respectively would be required (based on their calculated saturation concentrations); well in excess of the initial toluene mixing ratios. Providing some absorptive mass is present, a gaseous species can partition some of its mass into the aerosol phase below its saturation concentration (Pankow, 1994b, a; Kroll and Seinfeld, 2008). However, even taking this into account, it is clear that equilibrium partitioning cannot describe the observation of these relatively volatile species in the aerosol phase, during initial aerosol formation and growth (Figures 4.12 and 4.13).
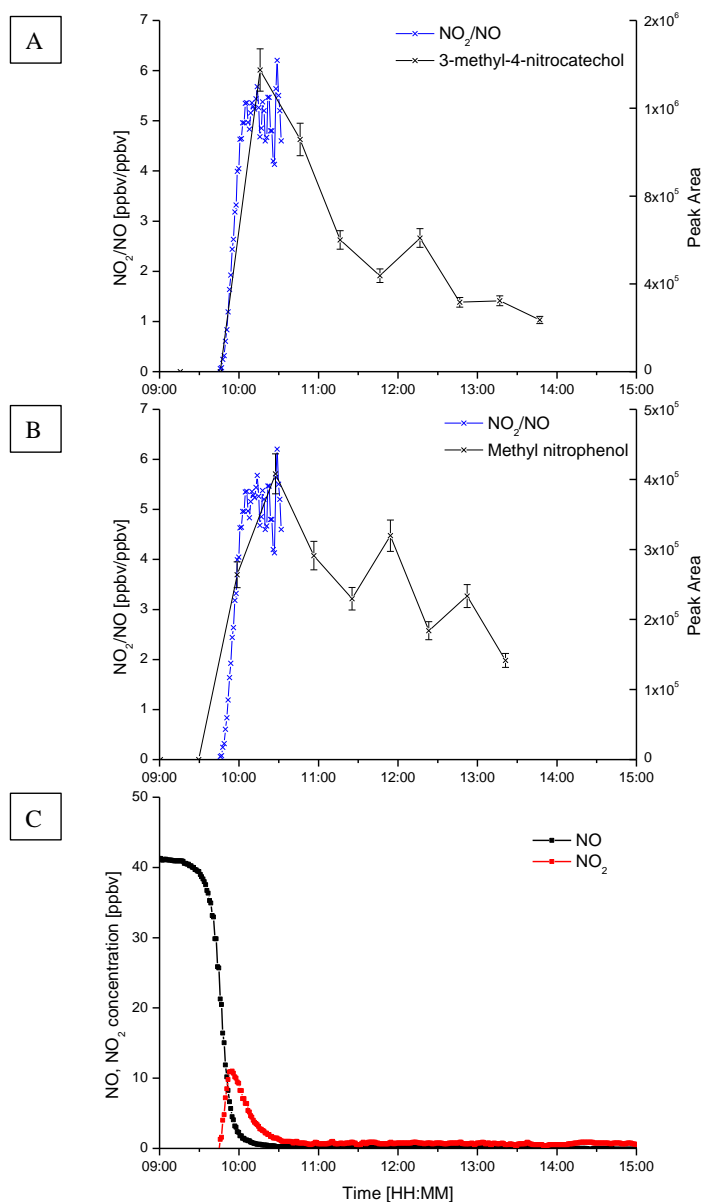
Figure 4.10 - Correlation of the NO_2/NO concentration ratio (ppbv/ppbv) with the particle phase temporal profiles of two toluene oxidation products, 3-methyl-4-nitrocatechol (A) and methyl nitrophenol (B) during Tol_{low}, with the NO and NO_2 temporal evolution shown in (C).
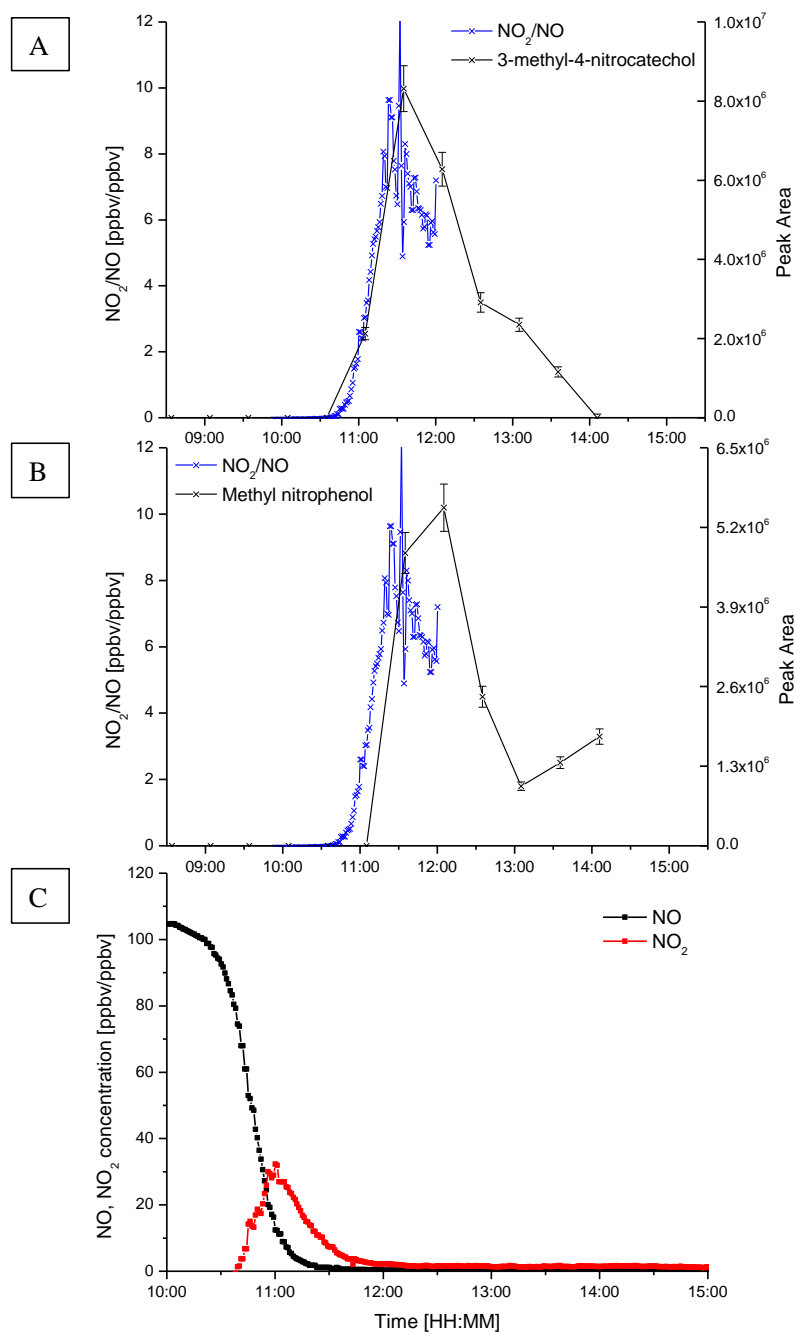
Figure 4.11 - Correlation of the NO_2/NO concentration ratio (ppbv/ppbv) with the particle phase temporal profiles of two toluene oxidation products, 3-methyl-4-nitrocatechol (A) and methyl nitrophenol (B) during Tol_{high}, with the NO and NO_2 temporal evolution shown in (C).
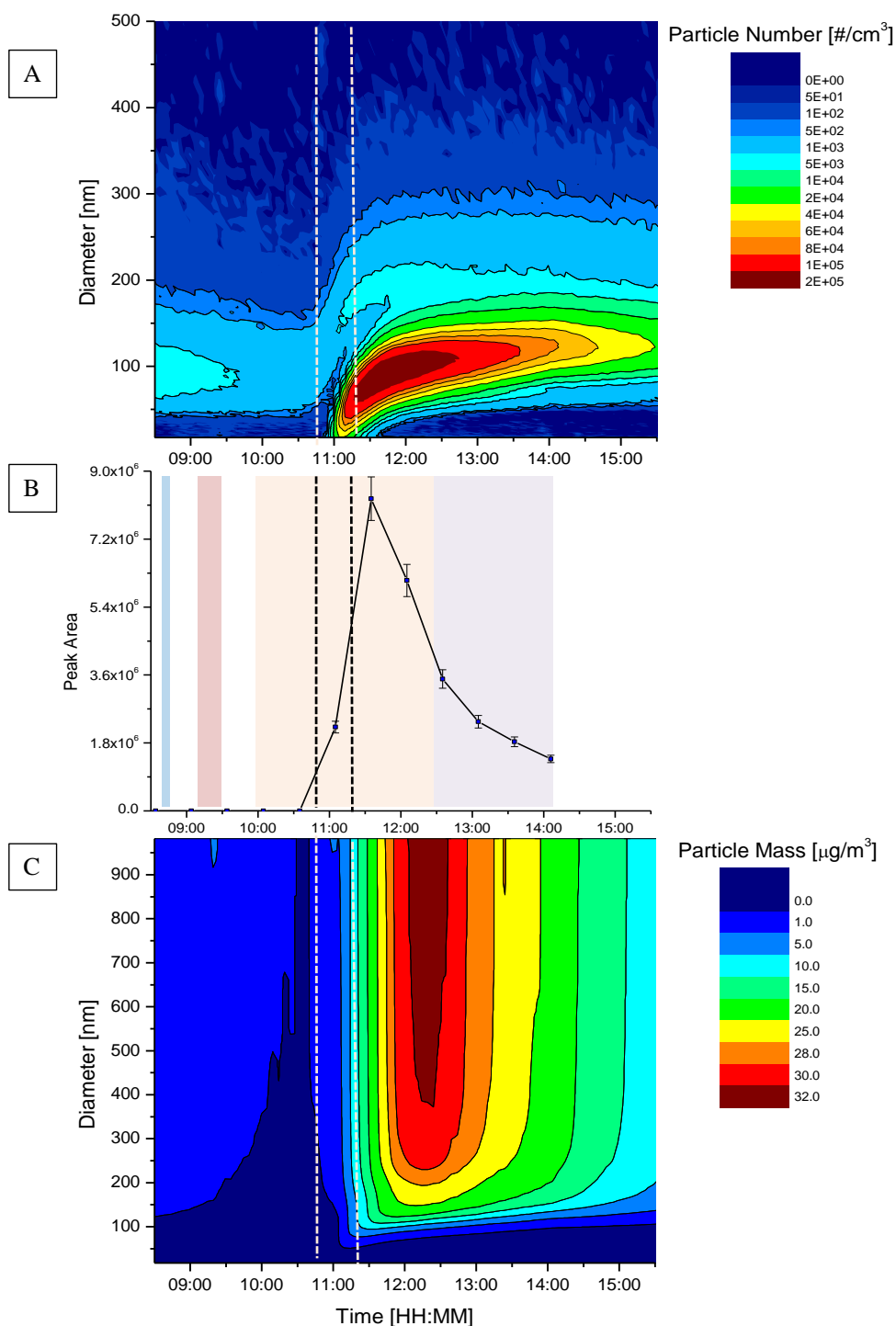
Figure 4.12 - Particle diameter *vs.* time with a coloured contour plot displaying increasing particle number (A) and particle mass (C), compared with the temporal profile of 3-methyl-4-nitrocatechol (B) during Tol$_{high}$. Shaded areas; Blue = toluene addition. Red = NO addition. Orange = Chamber covers fully open. Purple = chamber cover closed by 30˚. Dashed lines display the start and end time of the PILS sampling period. Methyl nitrophenol not shown as it was observed in the aerosol phase after initial aerosol growth was observed (up to 30 minutes later).
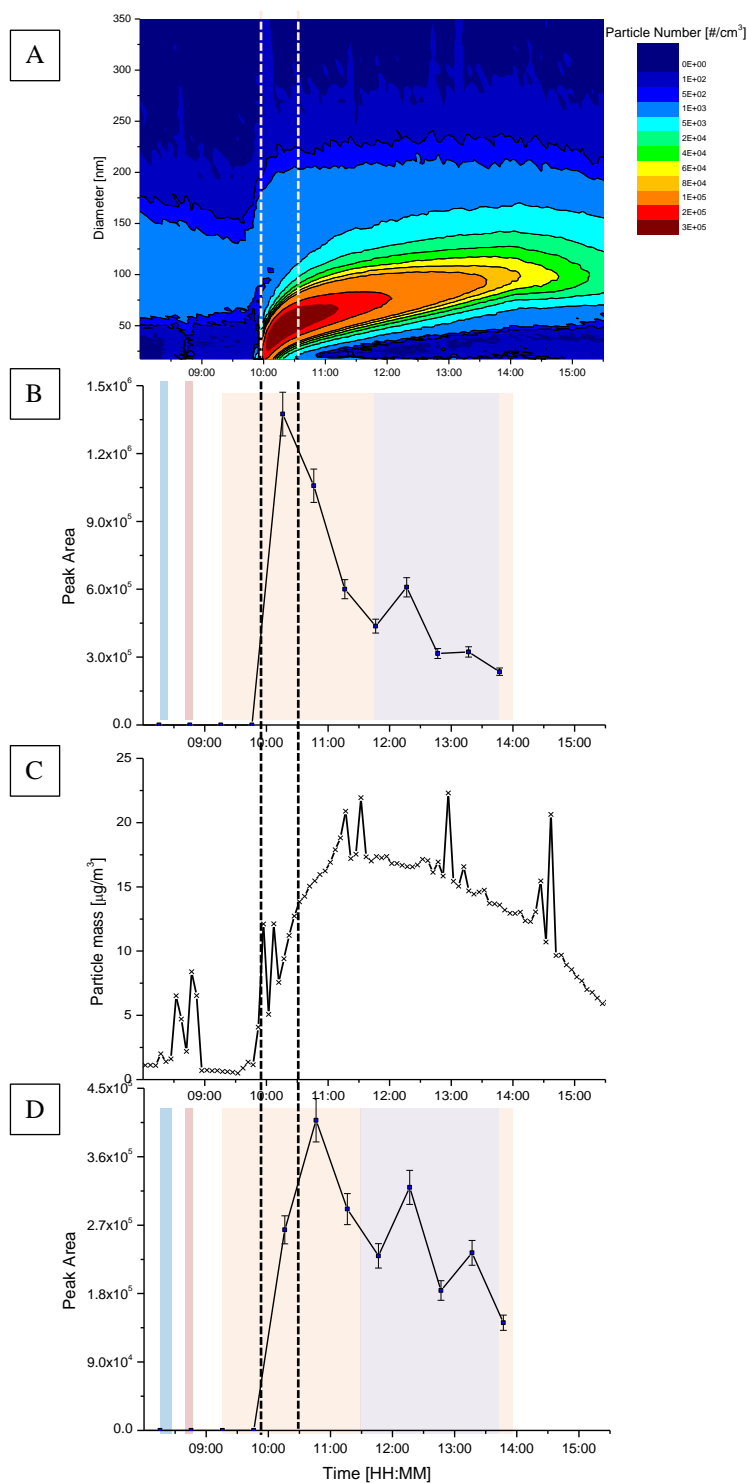
Figure 4.13 - Particle diameter *vs*. time with a coloured contour plot displaying increasing particle number (A) compared with increasing particle mass over time (C) and the temporal profile of 3-methyl-4-nitrocatechol (B) and methyl-nitrophenol (D) during Tol$_{low}$. Shaded areas; Blue = toluene addition. Red = NO addition. Orange = chamber covers fully open. Purple = chamber cover closed by 30˚. Dashed lines display the start and end time of the PILS sampling period.

The reason why these intermediate volatility compounds are observed in the aerosol phase during initial aerosol growth is currently unclear. However, a recent study has also observed a similar phenomenon with nitrophenols formed from the photo-oxidation of benzene (Sato et al., 2012). In their study, nitrophenols measured using HR-TOF-AMS were observed from the onset of SOA nucleation and rapidly decreased in concentration over the first hour (Sato et al., 2012). The composition of these compounds were determined from the collection of SOA onto filter samples, followed by HPLC-TOFMS analysis (Sato et al., 2012). Whilst no reference to volatility was made in their study, two of the nitrophenols identified using commercial available standards, 4-nitrophenol and 4-nitrocatechol, will be of even higher volatility (calculated $C^* = 3.19 \times 10^5$ and 4.70×10^3 μg m^{-3}) than the species identified in this study, due to the lack of a methyl group on the aromatic ring. Furthermore, Sato et al. (2012) observed that from the onset of SOA nucleation to the first 60 minutes of the experiment, nitrophenol formation was almost independent of the amount of absorptive mass present (Sato et al., 2012). One possible explanation for these observations, is the formation of gas phase clusters.

A number of studies have shown phenol-phenol or phenol-water clusters can form in the gas phase and produce stable clusters through hydrogen bonding (Benoit and Clary, 2000; Tsui and van Mourik, 2001; Cabral do Couto et al., 2002; Parthasarathi et al., 2005). Theoretical simulations predict the stability of phenol-water clusters to be comparable to that of water clusters, exhibiting similar hydrogen bonding energies. Nitrobenzene has also been found to produce gas phase clusters, recently being used as a modifier in the buffer gas of ion mobility mass spectrometry, to reduce the mobility of certain ions through gas phase cluster formation (Fernández-Maestre et al., 2012)). Whilst no studies, have investigated nitrophenol gas phase clustering, these compounds are known to form both intra- and inter-molecular hydrogen bonds; with very strong intra-molecular hydrogen bonding observed between the nitro and hydroxyl group (C-NO—HO-C) (Chen et al., 1998; Chen and Chen, 2001; An et al., 2011). Potentially, very strong inter-molecular hydrogen bonds could form with other nitrophenols, water, sulfuric acid, and/or other suitable species, resulting in stabilised cluster formation and new particle formation. If these compounds were to form stabilised clusters in the gas phase, this could explain why these species are observed in the aerosol phase from the onset of SOA nucleation, as shown in (Sato et al., 2012) and during initial aerosol growth, as shown in this study; potentially uncovering a new mechanism for new particle formation and/or growth of SOA.

In contrast to the other two aromatic systems investigated, the photo-oxidation of 4-methylcatechol did not result in the formation of nitrophenols in the aerosol phase during

initial SOA growth. In this experiment (Table 4.1), only one nitrophenol compound (MW 168 g mol^{-1}, 4-methyl-5-nitrocatechol) was observed in the PILS SOA samples. The fragmentation patterns and structural assignment of this species is discussed in Section 4.3.2.1. Interestingly, 4-methyl-5-nitrocatechol was not observed in the aerosol phase until the chamber covers were closed, approximately 2.5 hours after irradiation was initiated (Figure 4.14). The observation of this species in the aerosol phase after irradiation had stopped, suggests photolytic dissociation is preventing this compound from accumulating in the gas phase and partitioning into the aerosol phase. The location of aromatic substitutions can affect the rate of reaction (Bejan, 2006), photolysis dissociation (Bejan, 2006; Chen et al., 2011) (including HONO formation (Bejan et al., 2006)) and the strength of hydrogen bonds due to the change in resonance stability of the aromatic ring (should these species undergo gas phase clustering) (Chen et al., 1998; Chen and Chen, 2001; An et al., 2011). It is therefore likely that location of aromatic substitutions in 4-methyl-5-nitrocatechol makes this compound more susceptible to a loss process such as photolysis degradation than 3-methyl-4-nitrocatechol (observed from the photo-oxidation of toluene), accounting for the differences in the timing of partitioning observed; highlighting the importance of studying SOA formation at molecular level.
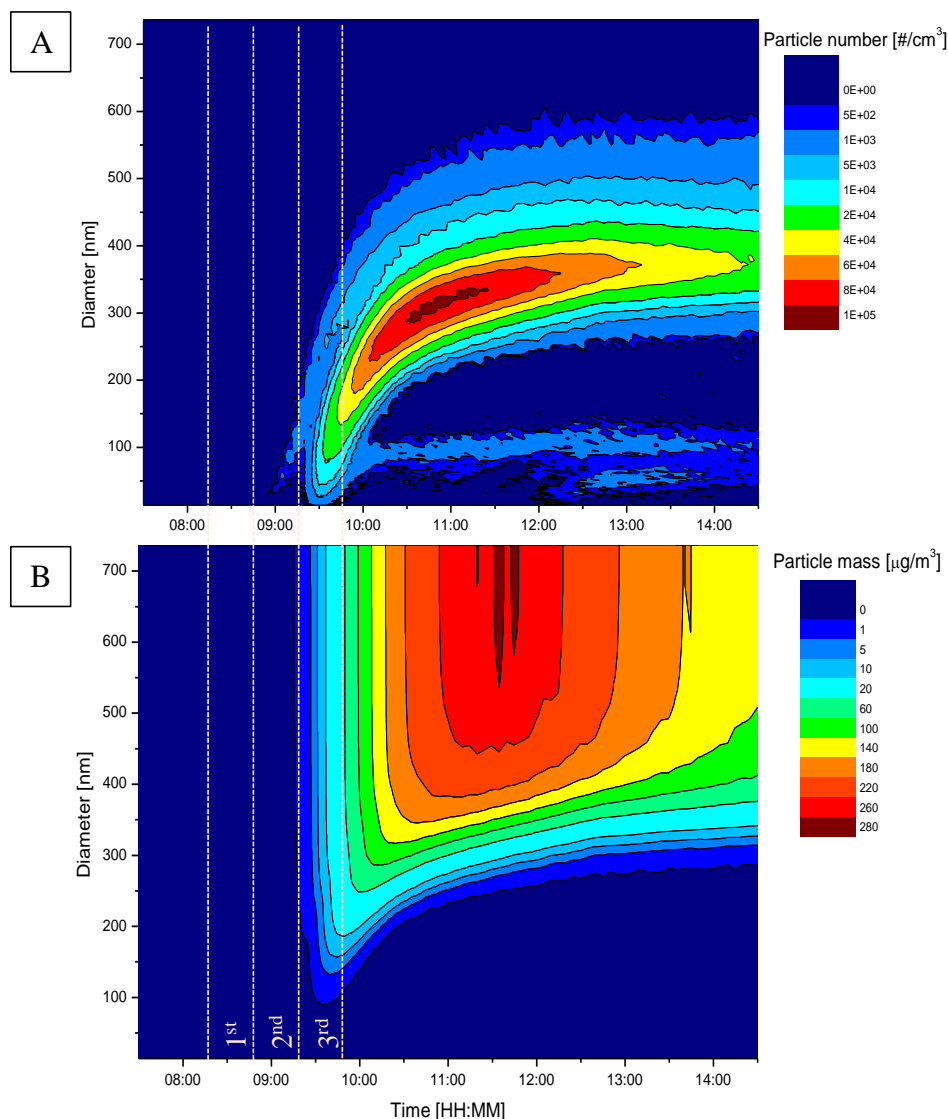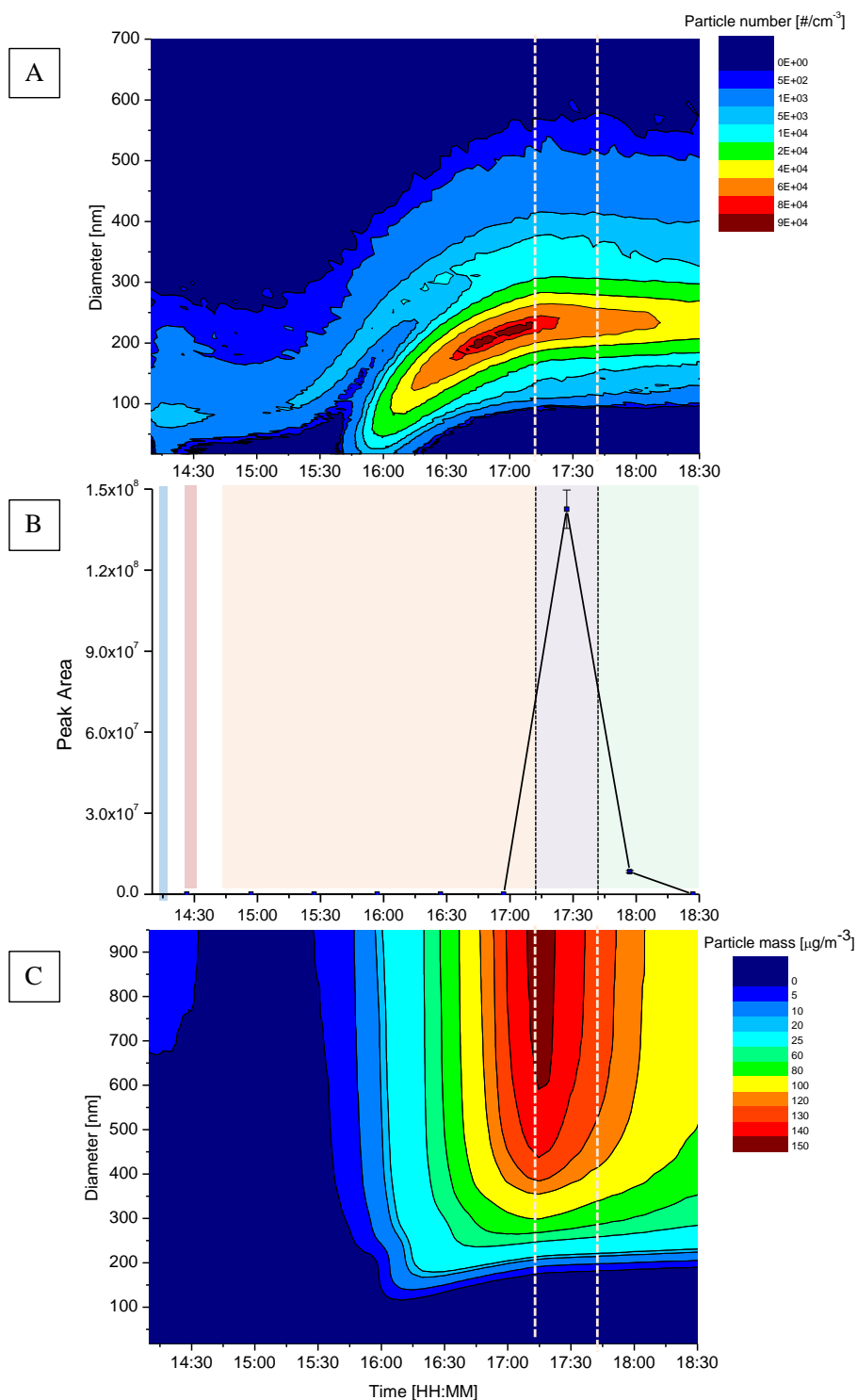
Figure 4.14 - Particle diameter *vs*. time with a coloured contour plot displaying increasing particle number (A) and particle mass (C), compared with the temporal profile of 4-methyl-5-nitrocatechol (B) during 4-MCat. Shaded areas; Blue = 4-methyl catechol addition. Red = NO addition. Orange = chamber covers fully open. Purple = chamber cover closed. Green = filter sampling period, chamber covers still closed. Dashed lines display the start and end time of the PILS sampling period.

4.3.2.1 Compound Structure Assignment

The deprotonated molecular species fragmentation data obtained from the HPLC-ITMS[2] analysis for toluene photo-oxidation product with a MW of 168 g mol^{-1} is shown in Table 4.6 and the proposed fragmentation is shown in Figure 4.15. This compound was assigned as 3-methyl-4-nitrocatechol. The fragment ion at m/z 138 is due to the loss of NO. As previously discussed, the loss of NO occurs from the intermolecular re-arrangement of R-NO_2 to R-O-N=O which is resonance stabilised through an electron donating substituent (*i.e.* an alcohol group) in the para position to the NO_2 group (Figure 4.15B). The fragment ion at m/z 123 is due to the loss of CH_3NO from the deprotonated molecular species, suggesting the NO_2 group is located next the methyl group, as shown in Figure 4.15C. This is further supported by the fragment ion at m/z 121 which is due to the loss of HNO_2 (Figure 4.15D) and the fragment ion at m/z 107 which is due to the loss of CH_3NO_2 (Figure 4.15E). The fragment ion at m/z 148 can be attributed to the loss of H_2O occurring through H-atom abstraction. This loss suggests an alcohol group is attached to the aromatic ring and is most likely located next to the methyl group; where hydrogen atom abstraction would be more favoured than from the resonance stabilised ring structure (Figure 4.15A). This is also supported by considering the gas-phase mechanisms of formation, where the initial addition of an ˙OH radical to toluene would be most favoured in the ortho position to the methyl group (Forstner et al., 1997; Nakao et al., 2011). Thus, the most likely compound based on the fragmentation patterns and gas-phase mechanisms of formation is 3-methyl-4-nitrocatechol.

The deprotonated molecular species fragmentation data obtained from the HPLC-ITMS[2] analysis for 4 -methyl catechol photo-oxidation product with a MW of 168 g mol^{-1} is shown in Table 4.7 and the proposed fragmentation is shown in Figure 4.16. This compound was assigned as 4-methyl-5-nitrocatechol. For this compound, only the location of the NO_2 group is required. The same fragment ions at m/z 138 (Figure 4.16A), 123 (Figure 4.16B) and 121 (Figure 4.16C) as observed with 3-methyl-4-nitrocatechol (toluene photo-oxidation product) were observed for fragmentation of 4-methyl-5-nitrocatechol. This suggests that the NO_2 group is located in the ortho position to the methyl group and an electron donating substituent is in the para position the NO_2 group. Considering this, the most likely compound structure is 4-methyl-5-nitrocatechol.

Table 4.6 - Deprotonated molecular species fragmentation for the toluene oxidation product with a MW of 169 g mol^{-1}, obtained from the use of the HPLC-ITMS[2]

(M-H)$^-$	Fragment ion [m/z]	Loss [Da]	Suspected Loss	Fragmentation shown
168	148	20*	H_2O	Figure 4.15A
	138	30	NO	Figure 4.15B
	123	**45**	**˙CH$_3$ from m/z 138 or CH$_3$NO**	**Figure 4.15C**
	121	47	HNO_2	Figure 4.15D
	107	61	CH_3NO_2	Figure 4.15E

The highest intensity fragment ion is shown in bold. * = attributed to the loss of H_2O.
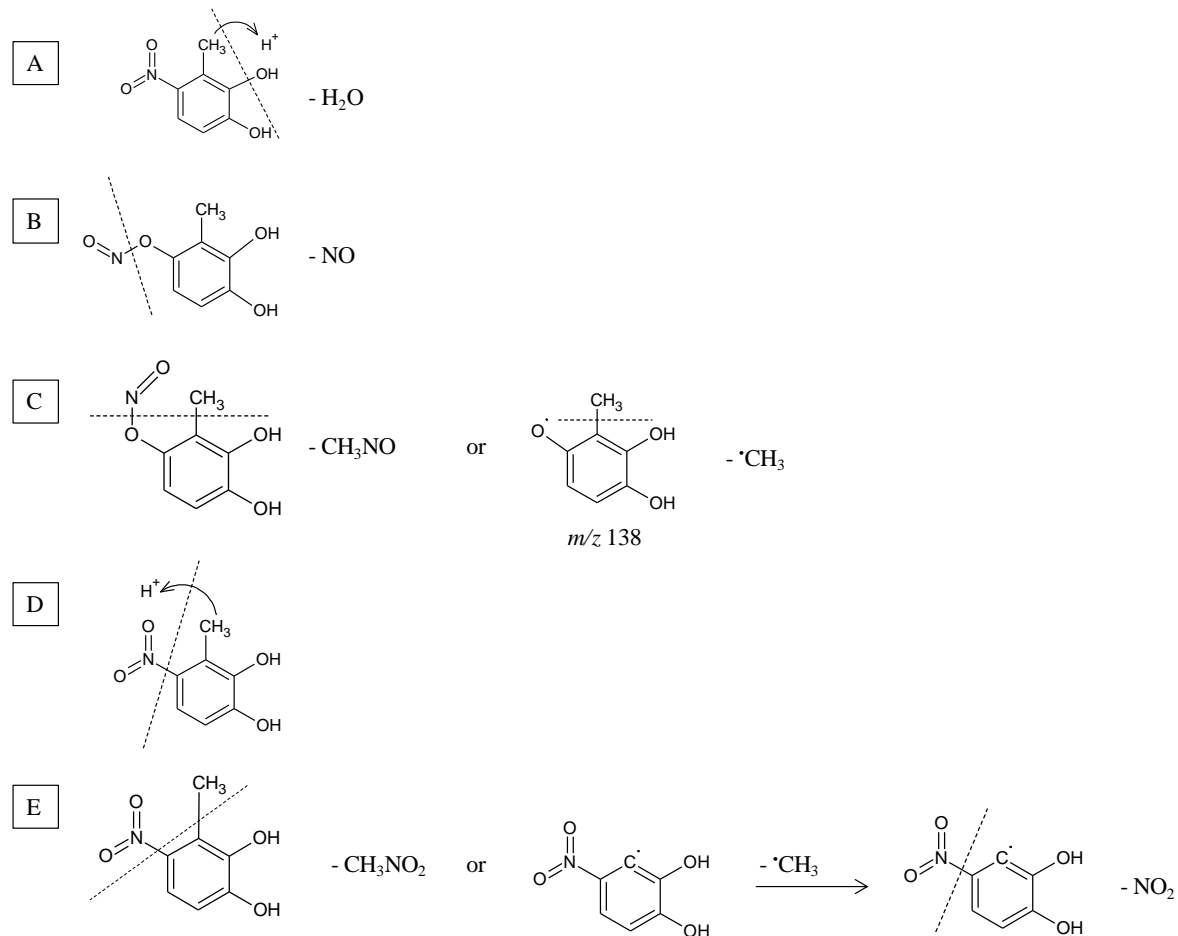
Figure 4.15 - Proposed deprotonated molecular species fragmentation for the toluene oxidation product with a MW of 169 g mol^{-1} in negative ionisation mode. Dashed lines indicate the location of fragmentation.

Table 4.7 - Deprotonated molecular species fragmentation for the 4-methyl catechol oxidation product with a MW of 169 g mol^{-1} obtained from the use of the HPLC-ITMS[2].

(M-H)⁻	Product ion [*m/z*]	Loss [Da]	Suspected Loss	Fragmentation shown
168	148	20*	H_2O	Figure 4.16A
	138	**30**	**NO**	**Figure 4.16B**
	123	45	CH_3 from m/z 138 or CH_3NO	Figure 4.16C
	121	47	HNO_2	Figure 4.16D

The highest intensity fragment ion is shown in bold. * = attributed to the loss of H_2O.
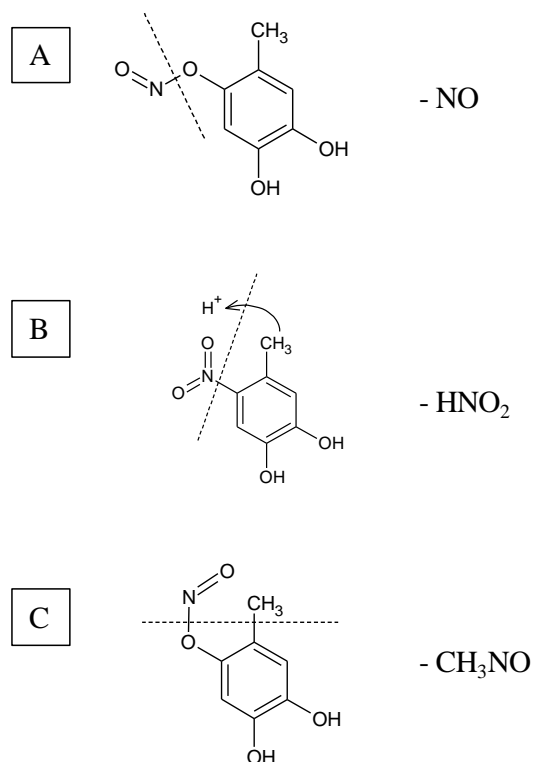
Figure 4.16 - Proposed deprotonated molecular species fragmentation of the 4-methyl catechol photo-oxidation product with a MW of 169 g mol^{-1} in negative ionisation mode. Dashed lines indicate the location of fragmentation.

4.3.3 Atmospheric Relevance

In chamber experiments, the $RO_2 + HO_2$ or RO_2 reaction pathway favoured in relatively "low NO environments" is thought to be key to new particle formation and SOA growth in the photo-oxidation of aromatic VOC systems. Here it is observed that both a low NO environment and sufficient NO_2 concentration is required for the formation of the nitrophenols, which in the photo-oxidation of methyl chavicol represented the majority of compounds in the aerosol phase when initial SOA growth was observed. In chamber experiments, where NO_x is not replenished, the NO_2 concentration decreases close to zero, which is likely to reduce the formation rate of the nitrophenols. However, in the atmosphere NO_2 continuously forms within the VOC-NO_x-O_3 cycle, which is likely to result continuous formation of these compounds in the ambient atmosphere. In the case of toluene (no kinetic data exists for methyl chavicol), hydrogen atom abstraction and addition of NO_2 to the aromatic ring is competitive with the addition of O_2 in polluted environments (Atkinson and Aschmann, 1994). However, downwind of pollution sources and in biomass burning plumes, the formation of these compounds, even if in very low yields, could lead to growth of new particles and potentially result in new particle formation.

The temporal evolution of the SOA species observed in this work may differ from ambient conditions, due to the multiple and complex processes affecting SOA evolution. However, using the techniques described, a greater insight and knowledge of the dynamic processes affecting SOA formation and evolution on a molecular level can be obtained. As shown in this work, the partitioning, formation and loss of individual compounds in the particle phase can vary considerably with only slight changes in the chemical composition and structure. Understanding why different compounds display different rates of formation and loss is critical to understanding SOA formation and evolution in ambient atmosphere.

Chapter 5 - The Use of Ultra-High Resolution Mass Spectrometry for the Compositional

Analysis of OA: Reproducibility and Reliability

5.1   Introduction

Ultra-high resolution mass spectrometry (UHR-MS) has revolutionised compositional analysis in many scientific areas such as; proteomics (study of the structure and function of proteins) (Kelleher, 2004; Macek et al., 2006; Zubarev and Mann, 2007), metabolomics (chemical characterisation of metabolites formed from cellular processes) (Aharoni et al., 2002; Kind and Fiehn, 2006), and petroleomics (chemical characterisation of the organic compounds present in petroleum and crude oil) (Marshall and Rodgers, 2004; Rodgers and Marshall, 2007; Marshall and Hendrickson, 2008; Marshall and Rodgers, 2008). The high mass-resolving power, peak resolution and mass accuracy achieved by these instruments, can allow the elemental composition of thousands of compounds in complex mixtures to be determined (Marshall and Hendrickson, 2008). As a result, UHR-MS has become a valuable tool for the chemical characterisation of compounds in many different scientific fields; including atmospheric aerosols.

The first use of UHR-MS for the compositional analysis of airborne particulate matter was reported in 1969 (Sharkey A. G. Jr. et al., 1969). However, from 1969 to approximately 2004, few studies reported the use of UHR-MS for the chemical characterisation of particulate matter. Only in the last decade has this method of analysis become a rapidly growing area within aerosol science (Nizkorodov et al., 2011). This rapid growth is in-part due to the application of high resolution plots (visualisation tools) for the compositional analysis of organic aerosol (OA). These plots were originally designed for the chemical sorting of individual compounds in complex mixtures; specifically, crude oil, petroleum and coal samples (Van Krevelen, 1950; Kendrick, 1963; Bostick and Daws, 1994; Curiale and Gibling, 1994; Grigsby and Green, 1997; Hughey et al., 2001; Qian et al., 2001; Rodgers et al., 2005). The sheer number of individual compounds present in OA samples and their continually evolving chemical composition, means that these visualisation tools can also be extremely useful for the compositional analysis of OA (Bateman et al., 2010).

The most common type of high resolution plots used for the chemical characterisation of OA are: Kendrick plots (Kendrick, 1963), van Krevelen diagrams (Van Krevelen, 1950), double bond equivalency index (Pellegrin, 1983; McLafferty, 1993), aromaticity index (AI) (Koch and Dittmar, 2006) and carbon oxidation state (Kroll et al., 2011). Using these visualisation tools, hundreds of compounds can be sorted by a wide variety of chemical properties, including: the degree of oxidation (oxygen-to-carbon ratio and carbon oxidation state), degree of unsaturation (double bond equivalency index and aromaticity index), heteroatom class (*e.g.* nitrogen-, sulfur- *etc.* containing compounds) and common "repeating

units" within the homologues series of species (*e.g.* CH_2, CH_2O, ${}^{\bullet}OH$ *etc.*). This visual representation of the spectral composition can allow patterns in the chemical and physical properties of individual compounds within complex mixtures to be observed. These patterns can aid in the identification of unknown compound structures (Hughey et al., 2001; Roach et al., 2011), allow sample contaminants to be identified (Lebedev, 2012), and allow the chemical properties of the individual compounds to be evaluated as a whole (Bateman et al., 2010; Heald et al., 2010; Nguyen et al., 2010)). However, whilst these UHR-MS visualisation tools and chemical descriptions can significantly aid in the chemical characterisation of OA, no studies have investigated the reproducibility and reliability of this data (Bateman et al., 2009).

This investigation is perhaps the most warranted within aerosol science due to the extensive use of "chemical metrics" for describing the overall chemical properties of OA samples (*e.g.* (Kroll and Seinfeld, 2008; Hallquist et al., 2009; Bateman et al., 2010; Heald et al., 2010; Nguyen et al., 2010; Mazzoleni et al., 2012; Schmitt-Kopplin et al., 2012; Hamilton et al., 2013; Zhao et al., 2013)). These OA metrics are determined from the molecular formulae provided from the UHR-MS spectral composition and often include; the average oxygen-to-carbon ratio (O:C), hydrogen-to-carbon ratio (H:C), degree of unsaturation (DBE) and intensity weighted O:C (<O:C>) and DBE (<DBE>) values. Studies will often use these metrics along with the appearance of the spectra and *m/z* distribution to compare the chemical properties of different OA samples within the literature (Reinhardt et al., 2007; Smith et al., 2008; Wozniak et al., 2008; Nguyen et al., 2010; Zhao et al., 2013; Kourtchev et al., 2014). The current lack of standardised instrument and/or data processing method means that users will often develop and optimise their own methods for the compositional analysis of OA. However, few studies have investigated whether the use of different instrument and/or data processing methods can affect the calculated spectral composition (Hang et al., 2003; These and Reemtsma, 2003; Payne et al., 2009; Reemtsma, 2009; Kido Soule et al., 2010), and no studies have investigated whether this can affect the commonly reported metrics used for describing the chemical properties of OA.

The following work investigates if the use of different instrument or data processing methods can affect the calculated spectral composition and thus, the commonly reported OA metrics. This investigation was performed using a Bruker Daltonics SolariX 9.4-T Fourier transform ion-cyclotron resonance mass spectrometer. To investigate the effect of different instrument methods, a common setting applicable to other mass spectrometers was changed; the quadrupole target mass. The transportation of ions from the ionisation source to the detector is usually achieved through a series of radio-frequency (RF)-only ion guides and

can consist of a range of different multipoles; such as quadrupoles, hexapoles and octapoles, with the most common being RF-only quadrupoles (Zekavat et al., 2014). These ion guides are designed to efficiently focus the trajectory of all ions over a wide *m/z* range and simultaneously transport them to the detector, usually through varying pressure regions within the mass spectrometer. The ability of a multipole to effectively focus and transmit all ions of differing *m/z* ratios to the detector can vary depending on the type of multipole used, and the RF applied (which is inversely proportional to the quadrupole target mass (*m/z*)). Poor ion focussing and transmission can result in the loss of ions, decreasing instrument sensitivity. In some cases, poor ion focussing can result in a "low mass cut off", where ions of a particular *m/z* do not reach the detector and are subsequently not observed (Hang et al., 2003; de Hoffmann and Stroobant, 2007; Zekavat et al., 2014).

Here, the effect of the quadrupole target mass on the ability of a quadrupole ion guide (QIG) to effectively focus and transmit ions over an *m/z* range of 50 - 800 is investigated. Initially, the effect of the quadrupole ion focussing on the *m/z* distribution and signal intensity of a standard of L-arginine, which is a commonly used mass accuracy calibrant, is shown. This methodology is then repeated for a water soluble extract of chamber generated SOA, which is used as a proxy for OA. The effect of the quadrupole ion focussing on the calculated spectral composition (and thus the OA metrics) of the SOA sample is determined. To investigate the use of different UHR-MS data processing methods on the commonly reported OA chemical metrics, three data analysis methods used within the literature for the compositional analysis of OA were chosen. These data processing methods were applied to nine SOA samples and the effect on the calculated OA metrics reported. Finally, the relevance of these findings within aerosol science is discussed.

5.2 Experimental

5.2.1 FTICR-MS

A solariX Fourier transform ion cyclotron resonance mass spectrometer with a 9.4-T superconducting magnet (Bruker Daltonics, Coventry, UK) was used. Ionisation was achieved through electrospray ionisation (ESI), with a dry gas flow rate of 3.7 L min^{-1}, dry gas temperature of 220 °C, and a nebulizer gas pressure of 1.2 bar (nitrogen, BOC, UK). Samples were introduced into the ESI source through direct infusion, using a 50 μL syringe (Hamilton, Switzerland) at a flow rate of 120 μL h^{-1}. The FTICR-MS was externally calibrated using a 10 ppm standard of L-arginine (Sigma Aldrich UK, purity 98%) prepared in 50:50 methanol: water (optima LC-MS grade, Fisher Scientific, UK). Spectra were

acquired in both positive and negative ionisation modes over a scan range of *m/z* 50 – 800. Broadband detection mode was used, with 64 spectra averages obtained for each spectrum. Ion accumulation in the ICR cell was set to 0.5 seconds with a source accumulation time of 0.002 seconds. The collision RF, ion cooler time and the quadrupole target mass was set to favour lower masses at 1300 Volts-peak-to-peak (Vpp), 0.010 seconds and *m/z* 120, respectively.

5.2.2   Quadrupole Ion Focussing

Two sets of experiments were performed. Initially, the effect of the quadrupole target mass on the spectra appearance and reproducibility of the signal intensity of a common mass accuracy standard, L-arginine, was investigated. The quadrupole target mass was investigated at *m/z* 120, 300 and 480. L-arginine (Sigma Aldrich, UK, purity 98%) was prepared in 50:50 methanol:water (optima LC-MS grade, Fisher Scientific, UK) at a concentration of 20 ppm for negative ionisation mode and 50 ppm for positive ionisation mode. Five spectra of L-arginine were acquired at each quadrupole target mass in both positive and negative ionisation modes. Only the quadrupole target mass was changed, all other instrument parameters remained the same as discussed above in Section 5.2.1.

The second set of experiments were performed to investigate the effect of the quadrupole target mass on the spectra appearance and calculated spectral composition. This was performed using the same methodology as discussed above, except using an SOA sample. The collection and sample preparation of the investigated SOA sample is discussed in Section 5.2.3. The spectral composition was calculated using DataAnalysis 4.0 software (Bruker Daltonics, Breman, Germany). The molecular formulae of the observed peaks were determined using the following parameters; unlimited C, H and O were allowed and up to 3 N atoms, O:C < 3, H:C > 0.5, DBE < 20, and in positive mode, Na and K adducts were also allowed. Any peaks with a molecular formulae error > 10 ppm and relative abundance < 0.01% were excluded from the calculated spectral composition.

5.2.3   SOA Samples

The SOA samples investigated in this study were collected during the atmospheric chemistry of methyl chavicol (ATMECH) project. The chamber setup and instrumentation used has previously been described in detail elsewhere and will not be discussed here (Chapter 3, Section 3.2.1). For the quadrupole ion focussing experiment, a SOA filter sample collected during the photo-oxidation of methyl chavicol, experiment MC$_{[high]}$, was

used (Table 5.1). The total aerosol volume sampled was 7.32 m^3. The filter was prepared using the same methods as discussed previously in Chapter 2, Section 2.2.4.1. Due to the lack of the sample volume, the same SOA sample could not be used to investigate the effect of different data processing methods on the calculated spectral composition. Instead, nine SOA samples collected during three ATMECH experiments were investigated. These samples were chosen to ensure a variation in the spectral composition, *m/z* distribution and signal intensities were included in the analysis. These SOA samples were collected using the PILS. The PILS aerosol collection method and sample preparation was the same as discussed previously and can be found in Chapter 3, Section 3.2.2.1. The initial mixing ratios, chamber temperature and relative humidity of the experiments discussed are shown in Table 5.1. The time period the aerosol samples were collected during each experiment using the PILS, is shown in Table 5.2.

Table 5.1 - The initial mixing ratios, chamber temperature and relative humidity of the experiments discussed.

Exp. type	Exp. ID	Exp. date	Exp. description	Initial mixing ratio[a]				VOC:oxidant ratio	Experimental range[b]	
				MC [ppbv]	NO [ppbv]	NO_2 [ppbv]	O_3 [ppbv]		Chamber temp [K]	RH [%]
Photo-oxidation	$MC_{[high]}$	15.05.12	High NO_x	460[c]	92	3	5	~ 5:1	297-306	2.1 - 10.7
Ozonolysis (dark)	$MC_{L(O3)}$	14.05.12	O_3 low [VOC]	228[c]	< LOD	2	958	~ 1:4	298-296	5.7 - 14.5
	$MC_{H(O3)}$	24.05.12	O_3 high [VOC]	464[d]	< LOD	< LOD	923	~ 1:2	299 - 302	0.6 - 1.8

[a] = Photo-oxidation; on the opening of the chamber covers. Ozonolyisis; on the addition of methyl chavicol. [b] = Photo-oxidation; from the opening to the closing of the chamber covers. Ozonolysis; from the addition of methyl chavicol to the start of the filter sampling. [c] = FTIR measurement. [d] = PTR-MS measurement.

Table 5.2 - The time period the PILS aerosol samples were collected during the experiments discussed.

Exp. type	Exp. date	Exp. ID	PILS sample	Sampling period into the experiment[a] [minutes]
Photo-oxidation	15.05.12	MC$_{[high]}$	1356	190 - 220
			1357	220 - 250
			1358	250 - 280
Ozonolysis (dark)	14.05.12	MC$_{L(O3)}$	1429	73 - 103
			1431	133 - 163
			1432	163 - 193
	24.05.12	MC$_{H(O3)}$	1342	115 – 145
			1343	145 – 175
			1344	175 - 205

[a] = Sampling time period from the start of the experiment. Start of experiment; photosmog = opening of the chamber covers. Ozonolysis = addition of methyl chavicol.

5.3 Results and Discussion

5.3.1 Quadrupole Ion Focusing

The user interface of Bruker Daltonics mass spectrometers require users to enter a *m/z* value for what is referred to as a "target mass". This setting allows users to control the ion focussing of the QIG, the location which is shown in Figure 5.1. Arguably, this setting is one of the most influential in the effective transmission of ions to the ion cyclotron resonance (ICR) cell (detector). If the target mass value is not in the *m/z* region of interest, ions are either poorly focussed or follow an unstable trajectory (March et al., 1989; de Hoffmann and Stroobant, 2007). This can result in a loss of ions, decreasing instrument sensitivity and/or resulting in some ions not being detected.
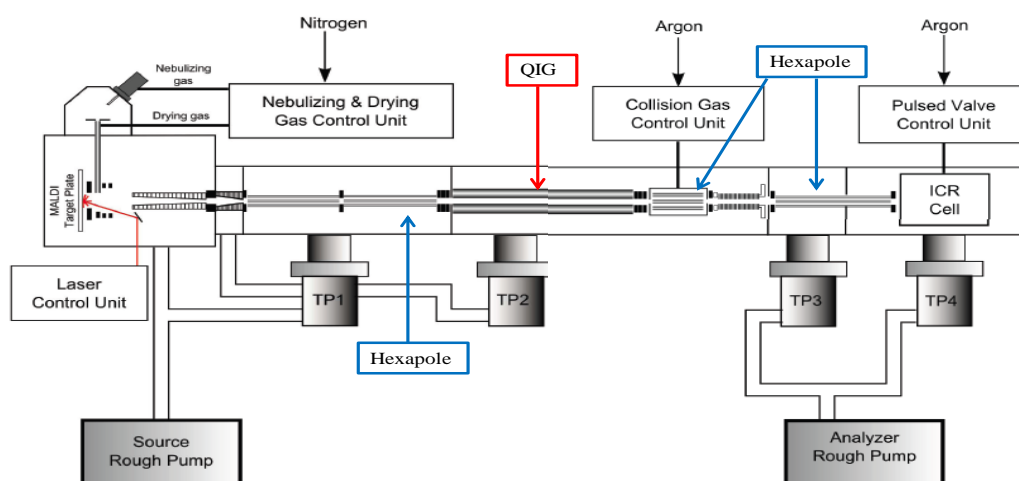
Figure 5.1 - Schematic diagram of the SolariX Bruker Daltonics FTICR-MS with the location of the quadrupole ion guide (QIG) shown in red. TP = turbo pump. Figure adapted from the Bruker Daltonics FTICR-MS user manual.

Initially, the effect of the quadrupole target mass on the signal intensity of a standard of L-arginine was investigated. This compound was chosen for a variety of reasons; primarily as its stability is known, but also as it is often used as a mass calibrant and has multiple peaks within the mass range investigated. L-arginine is a zwitterionic amino acid (Figure 5.2) which forms stabilised clusters during ESI (see Zhang et al. (2009) for further information). L-arginine (Arg) has four peaks in the mass range of *m/z* 50 - 800, at *m/z* 173 [(Arg)-H]⁻, 347 [(Arg)$_2$-H]⁻, 521 [(Arg)$_3$-H]⁻ and 695 [(Arg)$_4$-H]⁻ in negative ionisation mode, and *m/z* 175 [(Arg)+H]⁺, 349 [(Arg)$_2$+H]⁺, 523 [(Arg)$_3$+H]⁺ and 697 [(Arg)$_4$+H]⁺ in positive ionisation mode. The measured signal intensity of the four L-arginine peaks at quadrupole

target mass of *m/z* 120, 300 and 480, in positive and negative ionisation modes, are shown in Tables 5.3 and 5.4 respectively.
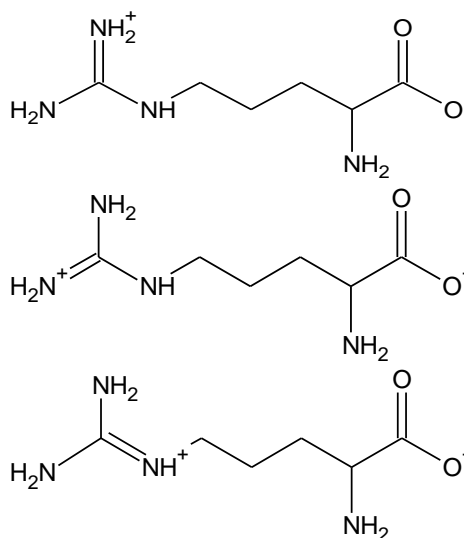
Figure 5.2 - Structure of L-arginine displaying the location of the negative charge and delocalisation of the positive charge.

From Tables 5.3 and 5.4, it can be observed that the measured signal intensities of each of the L-arginine peaks at the same quadrupole target mass are not reproducible, with the percentage relative standard deviation (%RSD) ranging from 9.1 to 124% for five replicate injections. Furthermore, it can be observed that the measured signal intensity of each of the L-arginine peaks varies significantly with the use of different quadrupole target masses. This can be observed more clearly in Figure 5.3, where the L-arginine peak with the closest *m/z* value to the quadrupole target mass has the highest measured signal intensity.

Table 5.3 - Measured signal intensity of the four L-arginine peaks in positive ionisation mode at a quadrupole target mass of *m/z* 120, 300 and 480.

			Measured signal intensity					
Quadrupole target mass *m/z* 120			Replicate injections					
m/z	1	2	3	4	5	Mean	SD	%RSD
175.118952	2.61×10^{10}	2.72×10^{10}	2.27×10^{10}	2.99×10^{10}	2.60×10^{10}	2.64×10^{10}	2.6×10^{9}	9.84
349.230628	1.25×10^{9}	9.95×10^{8}	1.79×10^{9}	1.58×10^{9}	9.48×10^{8}	1.31×10^{9}	3.67×10^{8}	27.94
523.342304	4.89×10^{8}	4.37×10^{8}	7.84×10^{8}	6.04×10^{8}	4.71×10^{8}	5.57×10^{8}	1.41×10^{8}	25.39
697.453979	1.43×10^{8}	1.40×10^{8}	3.03×10^{8}	2.52×10^{8}	1.74×10^{8}	2.02×10^{8}	7.2×10^{7}	35.64
Quadrupole target mass *m/z* 300								
m/z	1	2	3	4	5	Mean	SD	%RSD
175.118952	1.96×10^{8}	1.78×10^{8}	1.94×10^{8}	1.56×10^{8}	1.73×10^{8}	1.79×10^{8}	1.63×10^{7}	9.11
349.230628	1.99×10^{10}	2.46×10^{10}	2.15×10^{10}	2.02×10^{10}	1.99×10^{10}	2.12×10^{10}	1.99×10^{9}	9.40
523.342304	5.45×10^{9}	7.15×10^{9}	6.03×10^{9}	5.80×10^{9}	5.26×10^{9}	5.94×10^{9}	7.41×10^{8}	12.48
697.453979	9.30×10^{8}	1.16×10^{9}	1.01×10^{9}	1.10×10^{9}	8.49×10^{8}	1.01×10^{9}	1.28×10^{8}	12.63
Quadrupole target mass *m/z* 480								
m/z	1	2	3	4	5	Mean	SD	%RSD
175.118952	8.94×10^{7}	1.49×10^{8}	1.89×10^{8}	3.01×10^{8}	2.21×10^{8}	1.9×10^{8}	7.92×10^{7}	41.74
349.230628	1.03×10^{8}	1.83×10^{8}	2.38×10^{8}	3.01×10^{8}	2.57×10^{8}	2.16×10^{8}	7.62×10^{7}	35.22
523.342304	1.20×10^{9}	1.89×10^{9}	2.15×10^{9}	2.33×10^{9}	2.07×10^{9}	1.93×10^{9}	4.38×10^{8}	22.74
697.453979	8.79×10^{8}	1.04×10^{9}	1.22×10^{9}	1.21×10^{9}	1.05×10^{9}	1.08×10^{9}	1.41×10^{8}	13.10

Table 5.4 - Measured signal intensity of the four L-arginine peaks in negative ionisation mode at a quadrupole target mass of *m/z* 120, 300 and 480.

			Measured signal intensity					
Quadrupole target mass *m/z* 120			Replicate injections					
m/z	1	2	3	4	5	Mean	SD	%RSD
173.104399	8.27×10^8	6.43×10^8	7.67×10^8	8.11×10^8	9.22×10^8	7.94×10^8	1.01×10^8	12.78
347.216075	4.52×10^8	1.55×10^8	2.64×10^8	2.22×10^8	2.20×10^8	2.63×10^8	1.13×10^8	42.92
521.327751	2.07×10^8	3.69×10^7	8.64×10^7	5.68×10^7	4.73×10^7	8.70×10^7	6.98×10^7	80.29
695.439426	3.95×10^7	3.59×10^6	9.79×10^6	5.55×10^6	3.53×10^6	1.24×10^7	1.54×10^7	124.01
Quadrupole target mass *m/z* 300								
m/z	1	2	3	4	5	Mean	SD	%RSD
173.104399	1.22×10^7	1.84×10^7	1.72×10^7	1.73×10^7	2.03×10^7	1.71×10^7	2.99×10^6	17.46
347.216075	2.69×10^8	4.53×10^8	4.31×10^8	4.80×10^8	5.97×10^8	4.46×10^8	1.18×10^8	26.37
521.327751	9.02×10^7	1.80×10^8	1.66×10^8	1.81×10^8	2.44×10^8	1.72×10^8	5.48×10^7	31.86
695.439426	3.95×10^6	7.35×10^6	5.63×10^6	6.12×10^6	9.50×10^6	6.51×10^6	2.07×10^6	31.77
Quadrupole target mass *m/z* 480								
m/z	1	2	3	4	5	Mean	SD	%RSD
173.104399	1.19×10^7	9.33×10^6	1.20×10^7	9.55×10^6	9.73×10^6	1.05×10^7	1.32×10^6	12.54
347.216075	5.89×10^7	5.64×10^7	5.54×10^7	4.52×10^7	4.74×10^7	5.26×10^7	5.98×10^6	11.36
521.327751	3.80×10^8	3.37×10^8	5.11×10^8	3.52×10^8	4.03×10^8	3.96×10^8	6.91×10^7	17.43
695.439426	4.82×10^7	4.12×10^7	7.52×10^7	4.72×10^7	5.88×10^7	5.41×10^7	1.34×10^7	24.74
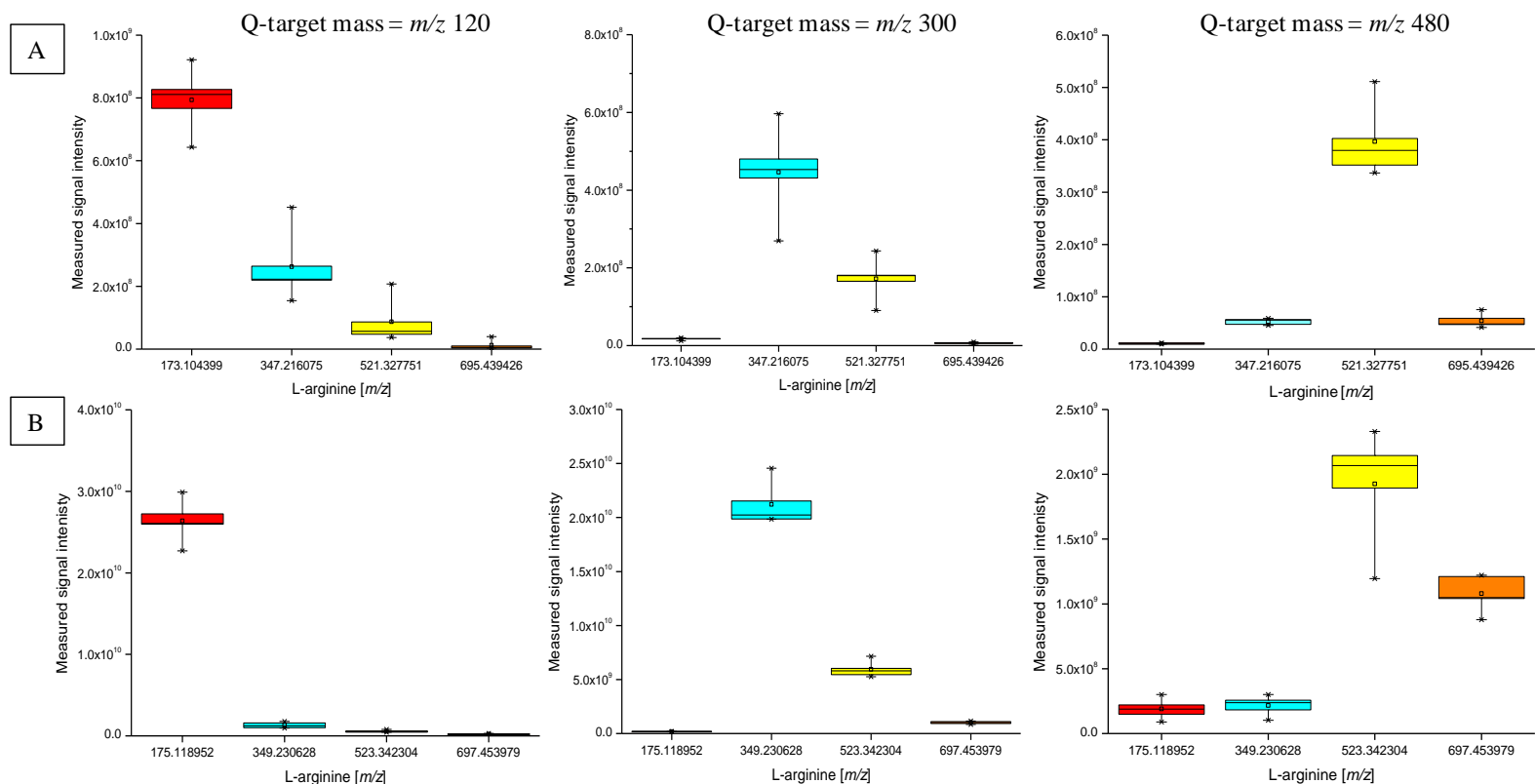
Figure 5.3 - Effect of the quadrupole target mass (Q-target mass) on the measured intensities of the four L-arginine peaks using the FTICR-MS. A = negative ionisation mode. B = positive ionisation mode. Q-target mass investigated at *m/z* 120, 300 and 480. Box plot; crosses display the minimum and maximum measured signal intensity. The 95th and 5th percentile is shown by the whiskers and the interquartile range (75th and 25th percentile) is shown by the boxes. The horizontal line within the box displays the median value and the mean is represented by the smaller square within the box.

This variation in the measured signal intensity is the result of the peaks location in the mass range investigated (Payne et al., 2009). The transmission of ions to the detector (and thus the measured signal intensity) is only stable within a certain *m/z* region, or so called "*m/z* window" (Southam et al., 2007; Payne et al., 2009; Kido Soule et al., 2010). Ions within the *m/z* window are in the optimum *m/z* range based on the instrument parameters used, and are thus, the most efficiently focused and transmitted ions. It is important to note however, that measured intensity within this *m/z* window does not guarantee a stable signal intensity. Other influences such as: space-charge effects (Payne et al., 2009), ion-ion interactions in the ICR cell (Gordon and Muddiman, 2001), ion suppression and enhancement during ionisation (Cech and Enke, 2001) and blockages in the ESI spray nozzle ("drop out") (Lewis et al., 2007), can all affect the measured signal intensity (Payne et al., 2009). The variation in the measured signal intensity of the L-arginine peaks with different quadrupole target masses, is the result of a shift in the optimum *m/z* range (*m/z* window), enhancing different *m/z* regions over the range investigated.

In other scientific areas, studies have used this *m/z* window to their advantage, by creating multiple *m/z* windows through selected ion monitoring (SIM) and "stitching" these windows together through the use of algorithms (Southam et al., 2007; Giavalisco et al., 2008; Kido Soule et al., 2010). Using this method, significantly more compounds have been observed in the spectra and the error in the measured signal intensities reduced (Southam et al., 2007; Giavalisco et al., 2008; Payne et al., 2009; Kido Soule et al., 2010). To achieve the desired *m/z* window of interest, all of these studies used SIM followed by the optimisation of the number of ions in the ICR cell (automatic gain control, AGC) using a Thermo Scientific FTICR-MS. However, the selection or identification of the *m/z* window in full scan mode with the use of a Bruker Daltonics FTICR-MS is significantly more complex. The user interface of the Bruker Daltonics FTICR-MS does not allow users to control the AGC. Instead, the desired *m/z* window must be achieved through a range of settings which control the focussing of ions into the ICR cell, including; the transfer time (ion time-of-flight), collision RF, ion cooler RF and the quadrupole target mass.

The effect of the quadrupole target mass on the observed spectra of L-arginine in negative and positive ionisation modes, is shown in Figures 5.4 and 5.5, respectively. In Figure 5.4, a significant amount of peaks can be observed in spectra. This is result of the methanol and water used to prepare the arginine standard and the instrument background, which is clearly very dirty. It is worth noting however, that the high signal intensity of the background ions does not affect the results shown here. The abundance of peaks in the spectra actually makes it easier to observe the effect of the quadrupole target mass on focussing of ions.

In both negative and positive ionisation modes, a significant decrease in the signal intensity of lower mass ions is observed when the quadrupole target mass is increased. This is the result of the quadrupoles ability to effectively focus both low and high mass ions based on the chosen target mass, and thus the RF voltage (*e.g.* (Zekavat et al., 2014)). The successful transmission of ions through a quadrupole is dependent upon the *m/z* ratio of the ion, the RF voltage applied and the potential well within the quadrupole (*i.e.* the radial distance from the centre of the rods); the latter, which is only applicable to the use of different ion guides which is not considered here. The successful transmission of ions of differing *m/z* values through a quadrupole at different RF voltages, can be described as shown in Figure 5.6.
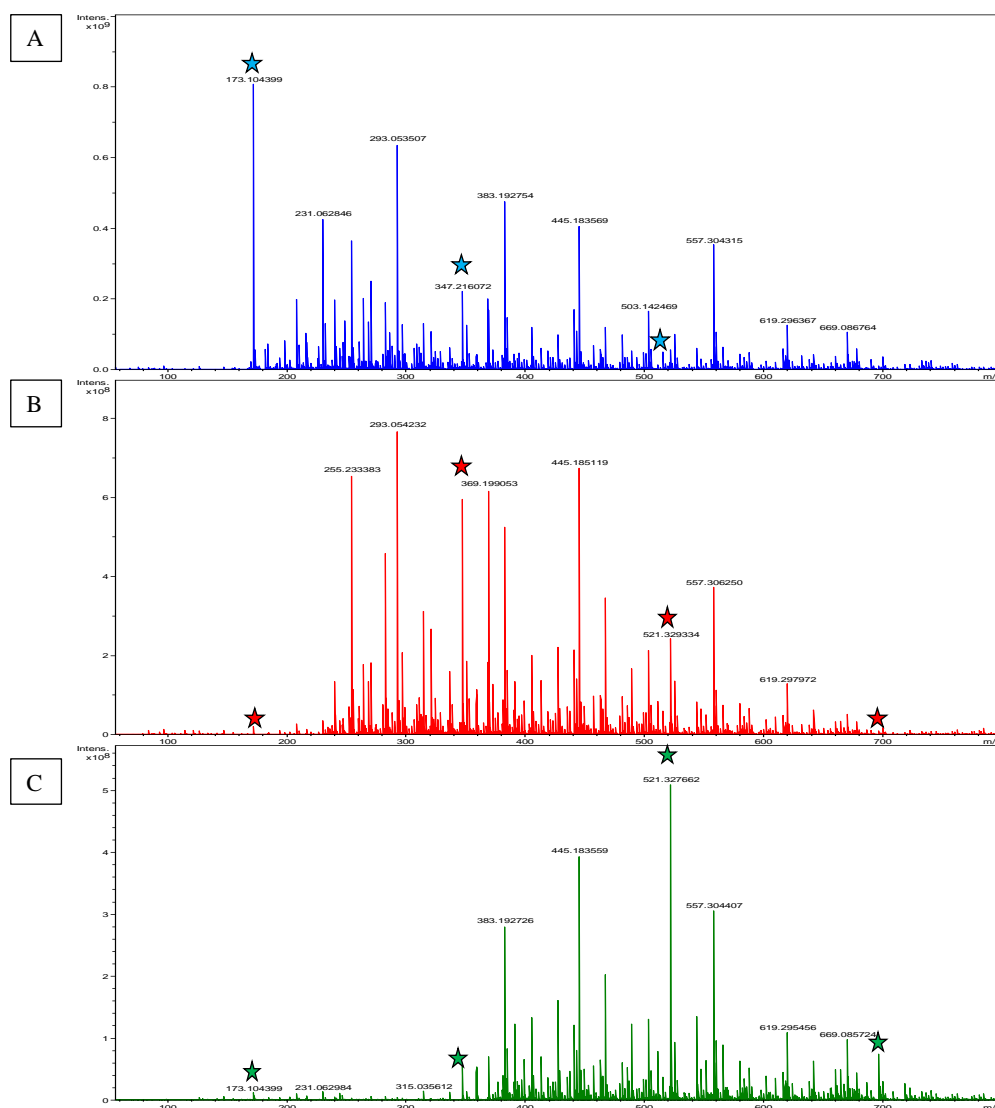
Figure 5.4 - FTICR-MS spectra of the four L-arginine peaks (shown by the use of stars) at different quadrupole target masses (Q-target mass) in negative ionisation mode. A = Q-target mass *m/z* 120 (L-arginine peak at *m/z* 695 cannot be observed). B = Q-target mass *m/z* 300. C = Q-target mass *m/z* 480.
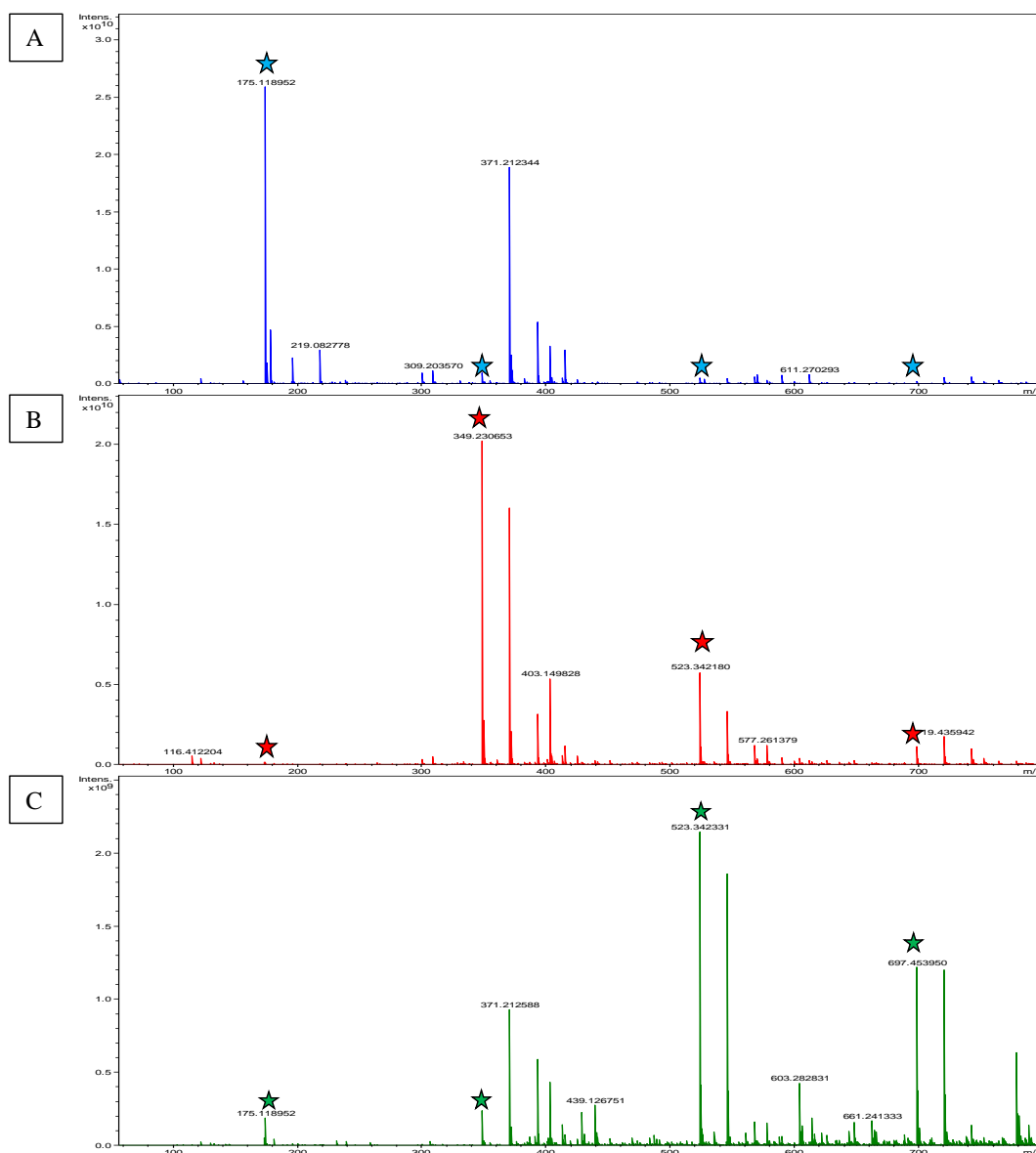
Figure 5.5 - FTICR-MS spectra of the four L-arginine peaks (shown by the use of stars) at different quadrupole target masses (Q-target mass) in positive ionisation mode. A = Q-target mass *m/z* 120. B = Q-target mass *m/z* 300. C = Q-target mass *m/z* 480.

In Figure 5.6, the stable trajectory of three ions of different mass values ($m_1 < m_2 < m_3$) through the quadrupole at different RF voltages is shown through the use of the coloured dashed lines (stability region). For a RF-only quadrupole, the direct current (DC) is equal to zero, thus ion stability within the quadrupole is determined by moving across the horizontal axis (*i.e.* differing RF voltages). For a low mass ion (m_1), a stable trajectory within the quadrupole is only achieved at low RF voltages, as shown for example, in Figure 5.6, RF voltage A. Outside this region (Figure 5.6 RF voltages B to D), the trajectory of the m_1 ion is unstable, resulting in the ion discharging itself on the rods of the quadrupole. This can

results in a low mass cut-off where significant decrease in the signal intensity is observed, often resulting the ion not being detected. This low mass cut-off can be observed in the spectra shown in Figures 5.3 and 5.4, where the use of a higher RF voltages results in a significant decrease in the signal intensity of the lower mass ions.
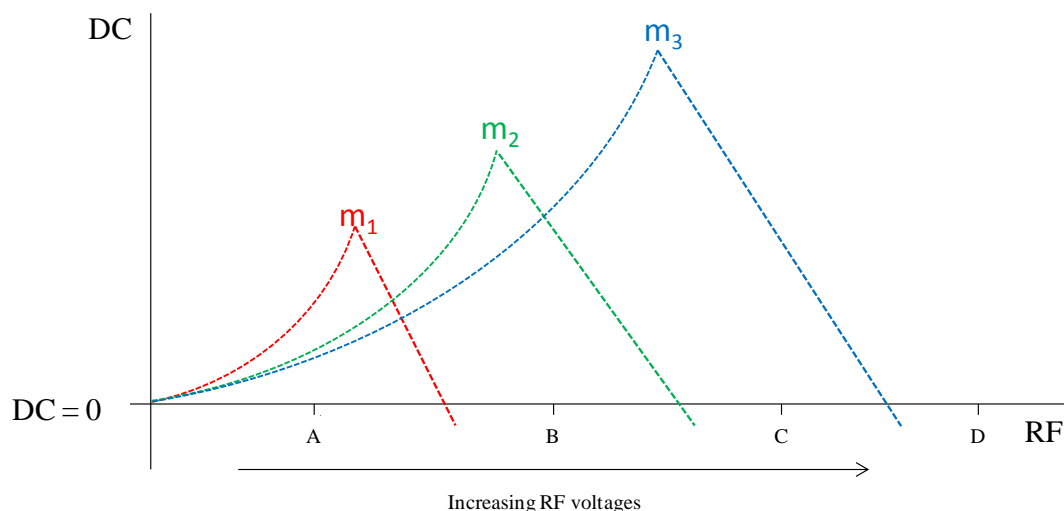
Figure 5.6 - An example of the stability areas of three different masses ($m_1 < m_2 < m_3$) within a quadrupole at different RF voltages (V_{RF}). Direct current (DC) is equal to zero in RF-only operating quadrupoles, stability region determined by moving horizontally across the x-axis. RF voltages; A = all masses within stability region. B = m_1 not in stability region (low mass cut off). C = m_1 and m_2 not in the stability region (low mass cut off). D = no masses stable (significant loss of ions). Adapted from de Hoffmann and Stroobant (2007).

From Figure 5.6, it can be observed that all three masses will have a stable trajectory through the quadrupole at RF voltage A. However, at low RF voltages, higher mass ions (m_3) are poorly focussed, resulting in a loss of ions and subsequently a decrease in instrument sensitivity. This can be observed in Figures 5.3, 5.4 and 5.5 where at higher RF voltages the signal intensity of the higher mass ions increases. Thus, higher mass ions at higher RF voltages are more efficiently focused. Therefore, achieving an appropriate RF voltage for the detection of all ions of differing *m/z* values, is a balance between the loss of low mass ions from an unstable trajectory and higher mass ions from poor ion focussing.

5.3.1.1 Quadrupole Ion Focussing: Elemental Composition

Owing to the clear importance of the quadrupole target mass on the spectra appearance and signal intensity of L-arginine, the same methodology was repeated but for an SOA sample

and any effect on the calculated spectral composition determined. The effect of the quadrupole target mass on the spectral distribution of a filter sample obtained during the photo-oxidation of methyl chavicol (experiment MC$_{[high]}$, Table 5.1) in negative and positive ionisation modes, is shown in Figures 5.7 and 5.8 respectively.
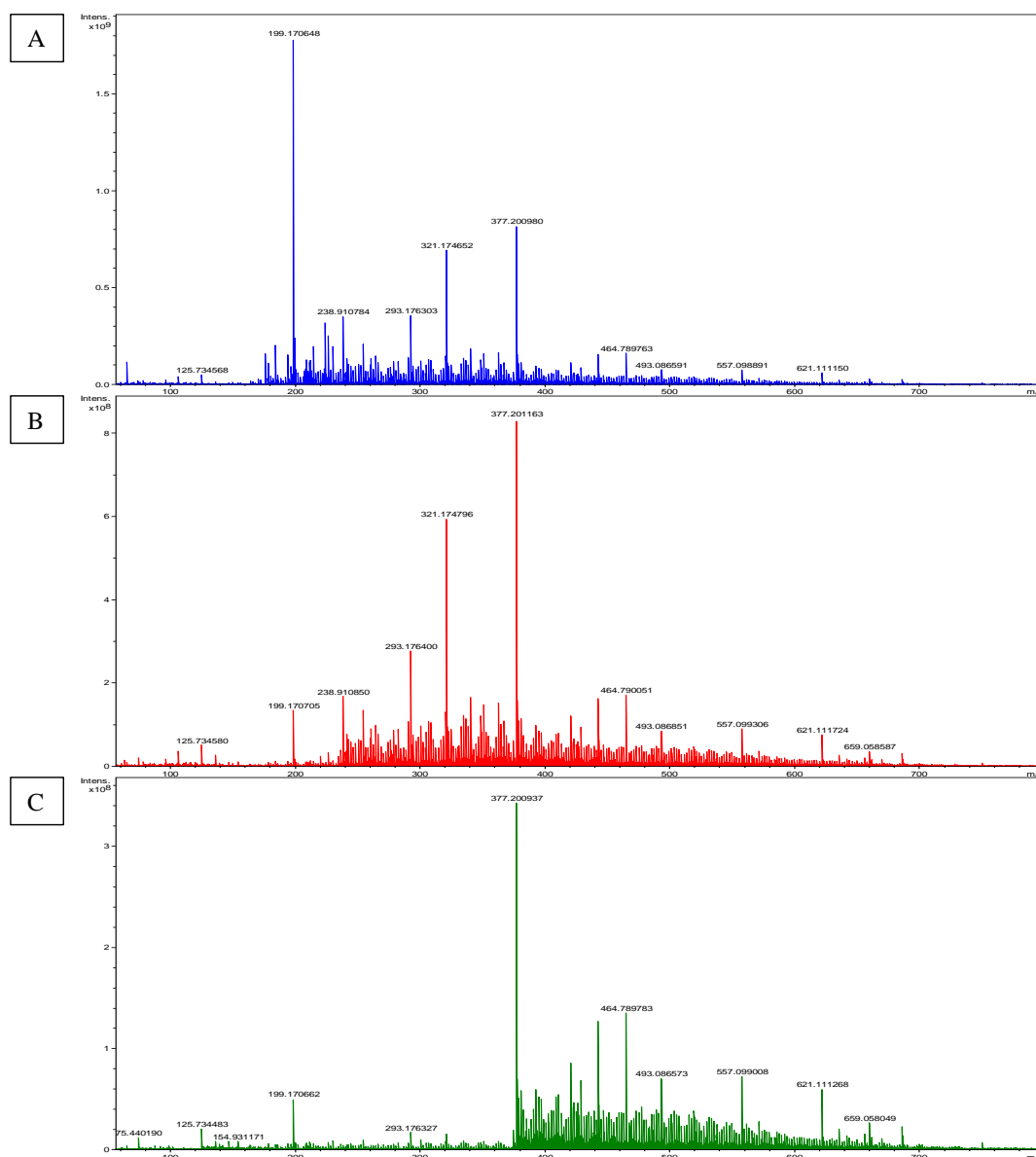
Figure 5.7 - FTICR-MS spectra of the SOA filter sample collected during experiment MC$_{[high]}$ (Table 5.1) at different quadrupole target masses (Q-target mass) in negative ionisation mode. A = Q-target mass *m/z* 120. B = Q-target mass *m/z* 300. C = Q-target mass *m/z* 480.

In negative ionisation mode, a significant decrease in the signal intensity of the lower mass ions is observed when the quadrupole target mass is increased, as observed with the spectra

of L-arginine. However, in positive ionisation mode, this low mass cut-off is not as evident. This is a result of the lack of species present in positive ionisation mode at high masses. However, it can be observed in Figure 5.8 that the signal intensity of *m/z* 205 decreases with increasing quadrupole target masses. Furthermore, higher mass ions, such as *m/z* 387, are most noticeable in the spectra when the quadrupole target mass is increased. Thus, the relative importance of the higher mass ions increases with the use of higher quadrupole target masses. Whilst this increase is only small, in OA samples this could potentially "artificially" enhance compounds of higher molecular weight, such as oligomers.
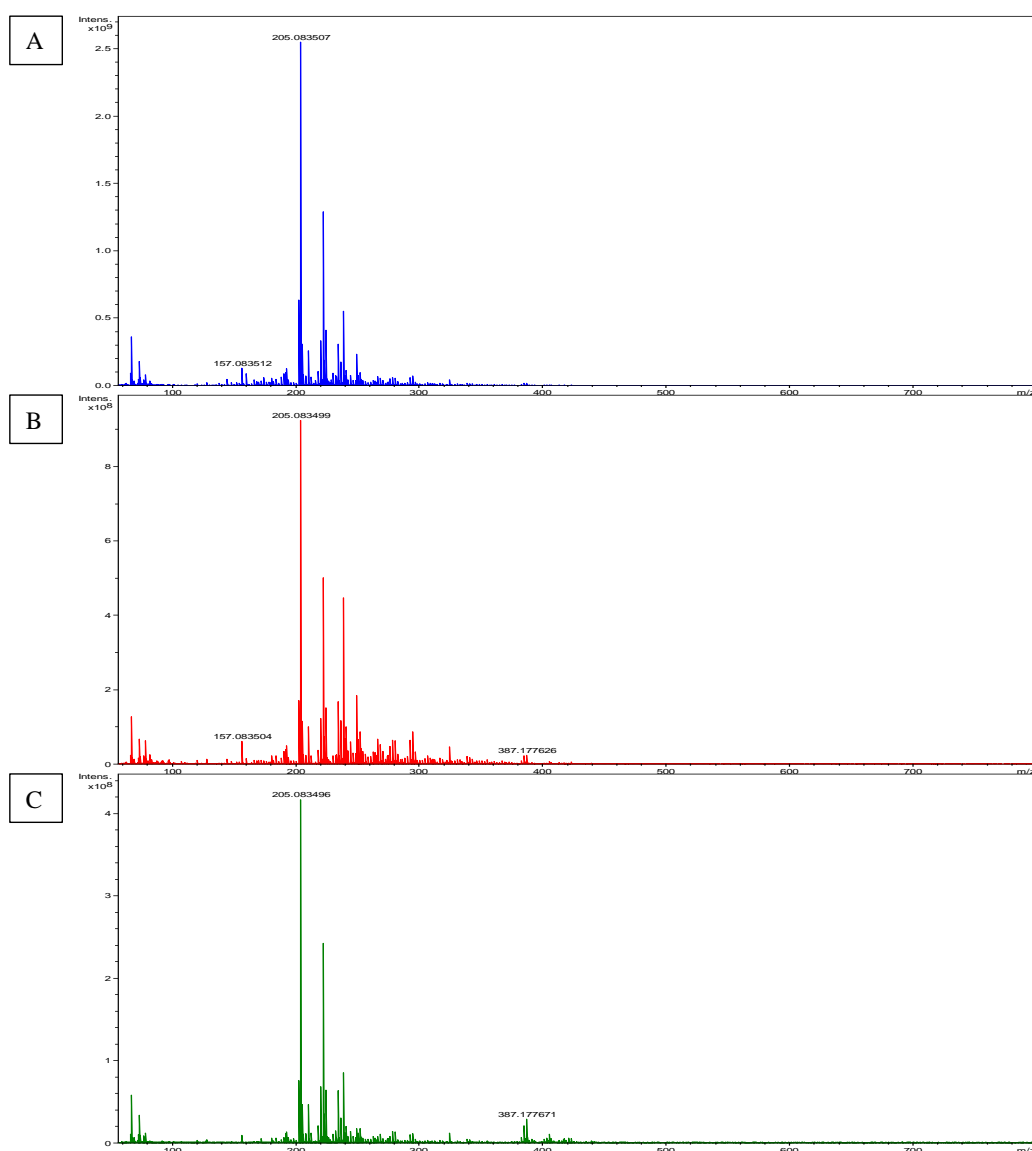
Figure 5.8 - FTICR-MS spectra of the SOA filter sample collected during experiment MC[high] (Table 5.1) at different quadrupole target masses (Q-target mass) in positive ionisation mode. A = Q-target mass *m/z* 120. B = Q-target mass *m/z* 300. C = Q-target mass *m/z* 480.

The effect of the quadrupole target mass on the calculated OA metrics is discussed here. Five replicate injections of the SOA filter sample obtained during experiment $MC_{[high]}$ (Table 5.1) was performed at each quadrupole target mass. The spectral composition was determined using the data analysis method described in Section 5.2.2. The SOA metrics were calculated from the spectral composition and included; the average O:C ratio, H:C ratio, DBE and intensity weighted <O:C> and <DBE> values. The intensity weighted <O:C> ratio was calculated using the equation shown in Eq. 5.1; where the O:C ratio of compound i ($O:C_i$) was multiplied by the measured signal intensity of compound i (I_i). This was performed for all of the compounds ranging from i to n. The sum of the O:C ratio multiplied by I for all the compounds i to n, divided by the sum of the measured signal intensities of compounds i to n, gives the <O:C> ratio. The substitution the O:C ratio for the DBE value in Eq. 5.1, gives the intensity weighted <DBE> value, as shown in Eq. 5.2.

Eq.5.1
$$< O:C > = \frac{\sum_n^i (I_i \times O:C)_{i,\,n}}{\sum_n^i I}$$

Eq.5.2
$$< DBE > = \frac{\sum_n^i (I_i \times DBE)_{i,\,n}}{\sum_n^i I}$$

The effect of the quadrupole target mass on the calculated SOA metrics in negative and positive ionisation modes, is shown in Tables 5.5 and 5.6 respectively. From Tables 5.5 and 5.6, it can be observed that replicate injections of the same SOA sample, at the same quadrupole target mass, results in little variation of the calculated SOA metrics; with a % RSD < 4.32% for both negative and positive ionisation modes. To evaluate the overall effect of the different quadrupole target masses on the calculated OA metrics, the percentage variation from the mean was used. This was calculated using the equation shown in Eq. 5.3; where the mean value of the 5 replicate measurements of each of the calculated OA metrics, at the different quadrupole target masses, were combined into a separate data set. For each OA metric (i), the maximum (max_i) value was subtracted from the minimum (min_i) value to obtain the range of the data set. The range was then divided by the average value of the data set and multiplied by 100, to give the percentage variation from the mean. This was performed as the %RSD can only be used where all the investigated parameters are kept constant. The use of different quadrupole target masses meant that the %RSD would not accurately represent the variation in the calculated OA metrics, and thus the percentage variation from the mean was used.

Eq.5.3 $\quad\quad \text{variation from the mean}_i\,[\%] = \left(\frac{(max_i - min_i)}{average_i}\right) \times 100$

The effect of the different quadrupole target masses on the calculated OA metrics is shown in Table 5.7. Surprisingly, the use of different quadrupole target masses did not have a significant effect on the average O:C, H:C and DBE values, with a percentage variation from the mean < 8.5%, in both positive and negative ionisation modes. This is the result of the signal intensity of the low mass ions being greater than the relative signal intensity used to calculate the spectral composition. The majority of the low mass ions had a measured relative signal intensity of ~ 1%, greater than the 0.01% relative signal intensity used for the calculation of the spectral composition. However, as expected, a higher variation in the calculated OA metrics were obtained for the intensity weighted <DBE> and <O:C> values. The percentage variation from the mean for the intensity weighted <O:C> and <DBE> values was determined as 14.89% and 30.28% in negative ionisation mode, and 15.38% and 2.68% in positive ionisation mode, respectively. The increase in the quadrupole target mass from *m/z* 120 to 480 in negative ionisation mode, resulted an increase in the <DBE> value by ~ 2 and the <O:C> by 0.07. Thus, whilst a significant variation in the average O:C, H:C and DBE values were not observed, the use of different quadrupole target masses did effect the intensity weighted <O:C> and <DBE> values. From these results, it is suggested that the comparison of the spectral appearance (*i.e.* spectral distribution and abundance) and intensity weighted <O:C> and <DBE> values is not performed unless the same instrument parameters have been used.

Table 5.5 - The effect of the quadrupole target mass on the calculated OA metrics of the SOA filter sample collected during $MC_{[high]}$, using the FTICR-MS in negative ionisation mode. The quadrupole target mass was investigated at m/z 120, 300 and 480. The calculation of <O:C> and <DBE> can be found in Eq. 5.1 and 5.2, respectively.

	Replicate injections	No. of compounds	Average			Intensity weighted	
			O:C	H:C	DBE	<O:C>	<DBE>
Quadrupole target mass = m/z 120	1	1601	0.54	1.35	6.52	0.48	6.59
	2	1624	0.51	1.35	6.64	0.47	6.70
	3	1596	0.53	1.36	6.54	0.47	6.66
	4	1568	0.52	1.35	6.67	0.46	6.72
	5	1546	0.52	1.35	6.53	0.46	6.70
	Mean	1587	0.52	1.35	6.58	0.47	6.67
	STDEV	30.36	0.01	0.01	0.07	0.01	0.05
	%RSD	1.91	1.94	0.46	1.05	1.44	0.78
Quadrupole target mass = m/z 300	1	1477	0.53	1.35	6.72	0.49	7.76
	2	1469	0.51	1.35	6.78	0.49	7.80
	3	1459	0.51	1.35	6.67	0.49	7.72
	4	1462	0.50	1.34	6.81	0.48	7.79
	5	1453	0.51	1.36	6.63	0.49	7.73
	Mean	1464	0.51	1.35	6.72	0.49	7.76
	STDEV	9.27	0.01	0.01	0.08	0.00	0.03
	%RSD	0.63	2.21	0.61	1.15	0.52	0.45
Quadrupole target mass = m/z 480	1	1027	0.53	1.35	7.05	0.54	8.67
	2	1008	0.52	1.34	7.19	0.54	8.69
	3	964	0.52	1.33	7.22	0.54	8.74
	4	1004	0.52	1.33	7.17	0.54	8.58
	5	1036	0.50	1.35	7.05	0.54	8.58
	Mean	1008	0.52	1.34	7.14	0.54	8.69
	STDEV	27.82	0.01	0.01	0.08	0.00	0.07
	%RSD	2.76	1.71	0.65	1.12	0.44	0.78

Table 5.6 - The effect of the quadrupole target mass on the calculated OA metrics of the SOA filter sample collected during $MC_{[high]}$, using the FTICR-MS in positive ionisation mode. The quadrupole target mass was investigated at m/z 120, 300 and 480. The calculation of <O:C> and <DBE> can be found in Eq. 5.1 and 5.2, respectively.

	Replicate injections	No. of compounds	Average			Intensity weighted	
			O:C	H:C	DBE	<O:C>	<DBE>
Quadrupole target mass = m/z 120	1	1199	0.48	1.61	3.63	0.37	2.78
	2	1081	0.53	1.57	3.88	0.39	3.03
	3	1059	0.52	1.59	3.81	0.39	3.02
	4	1039	0.54	1.59	3.75	0.39	3.04
	5	1072	0.52	1.59	3.82	0.39	3.02
	Mean	1090	0.52	1.59	3.78	0.39	3.02
	STDEV	62.94	0.02	0.01	0.09	0.01	0.11
	%RSD	5.77	4.32	0.89	2.51	1.71	3.67
Quadrupole target mass = m/z 300	1	1028	0.51	1.60	3.87	0.40	3.06
	2	1005	0.51	1.61	3.77	0.42	3.01
	3	973	0.54	1.61	3.80	0.43	3.05
	4	985	0.53	1.62	3.84	0.42	3.01
	5	934	0.52	1.62	3.71	0.42	3.00
	Mean	985	0.52	1.61	3.80	0.42	3.02
	STDEV	35.33	0.01	0.01	0.06	0.01	0.03
	%RSD	3.59	2.58	0.50	1.60	1.98	0.92
Quadrupole target mass = m/z 480	1	667	0.53	1.68	3.84	0.45	3.07
	2	611	0.52	1.63	3.89	0.46	3.09
	3	653	0.57	1.69	3.61	0.45	2.99
	4	733	0.53	1.66	3.77	0.44	3.07
	5	649	0.52	1.64	3.78	0.44	3.07
	Mean	663	0.53	1.66	3.78	0.45	3.06
	STDEV	44.48	0.02	0.02	0.11	0.01	0.04
	%RSD	6.71	3.69	1.37	2.84	1.72	1.33

Table 5.7 - The percentage variation from the mean of the calculated OA metrics (based on five replicate measurements, Tables 5.5 and 5.6) for each of the quadrupole target masses, using the SOA filter sample collected during experiment MC[high].

Ionisation mode	Quadrupole target mass [*m/z*]	No. of compounds	Average			Intensity weighted	
			O:C	H:C	DBE	<O:C>	<DBE>
Negative	120	1587	0.52	1.35	6.58	0.47	6.67
	300	1464	0.51	1.35	6.72	0.49	7.76
	480	1008	0.52	1.34	7.14	0.54	8.69
	Mean	1353	0.52	1.35	6.81	0.50	7.71
	Range	579	0.01	0.01	0.56	0.07	2.02
	Variation from the mean [%]	57.44	1.96	0.75	8.51	14.89	30.28
Positive	120	1090	0.52	1.59	3.78	0.39	2.98
	300	985	0.52	1.61	3.80	0.42	3.02
	480	663	0.53	1.66	3.78	0.45	3.06
	Mean	913	0.52	1.62	3.78	0.42	3.02
	Range	427	0.01	0.07	0.02	0.06	0.08
	Variation from the mean [%]	64.40	1.92	4.40	0.53	15.38	2.68

5.3.2 Impact of Data Analysis Parameters

Three different UHR-MS data analysis methods used within the literature for the compositional analysis of OA were chosen. These methods were used to investigate if different data processing methods affected the calculated chemical metrics used for describing OA. In total, nine SOA samples collected during three ATMECH experiments were investigated; three SOA samples per experiment (Tables 5.1 and 5.2). All samples were analysed using the same instrument parameters as discussed in Section 5.2.1. The lack of sample volume meant that repeat injections of the same SOA sample could not be performed. However, repeat injections of the same SOA sample would only measure the precision of the instrument, not the effect of using different data processing methods. The instrumental error associated with replicate injections of the same SOA sample was shown above in Section 5.3.1.1. The low %RSD ($< 4.32\%$) obtained for the replicate injections of the SOA filter sample collected during experiment $MC_{[high]}$, at the same quadrupole target mass, suggests that providing the same instrument parameters are used, the instrumental error will not have a large impact on the analysis performed here.

The three ATMECH experiments investigated were; (i) $MC_{[high]}$, a photo-oxidation experiment with an initial VOC and NO mixing ratio of 460 and 95 ppbv, respectively; (ii) $MC_{L(O3)}$, a dark ozonolysis experiment with an initial VOC and O_3 mixing ratio of 228 and 958 ppbv respectively, and; (iii) $MC_{H(O3)}$, a dark ozonolysis experiment with a higher VOC and O_3 initial mixing ratio of 464 and 923 ppbv, respectively. The spectral data of each of these samples were analysed in both positive and negative ionisation modes using the following data analysis parameters; (i) relative abundance $> 0.01\%$, with a molecular formulae error < 10 ppm (Hamilton et al., 2013); (ii) relative abundance $> 1\%$, with a molecular formulae error < 5 ppm (Hall and Johnston, 2011) and; (iii) signal-to-noise ratio > 10, with a molecular formulae error < 1 ppm (Altieri et al., 2009; Kourtchev et al., 2014). The spectral composition of each SOA sample was calculated using the same software and molecular formulae parameters as discussed in Section 5.2.2, except the relative signal intensities and molecular formulae error were changed to those shown in the three data processing methods.

For each SOA sample, the number of compounds, average O:C and H:C ratios, DBE and intensity weighted <O:C> and <DBE> values were calculated using the three data processing methods. The mean, range and percentage variation from the mean were determined for each of the chemical properties, using the three data processing methods. The use of the percentage variation from the mean allowed the chemical properties of all of

the SOA samples to be compared, irrespective of differing chemical compositions. The spectral data acquired in both positive and negative ionisation modes were treated as separate data sets. This was performed to account for different analyte selectivity and ionisation efficiencies during ESI (*e.g.* (Cech and Enke, 2001)).

The effect of using the three different data processing methods on the calculated chemical properties is shown in Appendix A, Tables 5.10 to 5.18; and a summary is shown in Table 5.8. The use of the three different data processing methods resulted in a significant variation in the number of compounds which were assigned a molecular formulae (Appendix A, Tables 5.10 to 5.18). For example, the use of data processing (i) for the analysis of the PILS SOA sample (1356, Appendix A, Table 5.16) collected during $MC_{[high]}$ resulted in 903 compounds being assigned a molecular formulae in positive ionisation mode. Conversely, the use of data processing method (iii) for the same SOA sample, resulted in only 20 compounds being assigned a molecular formulae. It is imperative to note, that those compounds which are not assigned a molecular formula are not included in the calculation of the OA metrics and are not observed in the high resolution plots. Thus, large variations in the number of compounds which are not assigned a molecular formula may result in a large variation in the molecular distribution of the high resolution plots and the values obtained for the calculated chemical metrics. This large variation can be in-part attributed to the mass accuracy of the external and/or internal calibration, and the signal intensities of the compounds in the spectrum (*i.e.* sample dependant). For example, if all the species in a spectrum had a signal intensity of 0.1% and a molecular formulae error of 8 ppm, the use of data processing method (i) will result in all of the compounds being assigned a molecular formula. Conversely, the use of a data processing method (ii) will result in zero compounds being assigned a molecular formula.

The effect of the number of compounds which are assigned a molecular formulae on the molecular distribution of a Van Krevelen diagram is shown in Figure 5.9. The use of data processing method (i) resulted in significantly more compounds being assigned a molecular formulae, in comparison to the other data processing methods. However, the use of this method is likely to result in considerably more solvent and background peaks being included in the Van Krevelen diagram, due to the very low relative signal intensity (0.01%) used to calculate the molecular formulae. Conversely, the use of data processing method (iii) resulted in loss of the characteristic molecular distribution (Figure 5.9 C) observed with the use of the other data processing methods (Figure 5.9 A and B). The effect of the different data processing methods on the calculated OA metrics is shown in Figure 5.10.

Table 5.8 - A summary of the percentage variation from the mean for the calculated chemical metrics of the nine SOA samples using the three different data processing methods. Summarised from Appendix A, Tables 5.10 to 5.18.

Negative ionisation mode		Average variation from the mean [%]				
Exp.	PILS Sample	O:C	H:C	DBE	<DBE>	<O:C>
3088	1429	29.82	9.89	15.56	11.92	1.94
	1431	17.76	19.79	20.51	8.05	2.90
	1432	11.48	8.40	15.73	1.86	2.30
3077	1342	16.39	12.91	39.92	15.98	41.07
	1343	11.86	2.33	23.11	3.57	31.27
	1344	10.47	0.76	25.27	1.84	30.12
3080	1356	20.75	6.56	14.59	14.00	18.56
	1357	20.75	15.70	9.28	12.16	8.66
	1358	18.99	8.85	9.68	18.88	16.15
Minimum % variation		10.47	0.76	9.28	1.84	1.94
Maximum % variation		29.82	19.79	39.92	18.88	41.07
Average % variation		17.59	9.47	19.29	9.81	17.00
Positive ionisation mode		Average variation from the mean [%]				
Exp.	PILS Sample	O:C	H:C	DBE	<DBE>	<O:C>
3088	1429	48.65	13.85	48.24	22.34	31.97
	1431	46.32	10.61	27.05	19.81	17.67
	1432	35.29	12.98	45.93	9.89	22.56
3077	1342	6.34	2.67	14.91	16.94	23.59
	1343	8.22	5.97	15.38	8.22	15.38
	1344	12.86	2.69	14.72	16.80	24.88
3080	1356	24.83	6.62	20.22	17.21	28.79
	1357	32.65	2.49	12.77	22.13	8.59
	1358	16.44	3.07	8.96	20.00	9.89
Minimum % variation		6.34	2.49	8.96	8.22	8.59
Maximum % variation		48.65	13.85	48.24	22.34	31.97
Average % variation		25.73	6.77	23.13	17.04	20.37
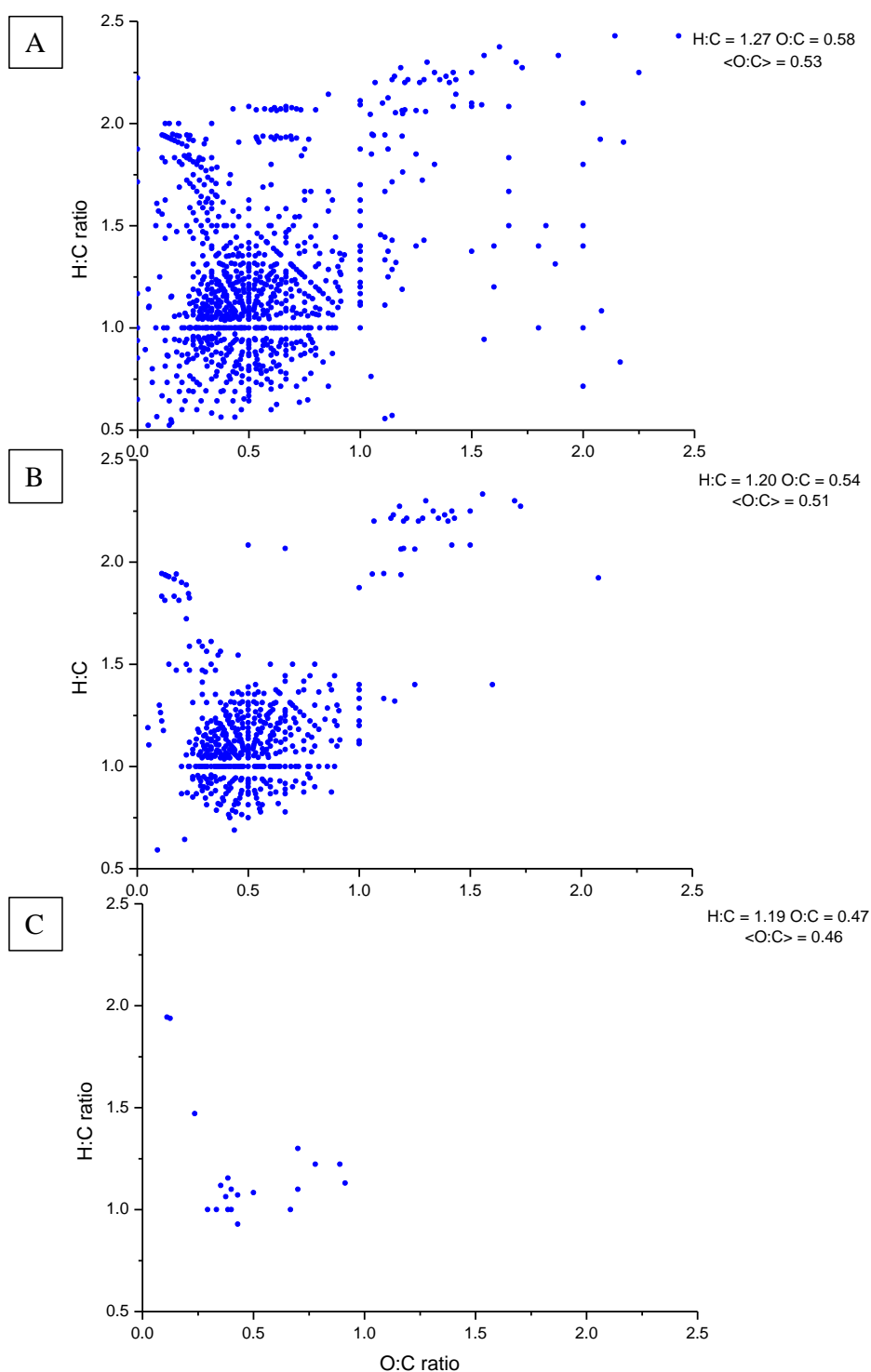
Figure 5.9 - Van Krevelen diagram to show the effect of the three different data processing methods on the molecular distribution of the compounds which have been assigned a molecular formula in experiment $MC_{[high]}$. Blue = PILS sample 1356 (Tables 5.1 and 5.2). A = Relative abundance > 0.01%, with a molecular formulae error < 10 ppm. B = Relative abundance > 1%, with a molecular formulae error < 5 ppm. C = S/N ratio > 10, with a molecular formulae error < 1 ppm.
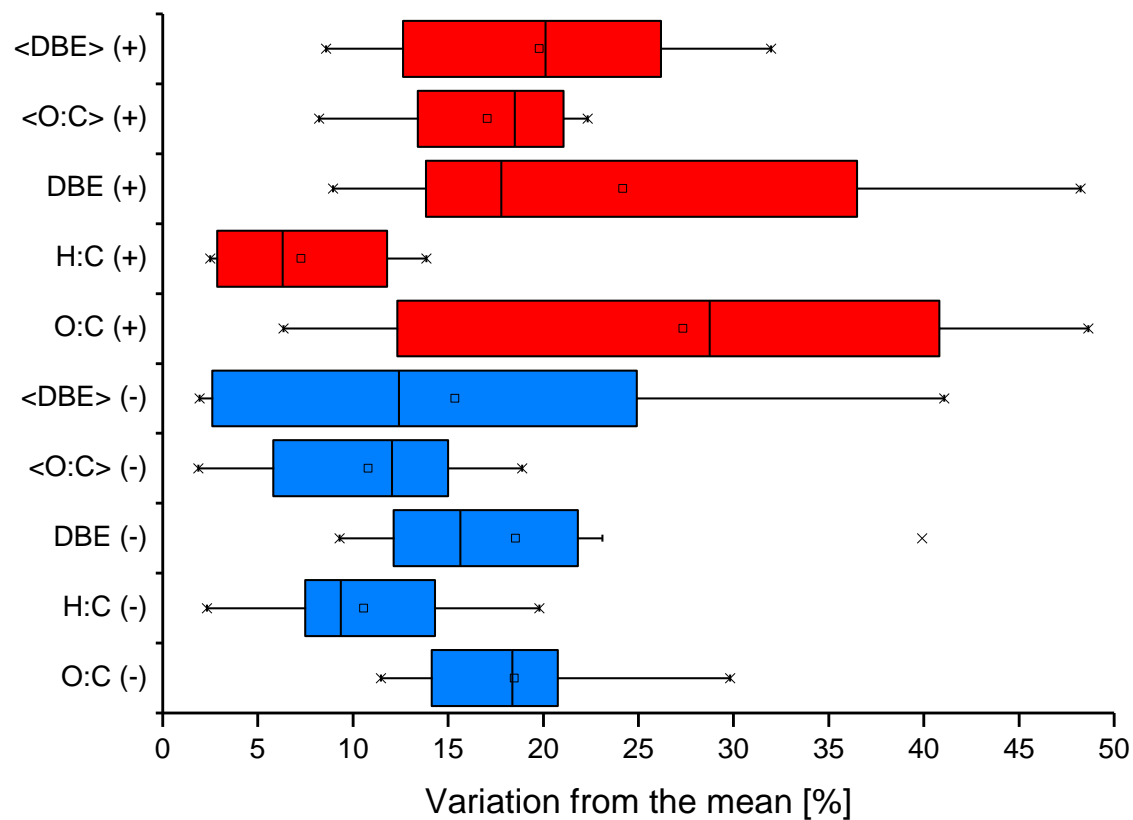
Figure 5.10 - Percentage variation from the mean for the investigated chemical properties for each of the SOA samples using the three different data processing methods, in negative and positive ionisation modes. Crosses display the minimum and maximum percentage variation from the mean. The 95th and 5th percentile is shown by the whiskers and the interquartile range (75th and 25th percentile) is shown by the boxes. The horizontal line in the middle of the boxes displays the median value, and the mean is represented by the smaller square within the box.

From Figure 5.10 it can be observed that the use of different data processing methods can have a large impact on the variation (and thus the reproducibility) of the reported chemical metrics. The average percentage variation from the mean ranged between 6.77 to 23.13% for the calculated chemical properties in both ionisation modes. However, the minimum and maximum percentage variation from the mean ranged between 0.76 to 48.65%. Generally, the percentage variation from the mean was lower in negative ionisation mode than in positive ionisation mode. This can be in-part attributed to internal mass calibration. In negative ionisation mode two compounds 4-methoxybenzoic acid and (4-methoxyphenyl)acetic acid previously identified during the ATMECH project were used to internally calibrate the mass accuracy (Chapter 3, Section 3.3.6). This could not be performed in positive ionisation mode due to the lack of known compounds observed in the spectra. Thus, any drift in the mass accuracy during sample analysis would of been reduced in negative ionisation mode.

The average percentage variation from the mean for the intensity weight <O:C> and <DBE> values is shown in Figure 5.11. From Figure 5.11 it can be observed that the intensity weighted <O:C> and <DBE> values displayed greater reproducibility than the non-intensity weighted O:C and DBE values. However, as shown in Section 5.3.1.1, the use of different quadrupole target masses had a larger effect on the reproducibility of the intensity weighted <O:C> and <DBE> values; highlighting the importance of using both a consistent instrument and data analysis method.

A summary of the average percentage variation from the mean for the calculated SOA metrics obtained from the use of the different quadrupole target masses (Table 5.7) and different data processing methods (Table 5.8), is shown in Table 5.9. From Table 5.9 it can be observed that a greater variation in the average O:C, H:C and DBE values were obtained with the use of different data processing methods, with the average percentage variation from the mean ranging between 6.77 to 25.73%, compared to 0.53 to 8.51% for the use of different quadrupole target masses. It is difficult to directly compare the variation of the OA metrics between the use of the different instrument or data processing methods due to the differing SOA composition and signal intensities (*i.e.* sample dependant). Nevertheless, it is clear that both the use of different instrument and data processing methods have an effect on the reported OA metrics.
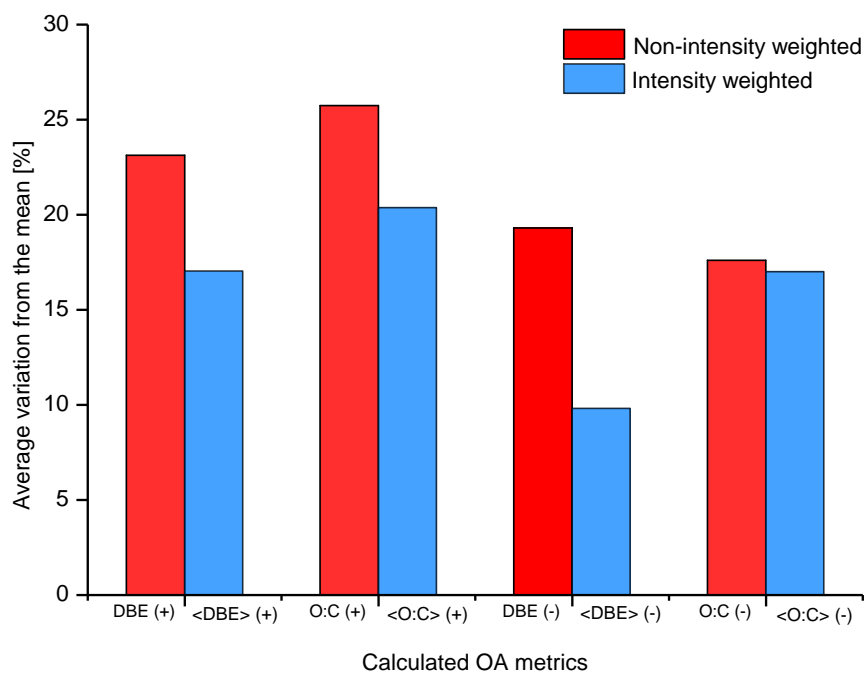
Figure 5.11 - Average percentage variation from the mean for the intensity weighted <O:C> and <DBE> values and the non-intensity weighted DBE and O:C values of the nine SOA samples investigated (Table 5.8), using the three different data processing methods in positive and negative ionisation modes.

Table 5.9 - Summary of average percentage variation from the mean of the calculated OA metrics using the three different quadrupole target masses (Q-target mass) and three data processing methods. Summarised from Tables 5.7 and 5.8.

		Average variation from the mean [%]				
Ionisation mode		O:C	H:C	DBE	<O:C>	<DBE>
Negative	Q-target mass	1.96	0.75	8.51	14.89	30.28
	Data analysis	17.59	9.47	19.29	17.00	9.81
Positive	Q-target mass	1.92	4.40	0.53	15.38	2.68
	Data analysis	25.73	6.77	23.13	17.04	20.37

5.4   Relevance of Findings within Aerosol Science

The instrument parameters investigated here will only be applicable to those mass spectrometers which use an RF-only quadrupole as an ion guide. The extremely large variation in the design of mass spectrometers and the lack of technical information provided, makes it very difficult to identify which instruments will be affected by the limited mass

ranged focussed by the QIG. Of the instruments for which the technical details could be obtained, the Bruker Daltonics SolariX FTICR-MS (as shown in this study) (Hamilton et al., 2011; Yassine et al., 2012; Hamilton et al., 2013; Pereira et al., 2014), Bruker Daltonics Apex-Qe FTICR-MS (Gao et al., 2010; Schmitt-Kopplin et al., 2010; Hall and Johnston, 2012), Thermo Orbitrap Fusion and Orbitrap QExactive all use a RF-only QIG. One of the main instruments used for the characterisation of OA, along with the Bruker Daltonics FTICR-MS, is the Thermo LTQ-Orbitrap (Reinhardt et al., 2007; Roach et al., 2010; O'Brien et al., 2013). However, it is currently unclear if this instrument also uses a RF-only QIG. It is also worth noting, that whilst the mass resolution is not high enough to distinguish the elemental composition, other commonly used mass spectrometers such as the ion-trap mass spectrometer will also be affected.

The use of different quadrupole target masses, as shown in this study, resulted in a significant variation in the *m/z* distribution of the mass spectra. For this reason, it is recommended that comparison of the spectral appearance of OA samples is not performed unless the same instrument parameters have been used. Furthermore, the use of different data processing methods was found to have significant impact on the number of compounds assigned a molecular formulae. As previously discussed, those compounds which are not assigned a molecular formulae are not included in the calculation of the OA metrics and the molecular distribution of high resolution plots. As observed in this study, stringent data analysis methods (*i.e.* S/N ratio > 10, molecular formula error < 1 ppm) can result in the loss of the characteristic molecular distribution observed with high resolution plots. Conversely, the use of a data analysis method which uses a very low relative signal intensity for the calculation of the molecular formulae is likely to result in more solvent and background peaks being included in the high resolution plots and calculated OA metrics. However, the manual extraction of known solvent or background peaks from an OA sample can be used to address this problem (Hamilton et al., 2013).

The average percentage variation from the mean for the calculated OA metrics was observed to range from 0.53 to 30.28% for the use of different quadrupole target masses, and 6.77 to 25.73% for the use of different data analysis methods. Based on the results shown in this study, this would mean an O:C ratio of 0.6 in positive ionisation mode would have an average variation of ± 0.17 using different data analysis methods and an average variation of ± 0.02 using different quadrupole target masses. Conversely, an intensity weighted <DBE> value of 5 in negative ionisation mode, would have an average variation of ± 0.49 using different data processing methods and an average variation of ± 1.51 using different quadrupole target masses. Whilst these variations may appear small, a variation of

$\pm$ 0.17 for an O:C ratio of 0.6 is the difference between whether the OA composition as a whole would be classified as semi-volatile oxygenated organic aerosol (SV-OOA) or low-volatility oxygenated organic aerosol (LV-OOA) using the AMS terminology (*e.g.* (Jimenez et al., 2009)). Thus, accurately determining these metrics is of critical importance for describing the chemical composition of OA. The combined effect of a different instrument and data processing method on the calculated OA metrics was not investigated here, but further study is warranted to investigate this. This work demonstrates the need for a standardised instrumental and data processing method for the inter-comparison of OA metrics; especially as the use of this method increases within aerosol science

5.5 Appendix A

Table 5.10 - The calculated SOA metrics of the PILS sample 1429 (Table 5.2) obtained during experiment $MC_{L(O3)}$ (Table 5.1), using the three different data processing methods in positive and negative ionisation modes. The spectral composition was obtained from the FTICR-MS using the data analysis method outlined in Section 5.3.2.

Experiment	No. of compounds	Average			Intensity weighted	
		O:C	H:C	DBE	\<O:C\>	\<DBE\>
Negative ionisation mode						
RA 0.01%, error 10 ppm	1379	0.65	1.27	7.06	0.53	8.18
RA 1%, error 5 ppm	958	0.58	1.22	7.82	0.51	8.34
S/N 10, error 1 ppm	323	0.48	1.15	8.26	0.47	8.26
Mean	887	0.57	1.21	7.71	0.50	8.26
Range	1056	0.17	0.12	1.2	0.06	0.16
% Variation	119.10	29.82	9.89	15.56	11.92	1.94
Positive ionisation mode						
RA 0.01%, error 10 ppm	1200	0.48	1.40	6.57	0.35	7.92
RA 1%, error 5 ppm	207	0.33	1.28	8.52	0.31	8.14
S/N 10, error 1 ppm	138	0.30	1.22	10.72	0.28	10.78
Mean	515	0.37	1.30	8.60	0.31	8.94
Range ±	1062	0.18	0.18	4.15	0.07	2.86
% Variation	206.21	48.65	13.85	48.24	22.34	31.97

Table 5.11 - The calculated SOA metrics of the PILS sample 1431 (Table 5.2) obtained during experiment $MC_{L(O3)}$ (Table 5.1), using the three different data processing methods in positive and negative ionisation modes. The spectral composition was obtained from the FTICR-MS using the data analysis method outlined in Section 5.3.2.

Experiment 3088	No. of compounds	Average			Intensity weighted	
		O:C	H:C	DBE	<O:C>	<DBE>
Negative ionisation mode						
RA 0.01%, error 10 ppm	2831	0.49	1.41	6.65	0.51	8.17
RA 1%, error 5 ppm	981	0.56	1.22	7.96	0.51	8.41
S/N 10, error 1 ppm	325	0.47	1.16	8.21	0.47	8.27
Mean	1379	0.51	1.26	7.61	0.50	8.28
Range	2506	0.09	0.25	1.56	0.04	0.24
% Variation	181.73	17.76	19.79	20.51	8.05	2.90
Positive ionisation mode						
RA 0.01%, error 10 ppm	1435	0.47	1.40	6.34	0.35	7.69
RA 1%, error 5 ppm	289	0.34	1.26	8.40	0.32	7.95
S/N 10, error 1 ppm	666	0.55	1.30	8.11	0.39	9.15
Mean	797	0.45	1.32	7.62	0.35	8.26
Range ±	1146	0.21	0.14	2.06	0.07	1.46
% Variation	143.85	46.32	10.61	27.05	19.81	17.67

Table 5.12 - The calculated SOA metrics of the PILS sample 1432 (Table 5.2) obtained during experiment $MC_{L(O3)}$ (Table 5.1), using the three different data processing methods in positive and negative ionisation modes. The spectral composition was obtained from the FTICR-MS using the data analysis method outlined in Section 5.3.2.

Experiment 3088	No. of compounds	Average			Intensity weighted	
		O:C	H:C	DBE	\<O:C\>	\<DBE\>
Negative ionisation mode						
RA 0.01%, error 10 ppm	1515	0.64	1.36	6.39	0.54	7.80
RA 1%, error 5 ppm	1034	0.62	1.32	7.10	0.54	7.91
S/N 10, error 1 ppm	436	0.57	1.25	7.49	0.53	7.73
Mean	995	0.61	1.31	6.99	0.54	7.81
Range ±	1079	0.07	0.11	1.1	0.01	0.18
% Variation	108.44	11.48	8.40	15.73	1.86	2.30
Positive ionisation mode						
RA 0.01%, error 10 ppm	1175	0.41	1.41	6.62	0.32	8.16
RA 1%, error 5 ppm	280	0.32	1.28	8.72	0.30	8.52
S/N 10, error 1 ppm	128	0.29	1.24	10.59	0.29	10.18
Mean	528	0.34	1.31	8.64	0.30	8.95
Range ±	1047	0.12	0.17	3.92	0.03	2.02
% Variation	198.42	35.29	12.98	45.93	9.89	22.56

Table 5.13 - The calculated SOA metrics of the PILS sample 1342 (Table 5.2) obtained during experiment $MC_{H(O3)}$ (Table 5.1), using the three different data processing methods in positive and negative ionisation modes. The spectral composition was obtained from the FTICR-MS using the data analysis method outlined in Section 5.3.2.

Experiment 3077	No. of compounds	Average			Intensity weighted	
		O:C	H:C	DBE	<O:C>	<DBE>
Negative ionisation mode						
RA 0.01%, error 10 ppm	1262	0.61	1.30	7.03	0.54	7.83
RA 1%, error 5 ppm	747	0.56	1.24	7.64	0.53	7.92
S/N 10, error 1 ppm	90	0.66	1.41	5.02	0.62	5.07
Mean	700	0.61	1.32	6.56	0.56	6.94
Range ±	1172	0.1	0.17	2.62	0.09	2.85
% Variation	167.51	16.39	12.91	39.92	15.98	41.07
Positive ionisation mode						
RA 0.01%, error 10 ppm	1275	0.49	1.51	6.23	0.39	7.15
RA 1%, error 5 ppm	227	0.46	1.47	7.25	0.39	7.40
S/N 10, error 1 ppm	122	0.47	1.51	7.05	0.46	5.80
Mean	541	0.47	1.50	6.84	0.41	6.78
Range ±	1153	0.03	0.04	1.02	0.07	1.6
% Variation	212.99	6.34	2.67	14.91	16.94	23.59

Table 5.14 - The calculated SOA metrics of the PILS sample 1343 (Table 5.2) obtained during experiment $MC_{H(O3)}$ (Table 5.1), using the three different data processing methods in positive and negative ionisation modes. The spectral composition was obtained from the FTICR-MS using the data analysis method outlined in Section 5.3.2.

Experiment 3077	No. of compounds	Average			Intensity weighted	
		O:C	H:C	DBE	\<O:C\>	\<DBE\>
Negative ionisation mode						
RA 0.01%, error 10 ppm	1133	0.62	1.29	7.01	0.55	7.68
RA 1%, error 5 ppm	951	0.60	1.30	7.12	0.56	7.63
S/N 10, error 1 ppm	58	0.55	1.27	5.60	0.57	5.51
Mean	714	0.59	1.29	6.58	0.56	6.94
Range ±	1075	0.07	0.03	1.52	0.02	2.17
% Variation	150.56	11.86	2.33	23.11	3.57	31.27
Positive ionisation mode						
RA 0.01%, error 10 ppm	1088	0.51	1.51	5.95	0.51	5.95
RA 1%, error 5 ppm	204	0.48	1.46	6.93	0.48	6.93
S/N 10, error 1 ppm	70	0.47	1.55	6.24	0.47	6.24
Mean	454	0.49	1.51	6.37	0.49	6.37
Range ±	1018	0.04	0.09	0.98	0.04	0.98
% Variation	224.23	8.22	5.97	15.38	8.22	15.38

Table 5.15 - The calculated SOA metrics of the PILS sample 1344 (Table 5.2) obtained during experiment $MC_{H(O3)}$ (Table 5.1), using the three different data processing methods in positive and negative ionisation modes. The spectral composition was obtained from the FTICR-MS using the data analysis method outlined in Section 5.3.2.

Experiment	No. of compounds	Average			Intensity weighted	
		O:C	H:C	DBE	\<O:C\>	\<DBE\>
Negative ionisation mode						
RA 0.01%, error 10 ppm	1203	0.60	1.32	6.78	0.54	7.41
RA 1%, error 5 ppm	881	0.58	1.31	6.97	0.55	7.42
S/N 10, error 1 ppm	51	0.54	1.31	5.36	0.54	5.39
Mean	712	0.57	1.31	6.37	0.54	6.74
Range ±	1152	0.06	0.01	1.61	0.01	2.03
% Variation	161.87	10.47	0.76	25.27	1.84	30.12
Positive ionisation mode						
RA 0.01%, error 10 ppm	1299	0.50	1.51	6.10	0.40	6.69
RA 1%, error 5 ppm	212	0.46	1.47	6.98	0.39	6.84
S/N 10, error 1 ppm	100	0.44	1.48	7.09	0.46	5.28
Mean	537	0.46	1.48	6.72	0.42	6.27
Range ±	1199	0.06	0.04	0.99	0.07	1.56
% Variation	223.28	12.86	2.69	14.72	16.80	24.88

Table 5.16 - The calculated SOA metrics of the PILS sample 1356 (Table 5.2) obtained during experiment $MC_{[high]}$ (Table 5.1), using the three different data processing methods in positive and negative ionisation modes. The spectral composition was obtained from the FTICR-MS using the data analysis method outlined in Section 5.3.2.

Experiment 3080	No. of compounds	Average			Intensity weighted	
		O:C	H:C	DBE	<O:C>	<DBE>
Negative ionisation mode						
RA 0.01%, error 10 ppm	903	0.58	1.27	6.96	0.53	7.18
RA 1%, error 5 ppm	498	0.54	1.20	7.52	0.51	7.48
S/N 10, error 1 ppm	20	0.47	1.19	6.50	0.46	6.19
Mean	474	0.53	1.22	6.99	0.50	6.95
Range ±	883	0.11	0.08	1.02	0.07	1.29
% Variation	186.42	20.75	6.56	14.59	14.00	18.56
Positive ionisation mode						
RA 0.01%, error 10 ppm	1136	0.54	1.53	5.86	0.43	5.33
RA 1%, error 5 ppm	70	0.42	1.55	6.27	0.36	4.40
S/N 10, error 1 ppm	92	0.49	1.45	7.16	0.43	5.90
Mean	433	0.48	1.51	6.43	0.40	5.21
Range ±	1066	0.12	0.1	1.3	0.07	1.5
% Variation	246.38	24.83	6.62	20.22	17.21	28.79

Table 5.17 - The calculated SOA metrics of the PILS sample 1357 (Table 5.2) obtained during experiment $MC_{[high]}$ (Table 5.1), using the three different data processing methods in positive and negative ionisation modes. The spectral composition was obtained from the FTICR-MS using the data analysis method outlined in Section 5.3.2.

Experiment 3080	No. of compounds	Average				Intensity weighted	
		O:C	H:C	DBE		<O:C>	<DBE>
Negative ionisation mode							
RA 0.01%, error 10 ppm	968	0.58	1.29	6.83		0.52	7.08
RA 1%, error 5 ppm	517	0.54	1.24	7.32		0.50	7.37
S/N 10, error 1 ppm	10	0.47	1.10	7.50		0.46	7.72
Mean	498	0.53	1.21	7.22		0.49	7.39
Range ±	958	0.11	0.19	0.67		0.06	0.64
% Variation	192.24	20.75	15.70	9.28		12.16	8.66
Positive ionisation mode							
RA 0.01%, error 10 ppm	1087	0.57	1.58	5.36		0.43	5.03
RA 1%, error 5 ppm	57	0.41	1.62	4.96		0.35	4.67
S/N 10, error 1 ppm	88	0.49	1.61	4.72		0.44	4.62
Mean	411	0.49	1.60	5.01		0.41	4.77
Range ±	1030	0.16	0.04	0.64		0.09	0.41
% Variation	250.81	32.65	2.49	12.77		22.13	8.59

Table 5.18 - The calculated SOA metrics of the PILS sample 1358 (Table 5.2) obtained during experiment $MC_{[high]}$ (Table 5.1), using the three different data processing methods in positive and negative ionisation modes. The spectral composition was obtained from the FTICR-MS using the data analysis method outlined in Section 5.3.2.

Experiment	No. of compounds	Average			Intensity weighted	
		O:C	H:C	DBE	<O:C>	<DBE>
Negative ionisation mode						
RA 0.01%, error 10 ppm	962	0.57	1.31	6.70	0.51	7.05
RA 1%, error 5 ppm	480	0.54	1.22	7.38	0.50	7.34
S/N 10, error 1 ppm	12	0.47	1.20	7.00	0.42	6.23
Mean	485	0.53	1.24	7.03	0.48	6.88
Range ±	950	0.1	0.11	0.68	0.09	1.11
% Variation	196.01	18.99	8.85	9.68	18.88	16.15
Positive ionisation mode						
RA 0.01%, error 10 ppm	1060	0.54	1.60	5.21	0.42	5.10
RA 1%, error 5 ppm	47	0.46	1.65	5.10	0.35	4.84
S/N 10, error 1 ppm	93	0.46	1.64	4.76	0.43	4.62
Mean	400	0.49	1.63	5.02	0.40	4.85
Range ±	1013	0.08	0.05	0.45	0.08	0.48
% Variation	253.25	16.44	3.07	8.96	20.00	9.89

Chapter 6 - Summary and Future Work

6.1   Summary

SOA constitutes a significant proportion of ambient particulate matter. Whilst SOA formation is known to have adverse effects on climate and human health, the VOC oxidation pathways leading to SOA formation are poorly understood. The sheer number of compounds formed from the oxidation of VOCs, their low concentrations, and continually evolving chemical composition, makes the identification of the species involved in SOA formation and growth a highly complex and difficult task. Techniques such as mass spectrometry coupled with prior chromatographic separation, can allow individual species within complex mixtures to be isolated and identified. In this thesis, a number of new methods were developed to study the composition of SOA. These methods were tested on a range of aromatic VOC systems, which have received considerably less study in recent years. Initially, the SOA composition formed from the photo-oxidation of methyl chavicol was investigated. Methyl chavicol has been suggested to be an important SOA precursor in regions where there are oil palm plantations and pine forests. However, the SOA composition formed from the oxidation of methyl chavicol had largely been unexplored.

The photo-oxidation of methyl chavicol resulted in significant SOA formation, with the SOA yield determined to range between 19-31%, depending on the initial VOC:NO$_x$ mixing ratio. All of the identified SOA compounds were observed to retain the aromatic ring upon oxidation. This resulted in the formation of compounds with both low volatility and high O:C ratios (SVOOA and LVOOA); where functionalisation rather than fragmentation was mainly observed as a result of the stability of the aromatic ring. This leads to products that were more similar to ambient OA in terms C^* and O:C (measured using the AMS) than the majority of species previously observed in chamber studies from isoprene and monoterpene oxidation.

At lower VOC:NO$_x$ ratios (*i.e.* higher NO$_x$ concentrations), a larger amount of aerosol mass was formed for a smaller amount of methyl chavicol reacted during initial aerosol growth. This suggested that the products formed from the reaction with NO$_2$ (as no aerosol formation was observed until a relatively low NO environment was entered) were likely to be influencing SOA formation in the initial stages of aerosol growth. The use of a time resolved aerosol collection method followed by offline mass spectrometric analysis allowed this to be investigated further. The majority of the observed initial SOA composition was found to consist of substituted nitrophenols. These compounds had high O:C ratios and were of low volatility, with one of the structurally identified nitrophenols observed to be

fractionally outside the extremely low volatility "nucleator" region proposed in Donahue et al. (2013).

To further investigate the role of substituted nitrophenols during initial aerosol growth, two other aromatic photo-oxidation systems (toluene and 4-methyl catechol) were investigated. Substituted nitrophenols were also observed in the initial SOA composition collected during the photo-oxidation of toluene. However, based on the volatility of these species (IVOC) and the little amount of aerosol mass formed, these compounds would not be expected to be in the aerosol phase. From these observations, it is suggested that the presence of the nitro-group on the aromatic ring may be forming stabilised gas-phase clusters; resulting in new particle formation. The chemical composition and structure of these substituted nitrophenols were found to be critically important, as the methyl nitrocatechol formed during the photo-oxidation of 4-methyl catechol did not partition into the aerosol phase until irradiation had stopped, suggesting the location of aromatic substitutions made this compound more susceptible to a loss process such as photolysis; highlighting the importance of studying SOA formation and evolution at a molecular level.

The methods developed can be applied to a range of other systems and have the potential to lead to significant improvements in our understanding of the fundamentals of aerosol formation and ageing. The methods are now being applied to more complex systems, using real fuel emissions, in the first instance, the SOA formed from oxidation of diesel exhaust emissions.

Finally, the effect of different instrument and data processing methods on the commonly reported OA metrics (i.e. O:C, H:C ratio *etc*) were investigated. This was performed using ultra high resolution mass spectrometry. It was found that the use of different quadrupole target masses, used to represent different instrument parameters, can have an significant effect on the *m/z* distribution of a spectrum; considerably altering the appearance. Different data processing methods and different quadrupole target masses were observed to effect the calculated OA metrics, but it was difficult to provide the true effect of these parameters on the OA metrics as it was largely sample dependent. Nevertheless, this work demonstrated the need for a standardised instrument and data processing method for the inter-comparison of OA metrics within the literature from ultra high resolution mass spectrometric techniques.

6.2   Future Work

The occurrence of the nitrophenol compounds during new particle formation in the aromatic systems is a very interesting observation. The nitro group is a zwitterion and as such it could potentially be involved in the very initial stages of nucleation through the formation of gas phase clusters. Recent measurements with API-TOFMS shows the occurrence of clusters to be highly oxidised ELVOC compounds, hinting that in monoterpene oxidation, the oxidised products are involved in the initial cluster formation. At York, work has already begun to investigate whether the substituted nitrophenols observed in this work are able to form stabilised gas phase clusters with other nitrophenols, sulfuric acid or water molecules. This is work is being investigated using theoretical quantum chemistry simulations (Dr M. Cockett, University of York). However, further experimental work will also be required to investigate the role of these species in new particle formation and aerosol growth.

The use of the PILS followed by offline analysis provided information regarding how quickly first, second, third *etc* generation products formed in the gas phase, partitioned into aerosol phase. This information, with further work (*e.g.* application of this technique to other VOC systems), could be incorporated into the master chemical mechanism, highlighting the mechanisms for the formation of ELVOCs and potentially allowing further SOA precursors to be identified. Only the SOA composition formed from the photo-oxidation of methyl chavicol was investigated in this work. Further work is required to investigate the SOA formed from the oxidation of methyl chavicol with different oxidants (O_3, $\cdot NO_3$), relative humidities and seed aerosol, to further investigate the effect methyl chavicol emissions may have on regional atmospheric chemistry.

Finally, further work is required to determine which ultra high resolution mass spectrometric instruments may be affected by the limited mass ranged focussed by the QIG. In addition, further work is required to develop a suitable instrument and data processing method for the inter-comparison of OA metrics. As a starting point, the instrumental method could be developed by the optimisation of each *m/z* window in a selected mass range and stitching these windows together using the methodology detailed in (Payne, 2011). However, the development of a suitable instrumental method for the compositional analysis of all OA samples, with the use of different ultra high resolution mass spectrometric techniques is likely to be extremely complicated. The use of a standardised data processing method is likely to be considerably easier to implement, this alone may be sufficient for the comparison of OA metrics from ultra high resolution mass spectrometric techniques. A standardised instrument and/or data processing will allow the chemical properties of OA to

be reliably compared within the literature. This information could potentially be listed in a database and used to compare the chemical properties of different OA samples; potentially providing greater insight into important SOA precursors.

List of Abbreviations

AMS - Aerosol mass spectrometry

BPC - Base peak chromatogram

CID - Collision induced dissociation

EIC - Extracted ion chromatogram

ESI - Electrospray ionisation

ELVOOA - Extremely low volatility oxygenated organic aerosol

FTICR-MS - Fourier transform ion cyclotron resonance mass spectrometry

HILIC - Hydrophilic interaction liquid chromatography

HPLC - High performance liquid chromatography

LV-OOA - Low volatility oxygenated organic aerosol

m/z **-** Mass-to-charge ratio

MS^2 - Tandem mass spectrometry

(M-H)$^-$ - Deprotonated molecular species

(M+H)$^+$ - Protonated molecular species.

(M+Na)$^+$ - Sodiated molecular species

NP-LC - Normal phase liquid chromatography

OA - Organic aerosol

TIC - Total ion chromatogram

QIG - Quadrupole ion guide

QTOFMS - Quadrupole time-of-flight mass spectrometry

RP-LC - Reverse phase liquid chromatography

SV-OOA - Semi volatile oxygenated organic aerosol

References

Adams, R. P.: Identification of essential oil components by gas chromatography/mass spectrometry, 4th Edn, Allured Publishing Corporation, Carol Stream, 2007.

Aharoni, A., Ric de Vos, C., Verhoeven, H. A., Maliepaard, C. A., Kruppa, G., Bino, R., and Goodenowe, D. B.: Nontargeted metabolome analysis by use of Fourier transform ion cyclotron mass spectrometry, A Journal of Integrative Biology, 6, 217-234, 2002.

Ahmadov, R., McKeen, S. A., Robinson, A. L., Bahreini, R., Middlebrook, A. M., de Gouw, J. A., Meagher, J., Hsie, E. Y., Edgerton, E., Shaw, S., and Trainer, M.: A volatility basis set model for summertime secondary organic aerosols over the eastern United States in 2006, Journal of Geophysical Research: Atmospheres, 117, 6301, 2012.

Akimoto, H., Takagi, H., and Sakamaki, F.: Photoenhancement of the nitrous acid formation in the surface reaction of nitrogen dioxide and water vapor: Extra radical source in smog chamber experiments, International Journal of Chemical Kinetics, 19, 539-551, 1987.

Alfarra, M. R., Hamilton, J. F., Wyche, K. P., Good, N., Ward, M. W., Carr, T., Barley, M. H., Monks, P. S., Jenkin, M. E., Lewis, A. C., and McFiggans, G. B.: The effect of photochemical ageing and initial precursor concentration on the composition and hygroscopic properties of beta-caryophyllene secondary organic aerosol, Atmospheric Chemistry and Physics, 12, 6417-6436, 2012.

Alicke, B., Geyer, A., Hofzumahaus, A., Holland, F., Konrad, S., Pätz, H. W., Schäfer, J., Stutz, J., Volz-Thomas, A., and Platt, U.: OH formation by HONO photolysis during the BERLIOZ experiment, Journal of Geophysical Research: Atmospheres, 108, 8247, 2003.

Almeida, J., Schobesberger, S., Kurten, A., Ortega, I. K., Kupiainen-Maatta, O., Praplan, A. P., Adamov, A., Amorim, A., Bianchi, F., Breitenlechner, M., David, A., Dommen, J., Donahue, N. M., Downard, A., Dunne, E., Duplissy, J., Ehrhart, S., Flagan, R. C., Franchin, A., Guida, R., Hakala, J., Hansel, A., Heinritzi, M., Henschel, H., Jokinen, T., Junninen, H., Kajos, M., Kangasluoma, J., Keskinen, H., Kupc, A., Kurten, T., Kvashin, A. N., Laaksonen, A., Lehtipalo, K., Leiminger, M., Leppa, J., Loukonen, V., Makhmutov, V., Mathot, S., McGrath, M. J., Nieminen, T., Olenius, T., Onnela, A., Petaja, T., Riccobono, F., Riipinen, I., Rissanen, M., Rondo, L., Ruuskanen, T., Santos, F. D., Sarnela, N., Schallhart, S., Schnitzhofer, R., Seinfeld, J. H., Simon, M., Sipila, M., Stozhkov, Y., Stratmann, F., Tome, A., Trostl, J., Tsagkogeorgas, G., Vaattovaara, P., Viisanen, Y., Virtanen, A., Vrtala, A., Wagner, P. E., Weingartner, E., Wex, H., Williamson, C., Wimmer, D., Ye, P., Yli-Juuti, T., Carslaw, K. S., Kulmala, M., Curtius, J., Baltensperger,

U., Worsnop, D. R., Vehkamaki, H., and Kirkby, J.: Molecular understanding of sulphuric acid-amine particle nucleation in the atmosphere, Nature, 502, 359-363, 2013.

Alpert, A. J.: Hydrophilic-interaction chromatography for the separation of peptides, nucleic acids and other polar compounds, Journal of Chromatography A, 499, 177-196, 1990.

Altieri, K. E., Turpin, B. J., and Seitzinger, S. P.: Oligomers, organosulfates, and nitrooxy organosulfates in rainwater identified by ultra-high resolution electrospray ionization FT-ICR mass spectrometry, Atmospheric Chemistry and Physics, 9, 2533-2542, 2009.

An, X., Jing, B., and Li, Q.: Regulating function of alkali metal on the strength of OH···O hydrogen bond in phenol–water complex: Weak to strong and strong to weak, Computational and Theoretical Chemistry, 966, 278-283, 2011.

Andreae, M. O., and Merlet, P.: Emission of trace gases and aerosols from biomass burning, Global Biogeochemical Cycles, 15, 955-966, 2001.

Anttila, P., Hyotylainen, T., Heikkila, A., Jussila, M., Finell, J., Kulmala, M., and Riekkola, M. L.: Determination of organic acids in aerosol particles from a coniferous forest by liquid chromatography-mass spectrometry, Journal of Separation Science, 28, 337-346, 2005.

Arsene, C., Vione, D., Grinberg, N., and Olariu, R. I.: GC × GC-MS hyphenated techniques for the analysis of volatile organic compounds in air, Journal of Liquid Chromatography and Related Technologies, 34, 1077-1111, 2011.

Aschmann, S. M., Nishino, N., Arey, J., and Atkinson, R.: Products of the OH radical-initiated reactions of furan, 2- and 3-methylfuran, and 2, 3- and 2, 5-dimethylfuran in the presence of NO, The Journal of Physical Chemistry, 118, 457-466, 2013.

Atkinson, R.: Kinetics and mechanisms of the gas-phase reactions of the hydroxyl radical with organic compounds, Journal of Physical and Chemical Reference Data, 86, 69-201, 1989.

Atkinson, R., Aschmann, S. M., Tuazon, E. C., Arey, J., and Zielinska, B.: Formation of 3-methylfuran from the gas-phase reaction of OH radicals with isoprene and the rate constant for its reaction with the OH radical, International Journal of Chemical Kinetics, 21, 593-604, 1989.

Atkinson, R.: Gas-phase trosposheric chemistry of organic compounds, Journal of Physical and Chemical Reference Data, Monograph 2, 1-216, 1994.

Atkinson, R., and Aschmann, S. M.: Products of the gas-phase reactions of aromatic hydrocarbons: Effect of NO2 concentration, International Journal of Chemical Kinetics, 26, 929-944, 1994.

Atkinson, R.: Atmospheric reactions of alkoxy and beta-hydroxyalkoxy radicals, International Journal of Chemical Kinetics, 29, 99-111, 1997a.

Atkinson, R.: Gas-phase tropospheric chemistry of volatile organic compounds: 1. Alkanes and alkenes, Journal of Physical and Chemical Reference Data, 26, 215-290, 1997b.

Atkinson, R.: Atmospheric chemistry of VOCs and NOx, Atmospheric Environment, 34, 2063-2101, 2000.

Atkinson, R., and Arey, J.: Atmospheric degradation of volatile organic compounds, Chemical Reviews, 103, 4605-4638, 2003.

Banerjee, S., and Mazumdar, S.: Electrospray ionization mass spectrometry: A technique to access the information beyond the molecular weight of the analyte, International Journal of Analytical Chemistry, 2012, 40, 2012.

Barazani, O., Cohen, Y., Fait, A., Diminshtein, S., Dudai, N., Ravid, U., Putievsky, E., and Friedman, J.: Chemotypic differentiation in indigenous populations of Foeniculum vulgare var. vulgare in Israel, Biochemical Systematics and Ecology, 30, 721-731, 2002.

Bargsten, A., Falge, E., Huwe, B., and Meixner, F.: Laboratory measurements of nitric oxide release from forest soil with a thick organic layer under different understory types, Biogeosciences Discussions, 7, 203-250, 2010.

Barsanti, K. C., and Pankow, J. F.: Thermodynamics of the formation of atmospheric organic particulate matter by accretion reactions - Part 1: Aldehydes and ketones, Atmospheric Environment, 38, 4371-4382, 2004.

Barsanti, K. C., Carlton, A. G., and Chung, S. H.: Analyzing experimental data and model parameters: implications for predictions of SOA using chemical transport models, Atmospheric Chemistry and Physics, 13, 12073-12088, 2013.

Bateman, A. P., Nizkorodov, S. A., Laskin, J., and Laskin, A.: Time-resolved molecular characterization of limonene/ozone aerosol using high-resolution electrospray ionization mass spectrometry, Physical Chemistry Chemical Physics, 11, 7931-7942, 2009.

Bateman, A. P., Nizkorodov, S. A., Laskin, J., and Laskin, A.: High-resolution electrospray ionization mass spectrometry analysis of water-soluble organic aerosols collected with a particle into liquid sampler, Analytical Chemistry, 82, 8010, 2010.

Baykut, G., and Eyler, J.: Fourier transform ion cyclotron resonance mass spectrometry, Trends in Analytical Chemistry, 5, 44-49, 1986.

Becker, K.: EUPHORE: Final report to the European commission, Contract EV5V-CT92-0059, Bergische Universität Wuppertal, Germany, 1996.

Bejan, I., Abd El Aal, Y., Barnes, I., Benter, T., Bohn, B., Wiesen, P., and Kleffmann, J.: The photolysis of ortho-nitrophenols: a new gas phase source of HONO, Physical Chemistry Chemical Physics, 8, 2028-2035, 2006.

Bejan, I. G.: Investigations on the gas phase atmospheric chemistry of nitrophenols and catechols, PhD Thesis, Bergische University of Wupperthal, Germany, 2006.

Bell, M., Goldberg, R., Hogrefe, C., Kinney, P., Knowlton, K., Lynn, B., Rosenthal, J., Rosenzweig, C., and Patz, J.: Climate change, ambient ozone, and health in 50 US cities, Climatic Change, 82, 61-76, 2007.

Benoit, D. M., and Clary, D. C.: Quantum simulation of phenol−water clusters, The Journal of Physical Chemistry A, 104, 5590-5599, 2000.

Bierbach, A., Barnes, I., and Becker, K. H.: Product and kinetic-study of the OH-initiated gas-phase oxidation of furan, 2-methylfuran and furanaldehydes at 300 K, Atmospheric Environment, 29, 2651-2660, 1995.

Blake, R. S., Monks, P. S., and Ellis, A. M.: Proton-transfer reaction mass spectrometry, Chemical Reviews, 109, 861-896, 2009.

Bloss, C., Wagner, V., Bonzanini, A., Jenkin, M. E., Wirtz, K., Martin-Reviejo, M., and Pilling, M. J.: Evaluation of detailed aromatic mechanisms (MCMv3 and MCMv3.1) against environmental chamber data, Atmospheric Chemistry and Physics, 5, 623-639, 2005.

Bloss, W. J., Alam, M. S., Rickard, A. R., Hamilton, J. F., Pereira, K. L., Camredon, M., Muñoz, A., Vázquez, M., Alacreu, P., Ródenas, M., and Vera, T.: Atmospheric chemistry of methyl chavicol (estragole), AGU Fall Meeting, Fall meeting 3 to 7 December 2012, A33L-0313, San Francisco, 2012.

Bonn, B., von Kuhlmann, R., and Lawrence, M. G.: High contribution of biogenic hydroperoxides to secondary organic aerosol formation, Geophysical Research Letters, 31, L10108, 2004.

Bostick, N. H., and Daws, T. A.: Relationships between data from Rock-Eval pyrolysis and proximate, ultimate, petrographic, and physical analyses of 142 diverse U.S. coal samples, Organic Geochemistry, 21, 35-49, 1994.

Bouvier-Brown, N., Goldstein, A., Worton, D., Matross, D., Gilman, J., Kuster, W., Welsh-Bon, D., Warneke, C., de Gouw, J., and Cahill, M.: Methyl chavicol: characterization of its biogenic emission rate, abundance, and oxidation products in the atmosphere, Atmospheric Chemistry and Physics, 9, 2061-2074, 2009.

Bouvier-Brown, N. C.: Quantifying reactive biogenic volatile organic compounds: Implications for gas-and particle-phase atmospheric chemistry, PhD Thesis, Univeristy of California, Berkeley, 182 pp., 2008.

Bowman, F. M., Odum, J. R., Seinfeld, J. H., and Pandis, S. N.: Mathematical model for gas-particle partitioning of secondary organic aerosols, Atmospheric Environment, 31, 3921-3931, 1997.

Bröske, R., Kleffmann, J., and Wiesen, P.: Heterogeneous conversion of NO2 on secondary organic aerosol surfaces: A possible source of nitrous acid (HONO) in the atmosphere?, Atmospheric Chemistry and Physics, 3, 469-474, 2003.

Bruins, A. P.: Mechanistic aspects of electrospray ionization, Journal of Chromatography A, 794, 345-357, 1998.

Brunekreef, B., and Forsberg, B.: Epidemiological evidence of effects of coarse airborne particles on health, European Respiratory Journal, 26, 309-318, 2005.

Bursey, M. M., and McLafferty, F. W.: Rearrangements and "flat-topped metastable ions" in the mass spectra of substituted nitrobenzenes, Journal of the American Chemical Society, 88, 5023-5025, 1966.

Bursey, M. M.: Influence of steric inhibition of resonance on ion intensities in mass spectra, Journal of the American Chemical Society, 91, 1861, 1969.

Buszewski, B., and Noga, S.: Hydrophilic interaction liquid chromatography (HILIC) - a powerful separation technique, Analytical and Bioanalytical Chemistry, 402, 231-247, 2012.

Bzdek, B. R., DePalma, J. W., Ridge, D. P., Laskin, J., and Johnston, M. V.: Fragmentation energetics of clusters relevant to atmospheric new particle formation, Journal of the American Chemical Society, 135, 3276-3285, 2013.

Cabral do Couto, P., Guedes, R. C., Costa Cabral, B. J., and Martinho Simões, J. A.: Phenol O–H bond dissociation energy in water clusters, International Journal of Quantum Chemistry, 86, 297-304, 2002.

Cahill, T. M., Seaman, V. Y., Charles, M. J., Holzinger, R., and Goldstein, A. H.: Secondary organic aerosols formed from oxidation of biogenic volatile organic compounds in the

Sierra Nevada Mountains of California, Journal of Geophysical Research, 111, D16312, 2006.

Calvert, J., Derwent, R., Orlando, J., Tyndall, G., and Wallington, T.: Mechanisms of atmospheric oxidation of the alkanes, Oxford University Press, New York, 2008.

Calvert, J. G., Atkinson, R., Kerr, J., Madronich, S., Moortgat, G., Wallington, T. J., and Yarwood, G.: The mechanisms of atmospheric oxidation of the alkenes, Oxford University Press, New York, 2000.

Calvert, J. G., Atkinson, R., Becker, K. H., Kamens, R. M., Seinfeld, J. H., Wallington, T. J., and Yarwood, G.: The mechanisms of atmospheric oxidation of aromatic hydrocarbons, Oxford University Press, New York, 2002.

Calvo, A. I., Alves, C., Castro, A., Pont, V., Vicente, A. M., and Fraile, R.: Research on aerosol sources and chemical composition: Past, current and emerging issues, Atmospheric Research, 120, 1-28, 2013.

Camredon, M., Aumont, B., Lee-Taylor, J., and Madronich, S.: The SOA/VOC/NOx system: an explicit model of secondary organic aerosol formation, Atmospheric Chemistry and Physics Discussions, 7, 11223-11256, 2007.

Canagaratna, M., Jayne, J., Jimenez, J., Allan, J., Alfarra, M., Zhang, Q., Onasch, T., Drewnick, F., Coe, H., and Middlebrook, A.: Chemical and microphysical characterization of ambient aerosols with the aerodyne aerosol mass spectrometer, Mass Spectrometry Reviews, 26, 185-222, 2007.

Cappa, C. D., Zhang, X., Loza, C. L., Craven, J. S., Yee, L. D., and Seinfeld, J. H.: Application of the statistical oxidation model (SOM) to secondary organic aerosol formation from photooxidation of C12 alkanes, Atmospheric Chemistry and Physics, 13, 1591-1606, 2013.

Carlton, A., Wiedinmyer, C., and Kroll, J.: A review of secondary organic aerosol (SOA) formation from isoprene, Atmospheric Chemistry and Physics, 9, 4987-5005, 2009.

Carr, P. W., Li, J., Dallas, A. J., Eikens, D. I., and Tan, L. C.: Revisionist look at solvophobic driving forces in reversed-phase liquid chromatography, Journal of Chromatography A, 656, 113-133, 1993.

Carr, P. W., Tan, L. C., and Park, J. H.: Revisionist look at solvophobic driving forces in reversed-phase liquid chromatography III. Comparison of the behavior of nonpolar and polar solutes, Journal of Chromatography A, 724, 1-12, 1996.

Carter, W., Atkinson, R., Winer, A., and Pitts, J.: Evidence for chamber-dependent radical sources: Impact on kinetic computer models for air pollution, International Journal of Chemical Kinetics, 13, 735-740, 1981.

Carter, W., Atkinson, R., Winer, A., and Pitts, J.: Experimental investigation of chamber-dependent radical sources, International Journal of Chemical Kinetics, 14, 1071-1103, 1982.

Cech, N. B., and Enke, C. G.: Practical implications of some recent studies in electrospray ionization fundamentals, Mass Spectrometry Reviews, 20, 362-387, 2001.

Chacon-Madrid, H. J., and Donahue, N. M.: Fragmentation vs. functionalization: chemical aging and organic aerosol formation, Atmospheric Chemistry and Physics, 11, 10553-10563, 2011.

Chacon-Madrid, H. J., Henry, K. M., and Donahue, N. M.: Photo-oxidation of pinonaldehyde at low NOx: from chemistry to organic aerosol formation, Atmospheric Chemistry and Physics, 13, 3227-3236, 2013.

Chan, A. W. H., Kautzman, K. E., Chhabra, P. S., Surratt, J. D., Chan, M. N., Crounse, J. D., Kurten, A., Wennberg, P. O., Flagan, R. C., and Seinfeld, J. H.: Secondary organic aerosol formation from photooxidation of naphthalene and alkylnaphthalenes: implications for oxidation of intermediate volatility organic compounds (IVOCs), Atmospheric Chemistry and Physics, 9, 3049-3060, 2009.

Chen, J., Wenger, J. C., and Venables, D. S.: Near-ultraviolet absorption cross sections of nitrophenols and their potential influence on tropospheric oxidation capacity, The Journal of Physical Chemistry A, 115, 12235-12242, 2011.

Chen, P. C., Lo, W., and Tzeng, S. C.: Molecular structures of mononitrophenols and their thermal decomposition tautomers, Journal of Molecular Structure, 428, 257-266, 1998.

Chen, P. C., and Chen, S. C.: Theoretical study of the internal rotational barriers in nitrobenzene, 2-nitrotoluene, 2-nitrophenol, and 2-nitroaniline, International Journal of Quantum Chemistry, 83, 332-337, 2001.

Chirico, R., DeCarlo, P. F., Heringa, M. F., Tritscher, T., Richter, R., Prévôt, A. S. H., Dommen, J., Weingartner, E., Wehrle, G., and Gysel, M.: Impact of aftertreatment devices on primary emissions and secondary organic aerosol formation potential from in-use diesel vehicles: results from smog chamber experiments, Atmospheric Chemistry and Physics, 10, 11545-11563, 2010.

Ciccioli, P., Brancaleoni, E., Frattoni, M., Cecinato, A., and Pinciarelli, L.: Determination of volatile organic compounds (VOC) emitted from biomass burning of mediterranean vegetation species by GC-MS, Analytical Letters, 34, 937-955, 2001.

Claeys, M., Wang, W., Ion, A. C., Kourtchev, I., Gelencsér, A., and Maenhaut, W.: Formation of secondary organic aerosols from isoprene and its gas-phase oxidation products through reaction with hydrogen peroxide, Atmospheric Environment, 38, 4093-4098, 2004.

Cocker, D. R., Flagan, R. C., and Seinfeld, J. H.: State-of-the-art chamber facility for studying atmospheric aerosol chemistry, Environmental Science and Technology, 35, 2594-2601, 2001.

Crump, J. G., and Seinfeld, J. H.: Turbulent deposition and gravitational sedimentation of an aerosol in a vessel of arbitrary shape, Journal of Aerosol Science, 12, 405-415, 1981.

Crutzen, P. J.: The role of NO and NO2 in the chemistry of the troposphere and stratosphere, Annual Review of Earth and Planetary Sciences, 7, 443-472, 1979.

Cubbon, S., Bradbury, T., Wilson, J., and Thomas-Oates, J.: Hydrophilic interaction chromatography for mass spectrometric metabonomic studies of urine, Analytical Chemistry, 79, 8911-8918, 2007.

Curiale, J. A., and Gibling, M. R.: Productivity control on oil shale formation - Mae Sot Basin, Thailand, Organic Geochemistry, 21, 67-89, 1994.

Cvetanovic, R.: Chemical kinetic studies of atmospheric interest, 12th International Symposium on Free Radicals, 4-9 January, Laguna Beach, CA, 1976,

de Hoffmann, E., and Stroobant, V.: Mass spectrometry: Principles and applications, 3rd edition ed., John Wiley and Sons, Chichester, England, 502 pp., 2007.

De Vincenzi, M., Silano, M., Maialetti, F., and Scazzocchio, B.: Constituents of aromatic plants: II. Estragole, Fitoterapia, 71, 725-729, 2000.

DeCarlo, P. F., Kimmel, J. R., Trimborn, A., Northway, M. J., Jayne, J. T., Aiken, A. C., Gonin, M., Fuhrer, K., Horvath, T., and Docherty, K. S.: Field-deployable, high-resolution, time-of-flight aerosol mass spectrometer, Analytical Chemistry, 78, 8281-8289, 2006.

DeMore, W. B., Sander, S. P., Golden, D. M., Hampson, R. F., Kurylo, M. J., Howard, C. J., Ravishankara, A. R., Kolb, C. E., and Molina, M. J.: Chemical kinetics and photochemical data for use in stratospheric modeling, evaluation no. 12, NASA Panel for Data Evaluation, Pasadena, CA, January 15, 1997.

Derwent, R., Jenkin, M., Passant, N., and Pilling, M.: Reactivity-based strategies for photochemical ozone control in Europe, Environmental Science and Policy, 10, 445-453, 2007.

Donahue, N., Robinson, A., Stanier, C., and Pandis, S.: Coupled partitioning, dilution, and chemical aging of semivolatile organics, Environmental Science and Technology, 40, 2635-2643, 2006.

Donahue, N., Epstein, S., Pandis, S., and Robinson, A.: A two-dimensional volatility basis set: 1. organic-aerosol mixing thermodynamics, Atmospheric Chemistry and Physics, 11, 3303-3318, 2011a.

Donahue, N., Kroll, J., Pandis, S., and Robinson, A.: A two-dimensional volatility basis set–Part 2: Diagnostics of organic-aerosol evolution, Atmospheric Chemistry and Physics, 12, 615-634, 2012.

Donahue, N., Ortega, I., Chuang, W., Riipinen, I., Riccobono, F., Schobesberger, S., Dommen, J., Baltensperger, U., Kulmala, M., Worsnop, D., and Vehkamaki, H.: How do organic vapors contribute to new-particle formation?, Faraday Discussions, 165, 91 -104, 2013.

Donahue, N. M., Kroll, J. H., Anderson, J. G., and Demerjian, K. L.: Direct observation of OH production from the ozonolysis of olefins, Geophysical Research Letters, 25, 59-62, 1998.

Donahue, N. M., Robinson, A. L., and Pandis, S. N.: Atmospheric organic particulate matter: From smoke to secondary organic aerosol, Atmospheric Environment, 43, 94-106, 2009.

Donahue, N. M., Trump, E. R., Pierce, J. R., and Riipinen, I.: Theoretical constraints on pure vapor-pressure driven condensation of organics to ultrafine particles, Geophysical Research Letters, 38, L16801, 2011b.

Dorsey, J. G., and Dill, K. A.: The molecular mechanism of retention in reversed-phase liquid chromatography, Chemical Reviews, 89, 331-346, 1989.

Eddingsaas, N. C., Loza, C. L., Yee, L. D., Chan, M., Schilling, K. A., Chhabra, P. S., Seinfeld, J. H., and Wennberg, P. O.: Alpha-pinene photooxidation under controlled chemical conditions - Part 2: SOA yield and composition in low- and high-NOx environments, Atmospheric Chemistry and Physics, 12, 7413-7427, 2012.

Ehn, M., Thornton, J. A., Kleist, E., Sipila, M., Junninen, H., Pullinen, I., Springer, M., Rubach, F., Tillmann, R., Lee, B., Lopez-Hilfiker, F., Andres, S., Acir, I.-H., Rissanen, M.,

Jokinen, T., Schobesberger, S., Kangasluoma, J., Kontkanen, J., Nieminen, T., Kurten, T., Nielsen, L. B., Jorgensen, S., Kjaergaard, H. G., Canagaratna, M., Maso, M. D., Berndt, T., Petaja, T., Wahner, A., Kerminen, V.-M., Kulmala, M., Worsnop, D. R., Wildt, J., and Mentel, T. F.: A large source of low-volatility secondary organic aerosol, Nature, 506, 476-479, 2014.

Ellis, A. M., and Mayhew, C. A.: Proton transfer reaction mass spectrometry: Principles and applications, John Wiley and Sons, West Sussex, UK, 2013.

Food and Agriculture Organization of the United Nations http://faostat3.fao.org/faostat-gateway/, access: 08/11/2013, 2012.

Fenn, J. B.: Ion formation from charged droplets: roles of geometry, energy, and time, Journal of the American Society for Mass Spectrometry, 4, 524-535, 1993.

Fernández-Maestre, R., Wu, C., and Hill, H. H.: Buffer gas modifiers effect resolution in ion mobility spectrometry through selective ion-molecule clustering reactions, Rapid Communications in Mass Spectrometry, 26, 2211-2223, 2012.

Finlayson-Pitts, B. J., and Pitts, J. N.: Chemistry of the upper and lower atmosphere: Theory, experiments, and applications, Academic Press, London, UK, 994 pp., 2000.

Fitzherbert, E. B., Struebig, M. J., Morel, A., Danielsen, F., Brühl, C. A., Donald, P. F., and Phalan, B.: How will oil palm expansion affect biodiversity?, Trends in Ecology and Evolution, 23, 538-545, 2008.

Forstner, H. J., Flagan, R. C., and Seinfeld, J. H.: Secondary organic aerosol from the photooxidation of aromatic hydrocarbons: Molecular composition, Environmental Science and Technology, 31, 1345-1358, 1997.

Fu, X., Zhang, Y., Shi, S., Gao, F., Wen, D., Li, W., Liao, Y., and Liu, H.: Fragmentation study of hexanitrostilbene by ion trap multiple mass spectrometry and analysis by liquid chromatography/mass spectrometry, Rapid Communications in Mass Spectrometry, 20, 2906-2914, 2006.

Fuchs, H., Bohn, B., Hofzumahaus, A., Holland, F., Lu, K. D., Nehr, S., Rohrer, F., and Wahner, A.: Detection of HO2 by laser-induced fluorescence: calibration and interferences from RO2 radicals, Atmospheric Measurement Techniques, 4, 1209-1225, 2011.

Gai, Y., Wang, W., Ge, M., Kjaergaard, H. G., Jørgensen, S., and Du, L.: Methyl chavicol reactions with ozone, OH and NO3 radicals: Rate constants and gas-phase products, Atmospheric Environment, 77, 696-702, 2013.

Galloway, M. M., Loza, C. L., Chhabra, P. S., Chan, A. W. H., Yee, L. D., Seinfeld, J. H., and Keutsch, F. N.: Analysis of photochemical and dark glyoxal uptake: Implications for SOA formation, Geophysical Research Letters, 38, L17811, 2011.

Gao, S., Keywood, M., Ng, N. L., Surratt, J., Varutbangkul, V., Bahreini, R., Flagan, R. C., and Seinfeld, J. H.: Low-molecular-weight and oligomeric components in secondary organic aerosol from the ozonolysis of cycloalkenes and α-pinene, Journal of Physical Chemistry A, 108, 10147-10164, 2004a.

Gao, S., Ng, N. L., Keywood, M., Varutbangkul, V., Bahreini, R., Nenes, A., He, J., Yoo, K. Y., Beauchamp, J. L., Hodyss, R. P., Flagan, R. C., and Seinfeld, J. H.: Particle phase acidity and oligomer formation in secondary organic aerosol, Environmental Science and Technology, 38, 6582-6589, 2004b.

Gao, Y., Hall, W. A., and Johnston, M. V.: Molecular composition of monoterpene secondary organic aerosol at low mass loading, Environmental Science and Technology, 44, 7897-7902, 2010.

Gentner, D. R., Isaacman, G., Worton, D. R., Chan, A. W. H., Dallmann, T. R., Davis, L., Liu, S., Day, D. A., Russell, L. M., Wilson, K. R., Weber, R., Guha, A., Harley, R. A., and Goldstein, A. H.: Elucidating secondary organic aerosol from diesel and gasoline vehicles through detailed characterization of organic carbon emissions, Proceedings of the National Academy of Sciences, 109, 18318-18323, 2012.

George, I., and Abbatt, J.: Chemical evolution of secondary organic aerosol from OH-initiated heterogeneous oxidation, Atmospheric Chemistry and Physics, 10, 5551-5563, 2010.

Geyer, A., Bächmann, K., Hofzumahaus, A., Holland, F., Konrad, S., Klüpfel, T., Pätz, H.-W., Perner, D., Mihelcic, D., Schäfer, H.-J., Volz-Thomas, A., and Platt, U.: Nighttime formation of peroxy and hydroxyl radicals during the BERLIOZ campaign: Observations and modeling studies, Journal of Geophysical Research: Atmospheres, 108, 8249, 2003.

Giavalisco, P., Hummel, J., Lisec, J., Inostroza, A. C., Catchpole, G., and Willmitzer, L.: High-resolution direct infusion-based mass spectrometry in combination with whole 13C metabolome isotope labeling allows unambiguous assignment of chemical sum formulas, Analytical Chemistry, 80, 9417-9425, 2008.

Goldstein, A. H., and Galbally, I. E.: Known and unexplored organic constituents in the earth's atmosphere, Environmental Science and Technology, 41, 1514-1521, 2007.

Gómez-González, Y., Surratt, J. D., Cuyckens, F., Szmigielski, R., Vermeylen, R., Jaoui, M., Lewandowski, M., Offenberg, J. H., Kleindienst, T. E., Edney, E. O., Blockhuys, F., Van Alsenoy, C., Maenhaut, W., and Claeys, M.: Characterization of organosulfates from the photooxidation of isoprene and unsaturated fatty acids in ambient aerosol using liquid chromatography/(−) electrospray ionization mass spectrometry, Journal of Mass Spectrometry, 43, 371-382, 2008.

Gómez Alvarez, E., Borrás, E., Viidanoja, J., and Hjorth, J.: Unsaturated dicarbonyl products from the OH-initiated photo-oxidation of furan, 2-methylfuran and 3-methylfuran, Atmospheric Environment, 43, 1603-1612, 2009.

Gordon, E. F., and Muddiman, D. C.: Impact of ion cloud densities on the measurement of relative ion abundances in Fourier transform ion cyclotron resonance mass spectrometry: experimental observations of coulombically induced cyclotron radius perturbations and ion cloud dephasing rates, Journal of Mass Spectrometry, 36, 195-203, 2001.

Gordon, T. D., Presto, A. A., Nguyen, N. T., Robertson, W. H., Na, K., Sahay, K. N., Zhang, M., Maddox, C., Rieger, P., Chattopadhyay, S., Maldonado, H., Maricq, M. M., and Robinson, A. L.: Secondary organic aerosol production from diesel vehicle exhaust: impact of aftertreatment, fuel chemistry and driving cycle, Atmospheric Chemistry and Physics, 14, 4643-4659, 2014.

Graedel, T. E., Hawkins, D. T., and Claxton, L. D.: Atmospheric chemical compounds: sources, occurrence and bioassay, Academic Press, London, England, 478 pp., 1986.

Grigsby, R. D., and Green, J. B.: High-resolution mass spectrometric analysis of a vanadyl porphyrin fraction isolated from the >700 °C resid of cerro negro heavy petroleum, Energy and Fuels, 11, 602-609, 1997.

Gritti, F., and Guiochon, G.: Influence of the pressure on the properties of chromatographic columns: I. Measurement of the compressibility of methanol-water mixtures on a mesoporous silica adsorbent, Journal of Chromatography A, 1070, 1-12, 2005.

Guenther, A., Hewitt, C. N., Erickson, D., Fall, R., Geron, C., Graedel, T., Harley, P., Klinger, L., Lerdau, M., and McKay, W.: A global model of natural volatile organic compound emissions, Journal of Geophysical Research, 100, 8873-8892, 1995.

Guenther, A., Geron, C., Pierce, T., Lamb, B., Harley, P., and Fall, R.: Natural emissions of non-methane volatile organic compounds, carbon monoxide, and oxides of nitrogen from North America, Atmospheric Environment, 34, 2205-2230, 2000.

Guo, Y., and Gaiki, S.: Retention behavior of small polar compounds on polar stationary phases in hydrophilic interaction chromatography, Journal of Chromatography A, 1074, 71-80, 2005.

Guo, Y., and Gaiki, S.: Retention and selectivity of stationary phases for hydrophilic interaction chromatography, Journal of Chromatography A, 1218, 5920-5938, 2011.

Hall, W. A., and Johnston, M. V.: Oligomer content of α-pinene secondary organic aerosol, Aerosol Science and Technology, 45, 37-45, 2011.

Hall, W. A., and Johnston, M. V.: Oligomer formation pathways in secondary organic aerosol from MS and MS/MS measurements with high mass accuracy and resolving power, Journal of the American Society for Mass Spectrometry, 23, 1097-1108, 2012.

Hallquist, M., Wenger, J. C., Baltensperger, U., Rudich, Y., Simpson, D., Claeys, M., Dommen, J., Donahue, N. M., George, C., Goldstein, A. H., Hamilton, J. F., Herrmann, H., Hoffmann, T., Iinuma, Y., Jang, M., Jenkin, M. E., Jimenez, J. L., Kiendler-Scharr, A., Maenhaut, W., McFiggans, G., Mentel, T. F., Monod, A., Prévôt, A. S. H., Seinfeld, J. H., Surratt, J. D., Szmigielski, R., and J., W.: The formation, properties and impact of secondary organic aerosol: current and emerging issues, Atmospheric Chemistry and Physics, 9, 5155-5236, 2009.

Hamilton, J., Webb, P., Lewis, A., Hopkins, J., Smith, S., and Davy, P.: Partially oxidised organic components in urban aerosol using GCXGC-TOF/MS, Atmospheric Chemistry and Physics, 4, 1279-1290, 2004.

Hamilton, J. F., Webb, P. J., Lewis, A. C., and Reviejo, M. M.: Quantifying small molecules in secondary organic aerosol formed during the photo-oxidation of toluene with hydroxyl radicals, Atmospheric Environment, 39, 7263-7275, 2005.

Hamilton, J. F.: Using comprehensive two-dimensional gas chromatography to study the atmosphere, Journal of Chromatographic Science, 48, 274-282, 2010.

Hamilton, J. F., Alfarra, M. R., Wyche, K. P., Ward, M. W., Lewis, A. C., McFiggans, G. B., Good, N., Monks, P. S., Carr, T., White, I. R., and Purvis, R. M.: Investigating the use of secondary organic aerosol as seed particles in simulation chamber experiments, Atmospheric Chemistry and Physics, 11, 5917-5929, 2011.

Hamilton, J. F., Alfarra, M. R., Robinson, N., Ward, M. W., Lewis, A. C., McFiggans, G. B., Coe, H., and Allan, J. D.: Linking biogenic hydrocarbons to biogenic aerosol in the Borneo rainforest, Atmospheric Chemistry and Physics, 13, 11295-11305, 2013.

Hang, W., Lewis, C., and Majidi, V.: Practical considerations when using radio frequency-only quadrupole ion guide for atmospheric pressure ionization sources with time-of-flight mass spectrometry, Analyst, 128, 273-280, 2003.

Hao, Z., Xiao, B., and Weng, N.: Impact of column temperature and mobile phase components on selectivity of hydrophilic interaction chromatography (HILIC), Journal of Separation Science, 31, 1449-1464, 2008.

Harrison, R. M.: Pollution: causes, effects and control, Royal Society of Chemistry, Cambridge, UK, 562 pp., 2001.

Hatakeyama, S., Izumi, K., Fukuyama, T., Akimoto, H., and Washida, N.: Reactions of OH with α-pinene and β-pinene in air: Estimate of global CO production from the atmospheric oxidation of terpenes, Journal of Geophysical Research: Atmospheres, 96, 947-958, 1991.

Hayen, H., Jachmann, N., Vogel, M., and Karst, U.: LC-Electron capture APCI-MS for the determination of nitroaromatic compounds, Analyst, 127, 1027-1030, 2002.

Heald, C., Kroll, J., Jimenez, J., Docherty, K., DeCarlo, P., Aiken, A., Chen, Q., Martin, S., Farmer, D., and Artaxo, P.: A simplified description of the evolution of organic aerosol composition in the atmosphere, Geophysical Research Letters, 37, L08803, 2010.

Heald, C. L., Jacob, D. J., Park, R. J., Russell, L. M., Huebert, B. J., Seinfeld, J. H., Liao, H., and Weber, R. J.: A large organic aerosol source in the free troposphere missing from current models, Geophysical Research Letters, 32, L18807, 2005.

Heald, C. L., Coe, H., Jimenez, J. L., Weber, R. J., Bahreini, R., Middlebrook, A. M., Russell, L. M., Jolleys, M., Fu, T. M., Allan, J. D., Bower, K. N., Capes, G., Crosier, J., Morgan, W. T., Robinson, N. H., Williams, P. I., Cubison, M. J., DeCarlo, P. F., and Dunlea, E. J.: Exploring the vertical profile of atmospheric organic aerosol: comparing 17 aircraft field campaigns with a global model, Atmospheric Chemistry and Physics, 11, 12673-12696, 2011.

Healy, R. M., Temime, B., Kuprovskyte, K., and Wenger, J. C.: Effect of relative humidity on gas/particle partitioning and aerosol mass yield in the photooxidation of p-xylene, Environmental Science and Technology, 43, 1884-1889, 2009.

Hearn, J. D., Renbaum, L. H., Wang, X., and Smith, G. D.: Kinetics and products from reaction of Cl radicals with dioctyl sebacate (DOS) particles in O2: a model for radical-initiated oxidation of organic aerosols, Physical Chemistry Chemical Physics, 9, 4803-4813, 2007.

Hemström, P., and Irgum, K.: Hydrophilic interaction chromatography, Journal of Separation Science, 29, 1784-1821, 2006.

Hewitt, C. N., Hayward, S., and Tani, A.: The application of proton transfer reaction-mass spectrometry (PTR-MS) to the monitoring and analysis of volatile organic compounds in the atmosphere, Journal of Environmental Monitoring, 5, 1-7, 2003.

Hewitt, C. N., MacKenzie, A. R., Di Carlo, P., Di Marco, C. F., Dorsey, J. R., Evans, M., Fowler, D., Gallagher, M. W., Hopkins, J. R., Jones, C. E., Langford, B., Lee, J. D., Lewis, A. C., Lim, S. F., McQuaid, J., Misztal, P., Moller, S. J., Monks, P. S., Nemitz, E., Oram, D. E., Owen, S. M., Phillips, G. J., Pugh, T. A. M., Pyle, J. A., Reeves, C. E., Ryder, J., Siong, J., Skiba, U., and Stewart, D. J.: Nitrogen management is essential to prevent tropical oil palm plantations from causing ground-level ozone pollution, Proceedings of the National Academy of Sciences, 106, 18447-18451, 2009.

Hildebrandt, L., Henry, K. M., Kroll, J. H., Worsnop, D. R., Pandis, S. N., and Donahue, N. M.: Evaluating the mixing of organic aerosol components using high-resolution aerosol mass spectrometry, Environmental Science and Technology, 45, 6329-6335, 2011.

Ho, C., Lam, C., Chan, M., Cheung, R., Law, L., Lit, L., Ng, K., Suen, M., and Tai, H.: Electrospray ionisation mass spectrometry: principles and clinical applications, The Clinical Biochemist Reviews, 24, 3, 2003.

Hodzic, A., Jimenez, J., Madronich, S., Canagaratna, M., DeCarlo, P., Kleinman, L., and Fast, J.: Modeling organic aerosols in a megacity: potential contribution of semi-volatile and intermediate volatility primary organic compounds to secondary organic aerosol formation, Atmospheric Chemistry and Physics, 10, 5491-5514, 2010.

Holčapek, M., Lísa, M., Volná, K., Almonasy, N., and Přikryl, J.: Occurrence of radical molecular ions in atmospheric pressure chemical ionization mass spectra of heterocyclic compounds, Journal of Mass Spectrometry, 42, 1645-1648, 2007.

Holčapek, M., Jirásko, R., and Lísa, M.: Basic rules for the interpretation of atmospheric pressure ionization mass spectra of small molecules, Journal of Chromatography A, 1217, 3908-3921, 2010.

Holzinger, R., Lee, A., Paw, K., and Goldstein, U.: Observations of oxidation products above a forest imply biogenic emissions of very reactive compounds, Atmospheric Chemistry and Physics, 5, 67-75, 2005.

Holzinger, R., Kasper-Giebl, A., Staudinger, M., Schauer, G., and Röckmann, T.: Analysis of the chemical composition of organic aerosol at the Mt. Sonnblick observatory using a

novel high mass resolution thermal-desorption proton-transfer-reaction mass-spectrometer (hr-TD-PTR-MS), Atmospheric Chemistry and Physics, 10, 10111-10128, 2010.

Howard, G., and Martin, A.: The separation of the C12-C18 fatty acids by reversed-phase partition chromatography, Biochemical Journal, 46, 532, 1950.

Howard, J. A., and Ingold, K. U.: Self-reaction of sec-butylperoxy radicals. Confirmation of the Russell mechanism, Journal of the American Chemical Society, 90, 1056-1058, 1968.

Hu, D., Tolocka, M., Li, Q., and Kamens, R. M.: A kinetic mechanism for predicting secondary organic aerosol formation from toluene oxidation in the presence of NOx and natural sunlight, Atmospheric Environment, 41, 6478-6496, 2007.

Huang, M., Hao, L., Gu, X., Hu, C., Zhao, W., Wang, Z., Fang, L., and Zhang, W.: Effects of inorganic seed aerosols on the growth and chemical composition of secondary organic aerosol formed from OH-initiated oxidation of toluene, Journal of Atmospheric Chemistry, 70, 151-164, 2013.

Hughey, C. A., Hendrickson, C. L., Rodgers, R. P., Marshall, A. G., and Qian, K.: Kendrick mass defect spectrum: a compact visual analysis for ultrahigh-resolution broadband mass spectra, Analytical Chemistry, 73, 4676-4681, 2001.

Hurley, M. D., Sokolov, O., Wallington, T. J., Takekawa, H., Karasawa, M., Klotz, B., Barnes, I., and Becker, K. H.: Organic aerosol formation during the atmospheric degradation of toluene, Environmental Science and Technology, 35, 1358-1366, 2001.

Iinuma, Y., Böge, O., Gnauk, T., and Herrmann, H.: Aerosol-chamber study of the α - pinene/O3 reaction: Influence of particle acidity on aerosol yields and products, Atmospheric Environment, 38, 761-773, 2004.

Iinuma, Y., Muller, C., Berndt, T., Boge, O., Claeys, M., and Herrmann, H.: Evidence for the existence of organosulfates from beta-pinene ozonolysis in ambient secondary organic aerosol, Environmental Science and Technology, 41, 6678-6683, 2007.

Iinuma, Y., Böge, O., Keywood, M., Gnauk, T., and Herrmann, H.: Diaterebic acid acetate and diaterpenylic acid acetate: atmospheric tracers for secondary organic aerosol formation from 1,8-cineole oxidation, Environmental Science and Technology, 43, 280-285, 2008.

Jakober, C. A., Charles, M. J., Kleeman, M. J., and Green, P. G.: LC-MS analysis of carbonyl compounds and their occurrence in diesel emissions, Analytical Chemistry, 78, 5086-5093, 2006.

Jandera, P.: Stationary and mobile phases in hydrophilic interaction chromatography: a review, Analytica Chimica Acta, 692, 1-25, 2011.

Jang, M., and Kamens, R. M.: Characterization of secondary aerosol from the photooxidation of toluene in the presence of NOx and 1-propene, Environmental Science and Technology, 35, 3626-3639, 2001.

Jang, M., Czoschke, N. M., Lee, S., and Kamens, R. M.: Heterogeneous Atmospheric Aerosol Production by Acid-Catalyzed Particle-Phase Reactions, Science, 298, 814-817, 2002.

Jathar, S. H., Miracolo, M. A., Tkacik, D. S., Donahue, N. M., Adams, P. J., and Robinson, A. L.: Secondary organic aerosol formation from photo-oxidation of unburned fuel: Experimental results and implications for aerosol formation from combustion emissions, Environmental Science and Technology, 47, 12886-12893, 2013.

Jathar, S. H., Donahue, N. M., Adams, P. J., and Robinson, A. L.: Testing secondary organic aerosol models using smog chamber data for complex precursor mixtures: influence of precursor volatility and molecular structure, Atmospheric Chemistry and Physics, 14, 5771-5780, 2014.

Jenkin, M. E., Saunders, S. M., and Pilling, M. J.: The tropospheric degradation of volatile organic compounds: A protocol for mechanism development, Atmospheric Environment, 31, 81-104, 1997.

Jimenez, J. L., Jayne, J. T., Shi, Q., Kolb, C. E., Worsnop, D. R., Yourshaw, I., Seinfeld, J. H., Flagan, R. C., Zhang, X., Smith, K. A., Morris, J. W., and Davidovits, P.: Ambient aerosol sampling using the Aerodyne Aerosol Mass Spectrometer, Journal of Geophysical Research: Atmospheres, 108, 8425, 2003.

Jimenez, J. L., Canagaratna, M. R., Donahue, N. M., Prevot, A. S. H., Zhang, Q., Kroll, J. H., DeCarlo, P. F., Allan, J. D., Coe, H., Ng, N. L., Aiken, A. C., Docherty, K. S., Ulbrich, I. M., Grieshop, A. P., Robinson, A. L., Duplissy, J., Smith, J. D., Wilson, K. R., Lanz, V. A., Hueglin, C., Sun, Y. L., Tian, J., Laaksonen, A., Raatikainen, T., Rautiainen, J., Vaattovaara, P., Ehn, M., Kulmala, M., Tomlinson, J. M., Collins, D. R., Cubison, M. J., E., Dunlea, J., Huffman, J. A., Onasch, T. B., Alfarra, M. R., Williams, P. I., Bower, K., Kondo, Y., Schneider, J., Drewnick, F., Borrmann, S., Weimer, S., Demerjian, K., Salcedo, D., Cottrell, L., Griffin, R., Takami, A., Miyoshi, T., Hatakeyama, S., Shimono, A., Sun, J. Y., Zhang, Y. M., Dzepina, K., Kimmel, J. R., Sueper, D., Jayne, J. T., Herndon, S. C., Trimborn, A. M., Williams, L. R., Wood, E. C., Middlebrook, A. M., Kolb, C. E.,

Baltensperger, U., and Worsnop, D. R.: Evolution of organic aerosols in the atmosphere, Science, 326, 1525-1529, 2009.

Johnson, D., Jenkin, M. E., Wirtz, K., and Martin-Reviejo, M.: Simulating the formation of secondary organic aerosol from the photooxidation of toluene, Environmental Chemistry, 1, 150-165, 2004.

Kalberer, M., Paulsen, D., Sax, M., Steinbacher, M., Dommen, J., Prevot, A., Fisseha, R., Weingartner, E., Frankevich, V., and Zenobi, R.: Identification of polymers as major components of atmospheric organic aerosols, Science, 303, 1659-1662, 2004.

Kallio, M., Jussila, M., Rissanen, T., Anttila, P., Hartonen, K., Reissell, A., Vreuls, R., Adahchour, M., and Hyötyläinen, T.: Comprehensive two-dimensional gas chromatography coupled to time-of-flight mass spectrometry in the identification of organic compounds in atmospheric aerosols from coniferous forest, Journal of Chromatography A, 1125, 234-243, 2006.

Kampf, C. J., Bonn, B., and Hoffmann, T.: Development and validation of a selective HPLC-ESI-MS/MS method for the quantification of glyoxal and methylglyoxal in atmospheric aerosols (PM2.5), Analytical and Bioanalytical Chemistry, 401, 3115-3124, 2011.

Kanakidou, M., Seinfeld, J., Pandis, S., Barnes, I., Dentener, F., Facchini, M., Van Dingenen, R., Ervens, B., Nenes, A., and Nielsen, C.: Organic aerosol and global climate modelling: a review, Atmospheric Chemistry and Physics, 5, 1053-1123, 2005.

Kanawati, B., Herrmann, F., Joniec, S., Winterhalter, R., and Moortgat, G. K.: Mass spectrometric characterization of beta-caryophyllene ozonolysis products in the aerosol studied using an electrospray triple quadrupole and time-of-flight analyzer hybrid system and density functional theory, Rapid Communications in Mass Spectrometry, 22, 165-186, 2008.

Kappos, A. D., Bruckmann, P., Eikmann, T., Englert, N., Heinrich, U., Höppe, P., Koch, E., Krause, G. H. M., Kreyling, W. G., Rauchfuss, K., Rombout, P., Schulz-Klemp, V., Thiel, W. R., and Wichmann, H. E.: Health effects of particles in ambient air, International Journal of Hygiene and Environmental Health, 207, 399-407, 2004.

Kebarle, P., and Verkerk, U. H.: Electrospray: From ions in solution to ions in the gas phase, what we know now, Mass Spectrometry Reviews, 28, 898-917, 2009.

Keil, A., and Haywood, J. M.: Solar radiative forcing by biomass burning aerosol particles during SAFARI 2000: A case study based on measured aerosol and cloud properties, Journal of Geophysical Research, 108, 8467, 2003.

Kelleher, N. L.: Peer reviewed: top-down proteomics, Analytical Chemistry, 76, 196 A-203 A, 2004.

Kendrick, E.: A Mass Scale Based on CH_2= 14.0000 for High Resolution Mass Spectrometry of Organic Compounds, Analytical Chemistry, 35, 2146-2154, 1963.

Khan, M. A. H., Hoque, M. M. N., Alam, S. S., Ashfold, M. J., Nickless, G., and Shallcross, D. E.: Estimation and comparison of night-time OH levels in the UK urban atmosphere using two different analysis methods, Journal of Environmental Sciences, 23, 60-64, 2011.

Kido Soule, M. C., Longnecker, K., Giovannoni, S. J., and Kujawinski, E. B.: Impact of instrument and experiment parameters on reproducibility of ultrahigh resolution ESI FT-ICR mass spectra of natural organic matter, Organic Geochemistry, 41, 725-733, 2010.

Kind, T., and Fiehn, O.: Metabolomic database annotations via query of elemental compositions: mass accuracy is insufficient even at less than 1 ppm, BMC Bioinformatics, 7, 234, 2006.

Kirkby, J., Curtius, J., Almeida, J., Dunne, E., Duplissy, J., Ehrhart, S., Franchin, A., Gagne, S., Ickes, L., Kurten, A., Kupc, A., Metzger, A., Riccobono, F., Rondo, L., Schobesberger, S., Tsagkogeorgas, G., Wimmer, D., Amorim, A., Bianchi, F., Breitenlechner, M., David, A., Dommen, J., Downard, A., Ehn, M., Flagan, R. C., Haider, S., Hansel, A., Hauser, D., Jud, W., Junninen, H., Kreissl, F., Kvashin, A., Laaksonen, A., Lehtipalo, K., Lima, J., Lovejoy, E. R., Makhmutov, V., Mathot, S., Mikkila, J., Minginette, P., Mogo, S., Nieminen, T., Onnela, A., Pereira, P., Petaja, T., Schnitzhofer, R., Seinfeld, J. H., Sipila, M., Stozhkov, Y., Stratmann, F., Tome, A., Vanhanen, J., Viisanen, Y., Vrtala, A., Wagner, P. E., Walther, H., Weingartner, E., Wex, H., Winkler, P. M., Carslaw, K. S., Worsnop, D. R., Baltensperger, U., and Kulmala, M.: Role of sulphuric acid, ammonia and galactic cosmic rays in atmospheric aerosol nucleation, Nature, 476, 429-433, 2011.

Kirkland, J. R., Lim, Y. B., Tan, Y., Altieri, K. E., and Turpin, B. J.: Glyoxal secondary organic aerosol chemistry: effects of dilute nitrate and ammonium and support for organic radical–radical oligomer formation, Environmental Chemistry, 10, 158-166, 2013.

Kitanovski, Z., Grgic, I., and Veber, M.: Characterization of carboxylic acids in atmospheric aerosols using hydrophilic interaction liquid chromatography tandem mass spectrometry, Journal of Chromatography A, 1218, 4417-4425, 2011.

Kitanovski, Z., Grgic, I., Vermeylen, R., Claeys, M., and Maenhaut, W.: Liquid chromatography tandem mass spectrometry method for characterization of monoaromatic nitro-compounds in atmospheric particulate matter, Journal of Chromatography A, 1268, 35-43, 2012a.

Kitanovski, Z., Grgic, I., Yasmeen, F., Claeys, M., and Cusak, A.: Development of a liquid chromatographic method based on ultraviolet-visible and electrospray ionization mass spectrometric detection for the identification of nitrocatechols and related tracers in biomass burning atmospheric organic aerosol, Rapid Communications in Mass Spectrometry, 26, 793-804, 2012b.

Kleffmann, J.: Daytime sources of nitrous acid (HONO) in the atmospheric boundary layer, Journal of Chemical Physics and Physical Chemistry, 8, 1137-1144, 2007.

Klotz, B., Sørensen, S., Barnes, I., Becker, K. H., Etzkorn, T., Volkamer, R., Platt, U., Wirtz, K., and Martín-Reviejo, M.: Atmospheric oxidation of toluene in a large-volume outdoor photoreactor: In situ determination of ring-retaining product yields, The Journal of Physical Chemistry A, 102, 10289-10299, 1998.

Knowlton, K., Rosenthal, J. E., Hogrefe, C., Lynn, B., Gaffin, S., Goldberg, R., Rosenzweig, C., Civerolo, K., Ku, J.-Y., and Kinney, P. L.: Assessing ozone-related health impacts under a changing climate, Environmental Health Perspectives, 1557-1563, 2004.

Kocadağlı, T., and Gökmen, V.: Investigation of α-dicarbonyl compounds in baby foods by high-performance liquid chromatography coupled with electrospray ionization mass spectrometry, Journal of Agricultural and Food Chemistry, 62, 7714-7720, 2014.

Koch, B. P., and Dittmar, T.: From mass to structure: an aromaticity index for high-resolution mass data of natural organic matter, Rapid Communications in Mass Spectrometry, 20, 926-932, 2006.

Kourtchev, I., Fuller, S. J., Giorio, C., Healy, R. M., Wilson, E., O'Connor, I., Wenger, J. C., McLeod, M., Aalto, J., Ruuskanen, T. M., Maenhaut, W., Jones, R., Venables, D. S., Sodeau, J. R., Kulmala, M., and Kalberer, M.: Molecular composition of biogenic secondary organic aerosols using ultrahigh-resolution mass spectrometry: comparing laboratory and field studies, Atmospheric Chemistry and Physics, 14, 2155-2167, 2014.

Kroll, J. H., Ng, N. L., Murphy, S. M., Flagan, R. C., and Seinfeld, J. H.: Secondary organic aerosol formation from isoprene photooxidation, Environmental Science and Technology, 40, 1869-1877, 2006.

Kroll, J. H., Chan, A. W. H., Ng, N. L., Flagan, R. C., and Seinfeld, J. H.: Reactions of semivolatile organics and their effects on secondary organic aerosol formation, Environmental Science and Technology, 41, 3545-3550, 2007.

Kroll, J. H., and Seinfeld, J. H.: Chemistry of secondary organic aerosol: Formation and evolution of low-volatility organics in the atmosphere, Atmospheric Environment, 42, 3593-3624, 2008.

Kroll, J. H., Donahue, N. M., Jimenez, J. L., Kessler, S. H., Canagaratna, M. R., Wilson, K. R., Altieri, K. E., Mazzoleni, L. R., Wozniak, A. S., Bluhm, H., Mysak, E. R., Smith, J. D., Kolb, C. E., and Worsnop, D. R.: Carbon oxidation state as a metric for describing the chemistry of atmospheric organic aerosol, Nature Chemistry, 3, 133-139, 2011.

Kruve, A., Kaupmees, K., Liigand, J., Oss, M., and Leito, I.: Sodium adduct formation efficiency in ESI source, Journal of Mass Spectrometry, 48, 695-702, 2013.

Kulmala, M.: How particles nucleate and grow, Science, 302, 1000-1001, 2003.

Kulmala, M., Vehkamäki, H., Petäjä, T., Dal Maso, M., Lauri, A., Kerminen, V. M., Birmili, W., and McMurry, P. H.: Formation and growth rates of ultrafine atmospheric particles: a review of observations, Journal of Aerosol Science, 35, 143-176, 2004.

Kulmala, M., Kontkanen, J., Junninen, H., Lehtipalo, K., Manninen, H. E., Nieminen, T., Petäjä, T., Sipilä, M., Schobesberger, S., Rantala, P., Franchin, A., Jokinen, T., Järvinen, E., Äijälä, M., Kangasluoma, J., Hakala, J., Aalto, P. P., Paasonen, P., Mikkilä, J., Vanhanen, J., Aalto, J., Hakola, H., Makkonen, U., Ruuskanen, T., Mauldin, R. L., Duplissy, J., Vehkamäki, H., Bäck, J., Kortelainen, A., Riipinen, I., Kurtén, T., Johnston, M. V., Smith, J. N., Ehn, M., Mentel, T. F., Lehtinen, K. E. J., Laaksonen, A., Kerminen, V.-M., and Worsnop, D. R.: Direct observations of atmospheric aerosol nucleation, Science, 339, 943-946, 2013.

Laitinen, T., Junninen, H., Parshintsev, J., Ruiz-Jimenez, J., Petaja, T., Hautala, S., Hartonen, K., Worsnop, D., Kulmala, M., and Riekkola, M.-L.: Changes in concentration of nitrogen-containing compounds in 10 nm particles of boreal forest atmosphere at snowmelt, Journal of Aerosol Science, 70, 1-10, 2014.

Lammel, G., and Cape, J.: Nitrous acid and nitrite in the atmosphere, Chemical Society Reviews, 25, 361-369, 1996.

Langmann, B., Sellegri, K., and Freney, E.: Secondary organic aerosol formation during June 2010 in central Europe: measurements and modelling studies with a mixed

thermodynamic-kinetic approach, Atmospheric Chemistry and Physics, 14, 3831-3842, 2014.

Lanz, V., Alfarra, M., Baltensperger, U., Buchmann, B., Hueglin, C., and Prévôt, A.: Source apportionment of submicron organic aerosols at an urban site by factor analytical modelling of aerosol mass spectra, Atmospheric Chemistry and Physics, 7, 1503-1522, 2007.

Laskin, A., Smith, J. S., and Laskin, J.: Molecular characterization of nitrogen-containing organic compounds in biomass burning aerosols using high-resolution mass spectrometry, Environmental Science and Technology, 43, 3764-3771, 2009.

Laskin, A., Laskin, J., and Nizkorodov, S. A.: Mass spectrometric approaches for chemical characterisation of atmospheric aerosols: critical review of the most recent advances, Environmental Chemistry, 9, 163-189, 2012.

Laskin, J., Laskin, A., Roach, P. J., Slysz, G. W., Anderson, G. A., Nizkorodov, S. A., Bones, D. L., and Nguyen, L. Q.: High-resolution desorption electrospray ionization mass spectrometry for chemical characterization of organic aerosols, Analytical Chemistry, 82, 2048-2058, 2010.

Lebedev, A.: Comprehensive environmental mass spectrometry, ILM Publications, Herfordshire, UK, 2012.

Ledford, E., Phillips, J., Xu, J., Gaines, R., and Blomberg, J.: Ordered chromatograms: A powerful methodology in gas chromatography, American Laboratory, 28, 22-25, 1996.

Lee, A., Goldstein, A. H., Keywood, M. D., Gao, S., Varutbangkul, V., Bahreini, R., Ng, N. L., Flagan, R. C., and Seinfeld, J. H.: Gas-phase products and secondary aerosol yields from the ozonolysis of ten different terpenes, Journal of Geophysical Research, 111, D07302, 2006a.

Lee, A., Goldstein, A. H., Kroll, J. H., Ng, N. L., Varutbangkul, V., Flagan, R. C., and Seinfeld, J. H.: Gas-phase products and secondary aerosol yields from the photooxidation of 16 different terpenes, Journal of Geophysical Research: Atmospheres, 111, D17305, 2006b.

Lee, J. Y., Lane, D. A., Heo, J. B., Yi, S.-M., and Kim, Y. P.: Quantification and seasonal pattern of atmospheric reaction products of gas phase PAHs in PM2.5, Atmospheric Environment, 55, 17-25, 2012.

Lee, W., Baasandorj, M., Stevens, P. S., and Hites, R. A.: Monitoring OH-initiated oxidation kinetics of isoprene and its products using online mass spectrometry, Environmental Science and Technology, 39, 1030-1036, 2005.

Lewis, I. A., Schommer, S. C., Hodis, B., Robb, K. A., Tonelli, M., Westler, W. M., Sussman, M. R., and Markley, J. L.: Method for determining molar concentrations of metabolites in complex solutions from two-dimensional 1H−13C NMR spectra, Analytical Chemistry, 79, 9385-9390, 2007.

Li, L., Huang, C., Huang, H. Y., Wang, Y. J., Yan, R. S., Zhang, G. F., Zhou, M., Lou, S. R., Tao, S. K., Wang, H. L., Qiao, L. P., Chen, C. H., Streets, D. G., and Fu, J. S.: An integrated process rate analysis of a regional fine particulate matter episode over Yangtze River Delta in 2010, Atmospheric Environment, 91, 60-70, 2014.

Liggio, J., and Mclaren, R.: An optimized method for the determination of volatile and semi-volatile aldehydes and ketones in ambient particulate matter, International Journal of Environmental and Analytical Chemistry, 83, 819-835, 2003.

Lim, H. J., and Turpin, B. J.: Origins of primary and secondary organic aerosol in Atlanta: Results of time-resolved measurements during the Atlanta supersite experiment, Environmental Science and Technology, 36, 4489-4496, 2002.

Limbeck, A., Kulmala, M., and Puxbaum, H.: Secondary organic aerosol formation in the atmosphere via heterogeneous reaction of gaseous isoprene on acidic particles, Geophysical Research Letters, 30, 1996, 2003.

Liu, S., Ahlm, L., Day, D. A., Russell, L. M., Zhao, Y., Gentner, D. R., Weber, R. J., Goldstein, A. H., Jaoui, M., and Offenberg, J. H.: Secondary organic aerosol formation from fossil fuel sources contribute majority of summertime organic mass at Bakersfield, Journal of Geophysical Research: Atmospheres, 117, D00V26, 2012.

Logan, J. A.: Tropospheric ozone: Seasonal behavior, trends, and anthropogenic influence, Journal of Geophysical Research: Atmospheres, 90, 10463-10482, 1985.

Loza, C. L., Chan, A. W., Galloway, M. M., Keutsch, F. N., Flagan, R. C., and Seinfeld, J. H.: Characterization of vapor wall loss in laboratory chambers, Environmental Science and Technology, 44, 5074-5078, 2010.

Loza, C. L., Craven, J. S., Yee, L. D., Coggon, M. M., Schwantes, R. H., Shiraiwa, M., Zhang, X., Schilling, K. A., Ng, N. L., Canagaratna, M. R., Ziemann, P. J., Flagan, R. C., and Seinfeld, J. H.: Secondary organic aerosol yields of 12-carbon alkanes, Atmospheric Chemistry and Physics, 14, 1423-1439, 2014.

Lu, Z., Hao, J., Takekawa, H., Hu, L., and Li, J.: Effect of high concentrations of inorganic seed aerosols on secondary organic aerosol formation in the m-xylene/NOx photooxidation system, Atmospheric Environment, 43, 897-904, 2009.

Ma, Y.-C., and Kim, H.-Y.: Determination of steroids by liquid chromatography/mass spectrometry, Journal of the American Society for Mass Spectrometry, 8, 1010-1020, 1997.

Macek, B., Waanders, L. F., Olsen, J. V., and Mann, M.: Top-down protein sequencing and MS3 on a hybrid linear quadrupole ion trap-orbitrap mass spectrometer, Molecular and Cellular Proteomics, 5, 949-958, 2006.

MacKenzie, A. R., Langford, B., Pugh, T. A. M., Robinson, N., Misztal, P. K., Heard, D. E., Lee, J. D., Lewis, A. C., Jones, C. E., Hopkins, J. R., Phillips, G., Monks, P. S., Karunaharan, A., Hornsby, K. E., Nicolas-Perea, V., Coe, H., Gabey, A. M., Gallagher, M. W., Whalley, L. K., Edwards, P. M., Evans, M. J., Stone, D., Ingham, T., Commane, R., Furneaux, K. L., McQuaid, J. B., Nemitz, E., Seng, Y. K., Fowler, D., Pyle, J. A., and Hewitt, C. N.: The atmospheric chemistry of trace gases and particulate matter emitted by different land uses in Borneo, Philosophical Transactions of the Royal Society B: Biological Sciences, 366, 3177-3195, 2011.

Madronich, S., and Calvert, J. G.: Permutation reactions of organic peroxy radicals in the troposphere, Journal of Geophysical Research: Atmospheres, 95, 5697-5715, 1990.

March, J.: Advanced organic chemistry: reactions, mechanisms, and structure, John Wiley and Sons, New York, 1992.

March, R. E., Hughes, R. J., and Todd, J. F.: Quadrupole storage mass spectrometry, John Wiley and Sons, New York, 1989.

March, R. E.: An introduction to quadrupole ion trap mass spectrometry, Journal of Mass Spectrometry, 32, 351-369, 1997.

Marshal, A. G., Grosshans, P. B.: Fourier transform ion cyclotron resonance mass spectrometry: The teenage years, Analytical Chemistry, 63, 215A-229A, 1991.

Marshall, A. G.: Fourier transform ion cyclotron resonance mass spectrometry, Accounts of Chemical Research, 18, 316-322, 1985.

Marshall, A. G., Hendrickson, C. L., and Jackson, G. S.: Fourier transform ion cyclotron resonance mass spectrometry: a primer, Mass Spectrometry Reviews, 17, 1-35, 1998.

Marshall, A. G., and Rodgers, R. P.: Petroleomics: The next grand challenge for chemical analysis, Accounts of Chemical Research, 37, 53-59, 2004.

Marshall, A. G., and Hendrickson, C. L.: High-resolution mass spectrometers, Annual Review of Analytical Chemistry, 1, 579-599, 2008.

Marshall, A. G., and Rodgers, R. P.: Petroleomics: Chemistry of the underworld, Proceedings of the National Academy of Sciences, 105, 18090-18095, 2008.

Martín-Reviejo, M., and Wirtz, K.: Is benzene a precursor for secondary organic aerosol?, Environmental Science and Technology, 39, 1045-1054, 2005.

Mazzoleni, L. R., Saranjampour, P., Dalbec, M. M., Samburova, V., Hallar, A. G., Zielinska, B., Lowenthal, D. H., and Kohl, S.: Identification of water-soluble organic carbon in non-urban aerosols using ultrahigh-resolution FT-ICR mass spectrometry: organic anions, Environmental Chemistry, 9, 285-297, 2012.

McLafferty, F. W.: Interpretation of mass spectra, 4th Edn, University Science Books, Sausalito, CA,1993.

McLuckey, S. A., and Wells, J. M.: Mass analysis at the advent of the 21st century, Chemical Reviews, 101, 571-606, 2001.

McMurry, P. H., and Grosjean, D.: Gas and aerosol wall losses in Teflon film smog chambers, Environmental Science and Technology, 19, 1176-1182, 1985.

McMurry, P. H.: A review of atmospheric aerosol measurements, Atmospheric Environment, 34, 1959-1999, 2000.

Mirov, N. T.: Composition of gum turpentines of pines, technical bulletin No. 1239, USDA forest service, 158 pp.,1961.

Misztal, P. K., Owen, S., Guenther, A. B., Rasmussen, R., Geron, C., Harley, P., Phillips, G., Ryan, A., Edwards, D. P., and Hewitt, C. N.: Large estragole fluxes from oil palms in Borneo, Atmospheric Chemistry and Physics, 10, 4343-4358, 2010.

Moldoveanu, S. C., and David, V.: Chapter 1 - Basic Information about HPLC, in: Essentials in modern HPLC separations, edited by: Moldoveanu, S. C., and David, V., Elsevier, Waltham, USA, 1-51, 2013.

Monks, P. S.: Gas-phase radical chemistry in the troposphere, Chemical Society Reviews, 34, 376-395, 2005.

Mortier, K. A., Zhang, G.-F., Van Peteghem, C. H., and Lambert, W. E.: Adduct formation in quantitative bioanalysis: effect of ionization conditions on paclitaxel, Journal of the American Society for Mass Spectrometry, 15, 585-592, 2004.

MPOB - Offical Portal Of Malaysian Palm Oil Board: http://bepi.mpob.gov.my/ (last access: 11 April 2013), 2012.

Müller, L., Reinnig, M.C., Hayen, H., and Hoffmann, T.: Characterization of oligomeric compounds in secondary organic aerosol using liquid chromatography coupled to electrospray ionization Fourier transform ion cyclotron resonance mass spectrometry, Rapid Communications in Mass Spectrometry, 23, 971-979, 2009.

Naidong, W.: Bioanalytical liquid chromatography tandem mass spectrometry methods on underivatized silica columns with aqueous/organic mobile phases, Journal of Chromatography B, 796, 209-224, 2003.

Nakao, S., Clark, C., Tang, P., Sato, K., and Cocker Iii, D.: Secondary organic aerosol formation from phenolic compounds in the absence of NOx, Atmospheric Chemistry Physics, 11, 10649-10660, 2011.

Nannoolal, Y., Rarey, J., Ramjugernath, D., and Cordes, W.: Estimation of pure component properties: Part 1. Estimation of the normal boiling point of non-electrolyte organic compounds via group contributions and group interactions, Fluid Phase Equilibria, 226, 45-63, 2004.

Nannoolal, Y., Rarey, J., and Ramjugernath, D.: Estimation of pure component properties: Part 3. Estimation of the vapor pressure of non-electrolyte organic compounds via group contributions and group interactions, Fluid Phase Equilibria, 269, 117-133, 2008.

Neeb, P., Horie, O., and Moortgat, G. K.: Gas-phase ozonolysis of ethene in the presence of hydroxylic compounds, International Journal of Chemical Kinetics, 28, 721-730, 1996.

Ng, N., Kroll, J., Chan, A., Chhabra, P., Flagan, R., and Seinfeld, J.: Secondary organic aerosol formation from m-xylene, toluene, and benzene, Atmospheric Chemistry and Physics, 7, 3909-3922, 2007a.

Ng, N., Canagaratna, M., Zhang, Q., Jimenez, J., Tian, J., Ulbrich, I., Kroll, J., Docherty, K., Chhabra, P., and Bahreini, R.: Organic aerosol components observed in Northern Hemispheric datasets from Aerosol Mass Spectrometry, Atmospheric Chemistry and Physics, 10, 4625-4641, 2010.

Ng, N. L., Kroll, J. H., Keywood, M. D., Bahreini, R., Varutbangkul, V., Flagan, R. C., Seinfeld, J. H., Lee, A., and Goldstein, A. H.: Contribution of first- versus second-generation products to secondary organic aerosols formed in the oxidation of biogenic hydrocarbons, Environmental Science and Technology, 40, 2283-2297, 2006.

Ng, N. L., Chhabra, P. S., Chan, A. W. H., Surratt, J. D., Kroll, J. H., Kwan, A. J., McCabe, D. C., Wennberg, P. O., Sorooshian, A., Murphy, S. M., Dalleska, N. F., Flagan, R. C., and

Seinfeld, J. H.: Effect of NOx level on secondary organic aerosol (SOA) formation from the photooxidation of terpenes, Atmospheric Chemistry and Physics, 7, 5159-5174, 2007b.

Nguyen, T. B., Bateman, A. P., Bones, D. L., Nizkorodov, S. A., Laskin, J., and Laskin, A.: High-resolution mass spectrometry analysis of secondary organic aerosol generated by ozonolysis of isoprene, Atmospheric Environment, 44, 1032-1042, 2010.

Nguyen, T. B., Lee, P. B., Updyke, K. M., Bones, D. L., Laskin, J., Laskin, A., and Nizkorodov, S. A.: Formation of nitrogen- and sulfur-containing light-absorbing compounds accelerated by evaporation of water from secondary organic aerosols, Journal of Geophysical Research: Atmospheres, 117, D01207, 2012.

Nizkorodov, S. A., Laskin, J., and Laskin, A.: Molecular chemistry of organic aerosols through the application of high resolution mass spectrometry, Physical Chemistry Chemical Physics, 13, 3612-3629, 2011.

Nováková, L., Solichová, D., and Solich, P.: Hydrophilic interaction liquid chromatography–charged aerosol detection as a straightforward solution for simultaneous analysis of ascorbic acid and dehydroascorbic acid, Journal of Chromatography A, 1216, 4574-4581, 2009.

Nozière, B., Kalberer, M., Claeys, M., Allan, J., D'Anna, B., Decesari, S., Finessi, E., Glasius, M., Grgić, I., Hamilton, J. F., Hoffmann, T., Iinuma, Y., Jaoui, M., Kahnt, A., Kampf, C. J., Kourtchev, I., Maenhaut, W., Marsden, N., Saarikoski, S., Schnelle-Kreis, J., Surratt, J. D., Szidat, S., Szmigielski, R., and Wisthaler, A.: The molecular identification of organic compounds in the atmosphere: State of the art and challenges, Chemical Reviews, 2015.

O'Neal, H. E., and Blumstein, C.: A new mechanism for gas phase ozone–olefin reactions, International Journal of Chemical Kinetics, 5, 397-413, 1973.

O'Brien, R. E., Laskin, A., Laskin, J., Liu, S., Weber, R., Russell, L. M., and Goldstein, A. H.: Molecular characterization of organic aerosol using nanospray desorption/electrospray ionization mass spectrometry: CalNex 2010 field study, Atmospheric Environment, 68, 265-272, 2013.

Odum, J. R., Hoffmann, T., Bowman, F., Collins, D., Flagan, R. C., and Seinfeld, J. H.: Gas/Particle partitioning and secondary organic aerosol yields, Environmental Science and Technology, 30, 2580-2585, 1996.

Ohta, T.: Furan ring formation in OH-initiated photooxidation of 1, 3-butadiene and cis-1, 3-pentadiene, Bulletin of the Chemical Society of Japan, 57, 960-966, 1984.

Olsen, B. A., and Pack, B. W.: Hydrophilic Interaction Chromatography: A Guide for Practitioners, John Wiley and Sons, Hoboken, New Jersey, 2013.

Orlando, J. J., Tyndall, G. S., and Wallington, T. J.: The atmospheric chemistry of alkoxy radicals, Chemical Reviews, 103, 4657-4690, 2003.

Orsini, D. A., Ma, Y., Sullivan, A., Sierau, B., Baumann, K., and Weber, R. J.: Refinements to the particle-into-liquid sampler (PILS) for ground and airborne measurements of water soluble aerosol composition, Atmospheric Environment, 37, 1243-1259, 2003.

Orzechowska, G. E., and Paulson, S. E.: Photochemical sources of organic acids. 1. Reaction of ozone with isoprene, propene, and 2-butenes under dry and humid conditions using SPME, The Journal of Physical Chemistry A, 109, 5358-5365, 2005.

Pandis, S. N., Paulson, S. E., Seinfeld, J. H., and Flagan, R. C.: Aerosol formation in the photooxidation of isoprene and β-pinene, Atmospheric Environment. Part A. General Topics, 25, 997-1008, 1991.

Pankow, J. F.: An absorption model of gas/particle partitioning of organic compounds in the atmosphere, Atmospheric Environment, 28, 185-188, 1994a.

Pankow, J. F.: An absorption model of the gas/aerosol partitioning involved in the formation of secondary organic aerosol, Atmospheric Environment, 28, 189-193, 1994b.

Parthasarathi, R., Subramanian, V., and Sathyamurthy, N.: Hydrogen bonding in phenol, water, and phenol−water clusters, The Journal of Physical Chemistry A, 109, 843-850, 2005.

Paulson, S. E., and Orlando, J. J.: The reactions of ozone with alkenes: An important source of HOx in the boundary layer, Geophysical Research Letters, 23, 3727-3730, 1996.

Paulson, S. E., Sen, A. D., Liu, P., Fenske, J. D., and Fox, M. J.: Evidence for formation of OH radicals from the reaction of O3 with alkenes in the gas phase, Geophysical Research Letters, 24, 3193-3196, 1997.

Payne, T. G., Southam, A. D., Arvanitis, T. N., and Viant, M. R.: A signal filtering method for improved quantification and noise discrimination in Fourier transform ion cyclotron resonance mass spectrometry-based metabolomics aata, Journal of the American Society for Mass Spectrometry, 20, 1087-1095, 2009.

Payne, T. G.: Profiling the metabolome using Fourier transform ion cyclotron resonance mass spectrometry, optimised signal processing, noise filtering and constraints methods,

PhD Thesis, School of Electronic, Electrical and Computer Engineering, University of Birmingham, 2011.

Peeters, J., Boullart, W., Pultau, V., Vandenberk, S., and Vereecken, L.: Structure−activity relationship for the addition of OH to (poly)alkenes: Site-specific and total rate constants, The Journal of Physical Chemistry A, 111, 1618-1631, 2007.

Pellegrin, V.: Molecular formulas of organic-compounds - the nitrogen rule and degree of unsaturation, Journal of Chemical Education, 60, 626-633, 1983.

Pereira, K. L., Hamilton, J. F., Rickard, A. R., Bloss, W. J., Alam, M. S., Camredon, M., Muñoz, A., Vázquez, M., Borrás, E., and Ródenas, M.: Secondary organic aerosol formation and composition from the photo-oxidation of methyl chavicol (estragole), Atmospheric Chemistry and Physics, 14, 5349-5368, 2014.

Perri, M. J., Seitzinger, S., and Turpin, B. J.: Secondary organic aerosol production from aqueous photooxidation of glycolaldehyde: Laboratory experiments, Atmospheric Environment, 43, 1487-1497, 2009.

Peters, A., Wichmann, H. E., Tuch, T., Heinrich, J., and Heyder, J.: Respiratory effects are associated with the number of ultrafine particles, American Journal of Respiratory and Critical Care Medicine, 155, 1376-1383, 1997.

Pierce, J., Engelhart, G., Hildebrandt, L., Weitkamp, E., Pathak, R., Donahue, N., Robinson, A., Adams, P., and Pandis, S.: Constraining particle evolution from wall losses, coagulation, and condensation-evaporation in smog-chamber experiments: optimal estimation based on size distribution measurements, Aerosol Science and Technology, 42, 1001-1015, 2008.

Pierce, J. R., Riipinen, I., Kulmala, M., Ehn, M., Petäjä, T., Junninen, H., Worsnop, D. R., and Donahue, N. M.: Quantification of the volatility of secondary organic compounds in ultrafine particles during nucleation events, Atmospheric Chemistry and Physics, 11, 9019-9036, 2011.

Pitts, J. N., Biermann, H. W., Atkinson, R., and Winer, A. M.: Atmospheric implications of simultaneous nighttime measurements of NO3 radicals and HONO, Geophysical Research Letters, 11, 557-560, 1984.

Platt, U., LeBras, G., Poulet, G., Burrows, J. P., and Moortgat, G.: Peroxy radicals from night-time reaction of N03 with organic compounds, Nature, 348, 147-149, 1990.

Pope, C. A., Young, B., Dockery, DW.: Health effects of fine particulate air pollution: lines that connect, Journal of the Air and Waste Management Association, 56, 709-742, 2006.

Pratt, K. A., and Prather, K. A.: Mass spectrometry of atmospheric aerosols—Recent developments and applications. Part II: On-line mass spectrometry techniques, Mass Spectrometry Reviews, 31, 17-48, 2012a.

Pratt, K. A., and Prather, K. A.: Mass spectrometry of atmospheric aerosols—Recent developments and applications. Part I: Off-line mass spectrometry techniques, Mass Spectrometry Reviews, 31, 1-16, 2012b.

Presto, A. A., Hartz, K. E. H., and Donahue, N. M.: Secondary organic aerosol production from terpene ozonolysis. 2. Effect of NOx concentration, Environmental Science Technology, 39, 7046-7054, 2005.

Qian, K., Rodgers, R. P., Hendrickson, C. L., Emmett, M. R., and Marshall, A. G.: Reading chemical fine print: Resolution and identification of 3000 nitrogen-containing aromatic compounds from a single electrospray ionization Fourier transform ion cyclotron resonance mass spectrum of heavy petroleum crude oil, Energy and Fuels, 15, 492-498, 2001.

Rafferty, J. L., Siepmann, J. I., and Schure, M. R.: Mobile phase effects in reversed-phase liquid chromatography: A comparison of acetonitrile/water and methanol/water solvents as studied by molecular simulation, Journal of Chromatography A, 1218, 2203-2213, 2011.

Reemtsma, T.: Determination of molecular formulas of natural organic matter molecules by (ultra-) high-resolution mass spectrometry: status and needs, Journal of Chromatography A, 1216, 3687, 2009.

Reinhardt, A., Emmenegger, C., Gerrits, B., Panse, C., Dommen, J., Baltensperger, U., Zenobi, R., and Kalberer, M.: Ultrahigh mass resolution and accurate mass measurements as a tool to characterize oligomers in secondary organic aerosols, Analytical Chemistry, 79, 4074-4082, 2007.

Rickard, A. R., Wyche, K. P., Metzger, A., Monks, P. S., Ellis, A. M., Dommen, J., Baltensperger, U., Jenkin, M. E., and Pilling, M. J.: Gas phase precursors to anthropogenic secondary organic aerosol: Using the Master Chemical Mechanism to probe detailed observations of 1,3,5-trimethylbenzene photo-oxidation, Atmospheric Environment, 44, 5423-5433, 2010.

Riipinen, I., Pierce, J. R., Yli-Juuti, T., Nieminen, T., Häkkinen, S., Ehn, M., Junninen, H., Lehtipalo, K., Petäjä, T., Slowik, J., Chang, R., Shantz, N. C., Abbatt, J., Leaitch, W. R., Kerminen, V. M., Worsnop, D. R., Pandis, S. N., Donahue, N. M., and Kulmala, M.: Organic condensation: a vital link connecting aerosol formation to cloud condensation nuclei (CCN) concentrations, Atmospheric Chemistry and Physics, 11, 3865-3878, 2011.

Riipinen, I., Yli-Juuti, T., Pierce, J. R., Petaja, T., Worsnop, D. R., Kulmala, M., and Donahue, N. M.: The contribution of organics to atmospheric nanoparticle growth, Nature Geoscience, 5, 453-458, 2012.

Rivett, A., Martin, D., Gray, D., Price, C., Nickless, G., Simmonds, P., O'Doherty, S., Greally, B., Knights, A., and Shallcross, D.: The role of volatile organic compounds in the polluted urban atmosphere of Bristol, England, Atmospheric Chemistry and Physics, 3, 1165-1176, 2003.

Roach, P. J., Laskin, J., and Laskin, A.: Molecular characterization of organic aerosols using nanospray-desorption/ electrospray ionization-mass spectrometry, Analytical Chemistry, 82, 7979-7986, 2010.

Roach, P. J., Laskin, J., and Laskin, A.: Higher-order mass defect analysis for mass spectra of complex organic mixtures, Analytical Chemistry, 83, 4924-4929, 2011.

Robinson, A. L., Donahue, N. M., Shrivastava, M. K., Weitkamp, E. A., Sage, A. M., Grieshop, A. P., Lane, T. E., Pierce, J. R., and Pandis, S. N.: Rethinking organic aerosols: Semivolatile emissions and photochemical aging, Science, 315, 1259-1262, 2007.

Robinson, N., Hamilton, J., Allan, J., Langford, B., Oram, D., Chen, Q., Docherty, K., Farmer, D., Jimenez, J., and Ward, M.: Evidence for a significant proportion of secondary organic aerosol from isoprene above a maritime tropical forest, Atmospheric Chemistry and Physics, 11, 1039-1050, 2011.

Rodgers, R. P., Schaub, T. M., and Marshall, A. G.: Petroleomics: MS returns to its roots, Analytical Chemistry, 77, 20-27, 2005.

Rodgers, R. P., and Marshall, A. G.: Petroleomics: Advanced characterization of petroleum-derived materials by Fourier transform ion cyclotron resonance mass spectrometry (FT-ICR MS), in: Asphaltenes, Heavy Oils, and Petroleomics, Springer, New York, 63-93, 2007.

Roelofs, G.-J., and Lelieveld, J. O. S.: Model study of the influence of cross-tropopause O3 transports on tropospheric O3 levels, Tellus B: Chemical and Physical Meteorology, 49, 38-55, 1997.

Rohrer, F., Bohn, B., Brauers, T., Brüning, D., Johnen, F.-J., Wahner, A., and Kleffmann, J.: Characterisation of the photolytic HONO-source in the atmosphere simulation chamber SAPHIR, Atmospheric Chemistry and Physics, 5, 2189-2201, 2005.

Ruppert, L., and Becker, K.: A product study of the OH radical-initiated oxidation of isoprene: formation of C5-unsaturated diols, Atmospheric Environment, 34, 1529-1542, 2000.

Sakamaki, F., Hatakeyama, S., and Akimoto, H.: Formation of nitrous acid and nitric oxide in the heterogeneous dark reaction of nitrogen dioxide and water vapor in a smog chamber, International Journal of Chemical Kinetics, 15, 1013-1029, 1983.

Sakamaki, F., and Akimoto, H.: HONO formation as unknown radical source in photochemical smog chamber, International Journal of Chemical Kinetics, 20, 111-116, 1988.

Samy, S., and Hays, M. D.: Quantitative LC-MS for water-soluble heterocyclic amines in fine aerosols (PM2.5) at Duke Forest, USA, Atmospheric Environment, 72, 77-80, 2013.

Sander, S. P., Golden, D., Kurylo, M., Moortgat, G., Wine, P., Ravishankara, A., Kolb, C., Molina, M., Finlayson-Pitts, B., and Huie, R.: Chemical kinetics and photochemical data for use in atmospheric studies evaluation number 15, Jet Propulsion Laboratory, 6, 2006.

Sato, K., Hatakeyama, S., and Imamura, T.: Secondary organic aerosol formation during the photooxidation of toluene: NOx dependence of chemical composition, The Journal of Physical Chemistry A, 111, 9796-9808, 2007.

Sato, K., Takami, A., Kato, Y., Seta, T., Fujitani, Y., Hikida, T., Shimono, A., and Imamura, T.: AMS and LC/MS analyses of SOA from the photooxidation of benzene and 1, 3, 5-trimethylbenzene in the presence of NOx: effects of chemical structure on SOA aging, Atmospheric Chemistry and Physics, 12, 4667-4682, 2012.

Schade, G. W., and Goldstein, A. H.: Fluxes of oxygenated volatile organic compounds from a ponderosa pine plantation, Journal of Geophysical Research, 106, 3111-3123, 2001.

Schmidt, A.-C., Herzschuh, R., Matysik, F.-M., and Engewald, W.: Investigation of the ionisation and fragmentation behaviour of different nitroaromatic compounds occurring as polar metabolites of explosives using electrospray ionisation tandem mass spectrometry, Rapid Communications in Mass Spectrometry, 20, 2293-2302, 2006.

Schmitt-Kopplin, P., Gelencsér, A., Dabek-Zlotorzynska, E., Kiss, G., Hertkorn, N., Harir, M., Hong, Y., and Gebefügi, I.: Analysis of the unresolved organic fraction in atmospheric aerosols with ultrahigh-resolution mass spectrometry and nuclear magnetic resonance spectroscopy: Organosulfates as photochemical smog constituents, Analytical Chemistry, 82, 8017-8026, 2010.

Schmitt-Kopplin, P., Liger-Belair, G., Koch, B. P., Flerus, R., Kattner, G., Harir, M., Kanawati, B., Lucio, M., Tziotis, D., Hertkorn, N., and Gebefügi, I.: Dissolved organic matter in sea spray: a transfer study from marine surface water to aerosols, Biogeosciences, 9, 1571-1582, 2012.

Schumann, U., and Huntrieser, H.: The global lightning-induced nitrogen oxides source, Atmospheric Chemistry and Physics, 7, 3823-3907, 2007.

Schure, M. R., Jake, L., and Siepmann, J. I.: How reversed-phase liquid chromatography works, LC GC North America, 31, 630-637, 2013.

Schwarz, K., Filipiak, W., and Amann, A.: Determining concentration patterns of volatile compounds in exhaled breath by PTR-MS, Journal of Breath Research, 3, 027002, 2009.

Seaton, A., Godden, D., MacNee, W., and Donaldson, K.: Particulate air pollution and acute health effects, The Lancet, 345, 176-178, 1995.

Seinfeld, J.: Rethinking the ozone problem in urban and regional air pollution, National Academy of Science, USA, 524 pp., 1992.

Seinfeld, J. H., and Pandis, S. N.: Atmospheric chemistry and physics: From air pollution to climate change, John Wiley and Sons, New Jersey, 2012.

Sharkey A. G. Jr., J. L. Shultz., T. Kessler., and Friedel., R. A.: High resolution mass spectrometry has advantages in determining organic contaminants in air and water, Journal of Research and Development, 20, 30-32, 1969.

Shiraiwa, M., Yee, L. D., Schilling, K. A., Loza, C. L., Craven, J. S., Zuend, A., Ziemann, P. J., and Seinfeld, J. H.: Size distribution dynamics reveal particle-phase chemistry in organic aerosol formation, Proceedings of the National Academy of Sciences, 110, 11746-11750, 2013.

Sihto, S. L., Kulmala, M., Kerminen, V. M., Dal Maso, M., Petäjä, T., Riipinen, I., Korhonen, H., Arnold, F., Janson, R., Boy, M., Laaksonen, A., and Lehtinen, K. E. J.: Atmospheric sulphuric acid and aerosol formation: implications from atmospheric measurements for nucleation and early growth mechanisms, Atmospheric Chemistry and Physics, 6, 4079-4091, 2006.

Singh, H., Chen, Y., Tabazadeh, A., Fukui, Y., Bey, I., Yantosca, R., Jacob, D., Arnold, F., Wohlfrom, K., Atlas, E., Flocke, F., Blake, D., Blake, N., Heikes, B., Snow, J., Talbot, R., Gregory, G., Sachse, G., Vay, S., and Kondo, Y.: Distribution and fate of selected oxygenated organic species in the troposphere and lower stratosphere over the Atlantic, Journal of Geophysical Research: Atmospheres, 105, 3795-3805, 2000.

Sipilä, M., Berndt, T., Petäjä, T., Brus, D., Vanhanen, J., Stratmann, F., Patokoski, J., Mauldin, R. L., Hyvärinen, A.-P., Lihavainen, H., and Kulmala, M.: The role of sulfuric acid in atmospheric nucleation, Science, 327, 1243-1246, 2010.

Smith, J. S., Laskin, A., and Laskin, J.: Molecular characterization of biomass burning aerosols using high-resolution mass spectrometry, Analytical Chemistry, 81, 1512-1521, 2008.

Sogacheva, L., Saukkonen, L., Nilsson, E. D., Dal Maso, M., Schultz, D. M., De Leeuw, G., and Kulmala, M.: New aerosol particle formation in different synoptic situations at Hyytiälä, Southern Finland, Tellus B, 60, 485-494, 2008.

Solomon, S., Qin, D., Manning, M., Chen, Z., Marquis, M., Averyt, K., Tignor, M., and Miller, H.: IPCC, 2007: Climate change 2007: the physical science basis, contribution of workinggGroup I to the fourth assessment report of the Intergovernmental Panel on Climate Change, 2007.

Song, C., Na, K., and Cocker, D. R.: Impact of the hydrocarbon to NOx ratio on secondary organic aerosol formation, Environmental Science and Technology, 39, 3143-3149, 2005.

Sorooshian, A., Brechtel, F. J., Ma, Y., Weber, R. J., Corless, A., Flagan, R. C., and Seinfeld, J. H.: Modeling and characterization of a particle-into-liquid sampler (PILS), Aerosol Science and Technology, 40, 396-409, 2006.

Southam, A. D., Payne, T. G., Cooper, H. J., Arvanitis, T. N., and Viant, M. R.: Dynamic range and mass accuracy of wide-scan direct infusion nanoelectrospray Fourier transform ion cyclotron resonance mass spectrometry-based metabolomics increased by the spectral stitching method, Analytical Chemistry, 79, 4595-4602, 2007.

Southwell, I. A., Russell, M. F., Smith, R. L., and Vinnicombe, A.: Ochrosperma lineare, a new source of methyl chavicol, Journal of Essential Oil Research, 15, 329-330, 2003.

Spada, N., Fujii, E., and Cahill, T. M.: Diurnal cycles of acrolein and other small aldehydes in regions impacted by vehicle emissions, Environmetal Science and Technology, 42, 7084-7090, 2008.

Spanel, P., Ji, Y., and Smith, D.: SIFT studies of the reactions of H3O+, NO+ and O2+ with a series of aldehydes and ketones, International Journal of Mass Spectrometry and Ion Processes, 165, 25-37, 1997.

Spanel, P., and Smith, D.: SIFT studies of the reactions of H3O+, NO+ and O+ 2 with a series of volatile carboxylic acids and esters, International Journal of Mass Spectrometry and Ion Processes, 172, 137-147, 1998.

Spracklen, D., Carslaw, K., Kulmala, M., Kerminen, V.-M., Mann, G., and Sihto, S.-L.: The contribution of boundary layer nucleation events to total particle concentrations on regional and global scales, Atmospheric Chemistry and Physics, 6, 5631-5648, 2006.

Spracklen, D. V., Jimenez, J. L., Carslaw, K. S., Worsnop, D. R., Evans, M. J., Mann, G. W., Zhang, Q., Canagaratna, M. R., Allan, J., Coe, H., McFiggans, G., Rap, A., and Forster, P.: Aerosol mass spectrometer constraint on the global secondary organic aerosol budget, Atmospheric Chemistry and Physics, 11, 12109-12136, 2011.

Sprengnether, M., Demerjian, K. L., Donahue, N. M., and Anderson, J. G.: Product analysis of the OH oxidation of isoprene and 1,3-butadiene in the presence of NO, Journal of Geophysical Research: Atmospheres, 107, ACH 8-1-ACH 8-13, 2002.

Steiner, A. L., Cohen, R. C., Harley, R. A., Tonse, S., Millet, D. B., Schade, G. W., and Goldstein, A. H.: VOC reactivity in central California: comparing an air quality model to ground-based measurements, Atmospheric Chemistry Physics, 8, 351-368, 2008.

Stockwell, W. R., Middleton, P., Chang, J. S., and Tang, X.: The second generation regional acid deposition model chemical mechanism for regional air quality modeling, Journal of Geophysical Research, 95, 16343-16367, 1990.

Stone, E. A., Hedman, C. J., Sheesley, R. J., Shafer, M. M., and Schauer, J. J.: Investigating the chemical nature of humic-like substances (HULIS) in North American atmospheric aerosols by liquid chromatography tandem mass spectrometry, Atmospheric Environment, 43, 4205-4213, 2009.

Strollo, C. M., and Ziemann, P. J.: Products and mechanism of secondary organic aerosol formation from the reaction of 3-methylfuran with OH radicals in the presence of NOx, Atmospheric Environment, 77, 534-543, 2013.

Stull, R. B.: An introduction to boundary layer meteorology, Kluwer Academic Publishers, The Netherlands,1988.

Sullivan, A., Peltier, R. E., Brock, C., De Gouw, J., Holloway, J., Warneke, C., Wollny, A., and Weber, R.: Airborne measurements of carbonaceous aerosol soluble in water over northeastern United States: Method development and an investigation into water-soluble organic carbon sources, Journal of Geophysical Research: Atmospheres, 111, D23S46, 2006.

Surratt, J. D., Chan, A. W. H., Eddingsaas, N. C., Chan, M., Loza, C. L., Kwan, A. J., Hersey, S. P., Flagan, R. C., Wennberg, P. O., and Seinfeld, J. H.: Reactive intermediates revealed in secondary organic aerosol formation from isoprene, Proceedings of the National Academy of Sciences of the United States of America, 15, 6640-6645, 20010.

Svensson, R., Ljungström, E., and Lindqvist, O.: Kinetics of the reaction between nitrogen dioxide and water vapour, Atmospheric Environment, 21, 1529-1539, 1987.

Taipale, R., Rantala, P., Kajos, M., Patokoski, J., Ruuskanen, T., Aalto, J., Kolari, P., Bäck, J., Hari, P., and Kulmala, M.: Oxygenated VOC and monoterpene emissions from a boreal coniferous forest, EGU General Assembly Conference Abstracts, 14, 9735, 2012.

Tan, Y., Carlton, A. G., Seitzinger, S. P., and Turpin, B. J.: SOA from methylglyoxal in clouds and wet aerosols: Measurement and prediction of key products, Atmospheric Environment, 44, 5218-5226, 2010.

Tapia, A., Villanueva, F., Salgado, M., Cabañas, B., Martínez, E., and Martín, P.: Atmospheric degradation of 3-methylfuran: kinetic and products study, Atmospheric Chemistry and Physics, 11, 3227-3241, 2011.

These, A., and Reemtsma, T.: Limitations of electrospray ionization of fulvic and humic acids as visible from size exclusion chromatography with organic carbon and mass spectrometric detection, Analytical Chemistry, 75, 6275-6281, 2003.

Tolocka, M. P., Jang, M., Ginter, J. M., Cox, F. J., Kamens, R. M., and Johnston, M. V.: Formation of oligomers in secondary organic aerosol, Environmental Science and Technology, 38, 1428-1434, 2004.

Tsui, H. H. Y., and van Mourik, T.: Ab initio calculations on phenol–water, Chemical Physics Letters, 350, 565-572, 2001.

Tuazon, E. C., Alvarado, A., Aschmann, S. M., Atkinson, R., and Arey, J.: Products of the gas-phase reactions of 1,3-butadiene with OH and NO3 radicals, Environmental Science and Technology, 33, 3586-3595, 1999.

Turpin, B. J., and Huntzicker, J. J.: Identification of secondary organic aerosol episodes and quantitation of primary and secondary organic aerosol concentrations during SCAQS, Atmospheric Environment, 29, 3527-3544, 1995.

USDA - United States Department of Agriculture, Global Crop Production Analysis: http://www.pecad.fas.usda.gov, last access: 04/11/2013, 2013.

Vaden, T. D., Imre, D., Beránek, J., Shrivastava, M., and Zelenyuk, A.: Evaporation kinetics and phase of laboratory and ambient secondary organic aerosol, Proceedings of the National Academy of Sciences of the United States of America, 108, 2190-2195, 2011.

Vailaya, A., and Horváth, C.: Retention in reversed-phase chromatography: Partition or adsorption?, Journal of Chromatography A, 829, 1-27, 1998.

van Donkelaar, A., Martin, R. V., Brauer, M., Kahn, R., Levy, R., Verduzco, C., and Villeneuve, P. J.: Global estimates of ambient fine particulate matter concentrations from

satellite-based aerosol optical depth: development and application, Environmental Health Perspectives, 118, 847, 2010.

Van Eijck, A., Opatz, T., Taraborrelli, D., Sander, R., and Hoffmann, T.: New tracer compounds for secondary organic aerosol formation from β-caryophyllene oxidation, Atmospheric Environment, 80, 122-130, 2013.

Van Krevelen, D. W.: Graphical-statistical method for the study of structure and reaction processes of coal, Fuel, 29, 269-284, 1950.

Varutbangkul, V., Brechtel, F., Bahreini, R., Ng, N., Keywood, M., Kroll, J., Flagan, R., Seinfeld, J., Lee, A., and Goldstein, A.: Hygroscopicity of secondary organic aerosols formed by oxidation of cycloalkenes, monoterpenes, sesquiterpenes, and related compounds, Atmospheric Chemistry and Physics, 6, 2367-2388, 2006.

Venkatachari, P., and Hopke, P. K.: Characterization of products formed in the reaction of ozone with alpha-pinene: case for organic peroxides, Journal of Environmental Monitoring, 10, 966-974, 2008.

Volkamer, R., Platt, U., Wirtz, K., Barnes, I., and Sidebottom, H.: The European Photoreactor (EUPHORE), 3rd Annual Report 2000, Bergische Universität Wuppertal Wuppertal, Germany, 2001.

Volkamer, R., Jimenez, J. L., San Martini, F., Dzepina, K., Zhang, Q., Salcedo, D., Molina, L. T., Worsnop, D. R., and Molina, M. J.: Secondary organic aerosol formation from anthropogenic air pollution: Rapid and higher than expected, Geophysical Research Letters, 33, L17811, 2006.

Wang, J., Hu, Z., Chen, Y., Chen, Z., and Xu, S.: Contamination characteristics and possible sources of PM10 and PM2.5 in different functional areas of Shanghai, China, Atmospheric Environment, 68, 221-229, 2013.

Wang, P. G., and He, W.: Hydrophilic interaction liquid chromatography (HILIC) and advanced applications, CRC Press, US, 610 pp., 2011.

Wang, X., Manning, W., Feng, Z., and Zhu, Y.: Ground-level ozone in China: Distribution and effects on crop yields, Environmental Pollution, 147, 394-400, 2007.

Webb, P. J., Hamilton, J. F., Lewis, A. C., and Wirtz, K.: Formation of oxygenated-polycyclic aromatic compounds in aerosol from the photo-oxidation of o-tolualdehyde, Polycyclic Aromatic Compounds, 26, 237-252, 2006.

Weber, R., Orsini, D., Daun, Y., Lee, Y. N., Klotz, P., and Brechtel, F.: A particle-into-liquid collector for rapid measurement of aerosol bulk chemical composition, Aerosol Science and Technology, 35, 718-727, 2001.

Weber, R. J., McMurry, P. H., Eisele, F. L., and Tanner, D. J.: Measurement of expected nucleation precursor species and 3–500-nm diameter particles at mauna Loa observatory, Hawaii, Journal of the Atmospheric Sciences, 52, 2242-2257, 1995.

Werker, E., Putievsky, E., Ravid, U., Dudai, N., and Katzir, I.: Glandular hairs, secretory cavities, and the essential oil in the leaves of tarragon (artemisia dracunculus L.), Journal of Herbs, Spices and Medicinal Plants, 2, 19-32, 1994.

WHO: World Health Organization air quality guidelines for particulate matter, ozone, nitrogen dioxide and sulfur dioxide: global update 2005: summary of risk assessment, Germany, 2006.

Wiedinmyer, C., Guenther, A., Harley, P., Hewitt, N., Geron, C., Artaxo, P., Steinbrecher, R., and Rasmussen, R.: Global organic emissions from vegetation, in: Emissions of atmospheric trace compounds, Advances in global change research, edited by: Granier, C., Artaxo, P., and Reeves, C., Springer, Netherlands, 115–170, 2004.

Winer, A. M., Atkinson, R., and Pitts, J. N.: Gaseous nitrate radical: Possible nighttime atmospheric sink for biogenic organic compounds, Science, 224, 156-159, 1984.

Wozniak, A. S., Bauer, J. E., Sleighter, R. L., Dickhut, R. M., and Hatcher, P. G.: Technical Note: Molecular characterization of aerosol-derived water soluble organic carbon using ultrahigh resolution electrospray ionization Fourier transform ion cyclotron resonance mass spectrometry, Atmospheric Chemistry and Physics, 8, 5099-5111, 2008.

Xu, L., Zhao, T., Guan, X., Tang, W., Liu, X., and Zhang, H.: Preparation, chromatographic evaluation and comparison of cystine- and cysteine-bonded stationary phases, Analytical Methods, 6, 2205-2214, 2014.

Yang, X. J., Qu, Y., Yuan, Q., Wan, P., Du, Z., Chen, D., and Wong, C.: Effect of ammonium on liquid- and gas-phase protonation and deprotonation in electrospray ionization mass spectrometry, Analyst, 138, 659-665, 2013.

Yassine, M. M., Dabek-Zlotorzynska, E., Harir, M., and Schmitt-Kopplin, P.: Identification of weak and strong organic acids in atmospheric aerosols by capillary electrophoresis/mass spectrometry and ultra-high-resolution Fourier transform ion cyclotron resonance mass spectrometry, Analytical Chemistry, 84, 6586-6594, 2012.

Yinon, J., McClellan, J. E., and Yost, R. A.: Electrospray ionization tandem mass spectrometry collision-induced dissociation study of explosives in an ion trap mass spectrometer, Rapid Communications in Mass Spectrometry, 11, 1961-1970, 1997.

Yu, F.: A secondary organic aerosol formation model considering successive oxidation aging and kinetic condensation of organic compounds: global scale implications, Atmospheric Chemistry and Physics, 11, 1083-1099, 2011.

Zabel, F.: Unimolecular decomposition of peroxynitrates, Zeitschrift fur Physikalische Chemie, 188, 119-142, 1995.

Zare, A., Christensen, J. H., Gross, A., Irannejad, P., Glasius, M., and Brandt, J.: Quantifying the contributions of natural emissions to ozone and total fine PM concentrations in the Northern Hemisphere, Atmospheric Chemistry and Physics, 14, 2735-2756, 2014.

Zekavat, B., Szulejko, J. E., LaBrecque, D., Olaitan, A. D., and Solouki, T.: Efficient injection of low-mass ions into high magnetic field Fourier transform ion cyclotron resonance mass spectrometers, Rapid Communications in Mass Spectrometry, 28, 230-238, 2014.

Zhang, D., Wu, L., Koch, K., and Cooks, R.: Arginine clusters generated by electrospray ionization and identified by tandem mass spectrometry, European Journal of Mass Spectrometry, 5, 353-361, 1999.

Zhang, J., Huff Hartz, K. E., Pandis, S. N., and Donahue, N. M.: Secondary organic aerosol formation from limonene ozonolysis: Homogeneous and heterogeneous influences as a function of NOx, The Journal of Physical Chemistry A, 110, 11053-11063, 2006.

Zhang, Q., Worsnop, D., Canagaratna, M., and Jimenez, J.: Hydrocarbon-like and oxygenated organic aerosols in Pittsburgh: insights into sources and processes of organic aerosols, Atmospheric Chemistry and Physics, 5, 3289-3311, 2005.

Zhang, Q., Jimenez, J., Canagaratna, M., Allan, J., Coe, H., Ulbrich, I., Alfarra, M., Takami, A., Middlebrook, A., and Sun, Y.: Ubiquity and dominance of oxygenated species in organic aerosols in anthropogenically-influenced Northern Hemisphere midlatitudes, Geophysical Research Letters, 34, L13801, 2007.

Zhang, Q., Jimenez, J., Canagaratna, M., Ulbrich, I., Ng, N., Worsnop, D., and Sun, Y.: Understanding atmospheric organic aerosols via factor analysis of aerosol mass spectrometry: a review, Analytical and Bioanalytical Chemistry, 401, 3045-3067, 2011a.

Zhang, Q. J., Beekmann, M., Drewnick, F., Freutel, F., Schneider, J., Crippa, M., Prevot, A. S. H., Baltensperger, U., Poulain, L., and Wiedensohler, A.: Formation of organic aerosol in

the Paris region during the MEGAPOLI summer campaign: evaluation of the volatility-basis-set approach within the CHIMERE model, Atmospheric Chemistry and Physics, 13, 5767-5790, 2013.

Zhang, R., Suh, I., Zhao, J., Zhang, D., Fortner, E. C., Tie, X., Molina, L. T., and Molina, M. J.: Atmospheric new particle formation enhanced by organic acids, Science, 304, 1487-1490, 2004.

Zhang, R., Wang, L., Khalizov, A. F., Zhao, J., Zheng, J., McGraw, R. L., and Molina, L. T.: Formation of nanoparticles of blue haze enhanced by anthropogenic pollution, Proceedings of the National Academy of Sciences, 106, 17650-17654, 2009.

Zhang, R., Khalizov, A., Wang, L., Hu, M., and Xu, W.: Nucleation and growth of nanoparticles in the atmosphere, Chemical Reviews, 112, 1957-2011, 2011b.

Zhang, S.-H., Shaw, M., Seinfeld, J. H., and Flagan, R. C.: Photochemical aerosol formation from α-pinene- and β-pinene, Journal of Geophysical Research: Atmospheres, 97, 20717-20729, 1992.

Zhang, X., Cappa, C. D., Jathar, S. H., McVay, R. C., Ensberg, J. J., Kleeman, M. J., and Seinfeld, J. H.: Influence of vapor wall loss in laboratory chambers on yields of secondary organic aerosol, Proceedings of the National Academy of Sciences, 111, 5802-5807, 2014.

Zhao, J., Levitt, N. P., and Zhang, R.: Heterogeneous chemistry of octanal and 2, 4-hexadienal with sulfuric acid, Geophysical Research Letters, 32, L09802, 2005.

Zhao, X., and Yinon, J.: Identification of nitrate ester explosives by liquid chromatography-electrospray ionization and atmospheric pressure chemical ionization mass spectrometry, Journal of Chromatography A, 977, 59-68, 2002.

Zhao, Y., Hallar, A. G., and Mazzoleni, L. R.: Atmospheric organic matter in clouds: exact masses and molecular formula identification using ultrahigh-resolution FT-ICR mass spectrometry, Atmospheric Chemistry and Physics, 13, 12343-12362, 2013.

Zhou, Y., Zhang, H., Parikh, H. M., Chen, E. H., Rattanavaraha, W., Rosen, E. P., Wang, W., and Kamens, R. M.: Secondary organic aerosol formation from xylenes and mixtures of toluene and xylenes in an atmospheric urban hydrocarbon mixture: Water and particle seed effects (II), Atmospheric Environment, 45, 3882-3890, 2011.

Zi-feng, L., Ji-ming, H. A. O., Jing-chun, D., and Jun-hua, L. I.: Estimate of the formation potential of secondary organic aerosol in Beijing summertime, Huan Jing Ke Xue, 30, 969–975, 2009.

Ziemann, P. J., Atkinson, R.: Kinetics, products, and mechanisms of secondary organic aerosol formation, Chem Soc Rev, 41, 6582-6605, 2012.

Zimmerman, P. R.: Testing of hydrocarbon emissions from vegetation, leaf litter and aquatic surfaces, and development of a methodology for compiling biogenic emission inventories: Final report, Environmental Protection Agency, EPA-450, 112, 1979.

Zubarev, R., and Mann, M.: On the proper use of mass accuracy in proteomics, Molecular and Cellular Proteomics, 6, 377-381, 2007.